Investigating Secular Trends in Metamorphism through the Construction and Application of a Relational Database (MetRec)

A Thesis Submitted to the
College of Graduate and Postdoctoral Studies
In Partial Fulfillment of the Requirements
For the Degree of Master of Science – Geology
In the Department of Geological Sciences
University of Saskatchewan
Saskatoon

By

Peter Roy Hone

Permission to Use

In presenting this thesis/dissertation in partial fulfillment of the requirements for a Postgraduate degree from the University of Saskatchewan, I agree that the Libraries of this University may make it freely available for inspection. I further agree that permission for copying of this thesis/dissertation in any manner, in whole or in part, for scholarly purposes may be granted by the professor or professors who supervised my thesis/dissertation work or, in their absence, by the Head of the Department or the Dean of the College in which my thesis work was done. It is understood that any copying or publication or use of this thesis/dissertation or parts thereof for financial gain shall not be allowed without my written permission. It is also understood that due recognition shall be given to me and to the University of Saskatchewan in any scholarly use which may be made of any material in my thesis/dissertation.

Disclaimer

This thesis document was exclusively created to meet the thesis and/or exhibition requirements for the degree of Master of Science at the University of Saskatchewan. Reference in this thesis/dissertation to any specific commercial products, process, or service by trade name, trademark, manufacturer, or otherwise, does not constitute or imply its endorsement, recommendation, or favoring by the University of Saskatchewan. The views and opinions of the author expressed herein do not state or reflect those of the University of Saskatchewan and shall not be used for advertising or product endorsement purposes.

Requests for permission to copy or to make other uses of materials in this thesis/dissertation in whole or part should be addressed to:

Head of the Department of Earth Sciences
Geology Building
University of Saskatchewan
114 Science Place Campus Drive
Saskatoon, Saskatchewan S7N 5E2 Canada

OR

Dean
College of Graduate and Postdoctoral Studies
University of Saskatchewan
116 Thorvaldson Building, 110 Science Place
Saskatoon, Saskatchewan S7N 5C9 Canada

Abstract

Recent studies of metamorphic trends have used dT/dP to compare records. dT/dP is calculated as the temperature estimate divided by the pressure estimate. This approximates a geothermal gradient for the sample (written as °C/GPa). Records are typically categorized by dT/dP into low, medium, and high samples. Previous studies, using a dataset of dT/dP, have looked at cycles of metamorphic trends, including a stark shift away from medium and high-pressure samples towards low pressure samples around 750 Ma. This study created a multi-table relational database, which combines previously published datasets with data from a literature review, with ~1000 records. This study has updated statistical methods, improved methods for categorizing records using facies classifications, and analyzed spatial association using mapping software and plate reconstruction models. The range of modern (<750 Ma) subduction related samples is also compared to modelled ranges of metamorphic records to establish the range of subduction-related material.

It has been shown that subduction-related rocks younger than 750 Ma can span a broad range of dT/dP from less than ~175 °C/GPa to ~875 °C/GPa. This is far broader than previous authors have established (<440 °C/GPa) and records which overlap <750 Ma subduction-related records are far more numerous than previously noted. A comparison of the most common orogens sampled shows that the data is heavily skewed – 372 records from the database come from the Alpine-Himalayan complex, which accounts for 66% of blueschist samples in the database. This pulls the trends of modern data to match those of the Alps and Himalayas and has not previously been discussed in the literature. It is posited by this study that blueschists are much rarer than previously acknowledged and the prevalence of modern blueschist is due to the Alpine-Himalayan bias. There is little evidence for a bimodal distribution of dT/dP which has previously been used as a marker for modern metamorphism. The findings of this study show that metamorphic terranes, while being closely tied to supercontinent cyclicity, have remained relatively stable since the Archean and that all categories of dT/dP can be seen throughout time and back into the Archean.

Acknowledgments

This study would like to thank Dr. Bruce Eglington and Dr. Sally Pehrsson for their invaluable guidance. It would also like to thank Hoang Anh Tu Nguyen for her help with Python programming and her general support throughout the thesis.

Table of Contents

List of Figures

List of Tables

List of Equations

1 Introduction

Changes in the Earth over time are recorded in the rock record. Although sometimes incomplete and challenging to interpret, this record provides a surface-level account of proxies for geological processes and, consequently, geodynamic settings. While most rock samples are obtained from surface exposures, it is also possible to sample the lower crust and mantle through xenoliths brought to surface by intrusions or during tectonic processes. These rock samples offer various proxies, including lithology, geochemistry, metamorphic petrology, and others. Metamorphism serves as a valuable proxy as it induces predictable changes in rocks through the application of heat and pressure. Changes brought on by metamorphism have undergone extensive study and are generally well-understood. Metamorphism can be categorized into different grades, reflecting the level of heat and pressure experienced by the rock. By assessing metamorphic grade, researchers can interpret the geological processes that have influenced these rocks. Since metamorphic rocks provide a record of changes in pressure and temperature conditions, this record can be extrapolated to infer regional tectonic variations.

Common metamorphic rocks include those that have attained blueschist, amphibolite, greenschist, granulite, and eclogite grade. Each of these are often used as indicators for a specific geodynamic setting: blueschist grade representing subduction zones, greenschist grade representing low-pressure and low-temperature regions, eclogite (typically) representing subduction, amphibolite grade representing mid-grade metamorphism in the central and hinterland region of collisional belts, and finally, granulite grade representing high-grade metamorphism in orogenic areas experiencing magmatic addition or additional heat sources. Ultrahigh temperature (UHT) and contact metamorphism are also commonly observed throughout the rock record and are often associated with the intrusion and emplacement of magmatic bodies, rather than specific tectonic events. However, UHT and contact metamorphism are typically avoided in such studies to prevent contamination of the tectonic interpretation of the data. Nonetheless, it is important to acknowledge the possibility of igneous intrusions influencing

individual samples. Orogens can generate diverse metamorphic conditions depending on their location within the collisional area, with significant variations in temperature, pressure, and metamorphic fluids. Consequently, a single orogen can exhibit different metamorphic facies and grades, even when considering multiple protoliths. Understanding this variability is crucial for interpreting metamorphic data and spatial associations.

Our understanding of present-day orogens and tectonics relies on surface exposures and data obtained through geophysical methods. Rock samples provide insights into what is visible at the surface, but only in one layer. Geophysical techniques allow us to probe deeper into the crust and mantle, supplementing our observations from the surface or drill cores. These techniques provide valuable information about regions of the Earth that we may not have the opportunity to observe directly, except through xenoliths. Xenoliths from the lower crust and mantle offer a glimpse into the deeper parts of the crust that are otherwise inaccessible. While there may be some challenges with regard to their provenance, these xenoliths will be an essential tool going forward. The focus on surface sampling in orogens can introduce biases in our models. Consequently, our understanding of orogens is often limited, requiring us to integrate information from various orogens to construct a theoretical model of their characteristics and evolution over time.

The distribution of exposed metamorphic belts is highly uneven and our picture of modern orogens are often seen in time slices as these orogens erode. Working with surface exposures restricts us to samples that have returned to the surface which means that surface level sampling of an orogen will be affected by the level erosion. The same orogen may produce different outcrop samples after more erosion and that needs to be remembered during comparisons.

Geological eons are defined by major changes in the Earth's history. While the Phanerozoic era is characterized by a wealth of fossil evidence, the Archean era is marked by a scarcity of rock samples (Korenaga, 2013). The Hadean era even more so. This poses a significant challenge, particularly for authors seeking "direct geological evidence" (Stern, 2005). The absence of direct evidence presents a serious obstacle in understanding the onset of plate tectonics. Numerous authors have proposed that plate tectonics existed since the Archean or even the Hadean, but our ability to prove or disprove these hypotheses is severely limited. The current

debate revolves around what should be considered evidence, the required amount of evidence, and even how to define plate tectonics (in contrast to localized subduction).

Many researchers have employed different proxies to correlate metamorphic grade with geodynamic processes, including:

- Mineralogy (de Roever, 1956; Ernst, 1972; Guotana et al., 2022; Nutman, 2022; Stern, 2005)
- Geothermal gradients and thermobaric ratio (Brown and Johnson, 2019; Brown, 2007; Brown et al., 2020a, 2022; Brown and Johnson, 2018; Chowdhury et al., 2021; Grambling, 1981; Holder et al., 2019; Palin et al., 2020; Zheng and Zhao, 2020)
- Geochemistry (Nutman, 2022; Shirey et al., 2008a)
- Crustal models (Davies, 1992; Hastie and Fitton, 2019; Hawkesworth et al., 2010; Korenaga, 2021, 2018; Profeta et al., 2016; Tang et al., 2020)
- Mantle Potential Temperatures (Condie et al., 2016; Condie and Shearer, 2017; Davies, 2006, 2009; Ganne and Feng, 2017; Herzberg et al., 2010; Korenaga, 2008a)

Numerous studies have explored these different proxies, and authors have proposed different timings for the onset of plate tectonics, ranging from the Late Proterozoic to the Late Hadean. Supporters of a Hadean and Early Archean onset of plate tectonics cite geochemical research. Nutman et al. (2021) argues that the rock chemistry of the Isua Supracrustal Belt (ISB) indicates extensive recycling between the mantle and hydrosphere. A stagnant lid model of plate tectonics would not involve such element recycling between the crust and mantle. Brown et al. (2020a) suggests the onset of plate tectonics in the Early Proterozoic, with a transitional period beginning in the Archean. They consider the first instances of supercontinents as the initial manifestation of mobile lid tectonics, while isolated cases of subduction cannot be proven to be plate tectonics. Other authors have positioned their estimates between these extremes. Recent research focuses on secular trends in thermobaric ratio (dT/dP). This thesis will investigate these secular trends in plate tectonic regimes, primarily focusing on dT/dP alongside other proxies.

Most recent studies of metamorphism have focused on the conditions of peak metamorphism. Peak metamorphism is the highest point for temperature and/or pressure along the path of prograde heating and burial, prior to cooling and exhumation (Vernon and Clarke,

2008). These two values can be non-contemporaneous, and sometimes not even taken from the same sample. Figure 1.1 illustrates a common issue with using peak temperature and peak pressure as a proxy for peak metamorphism. Having temperature, pressure, and time estimates

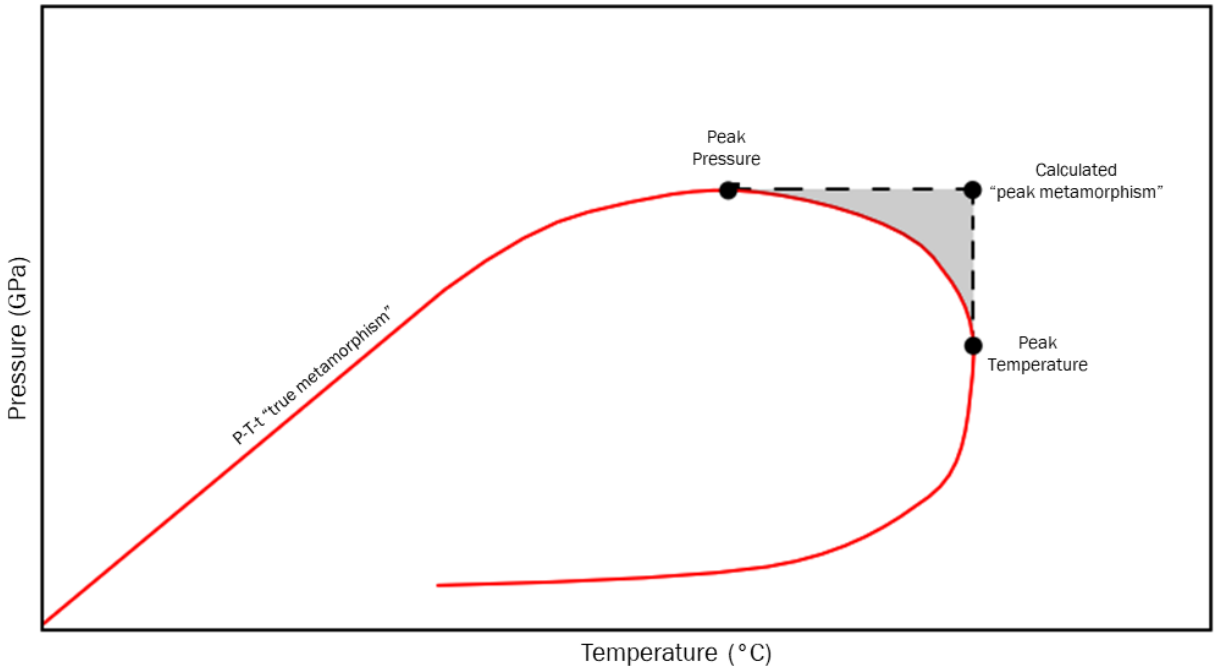

Figure 1.1 A hypothetical clockwise P-T-t path which demonstrates the difference between a "peak" metamorphism calculated from peak pressure over peak temperature the P-T-t path those rocks actually experience. The true P-T-t path touches the point labelled "peak pressure" and the one labelled "peak temperature", but never crosses through the point labelled "peak metamorphism." This means that records show a peak metamorphism which is slightly deeper and hotter than the PT-space that the record experienced.

taken from the same sample is increasingly commonplace but is not always the case. In many cases, estimates from different parts of an orogen or different studies of the same orogen are combined to derive pressure, temperature, and age. Many compilations have looked at dT/dP values for trends in secular change (Brown and Johnson, 2019; Brown, 2006, 2010; Brown and Johnson, 2018; Holder et al., 2019; Palin et al., 2020; Palin and Santosh, 2021a; Spencer et al., 2021; Zheng and Zhao, 2020). Categorizing samples through dT/dP approximates geothermal gradients which in turn are used to approximate different processes and geodynamic settings. Statistical analysis of dT/dP is driving much of the current research. Many geological problems do not confer themselves to quantitative means and historically. This quantification is not simply an issue for this study but for the discipline of geology as a whole.

Limitations with the previous mentioned compilations include small datasets, large biases in data (spatially and temporally), and limited statistical analysis. Previous compilations have been limited to <600 record data sets contained in spreadsheets. These spreadsheets lack uncertainties, detailed locality information, and ownership details (making it difficult to determine which samples had been added by which authors). There is a concern that with weighted analyses, oversampling of an area will bias the results. This can be the case for areas such as the Alps, while many areas (South America for example) have very few samples. There is also a temporal bias in the data – there are as many samples for the Phanerozoic (541 m.y.) as there are for the remainder of the geologic history (>3500 m.y.). Similarly, the analysis methods from recent studies bias the results, largely with respect to the classification of metamorphic samples. Different authors looking at dT/dP and secular trends have used different cut-offs for metamorphic samples (Brown and Johnson, 2019; Holder et al., 2019; Palin et al., 2020; Zheng and Zhao, 2020). Each of these cut-offs creates categories of samples which are assigned to geodynamic settings. When compilations note a lack of low-dT/dP samples, this is partly an artefact of where the cut-off for low-dT/dP samples is (see 2.1.9 The Range of Modern Subduction [Penniston-Dorland et al. (2015)). Modern studies have relied heavily on statistical analysis based on these datasets. The problem arises, however, that there are diminishing returns on running many statistical analyses on the same dataset. To make progress, there needs to be an update for the dataset or a shift in the analytical approach. This study does both.

This study was undertaken to create a metamorphic database which would increase the accuracy of metamorphic interpretations. This was accomplished by providing a multi-table relational database which reinforces referential integrity to provide a platform for future research. A literature review was undertaken to increase the number of samples – to increase the amount of data, and to fill in gaps in time and space. Ideally, a database would be able to contain all the available data from all metamorphic estimates that have been published. This literature review was constrained by the needs of the master's thesis to be completed in a couple of years and so as many new records have been added as has been available in the time allotted. For the purpose of spatial associations and weighted statistical analyses, the ideal process would be to ensure an equal spread – spatially and temporally – across the globe. This is as yet beyond our ability.

One major improvement is the introduction of uncertainties. Previous compilations, exclusively spreadsheets, did not publish uncertainties with their samples. The process for

introducing uncertainties is covered in 3.1.2 Introducing New Fields. This study has built a workflow to assign uncertainties and calculate uncertainties for dT/dP. Additionally, the database publishes methods for most samples which allows future work to evaluate samples and determine which samples are still suitable. With the use of this database, this study also publishes updated methods for analyzing metamorphic data, including the categorization of dT/dP samples, improved analysis, and spatial methods. The data and methods published here provide a platform for future research.

2 Literature Review & Previous Studies

While plate tectonics provides a framework for the understanding of orogens, questions about mountain-building events have been asked since the late 18th century. Since then, studies have looked at classification of metamorphic grade and metamorphic facies with papers, such as de Roever (1956) noting the occurrence of lawsonite and jadeite through time. Most studies since 2006 have taken on numerical approaches, taking pressure and temperature estimates, and calculating thermobaric ratio (dT/dP), to use increasingly sophisticated statistical analysis.

Current consensus is that some form of plate tectonics has happened since the Archean, with the nature of that those movements being under debate Brown et al. (2022). Korenaga (2013) identifies many geological indicators of plate tectonics in his compilation of data, many of which extend back to the Archean. These Precambrian indicators include: the assembly of the supercontinent of Kenorland (~2.7Ga), eclogite xenoliths (~3Ga) in the Kaapvaal craton, evidence of continental rifting in the Pilbara craton (~3.2Ga), and a structure interpreted as a suture zone in the Itsaq Gneiss Complex (~3.6Ga) along with structures in the Isua Supracrustal belt that has been interpreted to contain the world's oldest accretionary complex (~3.8Ga). While it is important to note that some of these proxies are under discussion and scrutiny, these are the sorts of geological events and structures that point to plate tectonic activity. These and other proxies for plate tectonic movements will be discussed in later chapters.

This chapter will provide an overview to the many lenses through which to view secular trends in metamorphism: metamorphic index mineral occurrences, geochemistry, geophysical methods, computer modelling, and thermobaric ratio (dT/dP) estimates through time. dT/dP comparisons provide a quick, easy way to compare orogens and metamorphic events and so have become the standard for modern research focuses heavily on dT/dP (Brown and Johnson, 2019; Brown, 2006, 2007; Brown et al., 2020a; Brown and Johnson, 2018; Chowdhury et al., 2021; Holder et al., 2019; Palin et al., 2021; Palin and Dyck, 2018; Palin and Santosh, 2021b; Zheng and Zhao, 2020) but combines geochemistry, crustal models, and geophysical modelling to create

a better picture. These studies are compiled here for review and are organized by main proxy studied.

2.1.1 **Mineralogy**

Metamorphic assemblages are unique to pressure, temperature, and compositional conditions (both rock and fluids). Studying the complex interplay between mineral occurrences and metamorphic conditions allows research to get measurements of the conditions that rocks and minerals formed under, as well at the processes that they underwent. One group of these assemblages are glaucophane, lawsonite, and jadeite, the minerals that make up the blueschist facies. Blueschist is characterized by very high pressure and low temperature. As such, they can only be formed in areas with an abnormally low geothermal gradient – subduction zones.

These minerals are extremely rare on the planet and only show up in few locations today (Figure 2.1). The presence or absence of these blueschist facies minerals has long been used to

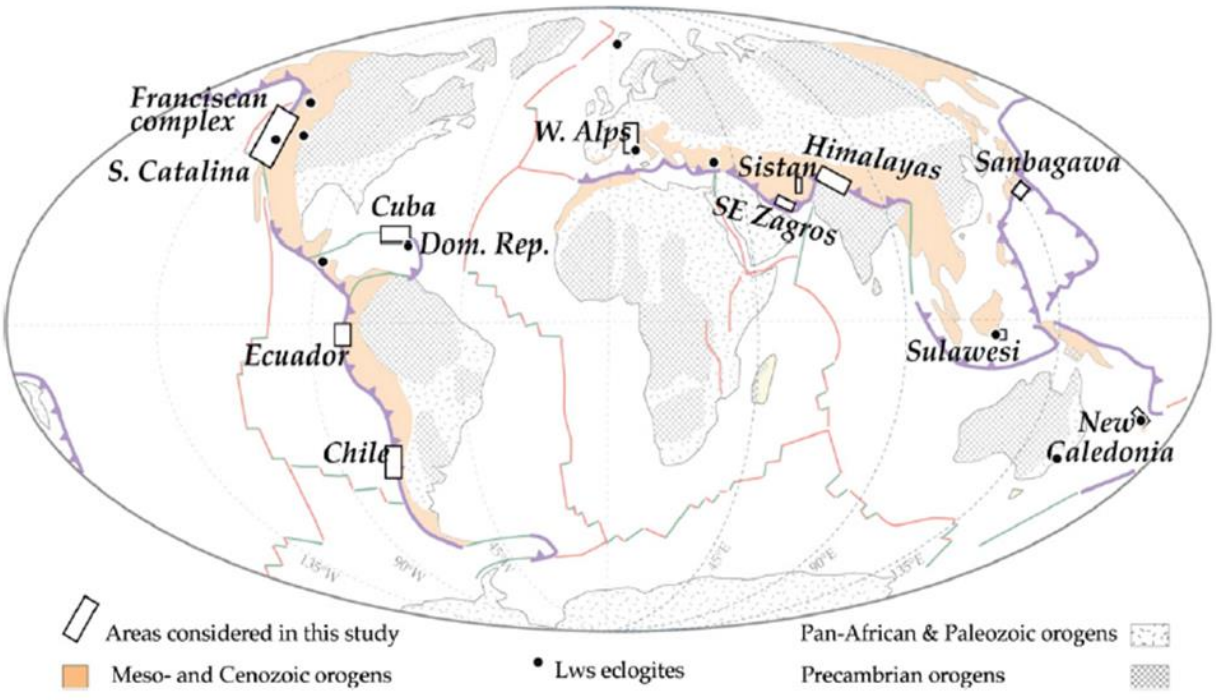

Figure 2.1 Global map showing current plate margins, High Pressure – Low Temperature (HP-LT) areas (black rectangles), lawsonite eclogite occurrences (black dots), and known orogens of different ages (shaded regions of peach, grey, and light grey). Taken from (Agard et al., 2009).

argue for the presence or absence of plate tectonics and subduction. There are some complications with this due to the rare exhumation and preservation of these assemblages. Arguments are made from different sources concerning the crust's ability to exhume these sorts of rock or the preservation of the rocks after exhumation (Palin et al., 2021).

de Roever (1956) and Ernst (1972) looked at the secular distribution of minerals as indicators for changing geodynamic settings. de Roever (1956) noted that lawsonite was exclusive to Phanerozoic rocks and indicating a change between the Precambrian and Phanerozoic geodynamic settings (Figure 2.2). Ernst (1972) looked at the distribution and first occurrence of subduction related mineral assemblages and argued that the oldest occurrence of epidote-bearing glaucophane schist, noted as product of subduction, is the prime indicator for subduction.

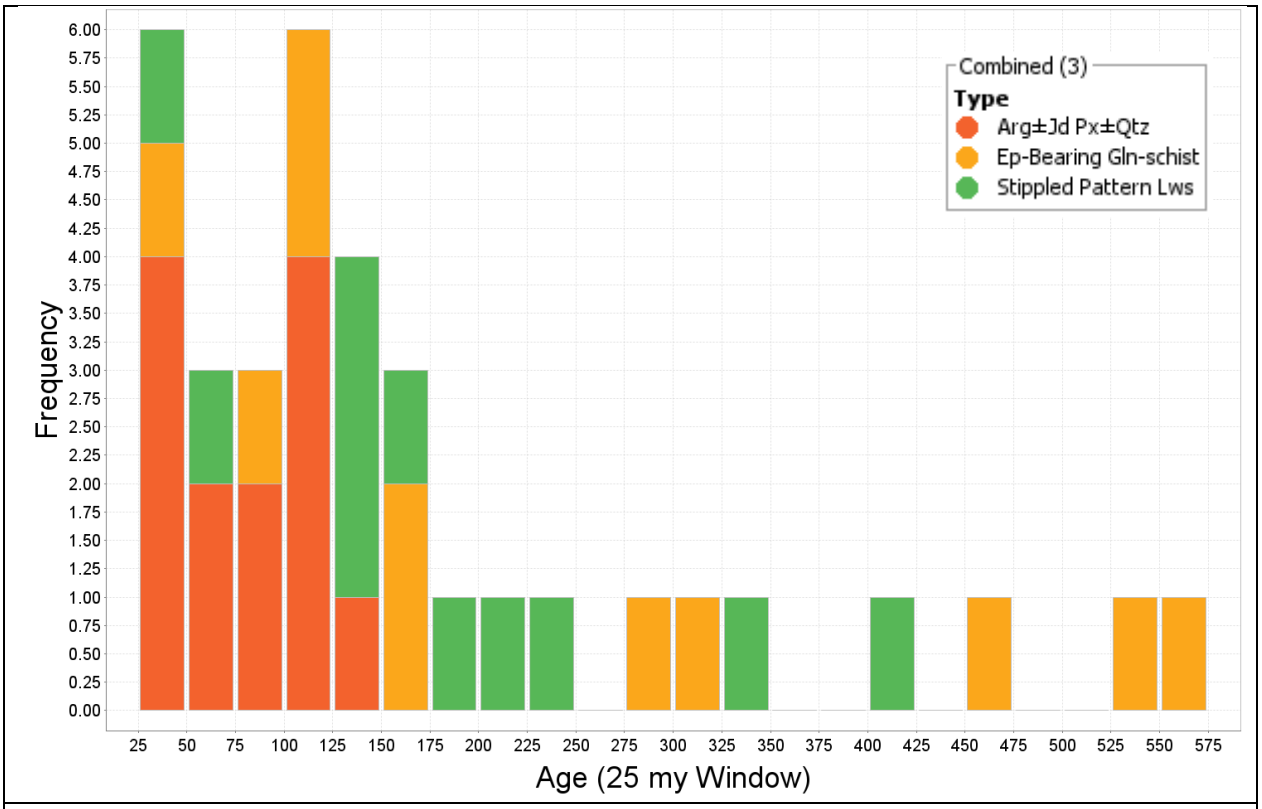

Figure 2.2 Frequency of distribution of subduction-related mineral assemblages through time, from 575 Ma to present day. Arg = aragonite, Jd Px = jadeitic pyroxene, Qtz = quartz, Ep = epidote, Gln = glaucophane, Lws = lawsonite. Modified from Ernst (1972).

Stern (2005) used blueschists, ultrahigh-pressure (UHP) metamorphic assemblages, and ophiolites as benchmarks for the onset of modern plate tectonics. Ophiolites are sections of preserved mafic crust which can be preserved in the rare instance that continental crust is subducted under oceanic crust. These provide rare examples of oceanic crust which is older than 180 Ma and clear markers for subduction. Stern (2005) argues that ophiolite obduction provides some of the only direct evidence for lateral movement associated with mobile lid tectonics. Blueschists as mentioned also provide key markers of subduction because they can't be produced anywhere else. Stern (2005) focuses on these two factors as "direct geological evidence" of subduction. Stern (2005) argues against other forms of evidence and largely eschews other proxies for subduction. Using the oldest samples of these lines of evidence, Stern puts the onset of plate subduction in the Late Proterozoic: "The oldest of each are not the same age—the oldest ophiolites, ca. 1.03 Ga, are significantly older than the oldest blueschists, ca. 800 Ma, and these are older than the oldest-known UHP terranes." There remain questions of preservation which will be discussed in section 2.4 Preservation Arguments.

Guotana et al. (2022) and Nutman et al. (2022) show evidence for UHP metamorphism in the Itsaq Gneiss Complex (IGC) and the ISB in Greenland. The IGC is one of the oldest (>3600 Ma Eoarchean) well preserved zones in the world and hosts the ISB (3.7-3.8 Ga). Nutman et al. (2021) presents rocks from the IGC that span a breadth of metamorphic assemblages relating to ultra-high-pressure, low-temperature assemblages to low-pressure, high-temperature assemblages. These samples are interpreted by Nutman (2022) to represent lower plate subduction zone metamorphism (250–400 °C/GPa) paired with upper plate granulite metamorphism (≥1000 °C/GPa). The pressure and temperature are estimated using the methods described in (Shen et al., 2015) and represent the oldest published subduction related metamorphism to date (Figure 2.3). As Nutman (2022) says "the world's best preserved and diverse Eoarchean record of the Itsaq Gneiss Complex provides evidence for both high and low T/P metamorphic regimes back to near the start of the rock record." Serpentine rocks were found in the Isua Supracrustal Belt (ISB), part of the IGC, which have been interpreted to have dehydrated and subsequently exhumed similar to UHP rocks in modern subduction zones (Guotana et al., 2022; Nutman et al., 2021). Serpentinization is a key factor for lowering frictional resistance which has been marked as a factor leading to the onset of subduction (Korenaga, 2013).

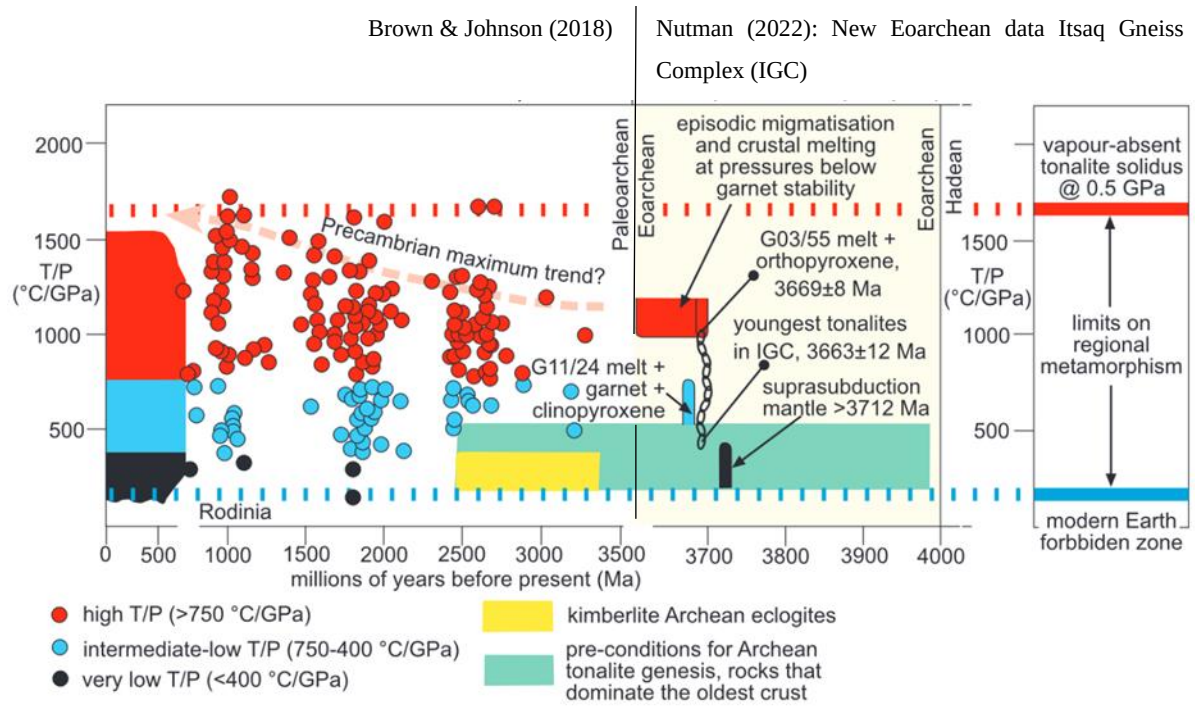

Figure 2.3 Comparison a data from the compilation by Brown and Johnson (2018) to the data of Nutman (2022). Figure shows the nature of Eoarchean tectonics from the lens of Itsaq Gneiss Complex, which includes migmatization and crustal melting, the inclusion of tonalites [noted by Nutman (2022) as markers of crustal growth]. Of note is the addition of ultra high pressure-low temperature samples in the Eoarchean. Righthand side shows the boundaries of regional metamorphic records. Taken from (Nutman (2022). G11/24 and G03/55 are sample numbers from Nutman (2022).

With this evidence, Nutman (2022) notes "[the] IGC removes the last argument against a form of plate tectonics operating throughout the Archean. Hence since the start of the rock record, a mobile lid plate tectonic regime contributed to interior heat loss, facilitating chemical communication and feedbacks between Earth's surface and its deep interior." Further, Nutman (2022) argues that the large amount of high Sr/Y tonalite that can be found in the Eoarchean would require a large amount of fluid flux into the mantle – each tonalite would "require partial melting of 3 to 5 times the volume of eclogitized mafic crust." This amount of fluid and dehydrating mafic crust would lend itself to a subduction-like model which would be able to draw down more rock and water than other proposed models. There remains debate regarding the significance of these findings: opponents question the of the use of titano-chondrite as a PT

estimate method and others remark that a single Archean terrane showing subduction does not prove a globally interconnected subduction network.

2.1.2 **Thermobaric Ratio & Geothermal Gradients**

Grambling (1981) focused on calculated geothermal gradients in the study of metamorphism. Grambling (1981) looked at approximately 100 samples ranging from Archean to Late Proterozoic (it is not clear in the published paper where the samples are derived from, but it is stated that they come from a literature review of published samples). The average geothermal gradient for these samples is compared in Table 2.1. Grambling noted a decreasing average geothermal gradient for the three age categories as well as increasing average depth (assuming 3.3 km/kbar). Figure 2.4 plots the individual samples for each age range. Grambling notes that Archean gradients vary from 21°C/km to 95°C/km.

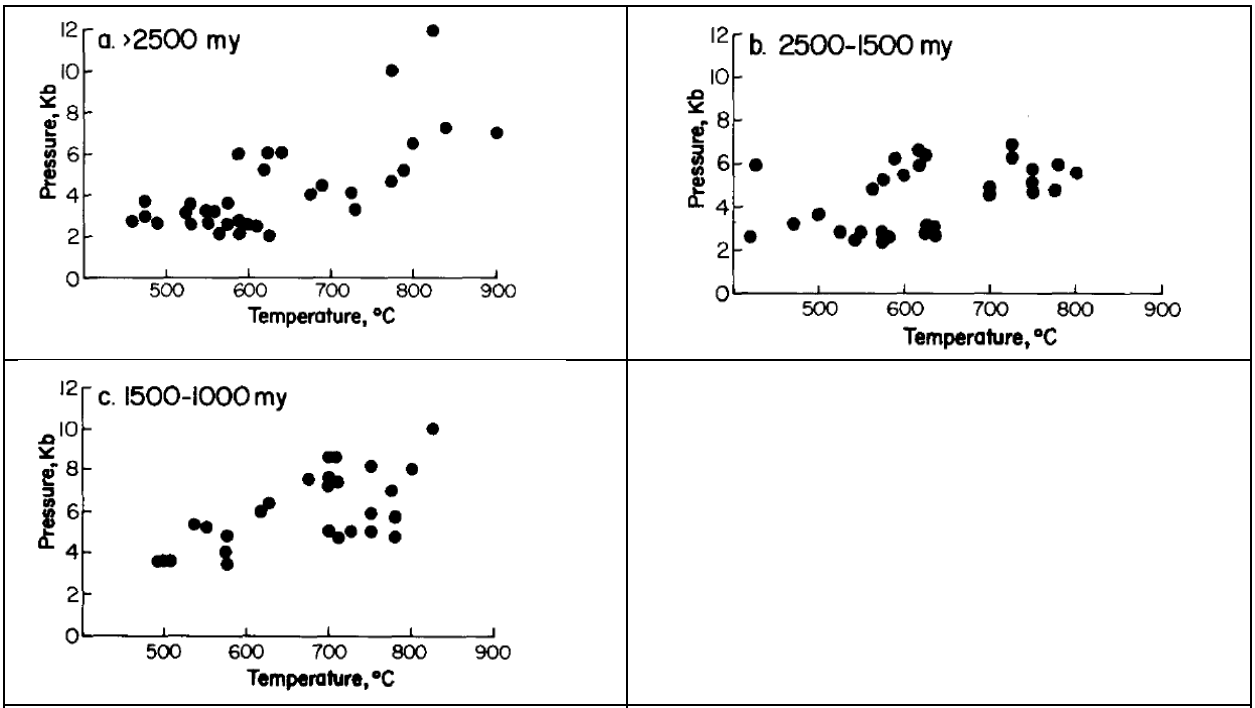

Figure 2.4 Pressure and temperature estimates for metamorphic samples broken into different ages. a) >2500 Ma, b) 2500-1500 Ma, c) 1500-1000 Ma. Taken from (Grambling, 1981).

Table 2.1 Age, calculated geotherm, pressure, and calculated depth (assuming 3.3km/kbar) for samples discussed by Grambling (1981).

Age	Gradient (°C/km)	Pressure (kbar)	Depth (km)	Sample Size
Archean	54	4.1	13.53	37
Early Proterozoic	47	4.3	14.19	36
Late Proterozoic	35	6	19.80	26

Brown and Johnson (2019), building on previous work of Brown (2006, 2007, 2010) and Brown and Johnosn (2018) assembled data from 564 samples globally and created the foundation for recent interpretations of metamorphic trends. Brown and Johnson (2019) used calculated average geothermal gradients from PT-estimates, similar to Grambling (1981). Plots involving pressure, temperature, and dT/dP through time were used to denote trends in dT/dP (Figure 2.5).

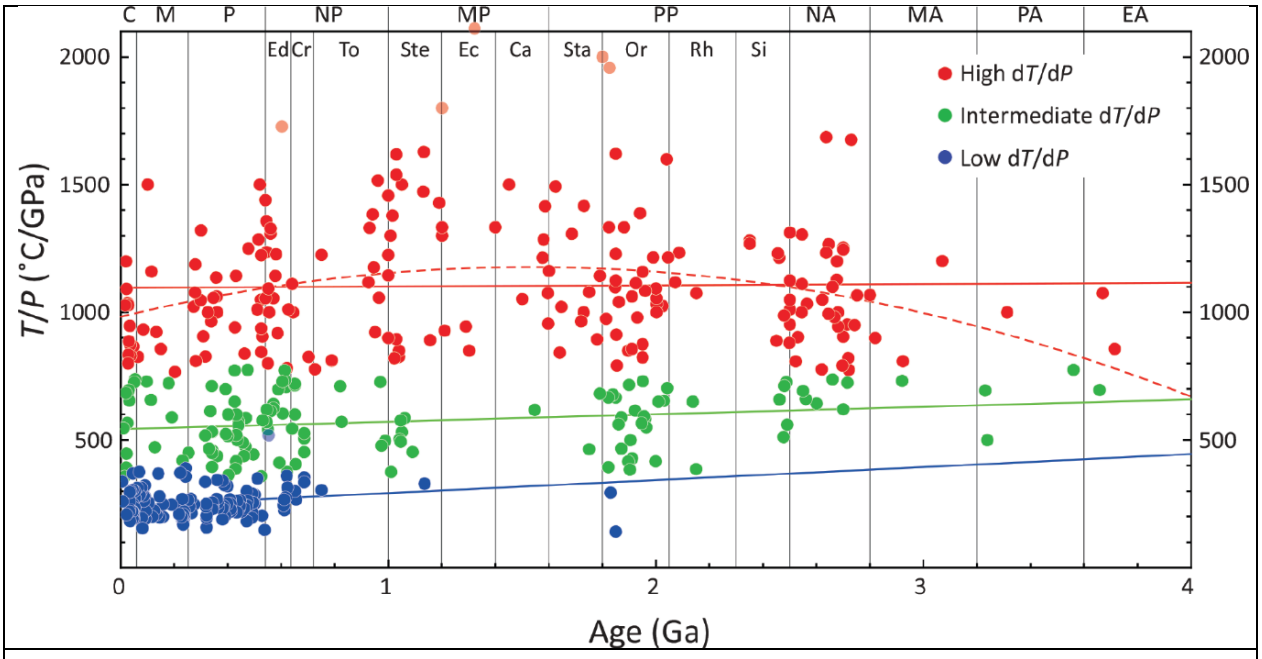

Figure 2.5 dT/dP through time for the (Brown and Johnson, 2018) dataset. Records are coloured according to the legend and coloured lines denote linear regression analysis, with the dashed lines represent second-order polynomial regression analysis. Vertical lines represent geological eras and periods (EA = Eoarchean, PA = Paleoarchean, MA = Mesoarchean, NA = Neoarchean, PP = Paleoproterozoic [Si = Siderian, Rh = Rhyacian, Or = Orosirian, Sta = Statherian], MP = Mesoproterozoic [Ca = Calymmian, Ec = Ectasian, Ste = Stenian], NP = Neoproterozoic [To = Tonian, Cr = Cryogenian, Ed = Ediacaran], P = Paleozoic, M = Mesozoic, and C = Cenozoic. Taken from Brown and Johnson (2018).

This paper also began the categorization of dT/dP into different levels (low, medium, high dT/dP) which is a staple of research today. Using statistical analysis (regression analysis, moving mean, etc.) they present secular trends in metamorphism as cycles using 2-dimensional plots (Figure 2.5). Brown and Johnson (2019) proposed a duality of thermal regimes where in one (intermediate and high dT/dP) metamorphism has occurred from the earliest records to present, and one (low dT/dP) which came to prominence as a result of cooling mantle potential temperatures. Brown and Johnosn (2018) used a moving mean and probability cure (Figure 2.6) to denote three different cycles for metamorphic assemblages. These cycles appear to have given way to the duality of metamorphic regimes declared in Brown and Johnson (2019). Korenaga (2013) states two main issues with the secular mantle cooling interpretation: while the mantle has certainly been cooling since the formation of the planet, it is not a simple correlation between mantle potential temperature and surface heat flux; and secondly, that Phanerozoic samples show no difficulty in producing high dT/dP samples.

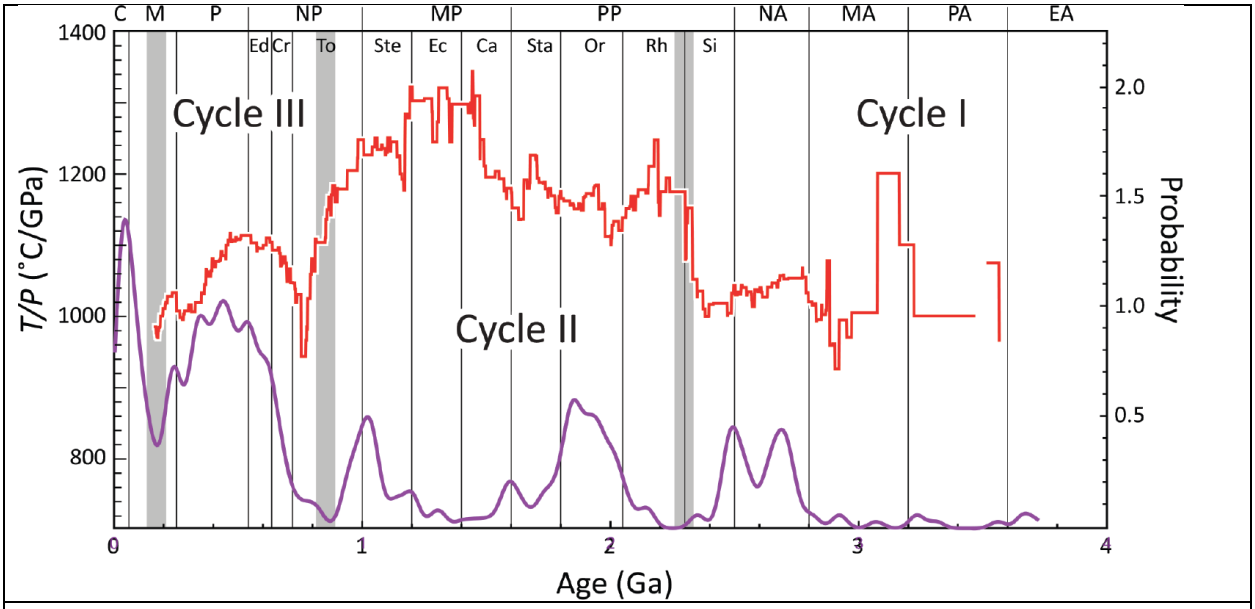

Figure 2.6 Moving mean (red) for dT/dP records plotted against probability curve (purple). Grey vertical bars represent times of interpreted supercontinent break up aligning with low probability of metamorphism. Cycle I, II, and III are interpreted by Brown and Johnson (2018) to be large-scale time periods of marked shifts in metamorphic activity. Labelling of the geological eras and periods at the top of the diagram are explained in Figure 2.5. Taken from Brown and Johnson (2018).

Chowdury et al. (2021) notes that the appearance of intermediate dT/dP rocks and high dT/dP rocks since the Proterozoic have been argued to represent paired metamorphism (e.g. (Brown and Johnson, 2019; Brown, 2006; Brown et al., 2020b)) but that "…notably, these rocks represent paired metamorphism in time but whether or not they were spatially paired, remains ambiguous." It's worth noting that Brown et al. (2021) presents two paired metamorphic belts of high-medium dT/dP and low dT/dP in the Proterozoic and one Phanerozoic, but that is all.

Holder et al. (2019) followed similar methods to Brown and Johnson (2019). They interpreted an increasing diversity in metamorphic environments [sic] from an increasing range of dT/dP. Figure 2.7 overlays dT/dP data from Brown and Johnson (2018) with two models for mantle potential temperature. Holder et al. (2019) is one of the first compilations to make direct comparisons to distinct models. As per Brown and Johnson (2019), a cooling mantle is linked to an increase in cooler metamorphic trends. Using log[T/P], Holder et al. (2019) divided samples into two categories (Figure 2.8) and argued for a bimodal metamorphic trend, similar to Brown and Johnson (2019).

Zheng and Zhao (2020) follow a similar style to Brown and Johnson (2018, 2019) with a numerical approach to the problem. Using the same dataset, Zheng and Zhao (2020) classified samples into Alpine (<10°C/km), Barrovian (10-30°C/km), and Buchan (>30°C/km). The lack of Alpine facies series before the Neoproterozoic is the main argument for a bimodal distribution of metamorphic trends – this would indicate that a large number of alpine samples can be found where previously none where. This idea falls in line with the conclusions of Brown and Johnson (2018, 2019) as well as the timing considerations of Palin et al. (2020).

Spencer et al. (2021) followed up Brown et al. (2020a) with similar statistical analyses and added modeling from Tang et al. (2020) to act as a proxy for crustal thickness. There are some issues with these methods which will be discussed herein. Figure 2.9 shows one of the figures from Spencer et al. (2021) which plots dT/dP against estimated duration of deformation and is coloured by age of final collision, for specific Proterozoic orogens. This figure shows a correlation between dT/dP and duration of deformation for the Proterozoic. There are outliers such as the Sveconorwegian and many modern orogens fall well outside of this trend.

Figure 2.10 shows dT/dP vs. Age from the dataset published by Brown and Johnson (2019). The figure includes a regression line by the locally weighted scatterplot smoothing

(LOWESS) method discussed in (Spencer et al., 2021), with a grey envelope representing a 95% confidence interval for the LOWESS line. Recently, (Tang et al., 2020) used Eu/$\sqrt{Sm \times Gd}$ (Eu/Eu* here after) as a proxy for crustal thickness. $\sqrt{Sm \times Gd}$ is used here a proxy for La/Yb. Tang et al. (2021) builds on this with a global dataset which approximates crust at a global scale, represented by the purple line and the 68% (dark green) and 95% (light green) confidence interval envelopes.

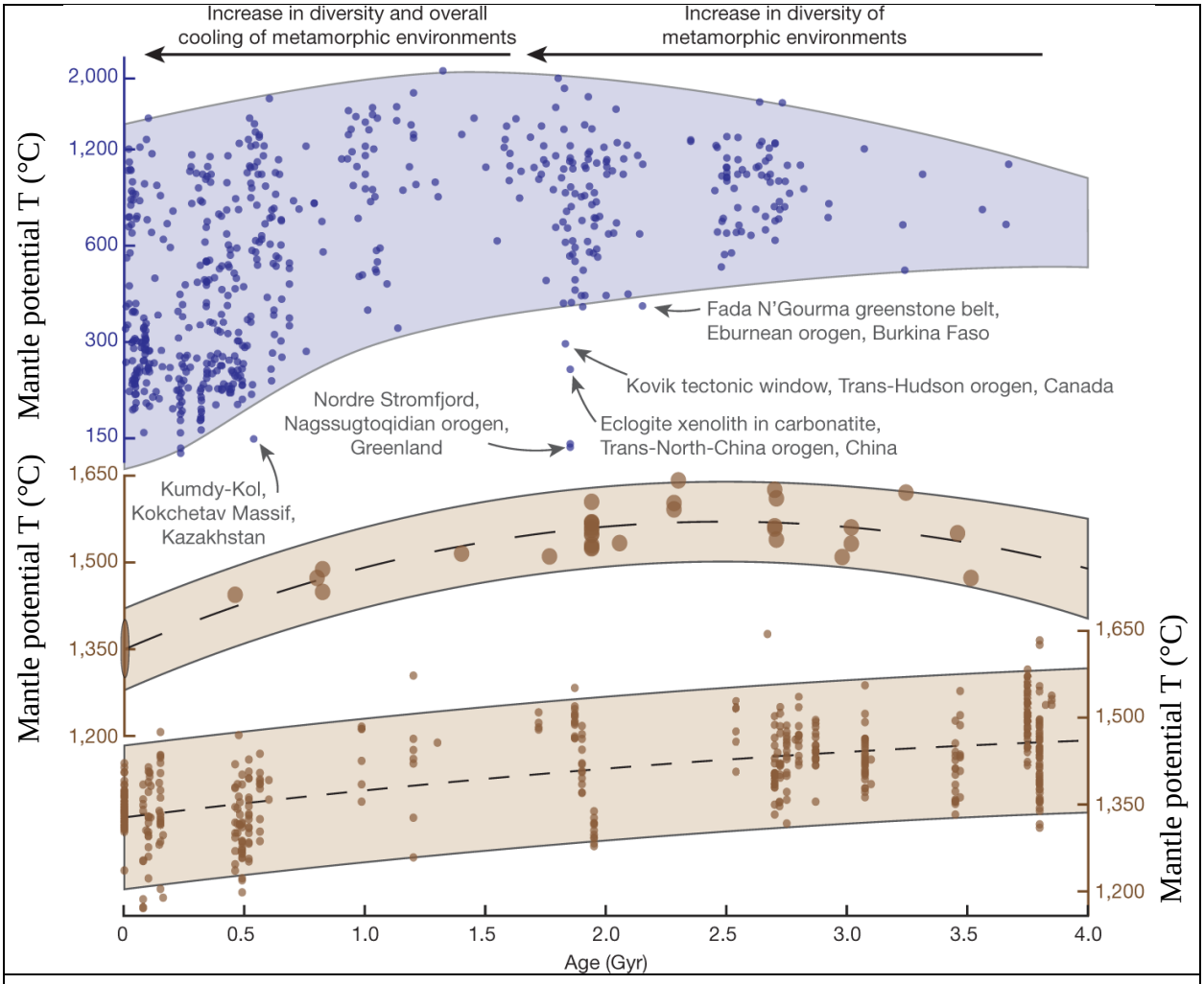

Figure 2.7 dT/dP from records from (Brown and Johnson, 2019) through time with an envelope capturing most samples (envelope shape chosen by (Holder et al., 2019)) (Top - blue), mantle potential temperature (°C) through time as in (Herzberg et al., 2010) (Middle - brown), and (Lower – brown) mantle potential temperature (°C) as in (Condie et al., 2016). Taken from Holder et al. (2019).

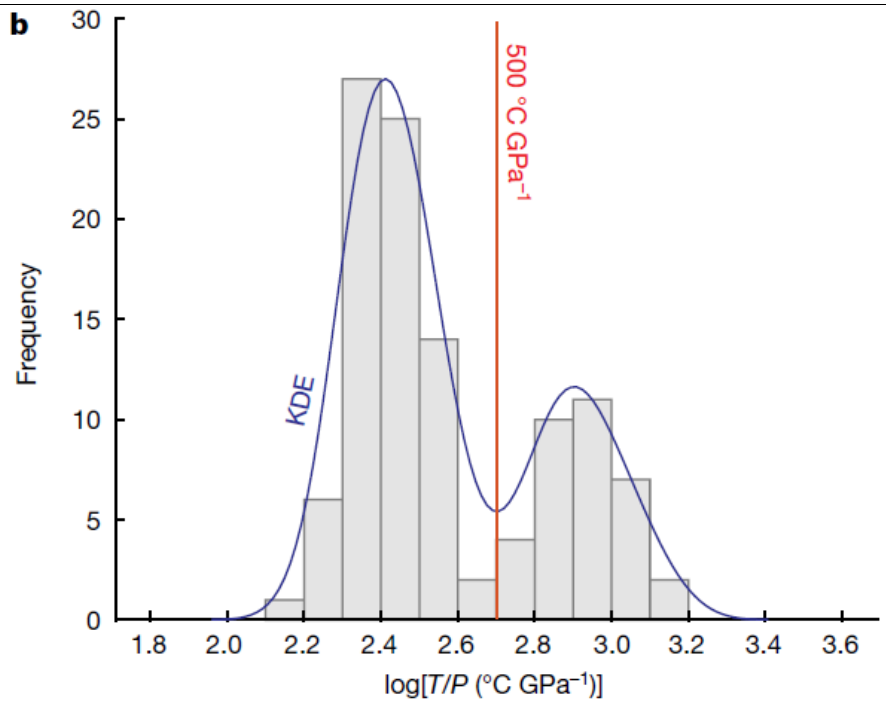

Figure 2.8 Histogram (grey boxes) of records younger than 200 Ma and Kernel-Density Estimate (blue line) for records from (Brown and Johnson, 2019). Records transformed to logarithm scale for comparison. Red centre line denotes the cut off for samples of 500 °C/GPa. From Holder (2019).

Figure 2.10 shows dT/dP vs. Age from the dataset published by Brown and Johnson (2019). The figure includes a regression line by the locally weighted scatterplot smoothing (LOWESS) method discussed in (Spencer et al., 2021), with a grey envelope representing a 95% confidence interval for the LOWESS line. Recently, (Tang et al., 2020) used Eu/$\sqrt{Sm \times Gd}$ (Eu/Eu* here after) as a proxy for crustal thickness. $\sqrt{Sm \times Gd}$ is used here a proxy for La/Yb. Tang et al. (2021) builds on this with a global dataset which approximates crust at a global scale, represented by the purple line and the 68% (dark green) and 95% (light green) confidence interval envelopes.

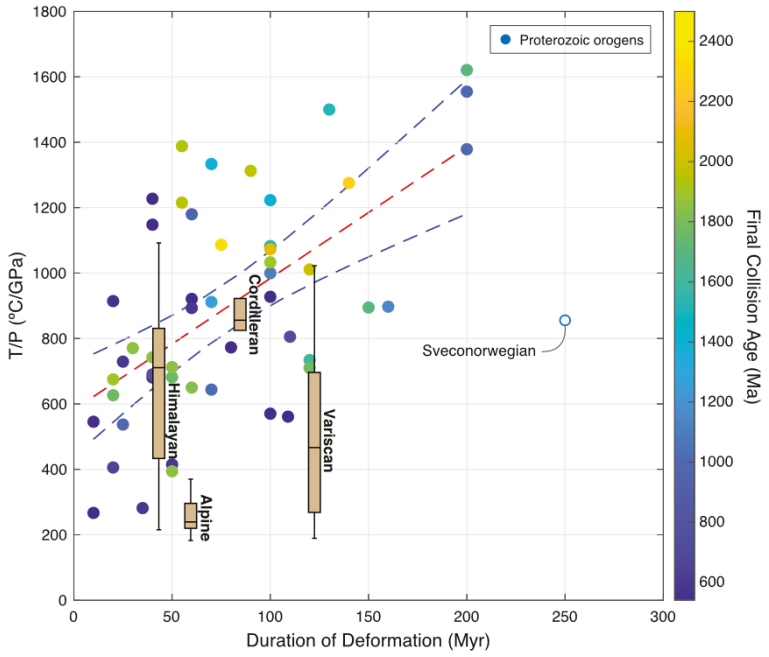

Figure 2.9 Duration of deformation plotted against dT/dP from the datasets of Brown and Johnson (2019). Coloured by age of end of collision. Taken from Spencer et al. (2021).

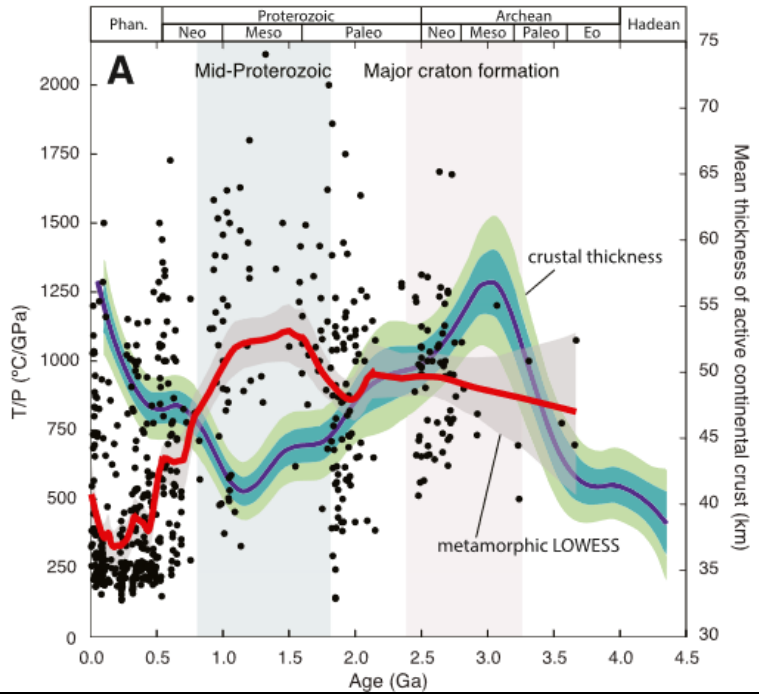

Figure 2.10 dT/dP vs. Age (Ga). Red line represents locally weighted scatterplot smoothing (LOWESS) regression on dT/dP with grey envelope representing a 95% confidence interval for that line. Purple line represents modelled crustal thickness from Tang, Chu, et al. (2021) with blue-green envelope representing 68% confidence, and light green envelope representing 95% confidence. Taken from Spencer et al. (2021).

2.1.2.1 Accepted Trends and Remaining Issues

Current accepted trends include: a change in the nature of most metamorphic samples from the Precambrian and the Phanerozoic (few low-dT/dP records in the Precambrian and many in the Phanerozoic); a higher number of low temperature samples in the Phanerozoic; increasing pressures throughout geological time; and a "bimodal distribution" of records which arises in the Late Proterozoic and continues to present day. Not every study agrees with each of these statements, but these are broadly agreed upon.

Issues that still remain include: datasets which are heavily biased towards Phanerozoic data and lack much Precambrian data; a focus on statistical methods which do not do the datasets justice in the sense that we are seeing a number of iterations of similar statistical methods on the same dataset; confidence intervals which are not representative of the dataset; a lack of uncertainties in datasets which occludes the interpretations of published studies; and a lack of spatial consideration when making interpretations of the data.

2.1.3 **Geochemistry**

Changing crustal geochemistry follows changes in the crust and mantle: as the mantle becomes more depleted over time, this is reflected in changing ratios of crustal rocks. These changes in crust and mantle can be tracked through time with geochemical analyses. One issue with the rock record arises with the lack of preservation of Hadean and Archean rocks. Low preservation means that geochemical signatures are often the only avenue for inquiry into many questions during these times. The rate and nature of crustal growth during the Hadean and Archean is one example of a question which largely relies on chemical evidence. Geochemical proxies rely on geochemical models which look at how different elements will become fractionated into or out of crust or the mantle during crystallization or melting. They often look to compare and contrast chemical trends in modern day rocks to older rocks. In many cases, these proxies are based around the idea of element compatibility/incompatibility. These ideas help geochemists build a framework for what chemicals will be fractionated in melts or crystallizations and which chemicals will be left behind in source rocks or melts. These fractionations create anomalies which can be tied to geodynamic settings or geological processes.

Shirey et al. (2008a) looked at the evidence for plate tectonics from geochemical analysis and concluded that plate tectonics would have initiated shortly after the Hadean. The compilation looked at crust-mantle recycling, mantle depletion, crustal evolution, zircon chemistry, mantle xenoliths, and evidence for the Archean lithosphere-hydrosphere. This synthesis provides geochemical context which points to subduction related activity around 3.9 Ga (Shirey et al., 2008b) which are summarized in Table 2.2.

Table 2.2 Summary of Early Earth events as compiled by geochemical analysis and geochemical modelling. Taken from Shirey et al. (2008a).

Time (Ga)	Event	Evidence
4.57	Accretion	Short- and long-lived isotopic systems in meteorites
4.57-4.51	Core formation	Composition, Hf-W
	First magma ocean	Modeling, energetics
	Separation of early enriched reservoir	Sm-Nd, composition, Hf-W, Sm-Nd
4.51-4.4	Giant impact to form Moon	Composition, modeling
	Second magma ocean	Modeling
	Persovskite fractionation	Lu-Hf, Sm-Nd
	Mantle overturn?	Hypothesis
4.4-3.9	Oceanic lithosphere (non-continental)	Hadean zircons, O, Lu-Hf
3.9	Onset of subduction, and first continental crust	Arc-like rocks, ophiolites
3.5	First mantle keels and permanent crust extraction	Nb-Th, Sm-Nd, samples
3.1-2.5	Terranes with direct subduction imprints	Preserved arcs, geophysics
Note: This table is compiled from the literature discussed in the text (Shirey et al., 2008b). Ages are meant to serve as guides, not firm boundaries, since future research will produce new age constraints.		

There would be marked differences in geochemical cycles between stagnant lid and mobile lid plate tectonics, other lines of evidence are presented by Nutman (2022). With a stagnant lid, there would be little recycling of material between the surface and mantle – magmas slowly carrying material to the surface. Mobile plate tectonics on the other hand brings material

down into the mantle through subduction and therefore recycles fluids, rocks, and other chemicals readily. There is evidence from the Barberton Greenstone Belt for crustal recycling of elements from the hydrosphere/lithosphere older than 3300 Ma (Sobolev et al., 2019). This recycling would need to be accomplished through the dehydration of oceanic crust which had previously been hydrated by seawater.

Archean crust production is a factor that is tied directly to questions of crustal thickness, mantle composition and depletion, and issues of preservation. Studies looking at these factors include Mo (McCoy-West et al., 2019) and Rb/Sr (Dhuime et al., 2018, 2015). McCoy-West et al. (2019) looked at molybdenum depletion in the mantle and came to the conclusion that the mantle was fully deplete by 3.5 Ga and mark billion as a time with large amounts of production and reworking of continental crust (Dhuime et al., 2015).

Condie and Shearer (2017) compared high field strength (HFS) incompatible element ratios in basalt through time. A transition period between 2 to 3 Ga is noted by the author in which the older basalts are interpreted to have a source similar to primitive mantle and the younger basalts a source more related to modern or depleted mantle. This transition is important because it relates to felsic continental crustal growth (which requires mobile lid plate tectonics) and the recycling of elements between the mantle and surface. This transition is interpreted by the authors as a transition from stagnant lid to mobile lid tectonics. It is important to note that this transition is seen in both hydrated and non-hydrated basalts. Hastie and Fitton (2019) modeled the geochemistry of Eoarchean Tonalite and Trondhjemite (ETT) to find a source rock and tie that to a geodynamic setting. Their findings - the requirement of partial melting in the presence of slab-derived fluids, non-primitive metabasic sources, or altered metabasic crust that is arc-like in composition, point to subduction as being a requirement for the production of ETT.

2.1.4 Crustal Thickness Models

Previous studies (Dhuime et al., 2018, 2015; Hawkesworth et al., 2010, 2009; Korenaga, 2021; Tang et al., 2021, 2020) have used hypothetical changes in crustal thickness to acknowledge and explain secular increases in pressure estimates for metamorphic records (seen in metamorphic datasets). The use of other proxies is often aligned with crustal modelling to show secular changes in crustal formation or crustal composition to show how a changing crust would affect/be affected by plate tectonics. The following papers are various models which

works have used to help understand changes in plate tectonics and secular variations in metamorphism. These models are all based on their own geochemical proxies for crustal thickness (La/Yb, Eu/Eu*, etc.). One caveat with these models is that large amounts of crust have been destroyed between the present day and the Archean which can greatly affect the preservation of crust and the rocks which researchers model from Hawkesworth (2009).

Hawkesworth et al. (2010) argues that the majority of crust was formed in the Archean and that only 7% remains today. This large deficit between the amount of Archean crust formed to the amount of crust we find today means that the almost all of the crust formed during the Archean has been destroyed or reworked. If the planet had the same volume of crust in the Archean as we do today as per Hawkesworth (2010), then we can assume that much evidence from the Archean about tectonic modes has been eradicated, but that also some large global mechanism must have caused the eradication. It is important to note however, that the processes destroying, or reworking Archean/Hadean crust may have occurred well after the Archean. Dhuime et al. (2018) modelled the production of juvenile continental crust through time. The paper notes that "…<25% of the volume of … continental crust preserved today is older than 3 Ga" and go on to state that models which have the majority of crust produced by the Late Archean (60-80%) would require large amounts of destruction and reworking of continental crust. The model from this paper shows a "marked decrease" in continental crust production, in the Archean, and a sharp increase in crustal destruction at the same time. The authors speculate that this increase in destruction could be associate with "… the widespread development of subduction zones." This interpretation agrees with the conclusions of Korenaga (2021) (discussed below) who argues that the large amounts of crust produced in the Archean requires plate tectonics.

Tang et al. (2021) building on the work of Tang et al. (2020), used a global dataset to model crustal evolution through time using Eu/Eu* (Figure 2.11). This model suggests increasing crustal thickness beginning from the Hadean (40 km) and peaking around the Mesoarchean (60 km)(3.0 Ga). In the model, crustal thickness drops to a minima in the Late Proterozoic (40 km)(~1.0-1.2 Ga) and climbs back up to 55-60 km during the present day. Tang et al. (2021) interpret these findings to represent major craton formation in the Archean (3.0 Ga maxima), the accretion of the supercontinent Nuna, and pseudo-breakup turning into accretion into Rodinia. This prolonged episode of supercontinent accretion – the inferred aborted rifting of Nuna to

create Rodinia – would mean a lull in orogenesis among other processes (Discussed further in 4.9 Supercontinent Cycles and Super GDU's).

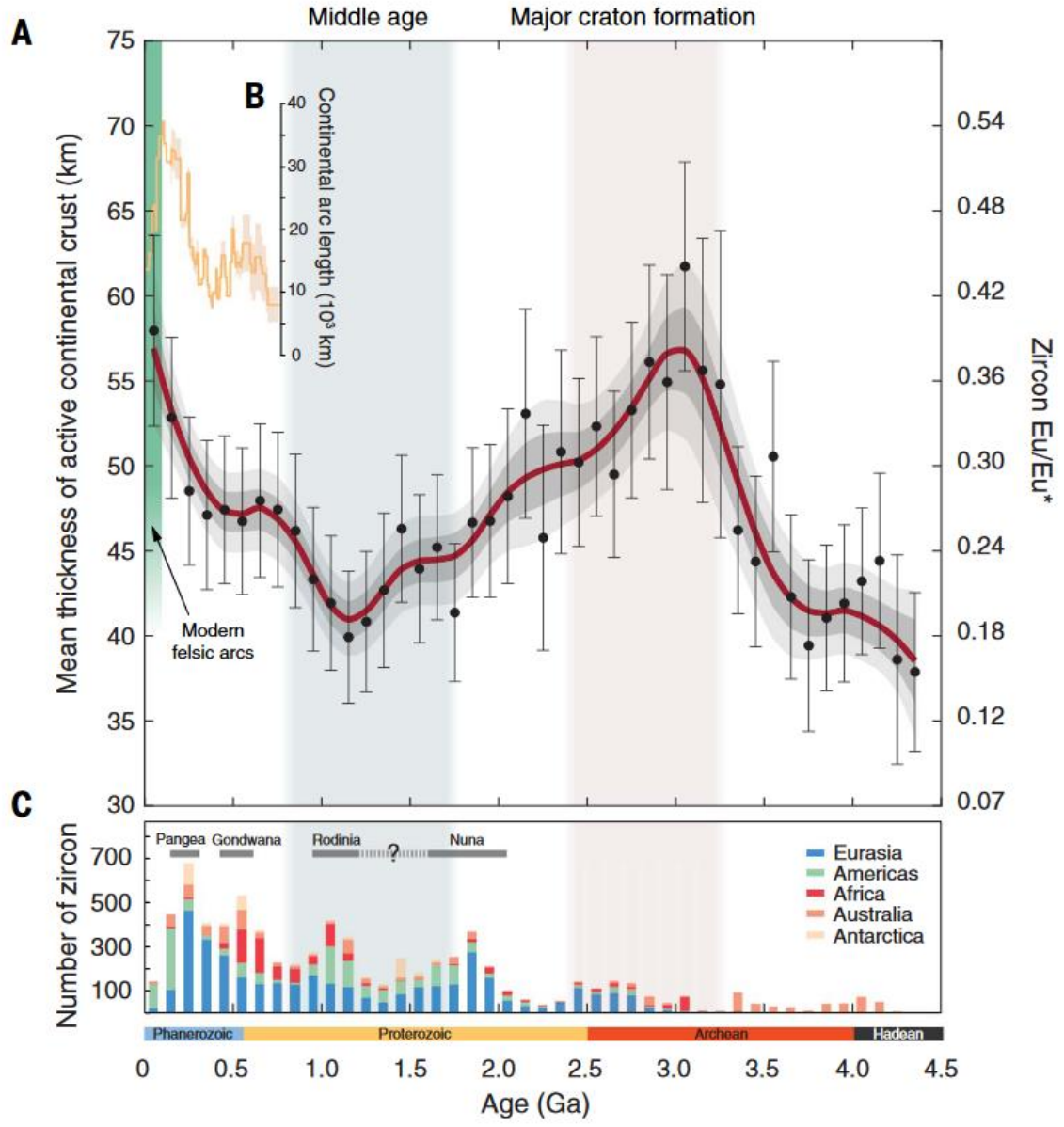

Figure 2.11 A) Model of crustal thickness through Eu/Eu* anomalies in detrital zircons. Sample points represent average from 100 m.y. bins with error bars at ±2 SEM. Grey envelopes represent 68% and 95% confidence levels for the red line (smoothed average crustal thickness). B) Continental arc length. C) Histogram of detrital zircons through time with 100 m.y. windows which represents an increase in continental crust being produced. Taken from Tang et al. (2021).

Korenaga (2021) reviewed recent models of Hadean chemistry and mantle dynamics to come up with a new hypothesis regarding the onset of plate tectonics in the Hadean. Key to this hypothesis is the notion that generating huge amounts of felsic crust requires plate tectonics and that the cooling of a magma ocean would allow for the onset of mantle convection. Korenaga proposes: "[one plausible scenario where] a chemically heterogeneous mantle resulting from the gravitational instability of a solidifying magma ocean allows rapid plate tectonics, which in turn leads to the early emergence of a habitable surface environment by efficiently sequestering atmospheric carbon" This scenario lines up with current models which have proposed large amounts of felsic crust being produced in the Hadean , and is in line with "self-consistent thermodynamics of lower mantle melting." Korenaga notes the two models, which combine to support the hypothesis, are independent of each other with each using different sources and methods.

2.1.5 **Age of Crust**

Subduction requires the subducting crust to have a certain amount of negative buoyancy. This has been the focus for many studies to explain the sharp change (the appearance of blueschists, UHP terranes, and large increase in low dT/dP category records) seen in the dataset around ~800 Ma. Changes in mantle potential temperature have been used as a mechanism to argue for thicker crust in the past. With a mantle crust there is deemed to be thicker oceanic crust being produced at mid-ocean rifts and thus the oceanic crust retains heat better and is more resistant to steep-angle subduction. Davies (1992) looked to quantify the buoyancy of oceanic crust through time to mark the beginning of modern subduction. If a cooler mantle produces thinner crust which cools faster, then it is less resistant to subduction. According to Davies (1992), currently oceanic crust takes about 20 m.y. to go from positively to negatively buoyant.

Whether oceanic crust would have become negatively buoyant before reaching opposing continental crust is a matter of crustal thickness (affecting rate of cooling) and time before reaching subduction. A hotter mantle would increase thickness (increasing buoyancy) and push oceanic crust faster (allowing less time for cooling). Davies (1992) modelled this interaction between these two factors and came to the conclusion that the conditions where oceanic crust would not achieve negative buoyancy is very close to modern day conditions, which led Davies to the conclusion that most oceanic crust would not be able to routinely sink at subduction zones (Figure 2.12). Davies (1992) notes that while it may not have been "expected" of oceanic crust to

sink at subductions zones, it is still possible crust that had sufficiently cooled to do so. It is important to note that the modelling of Davies (1992) is divorced from any spatial context and as such, it is unclear how changes in supercontinent cyclicity would affect the age of oceanic crust – that is to say whether a larger ocean would allow for a greater residence time cooling oceanic crust enough to create localized subduction.

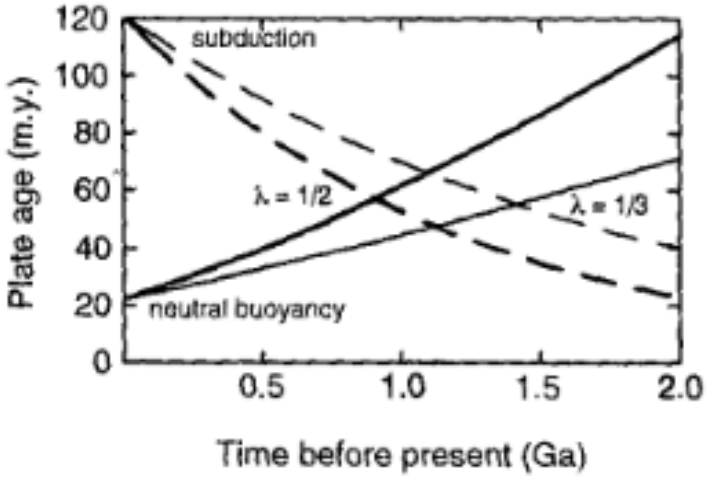

Figure 2.12 Model of average age of subducting plate (dashed lines) and average time for a oceanic plate to achieve neutral buoyancy (solid lines). Model assumes mantle temperature of 1280 °C. λ represents heat-flow decay constant. Taken from Davies (1992).

2.1.6 **Cooling Rates**

Chowdhury et al. (2021) focused on changes secular trends in cooling rates of metamorphic terranes. The paper found that Archean-Mesoproterozoic orogens cooled at a rate less than 50°C/Ma and that orogens that are Neoproterozoic and younger cooled at rates greater than 100°C/Ma. These findings are tempered by numerical experiments and the rock record which show that different P-T-t path shapes can be produced in the same orogen (Gerya and Stöckhert, 2006; Gerya et al., 2002; Krebs et al., 2008). This problem is similar to the issues mentioned with Spencer et al. (2021) (Figure 2.9) where complex orogens need to be simplified to just a few variables for us to compare them statistically. These complexities are clearly in mind for Chowdhury et al. (2021) as they note that Bhowmik and Chakraborty (2017) modeled the patterns of rocks at granulite-UHT grade facies and found that prolonged heating may represent "multiple pulses of heating and cooling instead of a single episode of protracted cooling."

Chowdhury et al. (2021) notes that cooling in metamorphic events is tectonically controlled and that as such secular changes in cooling are likely linked to secular changes in tectonic modes (Figure 2.13). One such change is the switch from peel-back orogenesis, a term coined by Chowdhury et al. (2021) to describe a method of orogenesis illustrated in (Figure 2.14), to modern subduction. This change would be characterized by modern collision zones having thicker, cooler crust resulting in the formation of intermediate dT/dP rocks (amphibolites and lower granulites), while peel-back orogenesis would have been thinner with a greater addition of magma mixing creating hotter, higher dT/dP rocks such a granulites and UHT granulites. This is once again referred to by Chowdhury et al. (2021) as being a possible progenitor of paired metamorphic belts.

The key take-away from Chowdhury et al. (2021) is the quickened cooling overall of younger orogens (Figure 2.13), which Chowdhury et al. (2021) describe as such, "…modern convergent plate margins are characterized by much more rapid cooling-exhumation often controlled by localized vertical extrusion and overall shorter durations of metamorphism, even if the shapes of some P-T paths may be quite similar to those of the early Precambrian high-grade rocks." Modern day events are marked more by isothermal exhumation and Precambrian events are marked more by isobaric cooling.

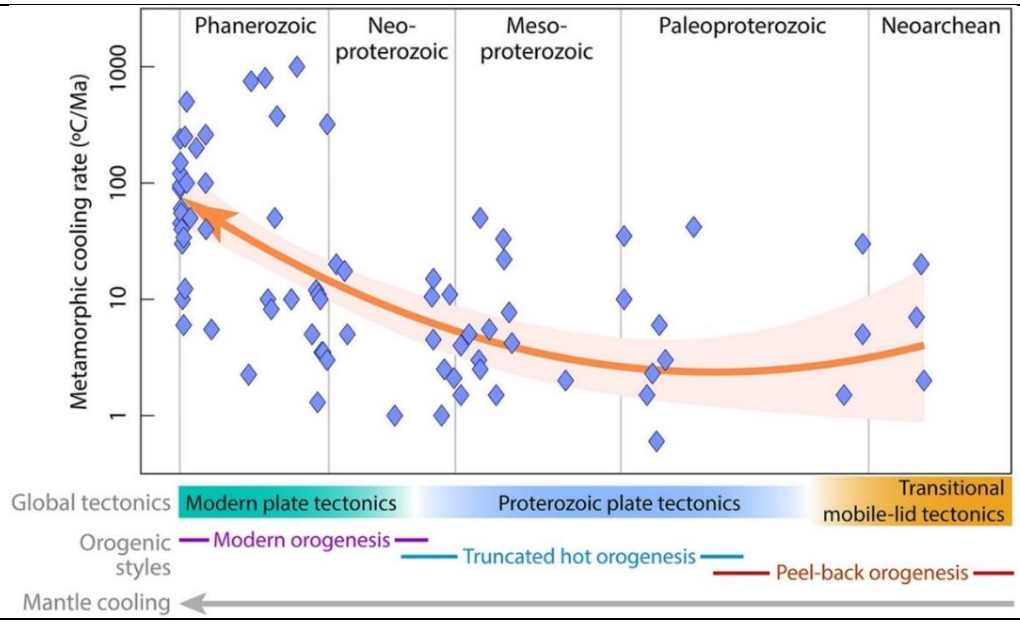

Figure 2.13 Cooling rates (blue diamonds) through time from the dataset of Chowdhury et al. (2021). Orange arrow represents regression line through the data. From Chowdhury et al. (2021).

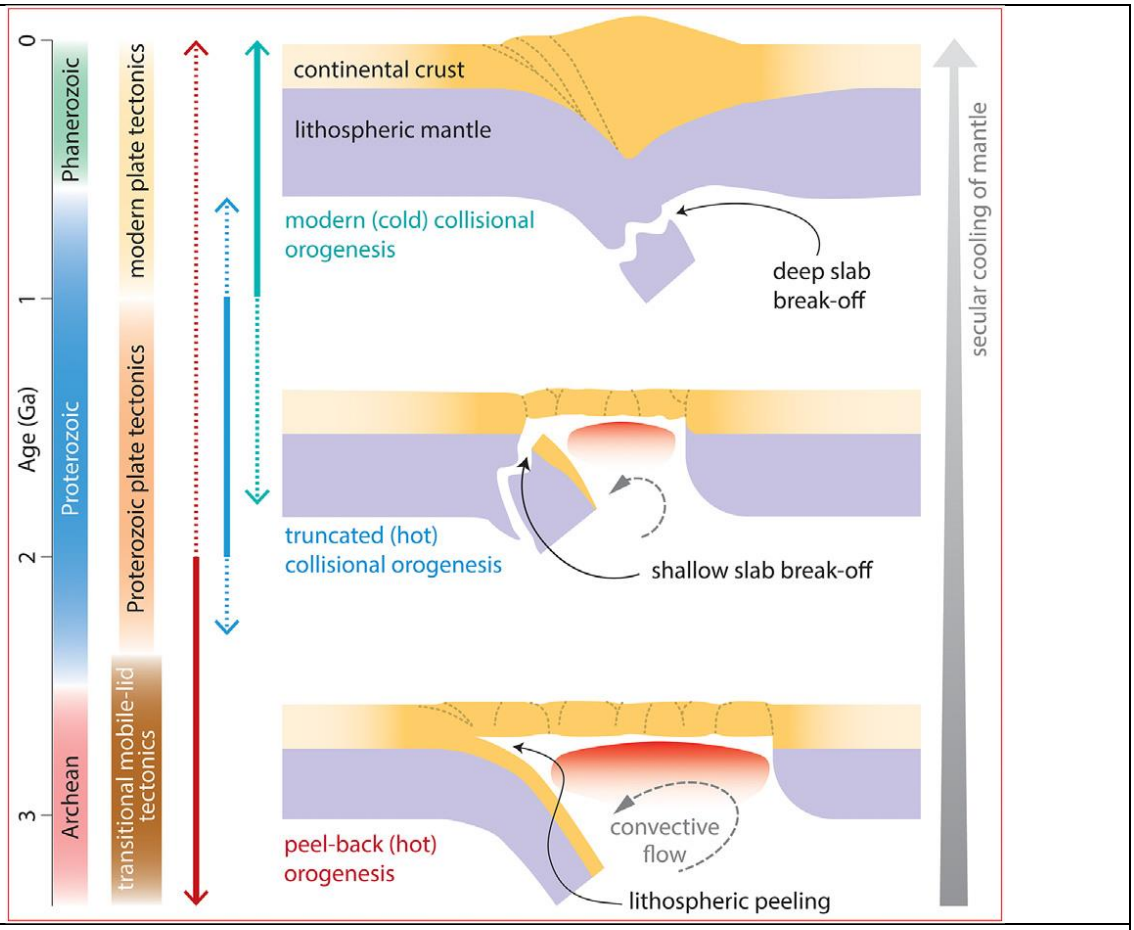

Figure 2.14 Changing orogenic patterns through time. Chowdhury et al. (2021).

Brown et al. (2022) identified "change points" relating to dT/dP and cooling rates through the evolution of the planet. Change points in this way are marked by large changes in temperature, pressure, or dT/dP. These points were marked at the mid-Paleoproterozoic, Mesoproterozoic, the late Paleozoic, and the Cenozoic (Figure 2.15). The relevance of these change points is somewhat obscured by large uncertainties in the data which are larger than the quoted drops or rises.

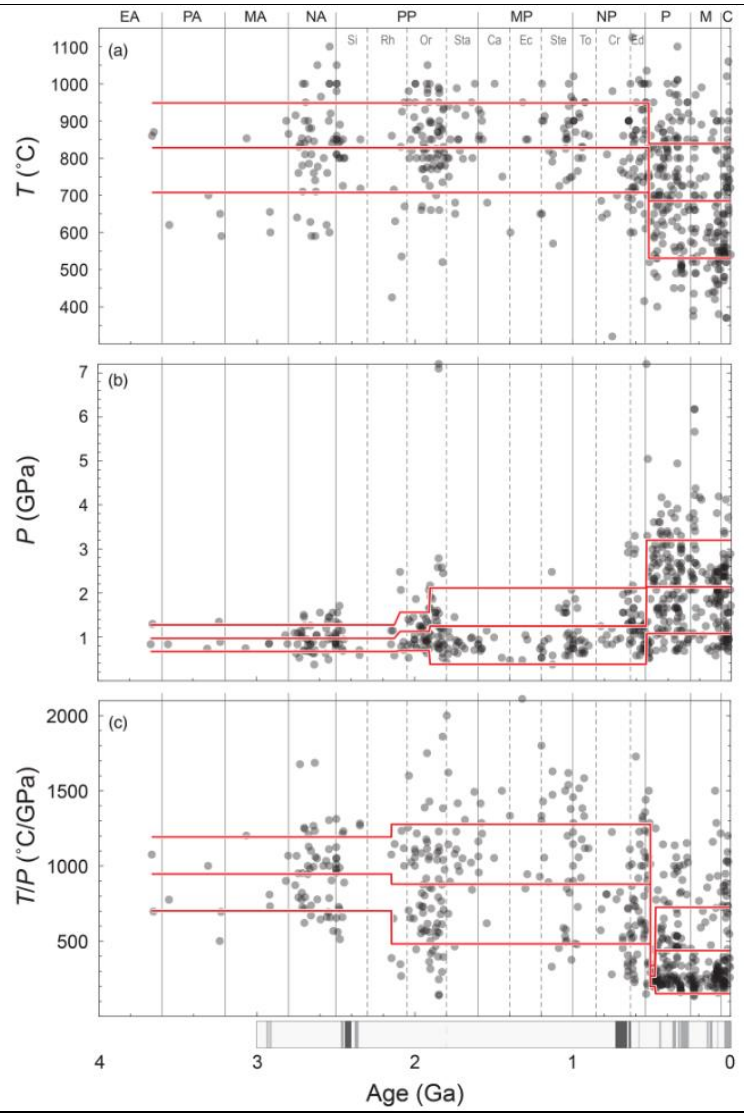

Figure 2.15 Comparison of temperature, pressure, and dT/dP through time. Grey circles represent metamorphic estimates. Red polyline represent median values and show drops/jumps which represent statistically significant change points. Taken from Brown et al. (2022). Grey vertical lines represent geological eras and periods (EA = Eoarchean, PA = Paleoarchean, MA = Mesoarchean, NA = Neoarchean, PP = Paleoproterozoic [Si = Siderian, Rh = Rhyacian, Or = Orosirian, Sta = Statherian], MP = Mesoproterozoic [Ca = Calymmian, Ec = Ectasian, Ste = Stenian], NP = Neoproterozoic [To = Tonian, Cr = Cryogenian, Ed = Ediacaran], P = Paleozoic, M = Mesozoic, and C = Cenozoic.

2.1.7 **Mantle Potential Temperatures**

When one considers secular changes in metamorphism, the state and nature of the mantle is a key issue. Since many of the modern papers look at dT/dP, it is important to understand how geothermal gradients have changed throughout the past. There are many factors which affect this and debate is ongoing. Some important papers which have considered this are summarized here.

Korenaga (2008a) modeled the thermal budget of the Earth, especially with regard to the Urey ratio – defined by Korenaga (2008b) as "…the contribution of internal heat production to planetary-scale energy balance…" and notes "the bulk Earth Urey ration today is probably ~0.35 [and] the convective Urey ration is estimated to be ~0.2." There are many factors which influence this, and the thermal budget of the Earth is still a subject of debate. The thermal budget affects how much energy can go towards things like mantle convection, etc. One factor, plate bending during subduction, was discussed by Davies (2009). Davies (2009) hypothesized that plate bending would create a slow down in mantle convection by causing "resistance to plate motions and mantle convection". This slowing down could allow plate tectonics to stay slow and keep mantle potential temperatures high. This would mean that there would need to be rapid cooling to today's mantle potential temperatures (Davies, 2009). Korenaga (2008a) considered plate bending to be a substantial factor, while Davies (2009) disagreed and concluded that plate bending is not a large factor to consider. Ganne & Feng (2017) calculated mantle potential temperatures for a large set of mafic samples to create a high-resolution timeline. Their findings are that the mantle has only cooled ~150°C since 2.5 Ga. This provides a strong record for a small time period. These findings are summarized in Figure 2.16.

2.1.8 **Compilations on the Onset of Plate Tectonics**

This paper is not the first to assess the largesse of the previous data from many geochemical, geophysical, and computational-modelling studies and the interpretations that have come from that data. Many authors have compiled data from many compilations and models to add to the growing number of interpretations for the onset of plate tectonics. These reviews are reviewed here below.

Condie & Kröner (2008) propose a model where plate tectonics begins as a localized subduction event (Early Archean) and proceeds to coalesce into a global network (Late Archean). By compiling the first instances of different plate tectonic indicators, they were able to set broad beginning and end dates for the onset and widespread distribution of subduction.

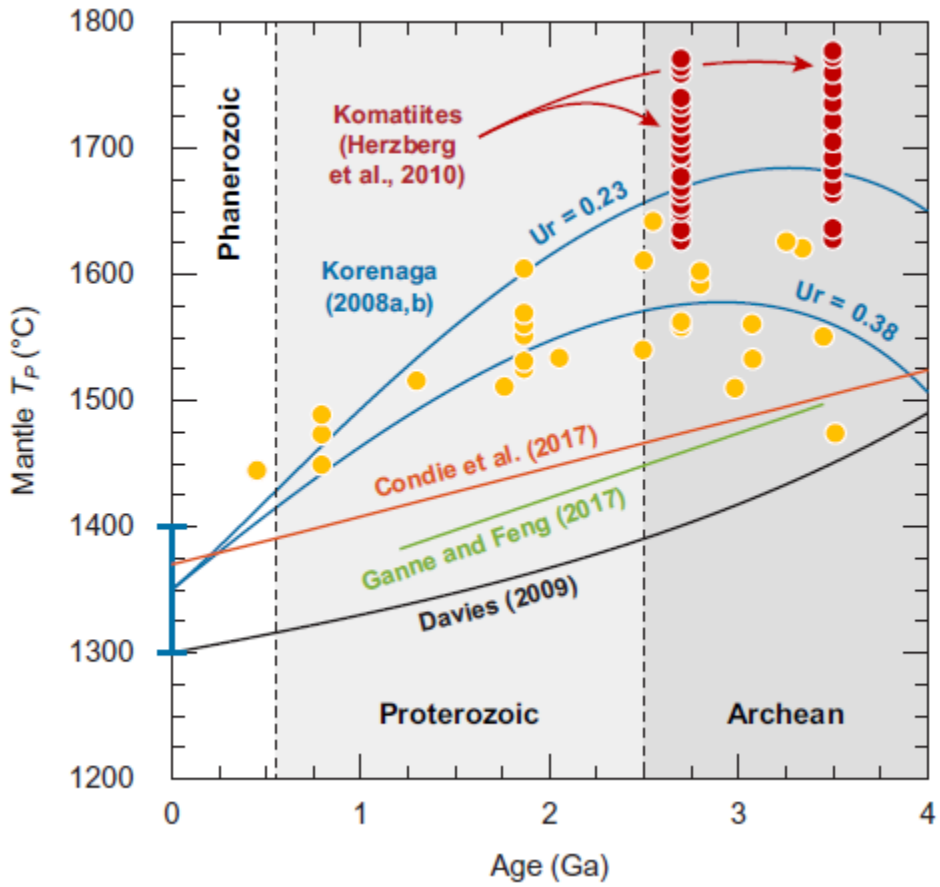

Figure 2.16 Coloured lines represent modelled mantle potential temperatures (°C) through time. Dots represent mantle temperature estimates (°C) from komatiites (red) and non-arc lavas, calculated by Herzberg et al. (2010). Taken from Palin et al. (2020).

This data (Figure 2.17) is split into two categories: first appearance and widespread distribution. These two columns provide instances of both the first appearance of subduction but also show when subduction probably became the norm. This data put the onset of subduction at 3.0Ga and widespread appearance around 2.7Ga (Condie and Kröner, 2008). Condie & Kröner (2008) note however the clash between the majority of the data and three key indicators for subduction: blueschist assemblages, ophiolites, and UHP metamorphism. These indicators have been the benchmark that many have used to mark the onset of modern plate tectonics and so must be resolved Stern (2005). There are many models proposed to answer these questions, largely revolving around mantle potential temperatures and the dynamics of Archean tectonics.

TABLE 1. PETROTECTONIC ASSEMBLAGES CHARACTERISTIC OF PLATE TECTONICS

Assemblage	Widespread distribution (Ga)	First appearance (Ga)
Ophiolites	≤1.0	3.8?
Arc–back-arc	2.7	3.1
Accretionary prisms & OPS	≤1.0	2.7 (3.8?)
Forearc basins	≤2.0	2.7 (3.25?)
Blueschists & UHP rocks	≤0.1	0.85 (1.0?)
Passive margins	≤2.0	2.7 (2.9?)
Continental rift	≤2.0	3.0
Metallic mineral deposits	≤2.7	3.5–3.4

Note: OPS—ocean plate stratigraphy; UHP—ultrahigh pressure.

TABLE 2. OTHER INDICATORS OF PLATE TECTONICS

Indicator	Widespread distribution (Ga)	First appearance (Ga)
UHP metamorphism	≤0.1	0.6
Paired metamorphic belts	≤2.7	3.3
Transcurrent faults & sutures	≤2.7	3.6 (?)
Collisional orogens	≤2.0	2.2
Accretionary orogens	≤2.7	3.8–3.7 (?)
Paleomagnetism	≤2.7	≥3.2 (?)
Geochemistry	≤2.7	3.1
Isotopes	≤3.0	≥4.0
Continents	≤2.7	≥3.0 (?)

Note: UHP—ultrahigh pressure.

Figure 2.17 Characteristic tectonic markers as defined by Condie and Kröner (2008).

Korenaga (2013) took an approach focused on the "relatively constant surface heat flux that is indicated by the likely thermal history of Earth." Korenaga (2013) states that most interpretations about plate tectonic indicators rely on assumptions about the mantle that are "demonstrably wrong or yet to be explored." This mantle-focused approach makes sense given the author's history of modelling mantle evolution and changes to mantle potential temperature. Korenaga (2013) first discusses the stresses and factors related to plate tectonics from a modelling and rock mechanics viewpoint, providing equations for modern plate tectonics today and discussing the changes different variables would take through time. One such section, concerning the effect of pore water pressure on subduction related friction, suggests that hydrostatic pressures (open cracks in the crust) would not be sufficient to ease friction between the upper and lower slab in a subduction zone. Korenaga (2013) states however that the

serpentinization reaction would be required to reduce this friction. Serpentinization is associated often with subduction zone assemblages and can be found as far back as Eoarchean rocks in the Isua Supracrustal Belt (Guotana et al., 2022). Additionally, Korenaga (2013) discusses the differences between Venus and Earth, which previous authors have used as a comparison to early Earth (Brown and Johnson, 2019; Stern Robert J., 2018). Korenaga (2013) states that "the absence of plate tectonics on Venus cannot be explained by this [grain size reduction via deformational work] mechanism alone, but it can be explained by the lack of shear strength reduction with high pore fluid pressure, which can operate only with surface water." This is significant because it would mean that Venus is not an appropriate proxy for early Earth.

Stern & Gerya (2018) approached the problem of the onset of plate tectonics by looking at: i) what pre-modern tectonics would look like, ii) what the transition to modern tectonics looked like, and iii) when modern tectonics became established. Stern begins with the first question by comparing Earth to other "large, rocky (silicate) bodies in our Solar System." These comparisons compare planetary diameter, mass, density, lithosphere, and some other factors. The key here is creating an early-Earth proxy by using other planets as benchmarks. Through this process, Stern proposes Venus as the closest proxy – it has similar characteristics to Earth, but shows single lid tectonics, and is obviously much hotter. Venus's single lid tectonics are driven by plumes and as such Stern proposes that is also the style for early-Earth. A key consideration is that Earth created a mobile lid tectonic style, while Venus did not. This could be a matter of mantle temperature differences between the two planets. Stern acknowledges that there is no *direct geological* evidence for stagnant lid episodes, however, notes that there is petrological evidence for a cooling mantle which may have better facilitated a single lid tectonic style. The second question is handled with many small pieces of circumstantial evidence which look at possible models for the transition to plate tectonics. These models look at things like zones of crustal weakness, oceanic crust thickness, and mantle plumes. The discussion is largely speculative but compiles many different theories about the onset of plate tectonics.

O'Neill (2018) compiled evidence for the initiation of plate tectonics and argues for a non-linear progression of a global network of plate tectonics. The progression of plate tectonics, the authors argue, shows "compelling [geochemical] evidence" for subduction as early as the Archean, but which conflicts with volcanic evidence and TTG's which do not show the involvement of subduction.

Sobolev and Brown (2019) argue that a lubricating effect of sediment building up in subduction zone trenches is the controlling factor in the speed and nature of plate tectonics. The authors cite two episodes of glaciation (Huronia global glaciations [2.45-2.2 Ga] and the Neoproterozoic glaciation [0.73-0.63 Ga]) which would have accrued large amounts of sediment at the edge of continents and in subduction zone trenches. These events would have enabled long-term subduction, according to the authors. These interpretations are most likely influenced by the work of Brown & Johnson (2019) which shows metamorphic samples beginning in the Late Archean as well as a low number of samples in the time called the "boring billion."

Brown et al. (2020a) push for the definition of plate tectonics to mean "…the creation and maintenance of a global network of narrow boundaries separating multiple plates…" arguing that "…then to argue for plate tectonics during the Archean requires more than a local record of subduction." This framing differentiates modern plate tectonics from limited and local subduction zones. One of the main differences being whether horizontal motion is the mode or the exception. This has implications to geochemical cycling, mountain building events, erosion, and land-mass estimates (Brown et al., 2020b; Nutman et al., 2021). This definition however may create a problem for marking the onset of plate subduction, namely that we have very little Archean crust preserved. There are different arguments made about the production and preservation of Hadean and Archean crust [those of Dhuime et al. (2015, 2018), Korenaga (2018), McCoy-West et al. (2019)], but the lack of rock record means making the case for a "global network" of subduction may be impossible to prove or disprove. Focusing on the time periods with more information Brown et al. (2020a) argue that plate tectonics require horizontal movement and bimodal distribution of metamorphism (Brown, 2006; Holder et al., 2019). Brown et al. (2020a) put the low end of the onset of plate tectonics around the formation of the supercontinent Columbia citing the accretion of proto-continents to reflect this horizontal motion and cite Brown and Johnson (2019) to show bimodal distribution of metamorphism. The paper acknowledges instances of Archean subduction and state that these instances can mark the onset of the transition from a pre-plate tectonic regime to plate tectonic regime. The paper puts the range of this transition period from the Archean to the Mesoproterozoic.

Palin & Santosh (2021b) break plate tectonics down into four time periods: No-tectonics, Stagnant-Lid tectonics, Global Plate tectonics, and Modern-day plate tectonics (Figure 2.18). This interpretation marries many different theories together: stagnant lid in the Archean, but with

enough subduction to satisfy questions about Archean subduction zones we find in the field; a clear transition from Archean-Proterozoic subduction and metamorphism to the Modern-day subduction we see today; and a separation for the "Boring Billion." This interpretation attempts to coerce several different and competing theories around the evolution of plate tectonics to work together, but it does not present a new way of thinking about the theory of plate tectonics. There are still questions around the effect of an evolving mantle through time, how energy from the mantle affected plate tectonic modes, the effect of a transition from a primitive mantle to a depleted mantle, among other questions.

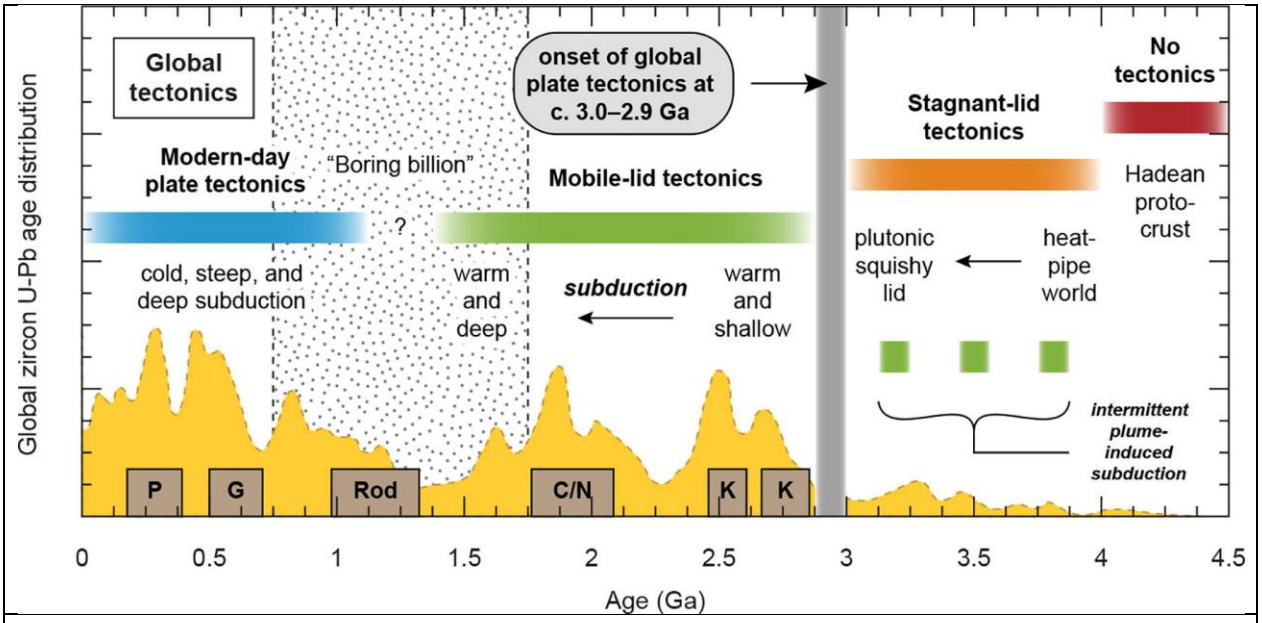

Figure 2.18 Graphical summary of the findings of Palin and Santosh (2021). Yellow peaks represent global zircon U-Pb age distribution, coloured stripes represent interpreted modes of tectonics. Labels at the bottom of diagram mark interpreted supercontinents: K = Kenorland, C/N = Columbia/Nuna supercontinent, Rod = Rodinia, G = Gondwana, P = Pangea. Taken from Palin and Santosh (2021).

2.1.9 **The Range of Modern Subduction [Penniston-Dorland et al. (2015)]**

Penniston-Dorland et al. (2015) compared PT estimates from subduction related metamorphism to comprehensive models of subduction pressure and temperature (Gerya et al., 2002; Syracuse et al., 2010). Pressure-temperature data was taken from the literature. A global dataset (Figure 2.19) made up of pressure-temperature estimates from maximum pressure

conditions ($P_{max} - T$). These estimates are from blueschists, eclogites, and "associated subduction-related metamorphic rocks" which are all 750 Ma or younger and published within the last 25 years (Penniston-Dorland et al., 2015). $P_{max} - T$ is usually associated closely with maximum temperature and estimates work best with $P_{max} - T$ (Penniston-Dorland et al., 2015). Penniston-Dorland et al. (2015) state: "the $P_{max} - T$ and prograde P–T path estimates cover a wide range of subduction conditions, including slow and fast convergence, old and young oceanic crust, and various subduction angles, in many ways analogous to the range of subduction conditions modeled by Syracuse et al. (2010). [Figure 2.19] … shows the locations of the studies used in this compilation."

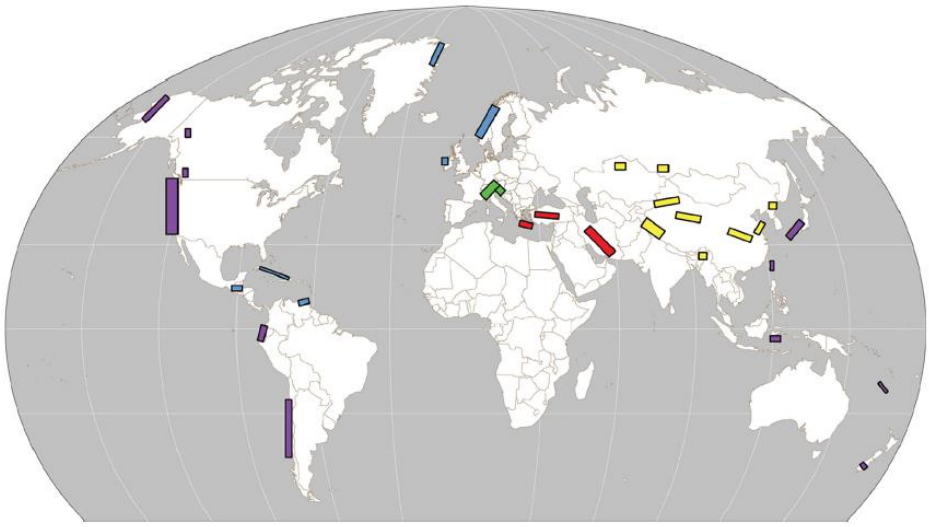

Figure 2.19 Distribution of samples from the Penniston-Dorland et al. (2015) dataset. Colours represent geographically distinct areas: Circum-Pacific (purple), Circum-Atlantic (blue), Alps (green), Turkey-Greece-Iran (red), and Continental Asia (yellow). Taken from Penniston-Dorland et al. (2015).

Figure 2.19 shows the distribution of the metamorphic samples in PT-space underlain by subduction-related metamorphic facies. These are contrasted against modelling by Syracuse et al. (2010) and Gerya et al. (2002), which represent average pressure-temperature paths for modelled oceanic subduction zones. Penniston-Dorland et al. (2015) notes that most samples are hotter than the models: "In general, discrepancies are greatest for P max < 2 GPa, where only a few of the highest-T model paths overlap petrologic observations and model averages are 100–300 ◦C colder than average conditions recorded by rocks." Agard et al. (2018) notes that the compilation

includes rocks from continental subduction areas, and that when those rocks are removed the data falls in line much closer to proposed models. For the purpose of this study, subduction – either oceanic or continental – represents horizontal movements associated with plate tectonics.

For the purpose of thermobaric analysis [as Brown & Johnson (2018), Palin et al. (2020), and Zheng and Zhao (2020)] it is important to note that every region sampled has points which plot hotter than the 10°C/km line shown. This line, representing the cutoff for "Alpine" metamorphism, is generally considered to be the cutoff for subduction-related metamorphism as well (see Table 2.3 for specifics). What this means, it is that large sections of subduction-related samples are plotting in historically agreed upon intermediate-category dT/dP sections. The lack of low-dT/dP samples, noted by Brown and Johnson (2018), has long been the hallmark for a lack of cold subduction – perhaps subduction zones are producing hotter rocks than previously understood as Penniston-Dorland et al. (2015) suggests and this is muddying the waters when it comes to pin-pointing the exact timing subduction. Figure 2.20 summarizes the range of dT/dP found in the dataset and Table 2.3 summarized the ranges of dT/dP classifications from previous authors. One can see in Figure 2.20 the median value for samples is 312°C/GPa, within the Alpine system (10°C/km or 300°C/GPa), but that much of the data sits outside of it. 61 samples in the dataset (17% of the total dataset) are higher than even the highest dT/dP lineation [440°C/GPa from Palin et al. (2020)] with the highest dT/dP samples reaching 875°C/GPa where previous compilations would have grouped it with granulite grade metamorphism and the like. Figure 2.21 plots each sample from the dataset against a metamorphic facies framework.

As noted by Penniston-Dorland et al. (2015), these are not exactly dT/dP estimates, but d(T@P_{max})/dP_{max} estimates. If these P-T-t loops are broad and T_{max} is much hotter than T@P_{max} then one would expect to see lower values. It is difficult to quantify this discrepancy, however P-T-t path for these samples have been noted by Penniston-Dorland et al. (2015) to be largely tight prograde loops where "…usually these [$P_{max} - T$] also correspond with maximum T (Tmax)." It is reasonable to assume that these are close to how samples have been calculated by previous compilations.

Given the overlap between the dT/dP created by subduction-related samples and high-grade metamorphism it seems unlikely that a single linear category can separate data into dT/dP categories. This would suggest that many strictly non-subduction related metamorphic samples should be re-examined.

Table 2.3 Summary of the categories of low, intermediate, and high metamorphism from previous compilations (Brown and Johnson, 2019; Palin et al., 2020; Zheng and Zhao, 2020).

Compilation	Category	°C/km	°C/GPa
Brown et al.	Low	<11	<375
	Intermediate	11-23	375-750
	High	>23	>750
Palin et al.	Low	<13	<440
	Intermediate	13-23	440-775
	High	23-45	775-1500
	Contact	>45	>1500
Zheng and Zhao	Low	<10	<330
	Intermediate	10-30	330-990
	High	>30	>990

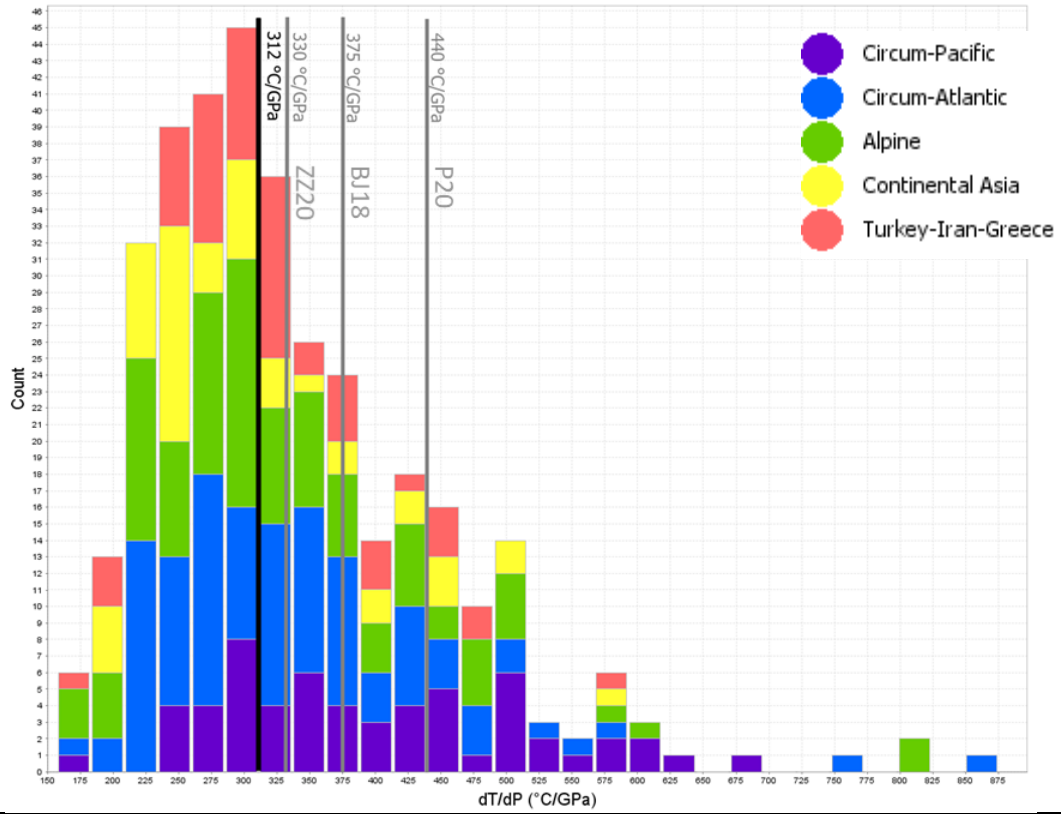

Figure 2.20 Histogram of subduction-related metamorphism samples from Penniston-Dorland et al. (2015). Samples are coloured as per Figure 2.19 (Circum-Pacific, Circum-Atlantic, Alpine, Continental Asia, and Turkey-Iran-Greece). Black line marks median dT/dP for the dataset, light grey lines represent upper boundary for what are considered low dT/dP conditions by previous authors (Zheng and Zhao 2020 [ZZ20]; M Brown and Johnson 2018 [BJ18]; Richard M. Palin et al. 2020 [P20]).

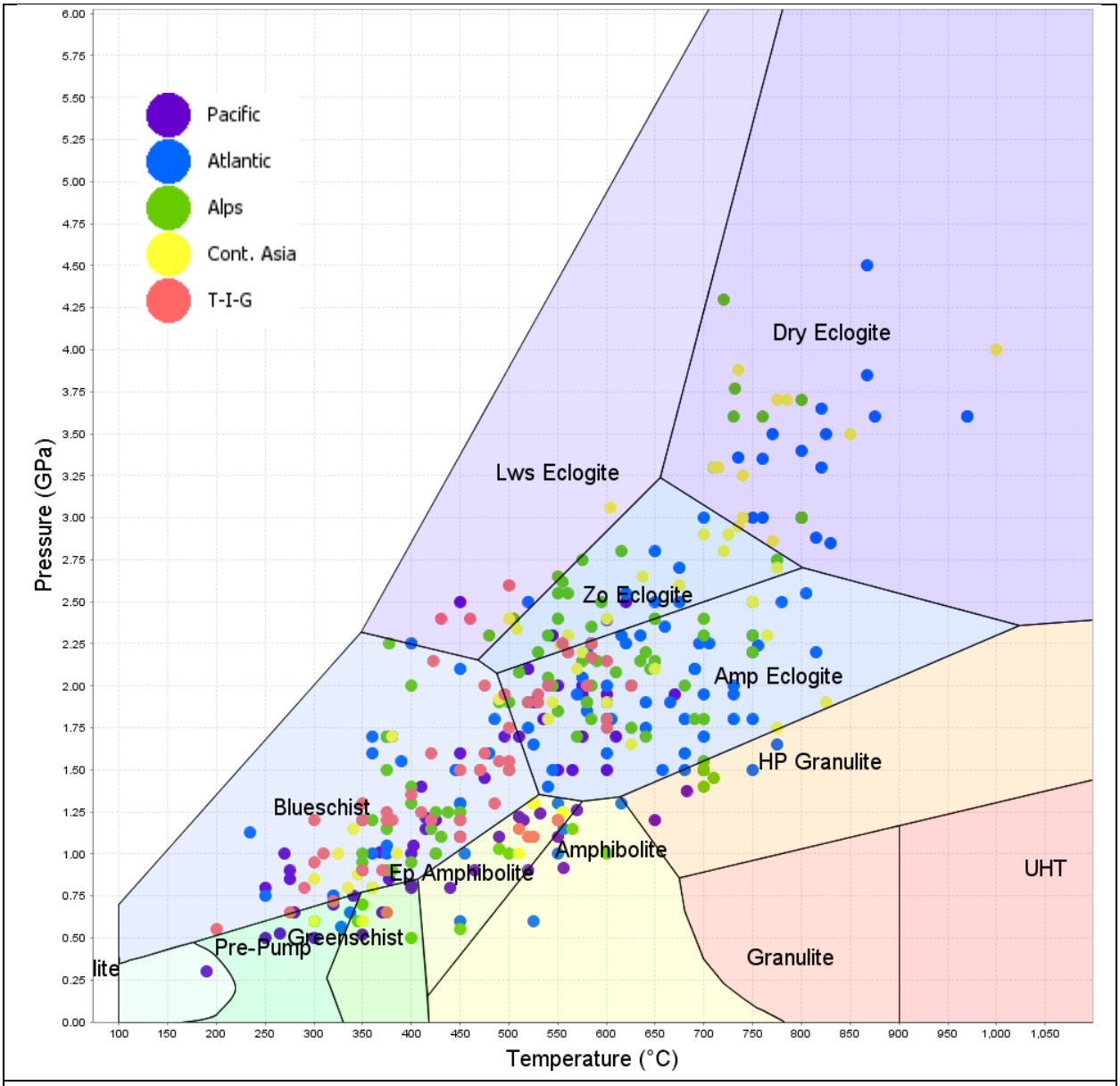

Figure 2.21 Pressure against temperature for the Penniston-Dorland (2015) dataset. Diagram in the background is metamorphic facies diagram. Points coloured according to geographic classification (see Figure 2.19).

2.2 Limitations

Peak PT conditions recorded in databases are snapshots of P-T-t paths. As shown in Figure 2.22, P-T-t paths will often pass through low-T, high-P zones before heating. These paths don't attempt to capture every possible P-T-t path, which would be impossible, but to illustrate commonalities between clockwise prograde metamorphic pathways. The issue with looking at

just peak P-T and arguing that there are no conditions with low T/P, is that it dismisses large sections of the pathway that the rock may have experienced. This won't be true for all samples: without P-T-t paths one cannot determine how many samples for which this is true. This limitation means that large amounts of the P-T-t pathway are not being accounted for during interpretation and current interpretations are thus overly simplified.

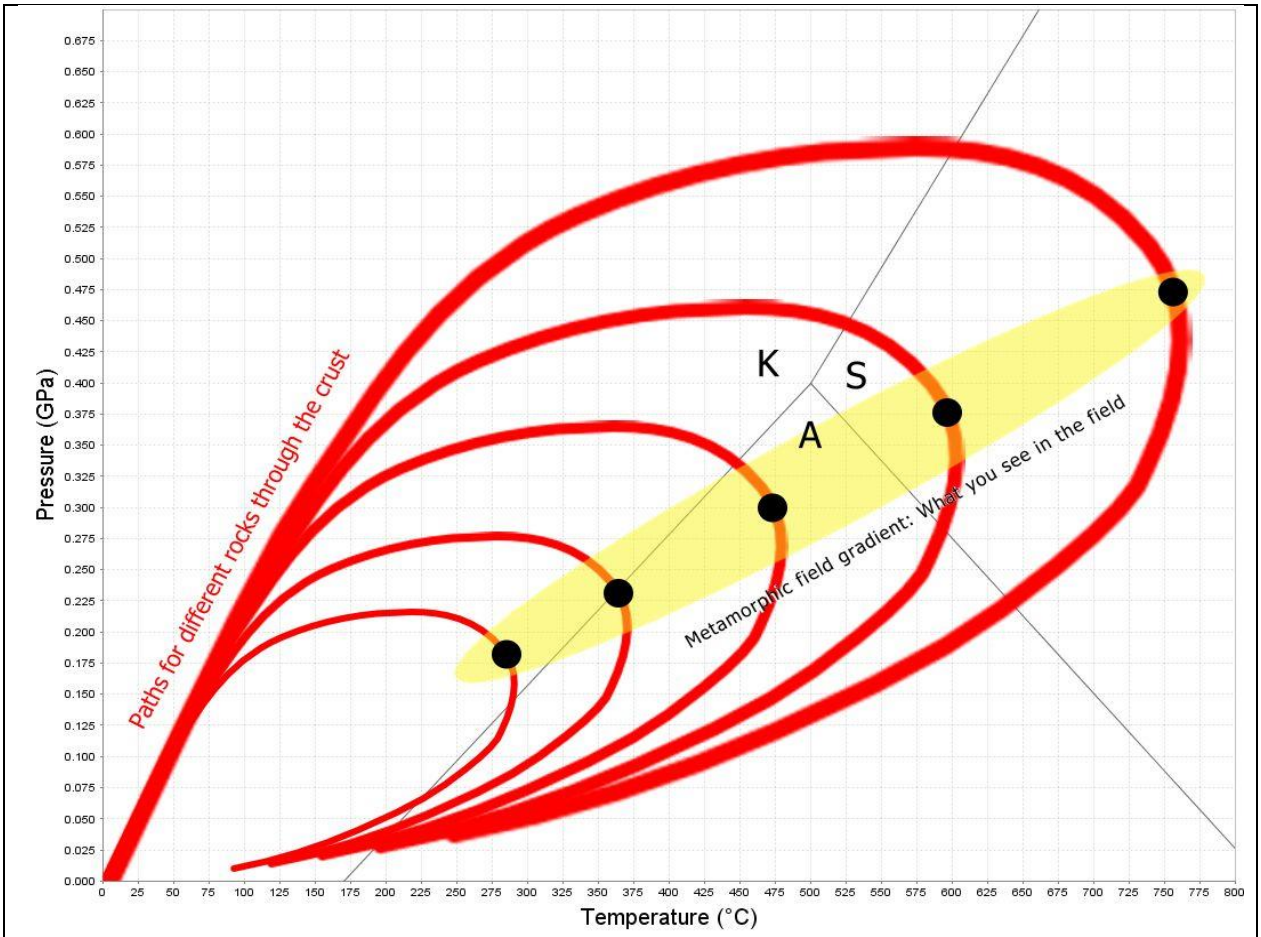

Figure 2.22 Diagram of pressure-temperature space showing different hypothetical clockwise P-T-t paths and comparing them to field assemblages. The hypothetical P-T-t paths show the path of prograde metamorphism to the yellow band which represents the field occurrence of that P-T-t path. Black dots represent the PT estimate for those hypothetical field rocks. K = Kyanite stability field, A = Andalusite stability field, S = Sillimanite stability field. Modified from Vernon & Clarke (2008).

2.2.1 **Spatial Limitations**

Orogenesis can be small or can span thousands of kilometers. One key limitation is our ability to capture complex spatial data. Computers are excellent at capturing and utilizing point

data (a singular point on the Earth's surface with latitude and longitude) but can struggle with polygons, 3D shapes, and gradients between values. Different programs tackle each of these problems individually, but nowhere have we seen the ability to put all these into one cohesive map or database.

Each sample is quantized, and workers will pick a handful of samples to represent a particular orogen or part of an orogen. To this end, one of the main conceits of this style of research is to use metamorphic samples as point samples. Each sample represents a point taken from within an orogen; together they represent the whole of an orogen, in principle at least. What this means is that orogens will always be far for more complex than we can capture or calculate. Our points are our best estimate for the range of each orogen.

Spatially, this means that we have little idea of the range of orogenic events when it comes to reconstruction modelling. When each sample is represented by a singular dot, one must visually collate groups of dots into an orogenic event. Given our difficulty with coming to a consensus on reconstruction modeling this means that certain orogens will be associated together (paired metamorphic belts, accretionary zones and metamorphic hinterlands, etc.) in some models and research and not in other models and research.

This doesn't touch on the matter of sampling bias. How many samples should represent an orogen? How many samples is too many? The trend of research to plot samples in 2-D space means that 1000 samples from one orogen will create more pull than 1 sample from a different orogen. It is an important decision for research moving forward to ascertain how to deal with this problem – especially with the proliferation of statistical methods to analyze data (linear regress, LOWESS, log distributions, histograms, etc.) which rely on the assessment of a population of data. The distribution of spatial samples against a modern map is given as a heatmap in Figure 2.23.

This study has taken to creating averages for over-represented orogens (see section: 3.2.3 Averaging Oversampled Areas). This is long and subjective work. It is beyond the scope of this project to create methods which will be able to normalize large swaths of data from the globe and it will be up to the community of researchers to determine how many samples is the correct number for representation of orogens.

One example of this disparity is between the North and South American Cordillera system and that of the Alpine-Himalayan system. The Alps and Himalaya have been the subject

of decades of geological observation and scrutiny. They are some of our best-studied orogens. By comparison, South America has a dearth of research and proves an extremely difficult part of the world to study. Comparing the samples which have been compiled in previous compilations, and this study which builds on those, we can see an order of magnitude difference in the number of samples being take from the Alpine-Himalaya belt compared to the North-South American cordillera. This bias is reflected in the data and thus the interpretations.

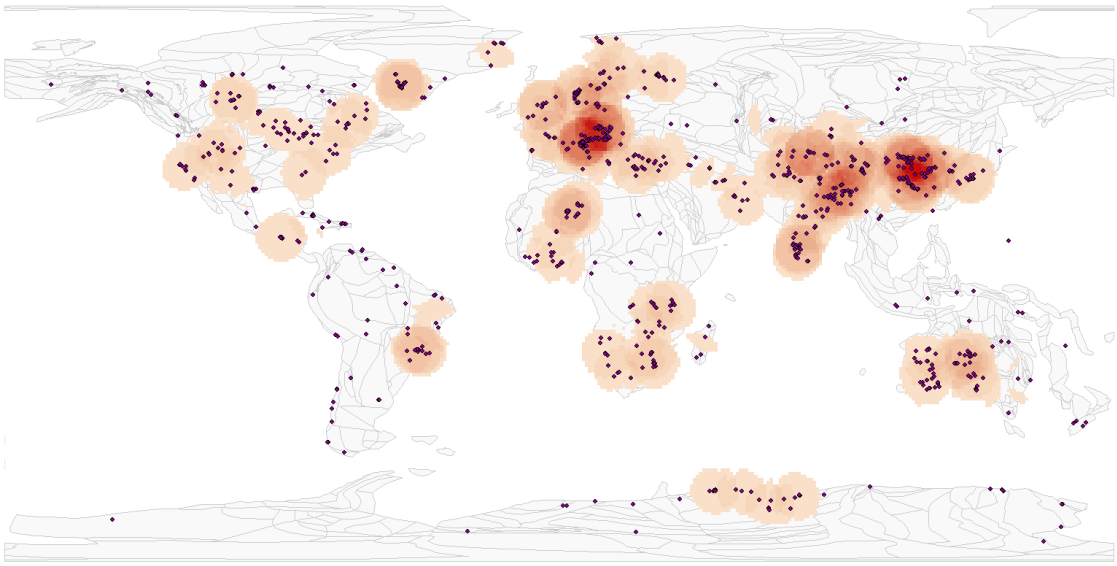

Figure 2.23 Heatmap of samples from combining the datasets of three significant compilations (Brown and Johnson, 2019; Palin et al., 2020; Penniston-Dorland et al., 2015). The heatmap represents areas of high sampling, especially noting the Alps and southern China.

Spatial bias is often a matter of rock availability, with well-populated areas with good exposure (Alps) being much better studied than remote areas with poor cover (Amazon). There remains the concern that well studied areas, such as collisional orogens like the Alps and the Himalayas are much better studies than accretionary orogens in the Phanerozoic Circum-Pacific. As mentioned, many areas in South America are difficult to study and to access. This leads to datasets which are weighted in favour of easy to access and heavily studied areas. Variations in sampling activity are likely to bias interpretations based on weighted averages or similar statistical methods. Table 2.4 and Table 2.5 compare the density of records from different regions of the world. Table 2.4 normalizes the number of samples in well-known orogens to calculate and

contrast record density. Table 2.5 shows the expected densities for well-known regions if they had been sampled with the same density as the Alps.

Table 2.4 Comparison of record density to orogen area (km^2) in (Brown and Johnson, 2019; Palin et al., 2020).

Orogen	Number of Records	Area km^2	Samples per km^2	Samples per 100'000 km^2
Himalaya	38	2510104	0.0000147	1.47
Alpine	25	254194	0.0000983	9.83
SAM Cordillera	5	3051784	0.0000016	0.16
NAM Cordillera	12	2910841	0.0000041	0.41

Table 2.5 Comparing the density of records in the Alps to the other well-known orogens. (Brown and Johnson, 2019; Palin et al., 2020).

Area	Alps Normalized	Normalized to Alps	Number of Records
Himalayas	4.25	691.2	38
SAM Cordillera	1.08	840.4	5
NAM Cordillera	1.92	801.6	12
Rest of the World	1.18	48045.3	552

As discussed in previous sections, the accretion of supercontinents represents times of increased metamorphism from accretionary orogens, while the breakups represent relative lulls. Figure 2.24 shows distinct crests of clustered records and relatively quiet troughs between. These crests and troughs have been interpreted to reflect metamorphism forming from the collision of multiple terranes to form supercontinents (Brown and Johnson, 2019). It is likely that these gaps represent a geologically relevant phenomenon which would survive an increase in sample size.

2.2.2 **Temporal Limitations**

Current datasets are small and sparse. Studies of metamorphic trends were less than a hundred samples [Ernst (1972) and Grambling (1981)] until Brown (2006). Since then, Brown (2006) has been the foundation which other papers have added to, with Brown et al. (2022) being

the current most complete dataset (n = 567). Despite this increase in data, there remain gaps in time and space which need to be addressed. These gaps are twofold: temporal and spatial gaps from sampling biases introduced from the rock record and rock availability, and temporal gaps interpreted to be connected to supercontinent cyclicity (as discussed in previous sections).

Figure 2.24 shows a histogram of the temporal distribution of records from previous major compilations. There remains significant bias in relation to Phanerozoic vs. Precambrian data, with the Phanerozoic containing roughly the same number of samples as the Precambrian (it is worth noting that this true even without the addition of the data from the Penniston-Dorland (2015) compilation which focused solely on orogens younger than 750 Ma). It was the goal of this project to undertake a literature review and fill the database with any relevant Precambrian records.

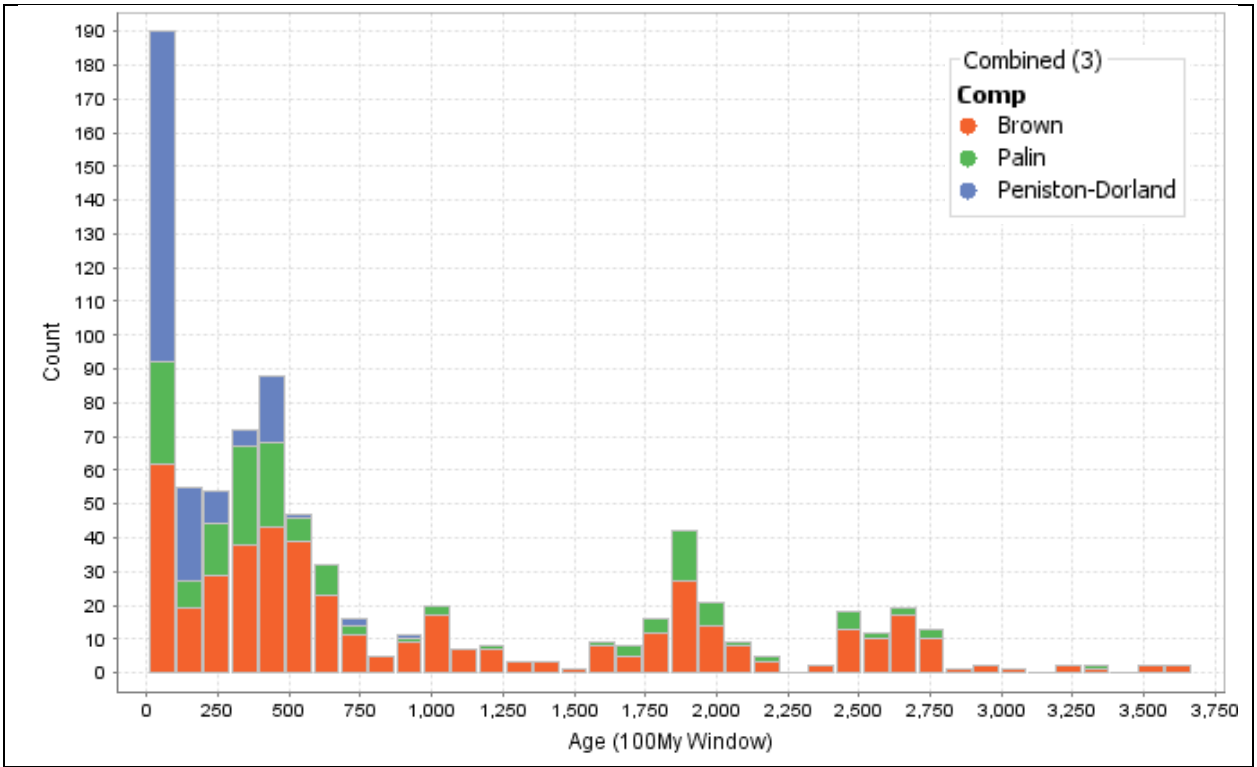

Figure 2.24 Histogram of samples from three significant compilations (100 m.y. age bins). (Brown et al., 2022; Palin et al., 2020; Penniston-Dorland et al., 2015).

A new database, MetRec, was created to address these gaps in the data. This was done through two methods: an extensive literature review was undertaken to increase the number of samples in the dataset; and results from areas considered to be oversampled relative to others

were averaged. It was the opinion of this project that because of the popularity of weighted averages to analyze metamorphic trends, the ability to best represent the density of samples across the planet was an important inclusion.

2.2.3 Thermobaric Exaggeration

Peak pressure and temperature are only snapshots of a much larger story. Orogens pass through pressure and temperature space to different degrees, at different rates, and different parts of the orogen will experience different conditions. One issue that hasn't been addressed by previous compilations is how calculated dT/dP differs from the true P-T-t path that an orogen takes during burial and exhumation. Illustrated in Figure 2.25, this point marked "calculated peak" is higher temperature and higher pressure than any point along the path of the orogen. This exaggeration can leave records which seem hotter and deeper than the rocks they represent have truly experienced. This can be especially critical for paths which may stray near metamorphic facies boundaries. Calculated dT/dP may plot in one facies while the rock itself has none of the qualifying minerals of that facies. Quantifying this discrepancy can be difficult. This study introduces a quantitative proxy called thermobaric exaggeration.

Thermobaric exaggeration (TBx) is the ratio of dT/dP at peak temperature to dT/dP at peak pressure:

Equation 1 Thermobaric exaggeration.

$$TbX = \frac{\frac{dT}{dP}@T_{max}}{\frac{dT}{dP}@P_{max}} \quad \text{.....(6.1)}$$

This equation creates a unitless value which compares the value of the peak-temperature slope to the peak-pressure slope. Where TbX equals 1, the dT/dP at the maximum temperature and pressure values are the same. Where TbX equals 0, these values are infinitely far apart. This allows one to examine the discrepancy between true and calculated peak metamorphism and compare these values. At the time of writing, compiling large numbers of TBx calculations from P-T-t paths is beyond the scope of this thesis. However, it will be a useful tool to quantify and categorize P-T-t paths moving forward.

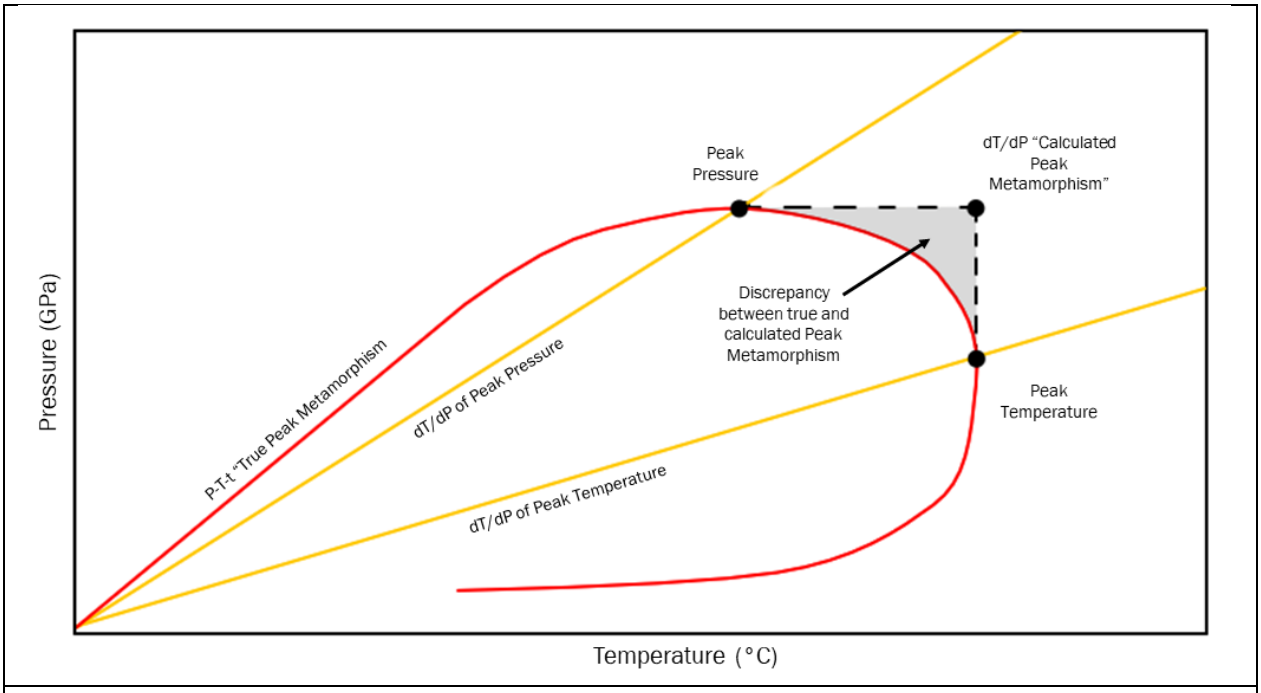

Figure 2.25 P-T-t path in PT space (red) showing clockwise prograde metamorphic path (true metamorphism). Peak pressure notes the highest pressure point on the loop and peak temperature notes the highest temperature point on the loop. Yellow lines show the difference between the ratio of dT/dP for the record at "peak pressure" and at "peak temperature." dT/dP "calculated" peak metamorphism is the point in PT space where peak temperature over peak pressure would be calculated. The greyed out box between the three peaks shows the discrepancy between PT space experience by the true P-T-t path and the space occupied by the calculated metamorphic peak.

2.3 Thermal Gradients are Associated with Types of Orogens in Modern versus Orogens in the Past

Currie & Hyndman (2006) investigate the thermal architecture of subduction zones (Figure 2.26). What they found from looking at the thermal structure of 10 circum-Pacific back arcs with no significant recent extension is that uniformly high temperatures can be found in the shallow mantle and thin lithosphere (1200 °C at ~60 km depth). These areas of elevated temperatures range from 250 km to greater than 900 km.

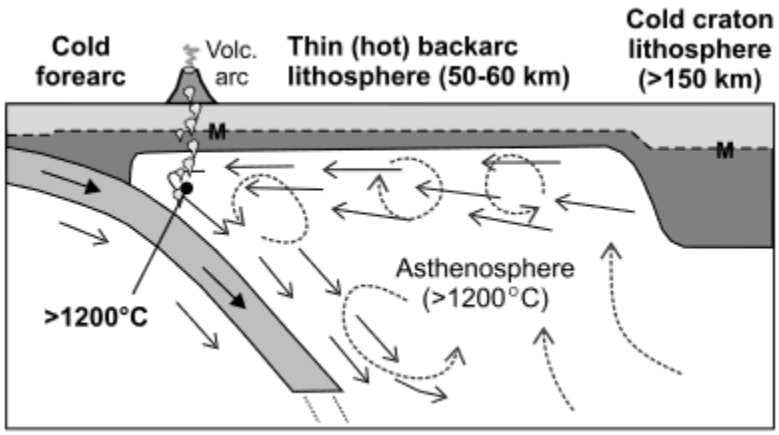

Figure 2.26 Cartoon summarizing the findings of (Currie and Hyndman, 2006), with different areas of the subduction zone, active arc, and back arc with associated temperatures. Taken from (Currie and Hyndman, 2006).

This is significant because the paper notes the existence of high upper mantle temperatures extending for several hundred kilometers orogenic hinterland even with no extension. The implication for this is that even modern subduction zones can show elevated temperatures (as seen in 2.1.9 The Range of Modern Subduction [Penniston-Dorland et al. (2015)) and that modern subduction zones can show great variation in temperatures across the length of them. Currie & Hyndman (2006) note that "most [modern] subduction zones are characterized by … the [presence of a] volcanic arc" (these can be interpreted from plate reconstruction models as in Figure 2.27).

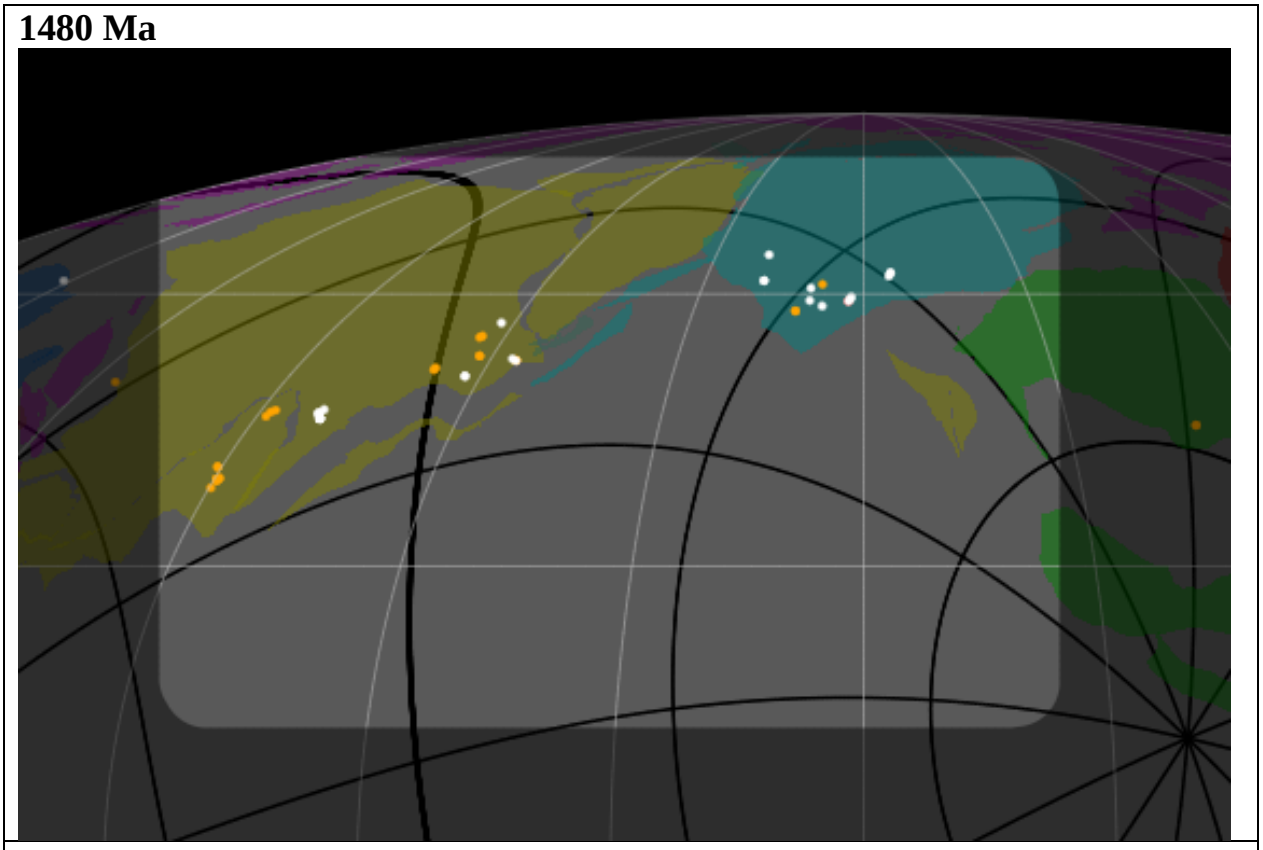

Figure 2.27 Paleoplates reconstruction model showing area of possible subduction at 1480 Ma (Eglington et al., 2017; Evans and Eglington, 2022). Orange dots represent volcanic igneous crystallization ages, white circles represent metamorphic ages. Each dot represents an occurrence of igneous activity or metamorphism at 1480 Ma. Coloured polygons represent continental material (yellow - North America, blue – Europe, green – South America, red – Africa, purple – Asia).

2.4 Preservation Arguments

Fluid loss and dehydration are key components of preserving low dT/dP assemblages. It is critical to minerals like lawsonite (a key indicator for subduction as it requires high pressure and great water contents) are dehydrated and summarily exhumed quickly before they can be rehydrated (Clarke et al., 2006). This sets a limit for how often these assemblages will be preserved and what sorts of environments will be able to exhume these assemblages quickly enough. “The inability of rocks to store fluid, owing to restricted or absent porosity, means that H_2O or CO_2 released as fluid by mineral breakdown is lost. Having lost a key potential reactant,

the products cannot react to reverse the prograde reactions during cooling, preserving peak assemblages, as mentioned previously" (Vernon and Clarke, 2008).

This ties into the findings of Chowdhury et al. (2021) which find secular changes in cooling over the last ~800 m.y. and that Phanerozoic rocks have been cooling faster. If previous Precambrian rocks were staying hotter longer this would allow for these very fragile assemblages to be reworked. Penniston-Dorland et al. (2015) show that modern subduction zones (the one that return to the surface at least) have tight hairpin PT paths. Maybe this is a survivorship bias and broad PT paths which cool slower aren't making it back to the surface or experience intense retrograde metamorphism which occludes their interpretations.

Wei and Clarke (2011) modeled mafic crust and found that mafic crust should be creating blueschists in subduction areas, effectively concluding that it's not a matter of whether they are being made, but if they are being preserved. Palin et al. (2021) looked at the possibility that UHP eclogite are not being exhumed by Archean crust. The team modelled Archean crust using the assumption that it was more mafic and therefore less buoyant. Using these assumptions, the paper makes the argument that there is a possibility that rheology and density of Archean crust are large factors in the exhumation (and therefore preservation) of UHP eclogite.

Different orogenic styles will preserve differently. There are many areas within an accretional orogen that will preserve rocks poorly or well. Rocks preserved in the extensional hinterland of the accretionary orogens will be preferentially preserved (Collins, 2002; Hawkesworth et al., 2009) [Figure 2.28]. This lines up with what we know of VMS deposits for which all the old VMS deposits that are preserved today are from back-arc basins. This could mean that intermediate-high dT/dP samples are preferentially preserved. From Hawkesworth et al. (2009): "These considerations show that preserved rocks tend to be from the end of the subduction-related and the collisional mountain building stages … because they are insulated in the cratonic interior and thus preserved from convergent plate margin erosion." There are some complications to this idea however, as many accretionary orogens can exhibit many instances of compression and extension throughout their life time before succumbing to a final collision (Collins, 2002).

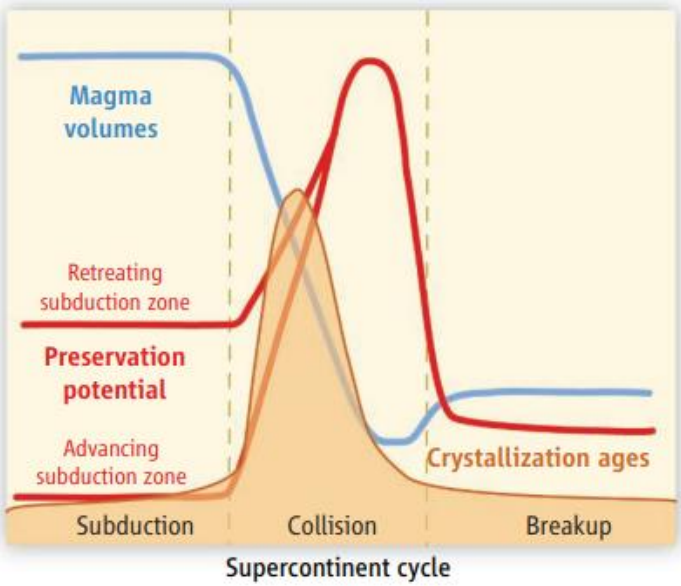

Figure 2.28 Illustrating the differences in preservation during the lifecycle of an accretionary orogen. Blue line shows the volume of magma being produced through time. Red lines show the preservation potential for subducting rocks. Orang spike represents crystallization ages. (Hawkesworth et al., 2009).

Tang et al. (2021) proposed a period of orogenic quiescence during the period typically called the "Boring Billion." The findings are summarized in Figure 2.29 and point to a prolonged period of supercontinent assemblage featuring reduced continent to ocean nutrient transport (due to a lack of orogenesis) which in turn meant a lack of primary production leading to decreases in uranium and molybdenum in black shales and of oxygen production. This lack of orogenesis lines up with gaps in previously published compilations the Nuna-Rodinia time period (Holder et al., 2019; Palin et al., 2020).

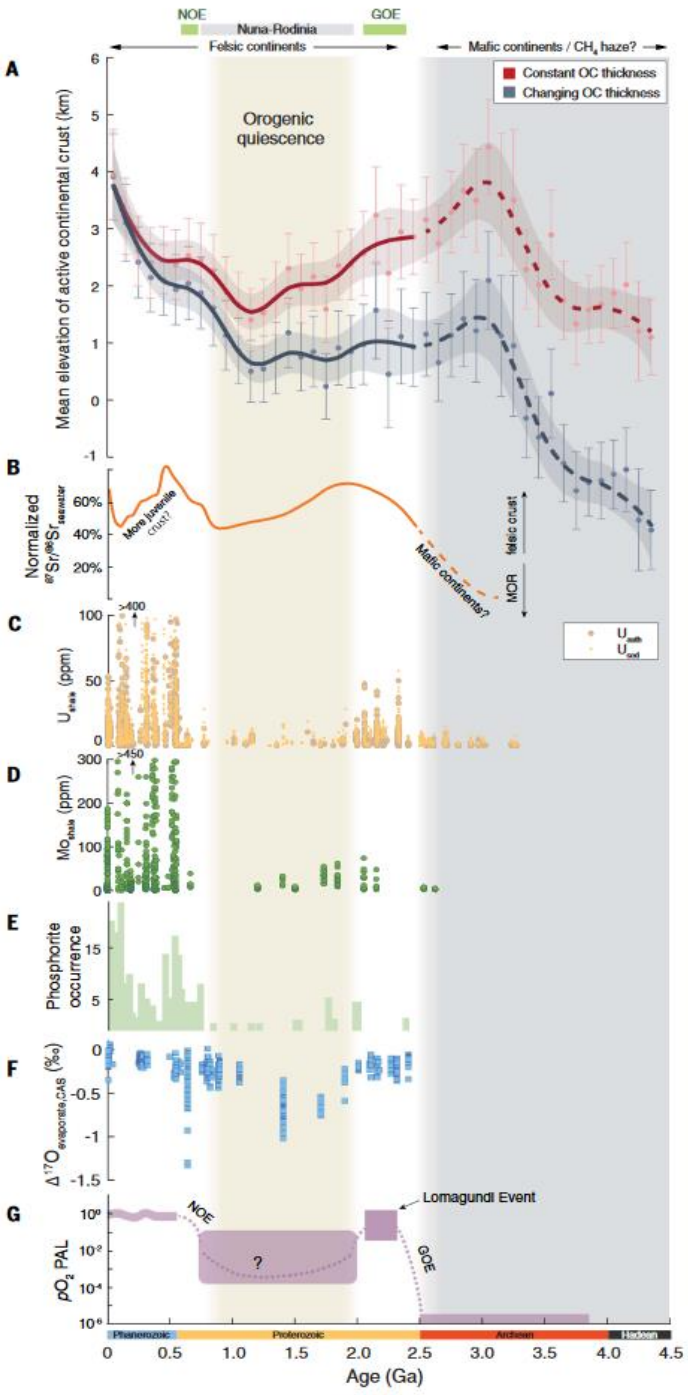
NOE
GOE
Nuna-Rodinia
Felsic continents
Mafic continents / CH4 haze?
A
Constant OC thickness
Changing OC thickness
Orogenic quiescence
Mean elevation of active continental crust (km)
B
Normalized 87Sr/86Sr seawater
More juvenile crust?
Mafic continents?
felsic crust
MOR
C
>400
U shale (ppm)
D
>450
Mo shale (ppm)
E
Phosphorite occurrence
F
Δ17O evaporites,CAS (‰)
G
Lomagundi Event
NOE
GOE
?
pO2 PAL
Phanerozoic
Proterozoic
Archean
Hadean
Age (Ga)

Figure 2.29 A) Calculated elevation (using an istosy model *) for two different crustal thickness models. B) Normalized seawater isotope curve. C)Uranium hosted in black shale. D) Molybdenum hosted in black shale. D) Phosphorus occurrences. F) Average $\Delta^{17}O$ in evaporites. G) Atmospheric partial pressure for $\Delta^{17}O$. The Lomagundi event is the event where marine carbonates experienced a large positive spike in $\delta\ ^{13}C$ Eguchi et al. (2020).Taken from Tang et al. (2021).

2.5 Supercontinent Cyclicity Concerns

The proposed cycle of supercontinent accretion-stability-rifting has some implications for the study of tectonics. Accretion of supercontinents would be times of increased collision between cratonic blocks, while periods of stability and rifting would have fewer instances of collision. These cycles have been associated with spikes and lulls in the metamorphic records (Brown and Johnson, 2018; Palin et al., 2020) [Figure 2.30].

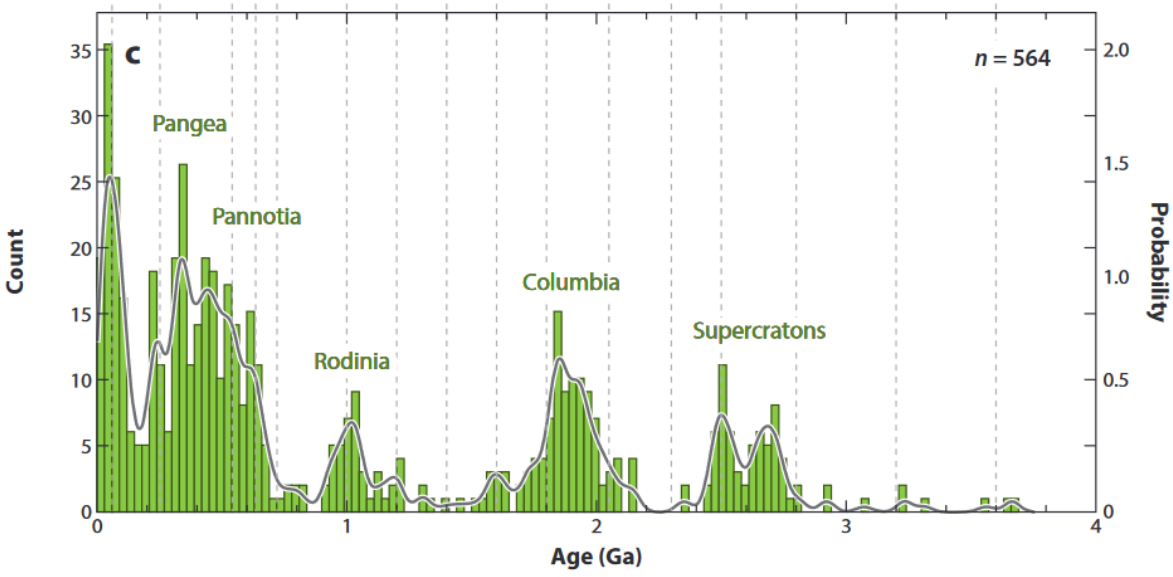

Figure 2.30 Histogram of metamorphic sample ages through time compared to inferred supercontinent accretion timings. Taken from (Brown et al., 2020).

2.6 Summary

Previous studies have looked at many proxies for the interpretation of metamorphism in the rock record (mineralogy, geochemistry, crustal models, thermobaric ratio, plate tectonic indicators, age of crust, cooling rates, and mantle potential temperature) and some have compiled

these data together to make assertions about what it all means (Palin et al., 2020). Each one of these studies has looked at a small slice of the metamorphic record and each one applies the findings of previous studies to inform their own. These studies, however, have struggled with small datasets. There are likely trends seen in small datasets that will not be true for larger datasets. Sometimes small sets can allow spurious results by nature of having a small dataset.

Much of the previous discussion has centered around the evolution and onset of plate tectonics. Given the massive influence that plate tectonics has on the planet, it makes sense that is a key discussion. The metamorphic rock record provides probably the best opportunity to study the onset and nature of early plate tectonics and what could have happened before that.

It has been shown by Penniston-Dorland et al. (2015) that modern subduction zones have a thermobaric range much broader than previous compilations have suspected. This information should be brought to the interpretation of previous subduction zones.

This study sets to bring together many more samples from under-sampled areas and times, build a workflow for dT/dP categorization that more closely resembles petrological differences in metamorphic rocks, investigate metamorphic rocks in terms of spatial associations through the use of plate reconstruction modelling, and interpret the data in ways that are more geologically relevant than simple statistical correlations.

3 Methods

This project created a database using Microsoft Access for use with spatial and statistical analysis. In addition to the creation of a database, this project introduces updated methods for the analysis of the data and for the classification of dT/dP records.

3.1 Data Compilation and Storage: The MetRec Database

The MetRec database is built from previous compilations and has been supplemented with a large literature review (n = 571 samples). It combines records from three previous compilations and fills out the records with spatial data, uncertainties, and estimate methods for P-T and age. The MetRec database will be hosted through the University of Saskatchewan and will be available for updates through the university.

3.1.1 Database Structure

MetRec is a multi-table relational database, this means that it is composed of many data tables which are linked through relationships that tie different fields together across data tables.

This structure allows greater flexibility in extracting, sorting, and searching the data. MetRec has included fields for RecordID to organize records, to facilitate links to associated information, fields for the authorship of previous compilations, and separate fields for each reference. Names and descriptions of fields are summarized in Table 3.1, while relationships between data tables are illustrated in Figure 3.1.

Table 3.1 Summary of MetRec's fields grouped by overall goal of the field groupings.

Group	Data Field	Description
Sample Details	Locality	Long form description of the sample area.
	Craton	The craton from which the sample was taken, where applicable.
	Orogen	The orogen that the metamorphic event is associated with.
	Met Facies	The metamorphic facies of the sample as published by the researcher who studied the sample.
	Peak Assemblage	Indicator minerals which indicate a specific metamorphic grade.
	Peak Condition	Denotes if age, pressure, and temperature where all taken from the same sample or if the estimates for this record are aggregated from multiple samples in the same event.
	PT Path	If the sample experienced clockwise or counter-clockwise PT path.
Location	Latitude & Longitude	Latitude and longitude in decimal degrees (WGS 84).
	Lat/Long Uncertainty	Uncertainty for latitude and longitude in decimal degrees.
	Country	Country of origin.
	Continent	Continent of origin.
Age	Isotope system	The radiometric isotope system (*i.e.*, U-Th-Pb, Rb-Sr, K-Ar, etc.)
	Minerals analyzed	Minerals analyzed in age dating.
	Age	Age of sample (Ma).
	Uncertainties	Uncertainty of the age (2σ).
	Pre-peak Age?	Binary field denotes if age records pre-peak conditions. Only used in cases when reporting peak conditions is unavailable.
	Cooling Age?	Binary field denotes if age records post-peak cooling. Only used in cases when reporting peak conditions is unavailable.
	Isotope system	Radiometric isotope system used (*i.e.*, U-Th-Pb, Rb-Sr, etc.)
Temperature and Pressure Estimates	P-T estimates	Reported pressure and temperature estimates.
	P-T uncertainties	Uncertainties for pressure and temperature estimates.
	Ana/Met	Denotes whether analytical or methodological uncertainties are reported.
	Range	Binary field denotes that estimate was reported as a range.
	Minimum	Binary field denotes that the estimate was reported as a minimum value.
	Methods	Method used for the P-T estimates.
	Minerals analyzed	Focus minerals for P-T estimates.
	Chemical systems for phase equilibrium modelling	Mineral system for pseudo-section modelling (FMASH, KFMASH, MnKFMASHTiO, etc.)

	PT estimate datasets	Main reference used in the P-T estimate method.
	dT/dP	Calculated from the temperature estimate over the pressure estimate.
	dT/dP Uncertainty	Uncertainty calculated according to Roddick (1987).
	dT/dP Category	Categorizes for dT/dP: low, medium, high, and contact.
Refs	Main Reference	Main reference.
	Subsequent References	Subsequent references are split into their own fields to aid in searching and sorting.
	Compilation	Author of the originally compiled dataset.
Notes	Notes	Notes section mentioning anything not covered in previous fields.

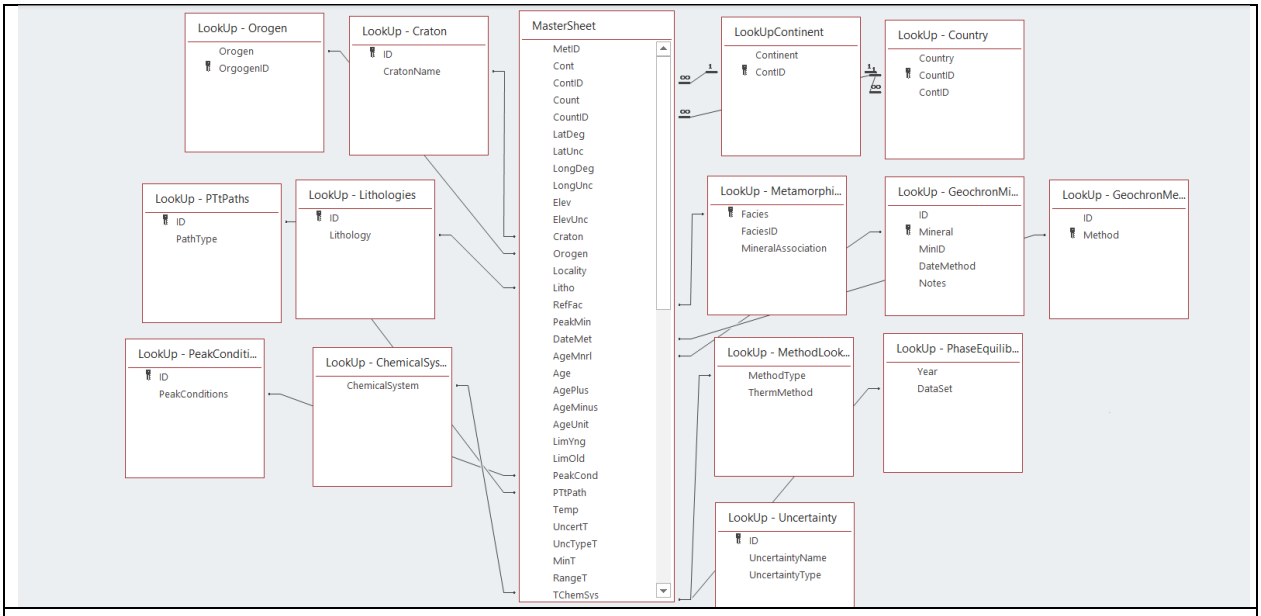

Figure 3.1 Structure of relationships between the multiple tables in the MetRec database. Titles of the table are at the top of each box. Lines connect one field to the coinciding field in another table. Relationships are either 1-to-1 or 1-to-many (symbolized with the '∞').

3.1.2 **Introducing New Fields**

In addition to the fields of previously published compilations, MetRec has added new fields. The MetRec database has added a number of new fields to previous compilations (PT estimate methods, age dating methods, and uncertainties, etc.) to aid in evaluating records,

sorting records, and for noting authorship and references of the compilations. The fields for the database are summarized in Table 3.1.

MetRec has added fields for the uncertainty (2σ) for the relevant fields: latitude, longitude, temperature, pressure, age, and dT/dP. The uncertainty for dT/dP is calculated from the uncertainties of temperature and pressure according to Roddick (1987).

3.1.2.1 Field Population Decisions

MetRec is populated from the published papers. When papers published more than one result for P-T-t estimates this project reported one to represent the sample. Pseudosection modelling took precedence over other methods where possible. Samples estimated by pseudosection modelling are marked in the database. Other estimate methods were taken on a case-by-case basis. With multiple papers, estimates from the newest paper were taken. Newest solutions models will incorporate updated mineral compositions and phase-stability which affects the pressure and temperature range for a given assemblage.

Pressure and temperature estimates are commonly reported as a range of values. Any time one of these values was reported as a range, that value was captured as halfway between the upper and lower end of the range. Uncertainties for ranges were reported as the difference from the halfway point to the end of the range (i.e. 500 – 600°C is reported as 550±50°C). Records whose values are reported as a range of values are marked under the "TRange" or "PRange" field (Table 3.1).

Uncertainties for pressure and temperature estimates are reported either as the assumed uncertainty published with a method (usually ±50°C and ±0.1GPa) or as the cited calculated analytical uncertainty. Analytical uncertainty was favoured, when available.

Latitude and longitude are stored in decimal degrees, with southern latitudes and western longitudes stated as negatives values. Latitude and longitude were taken from reported values where available. When reported, the available GPS coordinates are converted to WGS84 and reported with uncertainty ±0.000027°. Coordinate information was not provided for the majority of sample locations. In such cases, maps and diagrams were georeferenced. Location uncertainties for these samples were based on the scale of diagrams being georeferenced.

3.2 Analyzing Data

Analyzing data focused on two aspects: statistical analysis of the temperature, pressure, and dT/dP data as well as looking at spatial patterns in the data.

3.2.1 Software

IoGas is a plotting software for geochemical analysis. This study made use of the plotting features, including the ability to define polygons for diagrams which was used to categorize records.

ArcMap and ArcCatalog, part of the ArcGIS software package, were used to extract data from the database and plot onto georeferenced maps. This was used to assess data scarcity and identify areas of under- or over-sampling. Spatial joins were used to bind samples to an underlying polygon, in plate reconstructions, such as the Paleoplates model (Eglington et al., 2017; Evans and Eglington, 2022) (see 4.10 Spatial Associations) using GPlates software.

GPlates (https://www.gplates.org/) was used to visualize spatial interactions between records in the context of a plate reconstruction model. The plate reconstruction model is relative to mantle reference frame.

One limitation with plate reconstruction is the choice of plate reconstruction model. To combat this, this study has kept to those largescale accepted interpretations or interpretations which occur repeatedly throughout the model.

3.2.2 Nonlinear Categorization of dT/dP

This paper created petrologically meaningful categories for dT/dP, presented in Figure 3.2. The polygons shown follow the borders for a particular metamorphic facies, as defined by Zheng & Chen (2017), and the aluminosilicate polymorph boundaries defined by Pattison (1992). Using polygons instead of lines allows future workers much more flexibility in their interpretation and categorization.

Limitations with this approach include uncertainties with the metamorphic facies diagram - which is mostly relevant when samples plot next to a boundary, analytical uncertainties with the estimation of P-T-t, and uncertainties inherent to the estimation of P-T-t. There is currently no single diagram which would capture all aspects of the metamorphic process for all possible protoliths, but the metamorphic facies diagram covers many situations.

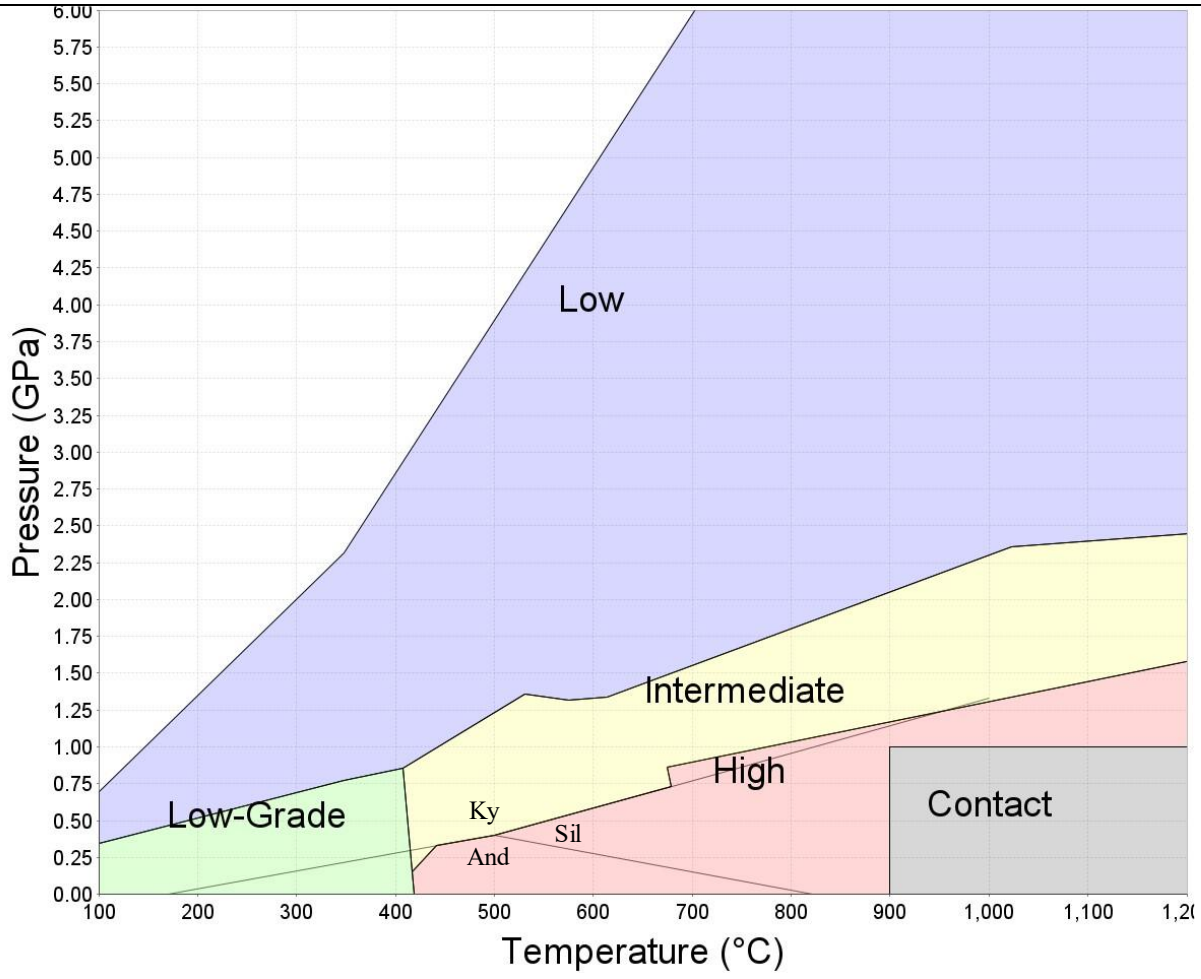

Figure 3.2 Polygonal classification for dT/dP used in this study. This classification is based on the shape territories of metamorphic facies and of the Ky-And-Sil aluminosilicate polymorph triple point. Green polygon represents Sub greenschist-Greenschist category, blue represents the low category, yellow represents the medium category, red represents the high category, and black represent the contact category.

3.2.3 **Averaging Oversampled Areas**

To mitigate oversampling, the study averaged samples for heavily studied areas into one record per event. An event is defined here as a grouping of records which are geographically close, share a geological unit, and share similar pressure, temperature, and age. For example: if we have 7 records marked ‘Unit X’ which are tightly grouped geographically and 6 of 7 are ~30-40 Ma and one is 80 Ma, then 6 records would be averaged to ‘Unit X (6 Samples)’ while the remaining sample is left alone.

The records which have been averaged remain in MetRec for reference and but are filtered out from weighted analysis. This process for the Alpine data is illustrated in Figure 3.3 for scale. Each group averaged is less than 100km across.

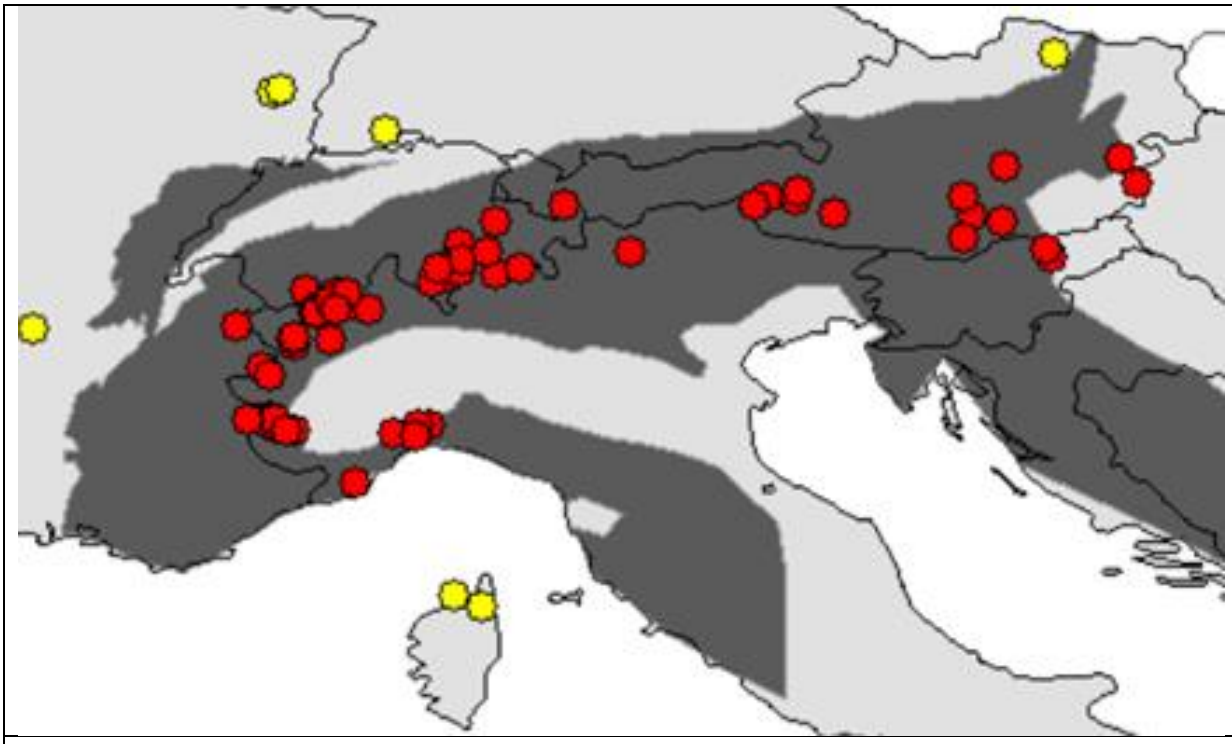

Figure 3.3 Polygon of the Alps, with Alpine samples shown in red. Samples outside of the Alps are shown in yellow. The incredible density of sampling within the Alps is greater that any other area and is a prime target for averaging of heavily studied areas.

Limitations with this process include the subjectivity of creating groups. The decision of this study has been to average judiciously and allow "singular" events to have multiple samples where it is not egregiously clear that there is oversampling. This mitigates concerns surrounding averaging too often or when it is not called for.

3.2.4 Spatial Associations and GDU/SuperGDU's

The main driving for non-contact metamorphism is the collision of tectonic plates as they travel horizontally across the globe. As such, an understanding – qualitative and quantitative – of the positioning and interactions between protocontinents, continents, supercontinents, and other (ribbon terranes, etc.) is imperative to understanding the secular trends in metamorphism.

This study utilized the modelling of Nguyen (2019) to address the total area of geodynamic units (GDU) and collated GDU's which move as one for a period of time

(SuperGDU). A superGDU is a group of GDU's which move together for a period time. In geological terms, a GDU represents a block of rock, while a SuperGDU represents the continental rocks which make up a plate. Oceanic crust is not considered or modelled beyond what oceanic crust survives today. Each GDU is a singular shape file representing one set of geologically continuous rock from the same time period. This work was done largely in GPlates, mentioned earlier.

The two main characteristics of SuperGDU's looked at in this study are those of SuperGDU area and the total number of SuperGDU's. This shows us the size of blocks moving together (during continental accretion the size of the largest SuperGDU will increase because the growing supercontinent will be the largest SuperGDU). The total number of SuperGDU's shows the number of independently moving blocks at any one time. During accretion this number will drop as more GDUs are amalgamated to the supercontinent. During times of continental breakup, SuperGDU count will increase as more and more blocks are moving independently.

3.2.5 Eschewed Metamorphic Samples

This study has not added any samples from known contact metamorphism but has created a polygon to mark contact metamorphic samples from previous compilations.

This study has chosen to include lower crustal and mantle xenolith samples. They are marked in the database under the field "Xeno" to allow future workers to filter them out as necessary.

Following the practice of other published compilations, this study has chosen not to add greenschist samples to the database because they are less diagnostic of tectonic process. There is a greenschist category to mark those samples, previously compiled, which fall under the sub-greenschist/greenschist facies. Because many terranes will retrograde and have overprinting metamorphism, there are many samples which prove to be too difficult to unravel at this time.

MetRec also contains records which act as place holders for future records. These placeholders are records which contain a significant amount of data for analysis but perhaps miss something important: typically, either age data, a PT-estimate, or location data. All reasonable efforts were taken to fill all data cells. When data uncertain, that is noted either in the uncertainty cell or in the note if required. These data were used where possible (i.e. a record with good PT-estimates and age data but no location data would have been used for statistical plotting but not

spatial associations). It total, 76 records are missing locations, 46 are missing ages, and 34 are missing PT-estimates, which leaves 1025 records which contain all three of these key areas. These records have been eschewed from analyses where appropriate but will remain to hopefully be filled out later when more data are available.

4 Results

The two main avenues of this study include: the construction of a multi-table relational database (MetRec) and the findings derived from the literature review and data analysis. Sections 4.1 and 4.2 provide an overview of the results of the literature review to the database (temporal and spatial coverage of the data) and highlights the key contributions made compared to previous compilations. Sections 4.3, 4.4, and 4.5 the ranges and broad trends of age, pressure and temperature, and dT/dP data. Section 4.6 presents the results of averaging records from the Alps and China, as described in section 3.2.3 (Averaging Oversampled Areas). Sections 4.7 to 4.9 analyze the data in terms of metamorphic facies, upper and lower plate classifications, and supercontinent cycles, respectively.

4.1 Spatial Coverage

Through the inclusion of previously under-used datasets (i.e. (Penniston-Dorland et al., 2015)) and a comprehensive literature review, MetRec increased the number of samples in the dataset by nearly double (n = 1037). It was also able to double the sample density for the North and South American cordilleras, which had a dearth of data.

The goal to enhance the amount of data captured for each record was achieved by reviewing the reference papers of previous datasets (refer to section 3.1.2 Introducing New Fields). A comparison of new fields to the field previously published is summarized in tables at the beginning of each heading. MetRec significantly augmented the quantity of location data available for each record, resulting in improved accuracy and user-friendliness.

Table 4.1 Comparison of location data captured by MetRec and previous compilations.

Previous Compilations:	MetRec Compilation:
• Location • Latitude • Longitude	• Continent • Country • Orogen • Location • Latitude • Longitude • Latitude Uncertainty • Longitude Uncertainty

Table 4.1 illustrates the amount of additional data for each record when compared to previously published datasets while Figure 4.1 compares the spatial distribution of samples of previous compilations and MetRec. Under-sampled areas and orogens were the main focus, as can be seen in Figure 4.1. It is important to acknowledge that the current geography does not reflect the paleogeography of past continents and supercontinents. However, meticulous efforts have been made to identify records from orogens that would have represented those ancient orogens. The objective is not to achieve a visually dense map of present-day records, but rather to accurately represent paleo-orogens. It should be noted that South America remains under-sampled and will be a priority for future research endeavors.

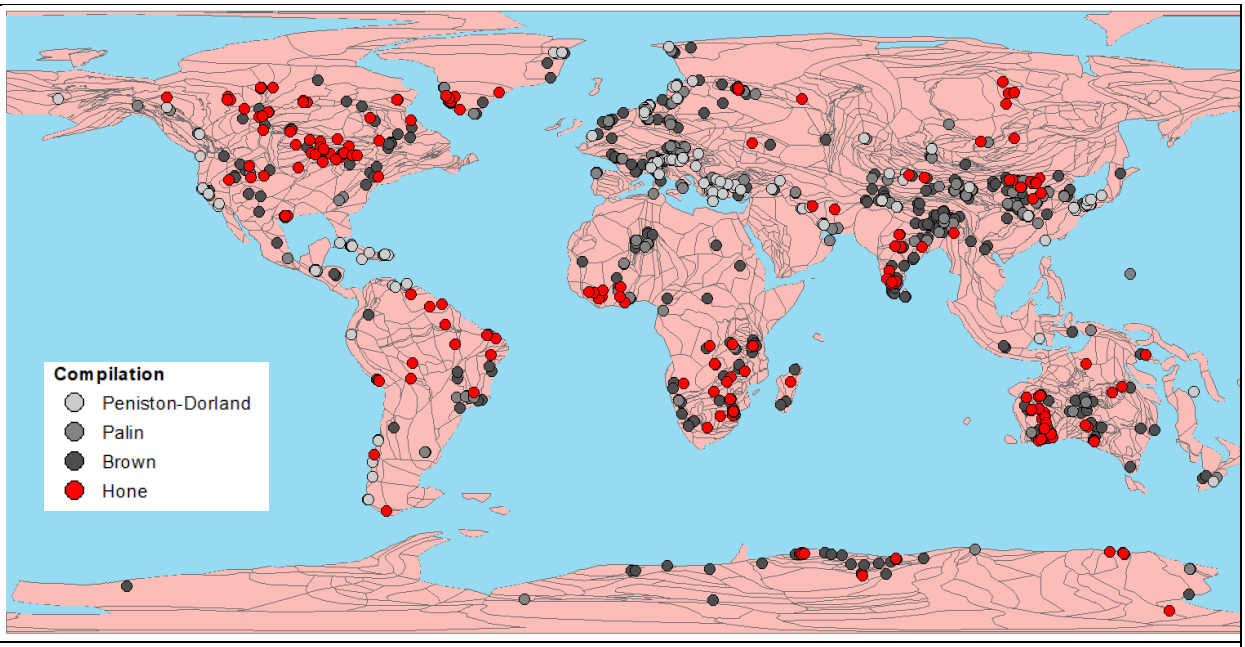

Figure 4.1 Comparison of data published in MetRec and datasets previously published. Grey circles are records from previous compilations. Red circles are what has been added by this study. Background polygons taken from the Paleoplates model (Eglington et al., 2017; Evans and Eglington, 2022).

Table 4.2 provides a comparison of record density between MetRec and previous studies for specific orogens. The focus of the project was not on areas that already had extensive coverage (e.g., the Alps), but even in those regions, the record density has increased due to the inclusion of available data. The methodology described in section 3.2.3 (Averaging Oversampled Areas) was employed to average samples in these oversampled regions (not shown on this map which includes all samples).

Table 4.2 and Table 4.3 clearly demonstrate a significant disparity between well-sampled orogens and those that are more challenging to access or sample. When comparing the sampling density of the Alps to the global average, it is evident that the Alps are sampled approximately 56 times more densely than the global average. This highlights the discrepancy in sampling efforts between different regions and emphasizes the need for further attention to under-sampled orogens.

Table 4.2 Comparison of the number of records to the areal extent of large orogens. This table shows the density of records in some different orogens across the planet.

Orogen	# of Records (Previous / MetRec[total data])		Area km^2	Records per 100,000 km^2 (Previous / MetRec [total data])	
Himalaya	37	42	2510104	1.47	1.67
Alpine	25	72	254194	9.83	28.23
SAM Cordillera	5	13	3051784	0.16	0.42
NAM Cordillera	12	22	2910841	0.41	0.75
Rest of the World	552	810	174469153	0.31	0.46

Table 4.3 A comparison of the record density for different orogens against the record density of the Alpine record density. The Alps normalized column shows how many records the Alps would need to achieve the same density as the orogen in the lefthand column. The Normalized to Alps column shows the number of records that other orogens would need to achieve the same record density as that of the Alps. The third column contrasts the previous density requirements with the reality of previous datasets and the MetRec database.

Area	If one sampled the Alps as densely as…	Sampled as Densely as Alps...	Current Samples (Previous / MetRec [total data])	
Himalayas	4.25	711	37	42
SAM Cordillera	1.08	864	5	13
NAM Cordillera	1.92	824	12	22
Rest of the World	1.18	49’418	552	810

4.2 **Temporal Coverage**

The inclusion of uncertainty, minerals and isotope systems analyzed significantly enhances the temporal information associated with individual records. As shown in

Table 4.4, this update includes the addition of age uncertainties, as well as the minerals and isotope systems used to determine the dates. Figure 4.2 shows a map of the location and distribution of Phanerozoic and Precambrian records across the planet.

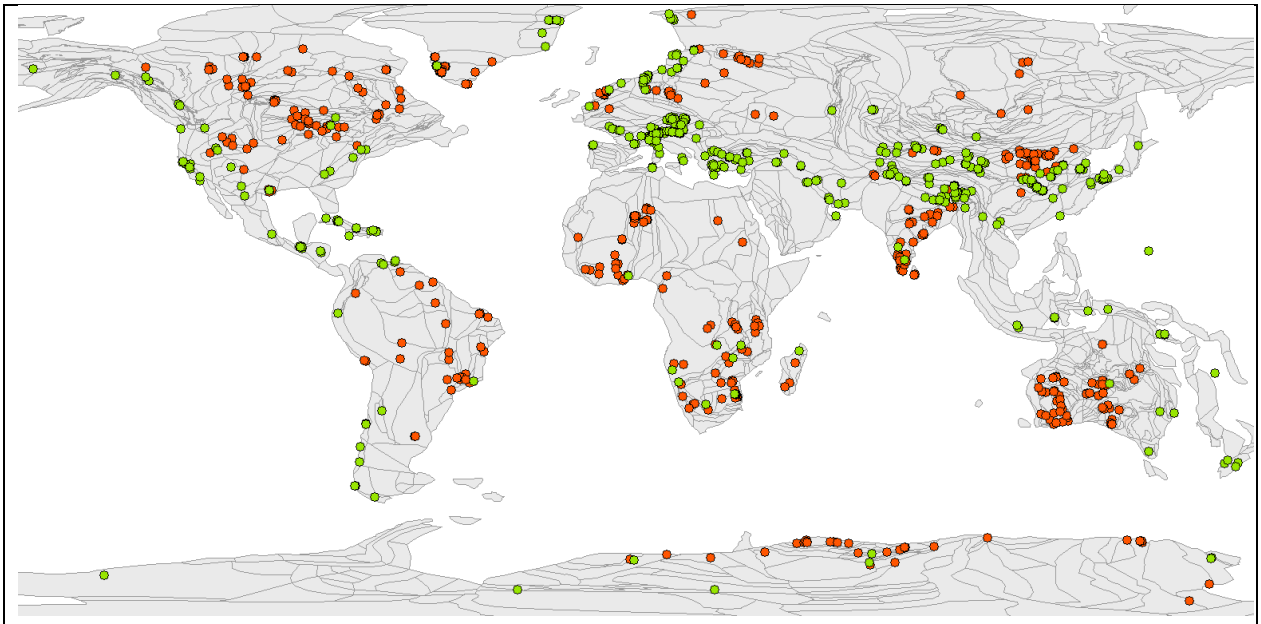

Figure 4.2 Spatial distribution of total MetRec records against continental blocks from the Paleoplates Model (Eglington et al., 2017; Evans and Eglington, 2022).. Greem = Phanerozoic records. Orange = Precambrian records.

Table 4.4 Comparison of age data captured by MetRec and previous compilations.

Previous Compilations:	MetRec Compilation:
• Age (Ga)	• Age (Ma) • Age Uncertainty • Mineral Analyzed • Isotope System • Pre-peak Age • Cooling Age

Figure 4.3 displays a histogram illustrating the density of records over time. The records from Penniston-Dorland (2015) have been integrated into the comprehensive database, where previously only specific records had been included in previous compilations. In this study, additional records from the literature review are highlighted in red. Specifically, 98 Archean records, 84 Proterozoic records, and 4 Phanerozoic records were incorporated as part of this study's contribution to the database. This increase in records numbers across different time

periods enhances the temporal coverage and improves the overall representation of geological eras in the dataset.

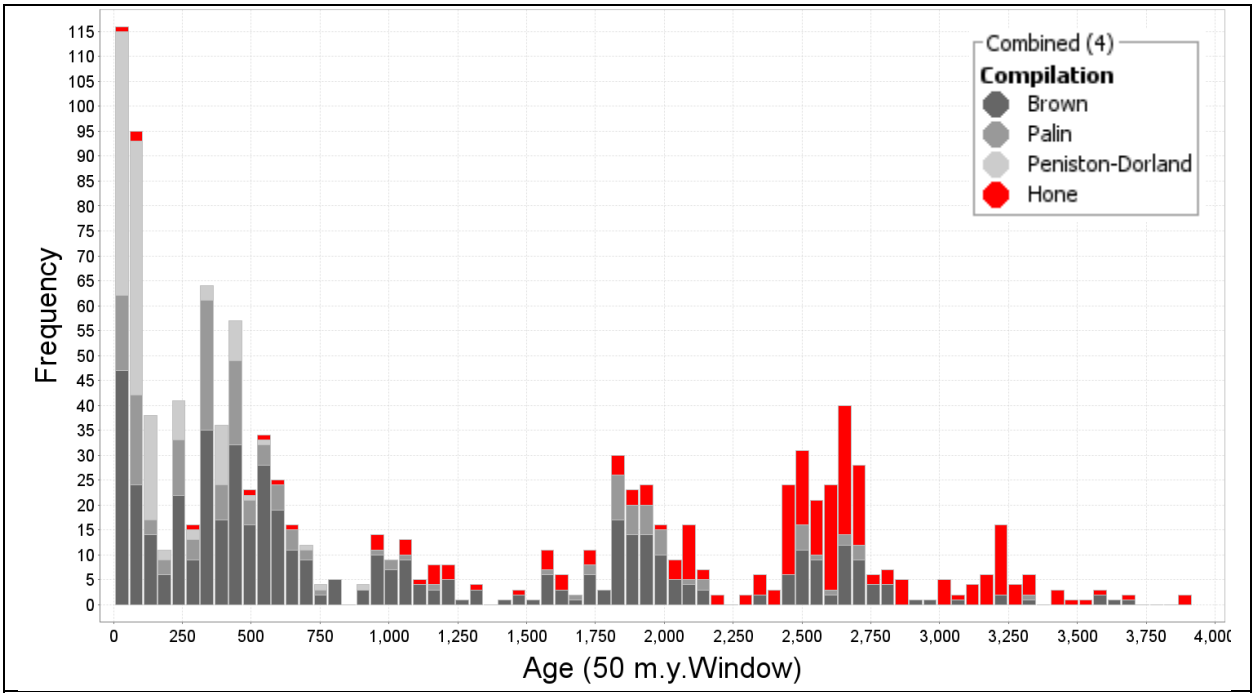

Figure 4.3 Histogram of records from MetRec by age. Records are colour according to legend, with red records showing the addition of records from this study's literature review. N = 1025 (Previous compilations = 755, Literature Review = 270 records).

4.3 **Age**

The dates in the MetRec database range from 3917 Ma to present. The uncertainties associated with age estimates vary from ±0.01 Ma (33.5 Ma, Ar^{40}-Ar^{39} on phengite) to ±127 Ma (689 Ma, U-Pb, zircon metamorphic rim). Figure 4.4 illustrates the frequency of the age data. Spikes appear in the data around 3200 Ma, 2750-2500 Ma, 2000-1800 Ma, 1250-1000 Ma, 600-300 Ma, and 50-0 Ma.

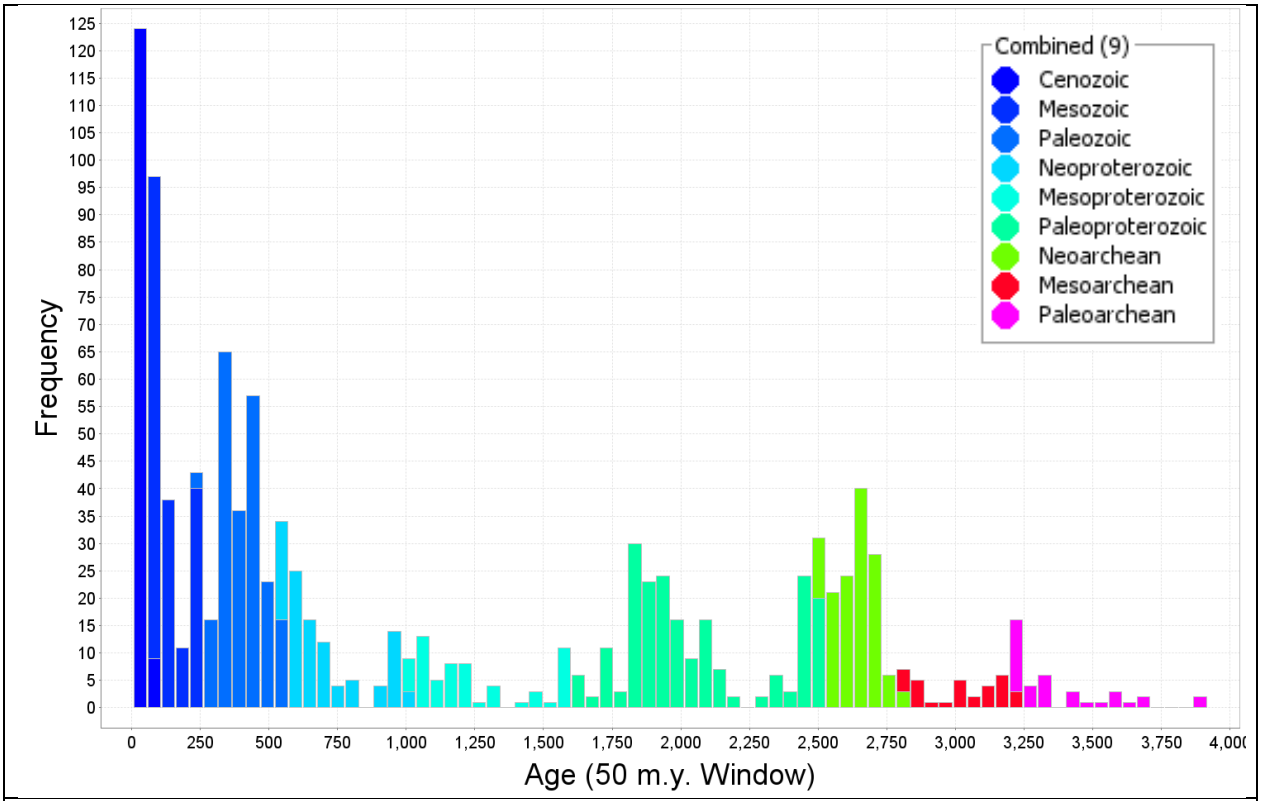

Figure 4.4 Histogram of ages for all records in MetRec with 150 m.y. windows.

Figure 4.5 presents heatmaps of dT/dP through time. The heatmaps highlight clusters of data that emerge during different times. In the Precambrian, notable clusters are observed around 3250 Ma, 2500 Ma, 2000 Ma, 1000 Ma, and 600 Ma. These clusters are interspersed with periods of relatively less data density or "stillness." In contrast, the Phanerozoic data displays clusters that are broader and more tightly clustered. These clusters are particularly evident between 500-300 Ma, approximately 235 Ma, and between 175-25 Ma. The wider and flatter nature of these clusters in the Phanerozoic era suggests a more continuous and extended range of dT/dP values compared to the distinct clusters observed in the Precambrian but the much greater number of samples can’t be discarded.

A)

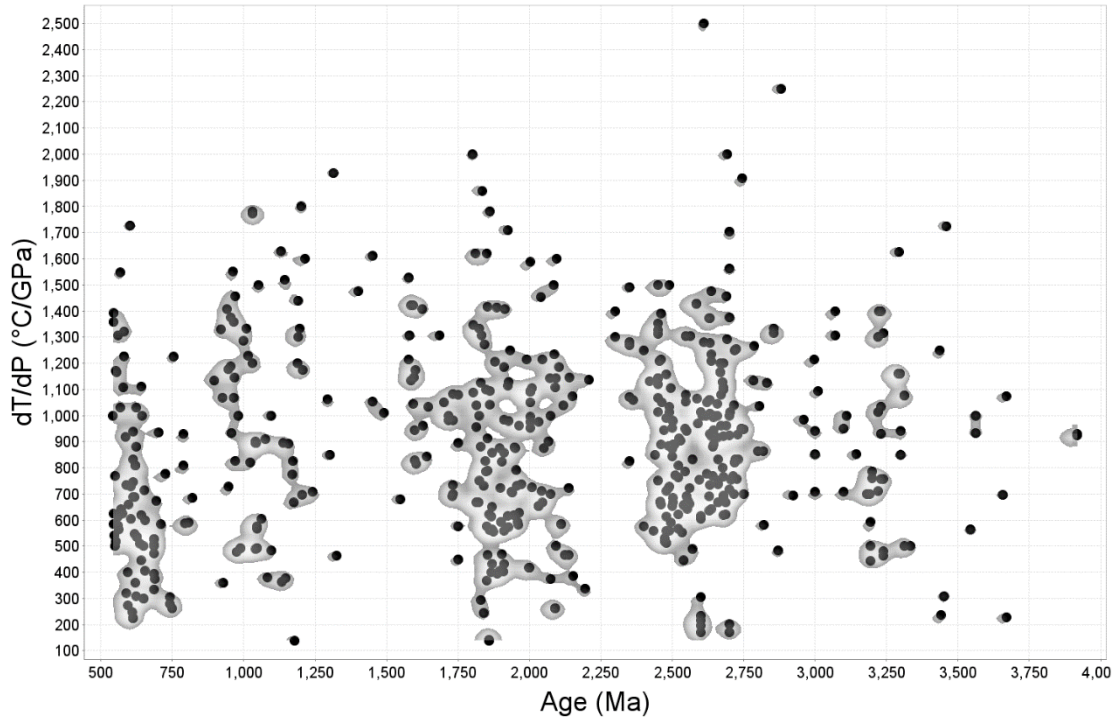
dT/dP (°C/GPa)
2,500
2,400
2,300
2,200
2,100
2,000
1,900
1,800
1,700
1,600
1,500
1,400
1,300
1,200
1,100
1,000
900
800
700
600
500
400
300
200
100
500
750
1,000
1,250
1,500
1,750
2,000
2,250
2,500
2,750
3,000
3,250
3,500
3,750
4,00
Age (Ma)

B)

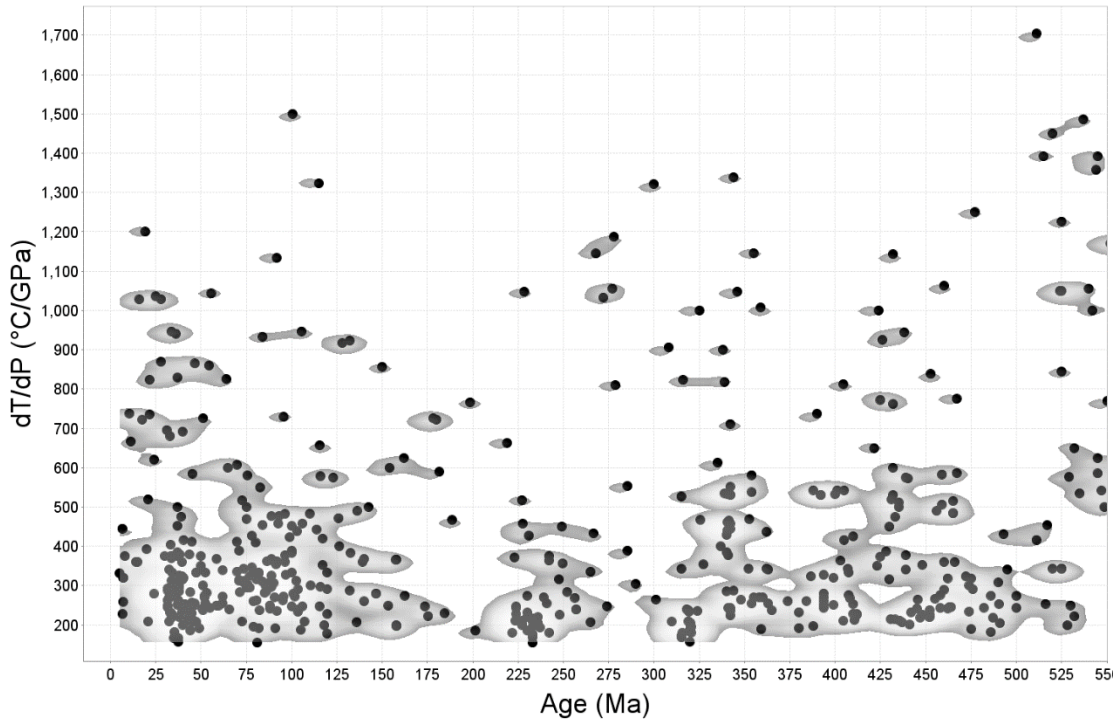
dT/dP (°C/GPa)
1,700
1,600
1,500
1,400
1,300
1,200
1,100
1,000
900
800
700
600
500
400
300
200
0
25
50
75
100
125
150
175
200
225
250
275
300
325
350
375
400
425
450
475
500
525
55
Age (Ma)

C)

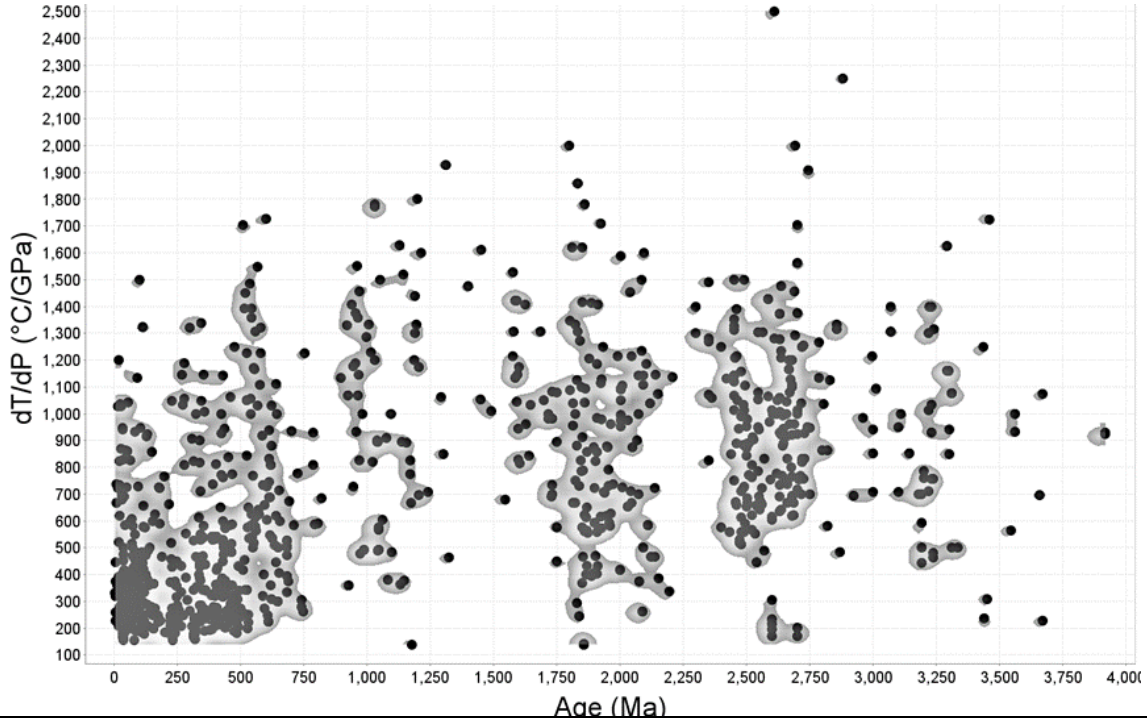

Figure 4.5 Heatmaps for dT/dP records through time. Time slices are arranged from youngest to oldest: A) Precambrian, B) Phanerozoic, C) All Data.

4.4 Pressure & Temperature

Table 4.5 provides a comparison of the temperature and pressure data captured by MetRec with previous compilations with the main addition being the inclusion of uncertainties and the estimate method.

Table 4.5 Comparison of temperature and pressure data captured by MetRec and previous compilations.

Previous Compilations:	MetRec Compilation:
• Temperature (°C) • Pressure (GPa)	• Temperature (°C) • Pressure (GPa) • Temperature Uncertainty (°C) • Pressure Uncertainty (GPa) • Uncertainty Type • Estimates minimum temperature/pressure? • Reported as range? • Chemical System (Pseudosection) • Geotherm/geobarometer • Estimate Method • Pseudosection Dataset

4.4.1 **Pressure**

The pressure data in the MetRec database exhibits a range from 0.2 GPa to 7 GPa. The uncertainties associated with pressure estimates vary from ±0.01 GPa to ±1.5 GPa, which can be compared with assumed pseudosection modeling uncertainty (±0.1 GPa.).

Figure 4.6 illustrates the distribution of pressures across different geological eras and the Phanerozoic. Looking at the Precambrian, median pressure increases from 0.79 GPa in the Paleoarchean to 1.15 GPa in the Neoproterozoic. These increases oscillate slightly but remain largely stable. The box representing the 50% of data shows relatively little change as well. The upper range of outliers increases from 5 GPa in the Paleoarchean to 6.5 GPa in the Neoarchean and further to 7 GPa in the Paleoproterozoic. The range of the upper whiskers increases from 1.35 GPa in the Paleoarchean to 2.35 GPa in the Neoproterozoic and the lower range of pressure estimates exhibits a slower increase, ranging from 0.2 GPa in the Paleoarchean to a high of 0.55 GPa in the Neoproterozoic. In contrast, the Phanerozoic data shows a median of 1.85 GPa, upper whisker range of 4.3 GPa, , and a lower range 0.42 GPa.

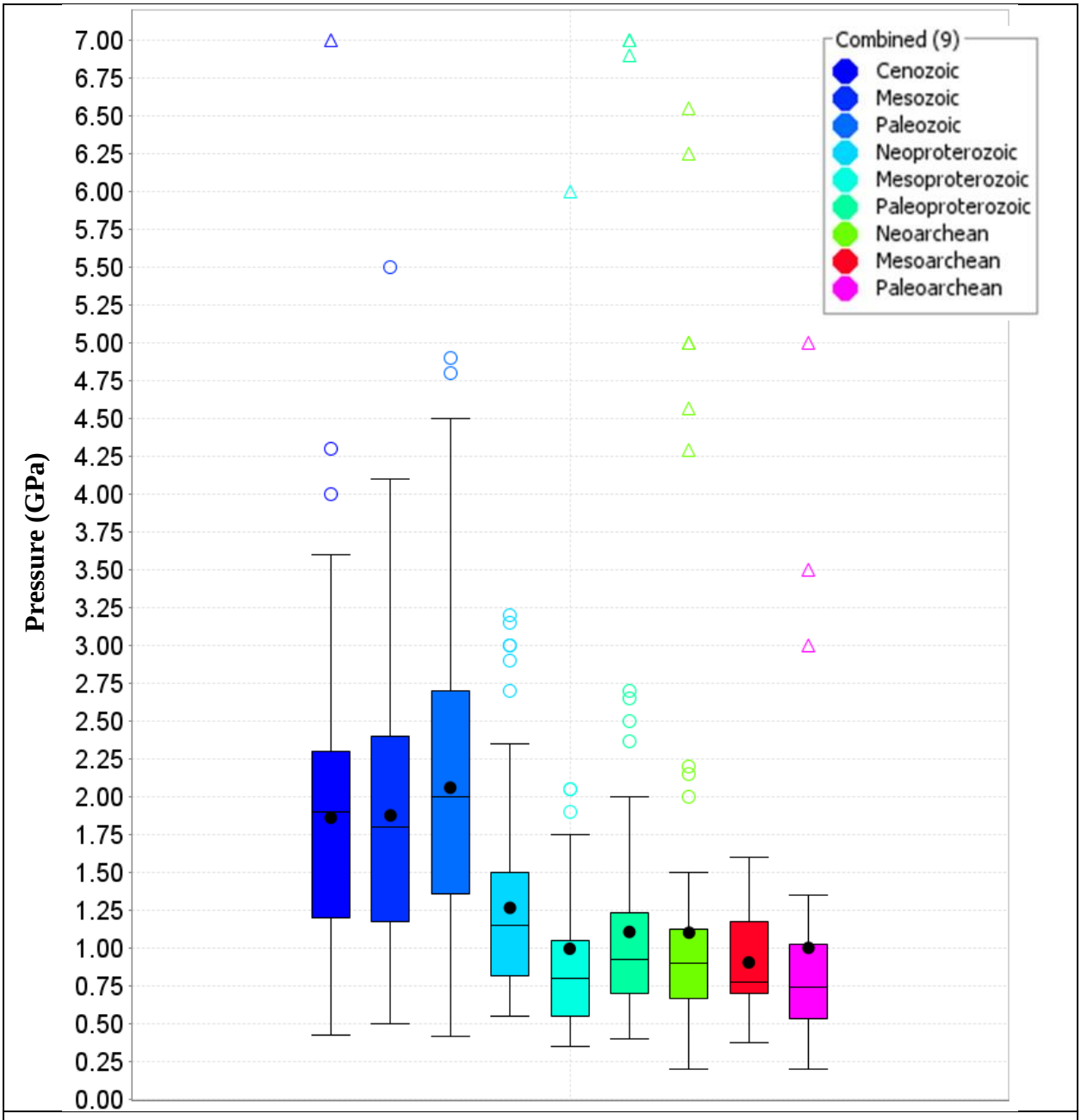

Figure 4.6 Box and whisker plot of pressure estimates for all samples in MetRec. Black circle represents the mean. Black line represents the median. Central box is the middle 50% of data. Circles are data that is further than 1.5 times distance the from the box. Triangles is more than 3 times distance from the box. The Whiskers are the extreme values that are not outliers (i.e. outside the 50% box but less than 1.5 times distance from the box).

Figure 4.7 depicts the frequency distribution of pressure data for the Phanerozoic and Precambrian records. The range of most Phanerozoic pressure data is broader than that of the

Precambrian data. Phanerozoic data ranges from 0.5 - 7 GPa with most data from 0.75 - 2.5 GPa. The Precambrian data ranges likewise from 0.2 - 7 GPa except that most data ranges from 0.5 - 1.5 GPa.

A)

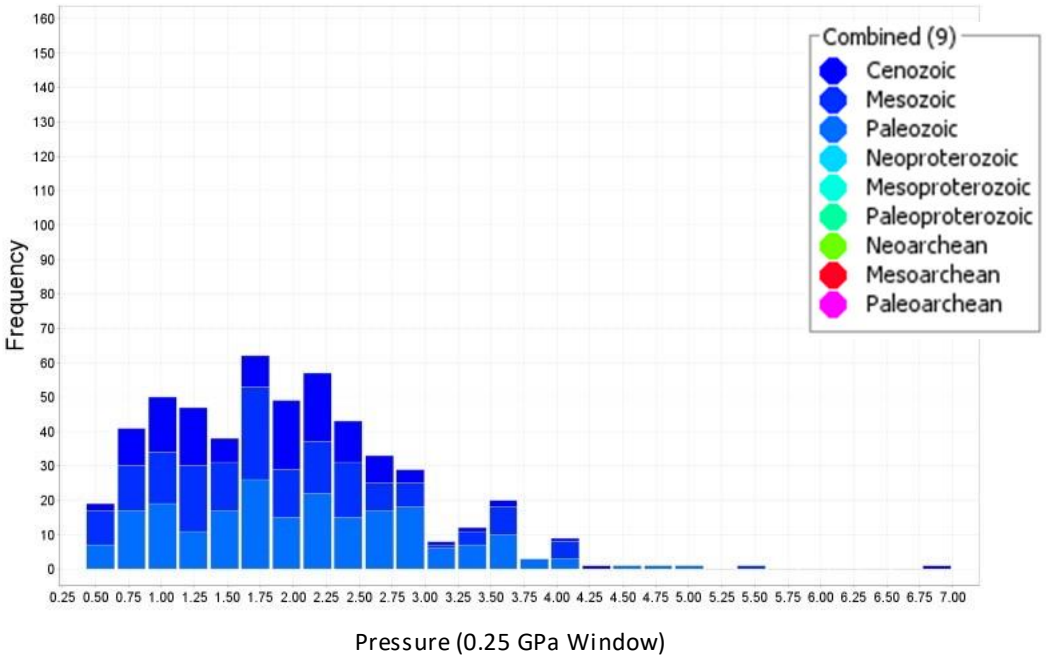

B)

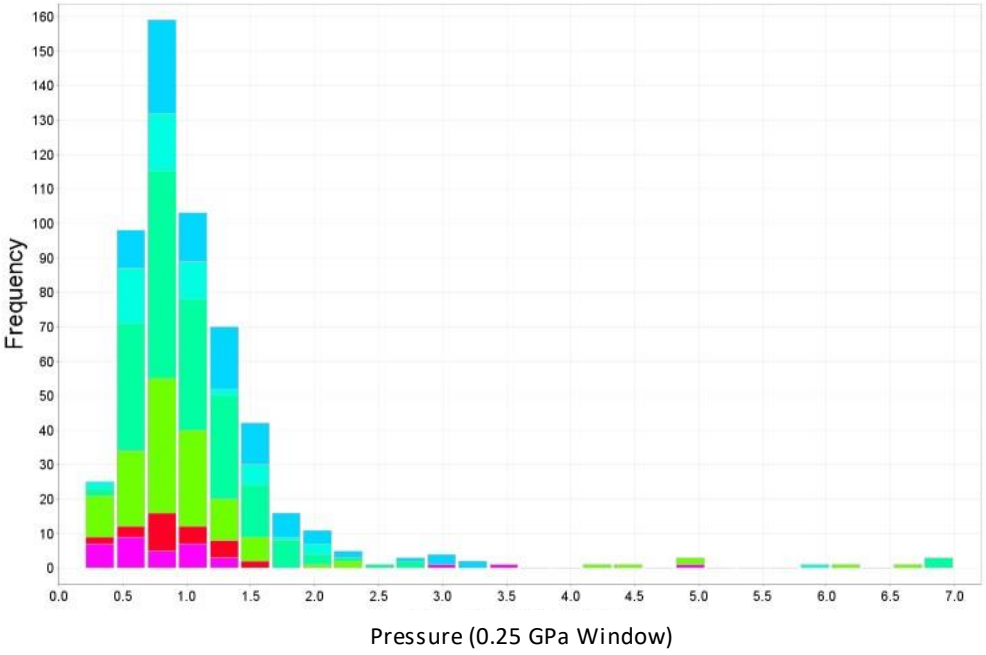

Figure 4.7 Histogram of pressure estimates for A) Phanerozoic and B) Precambrian records.

Figure 4.8 illustrates the range of pressure uncertainties at different pressures. 50% of all records are more certain than ± 0.3 GPa and 99% of the records are more certain ± 0.5 GPa.

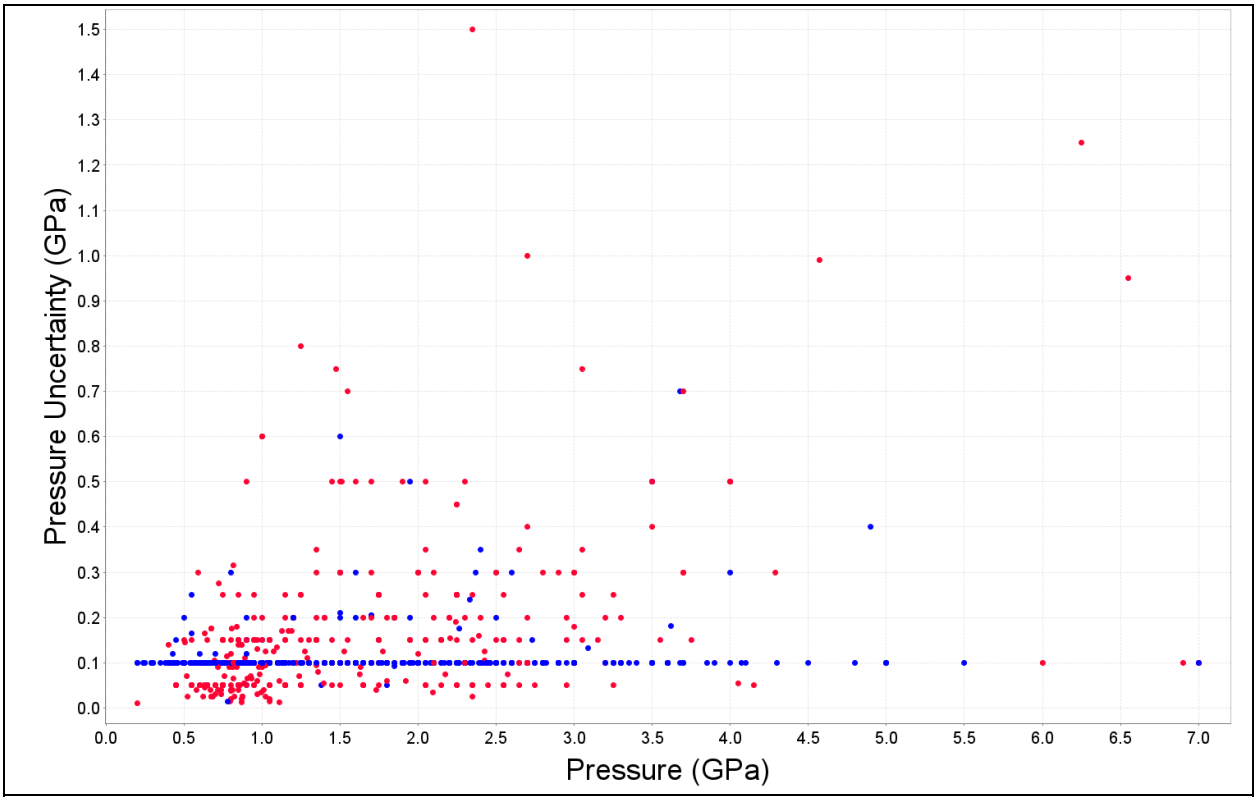

Figure 4.8 Pressure Uncertainty (GPa) against pressure (GPa) for all MetRec samples. Samples are divided into two categories: blue (assumed method uncertainty) and red (reported analytical uncertainty). See 3.1.2 Introducing New Fields for explanation of uncertainty types.

4.4.2 **Temperature**

Temperature estimates in the database range from 190 °C to 1254 °C. Temperature uncertainties range from ± 2.5 °C (572.5 °C) to ± 200 °C (800 °C). Uncertainties for pseudosection modelling are conventionally agreed to be ± 50 °C.

Figure 4.9 shows a box and whisker plot illustrating the ranges of temperature estimates across different geological eras. For the Precambrian, median values show a gradual increase from ~675 °C in the Paleoarchean to the Neoproterozoic (~800 °C), where the median temperature reaches a plateau until the Phanerozoic. The boxes, representing the central 50% of the data, follow a similar trend to the median values, indicating little change within these temperature ranges across the respective eras. The upper whiskers of the plot fluctuate between

930 °C in the Paleoarchean and 1124 °C in the Neoarchean. The lower whiskers show a steady rise from 345 °C in the Paleoarchean to 450 °C in the Neoproterozoic.

In the Paleozoic era, the median temperature drops to ~723 °C, further decreasing to ~570 °C in the Cenozoic era. The lower whiskers are much lower than in the Precambrian (275 °C, 234 °C, and 255 °C in the Paleozoic, Mesozoic, and Cenozoic eras, respectively).

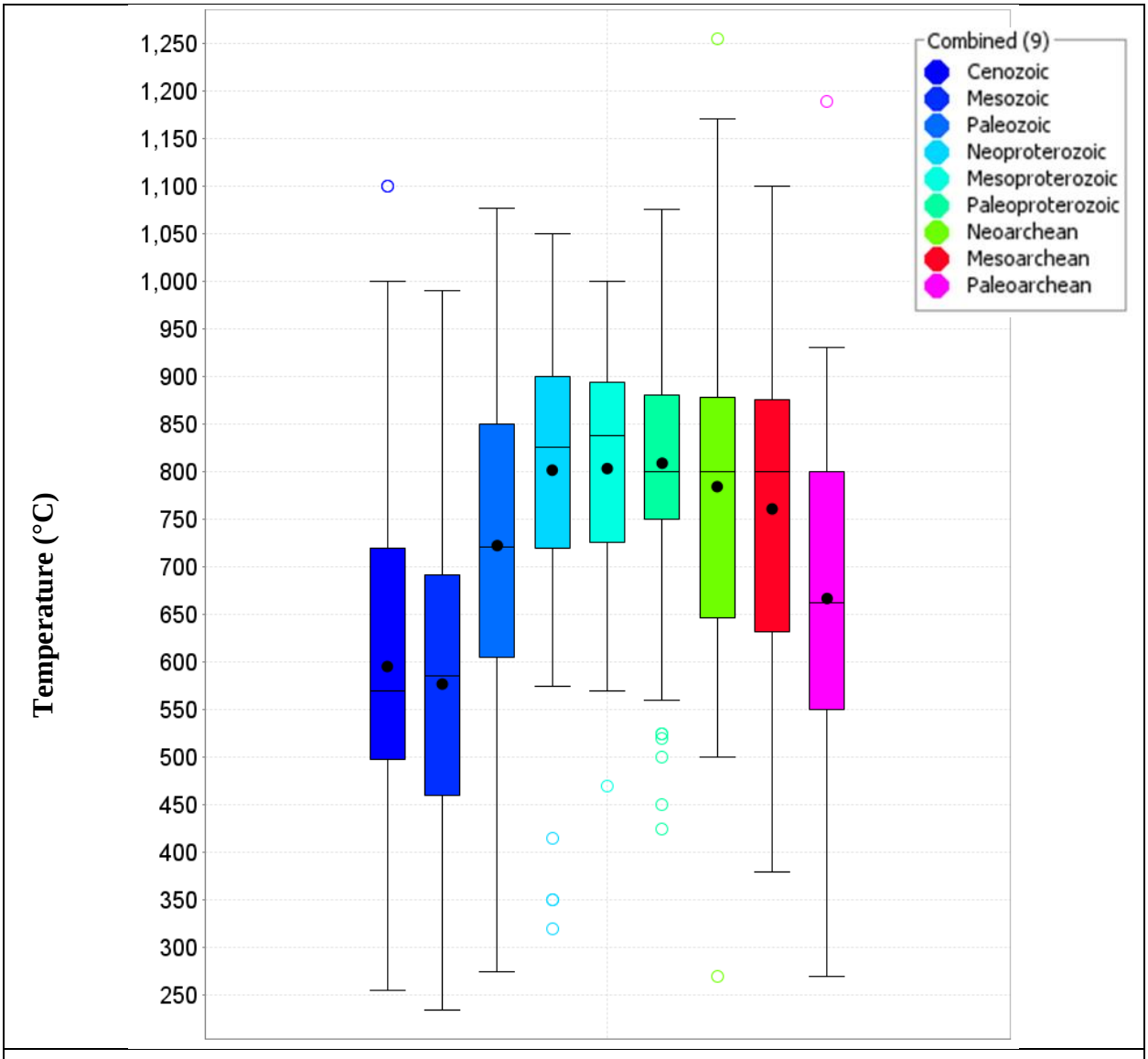

Figure 4.9 Box and whisker plots for temperature estimates for all records from MetRec. Black circle represents the mean. Black line represents the median. Central box is the middle 50% of data. Circles are data that is further than 1.5 times distance the from the box. Triangles is more than 3 times distance from the box. The Whiskers are the extreme values that are not outliers (i.e. outside the 50% box but less than 1.5 times distance from the box).

In Figure 4.10, the frequency of temperature estimates is depicted for both Phanerozoic and Precambrian data. The range of temperatures is the same between Phanerozoic and Precambrian data (250 – 1200°C). For the Phanerozoic data, the distribution is relatively well spread across the entire temperature range. There are noticeable spikes in frequency around 550 °C and 725 °C. In contrast, the Precambrian data exhibits a more tightly clustered distribution around 825 °C.

A)

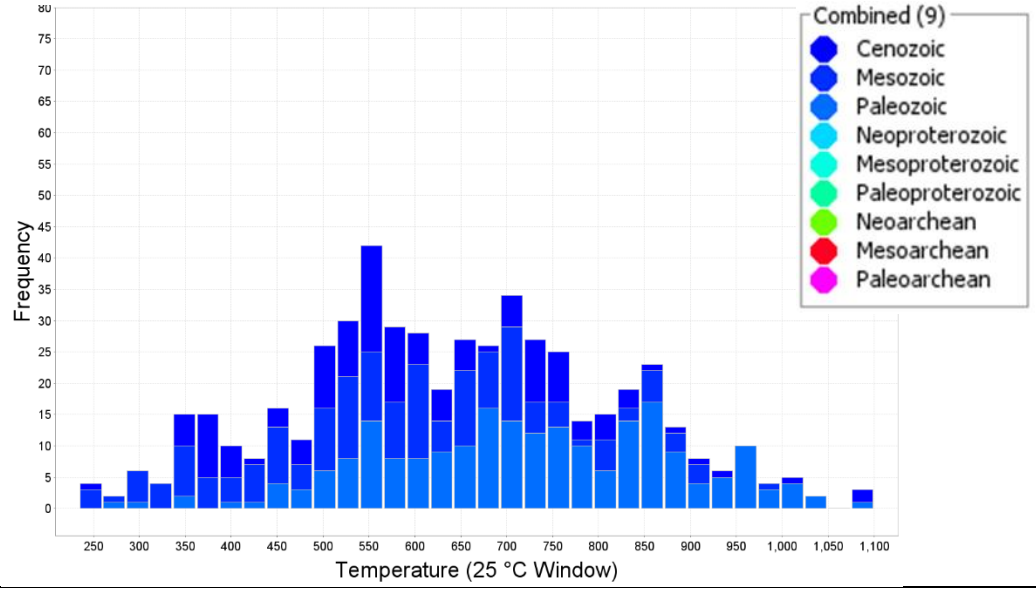

B)

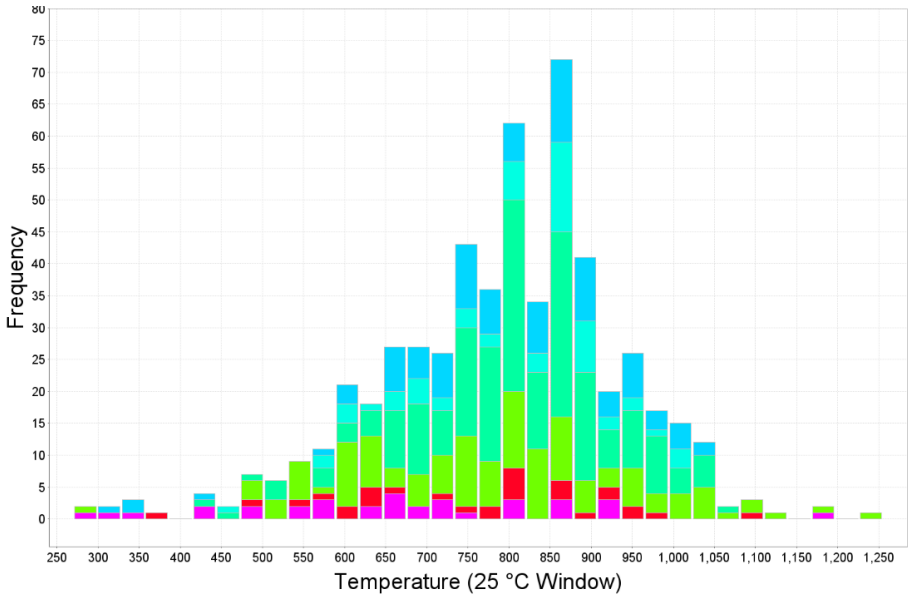

Figure 4.10 Histogram of temperature estimates for A) Phanerozoic data and B) Precambrian data.

Figure 4.11 illustrates the range of temperature uncertainties at different pressures. 50% of all records are more certain than ± 65 °C and 99% of the uncertainties are more certain than ± 100 °C.

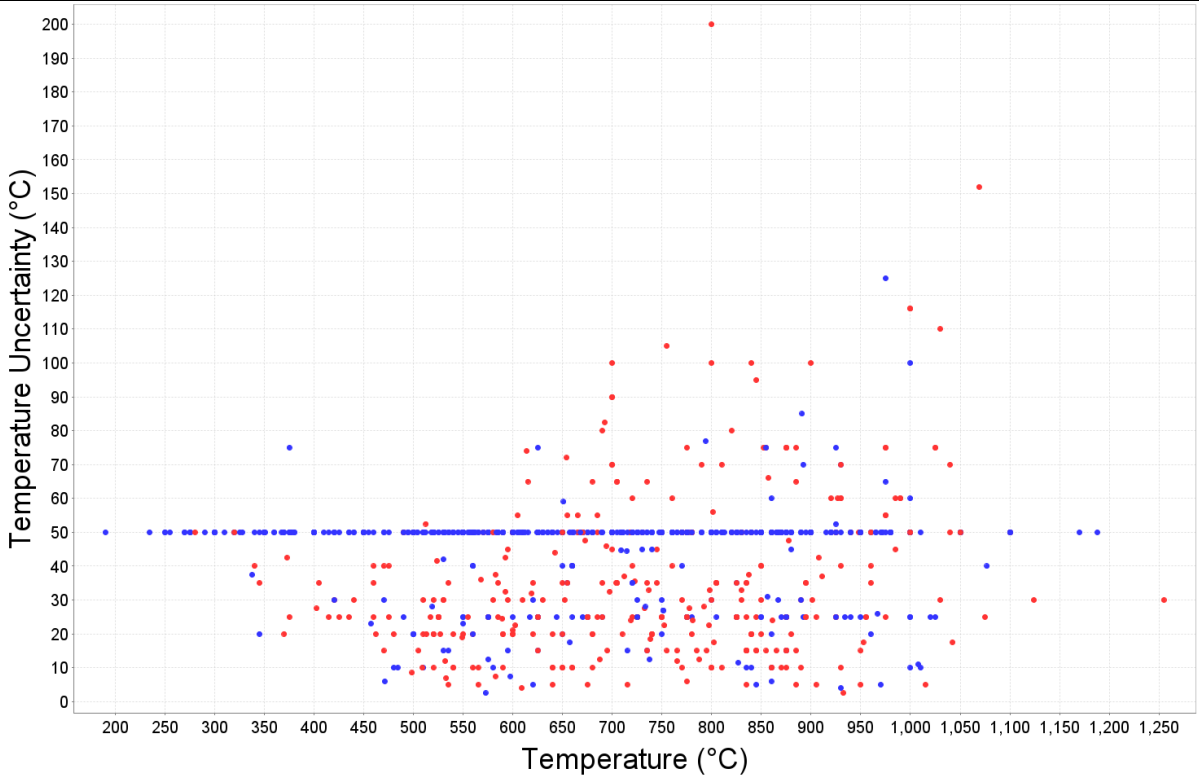

Figure 4.11 Temperature Uncertainty (°C) against temperature (°C) for all records in MetRec. Samples are divided into two categories: blue (assumed method uncertainty) and red (reported analytical uncertainty). See 3.1.2 Introducing New Fields for explanation of uncertainty types.

4.5 **dT/dP**

The records in the MetRec database range from 137 to 3525 °C/GPa. The uncertainties associated with dT/dP estimates vary from ±2.70 to ±1361 °C/GPa (a discussion of dT/dP uncertainty calculation can be found in 5.7 dT/dP Uncertainties and Pseudosection Modelling).

Since dT/dP is a calculated value from temperature and pressure, the main addition to the previous MetRec database has been dT/dP uncertainty.

Table 4.6 Comparison of dT/dP data captured by MetRec and previous compilations.

Previous Compilations:	MetRec Compilation:
• dT/dP (°C/GPa) • Type • PTt Path Type	• dT/dP (°C/GPa) • dT/dP Uncertainty (°C/GPa) • PTt Path Type

Figure 4.12 plots dT/dP broken down by geological era. The median values for dT/dP exhibit relatively stable temperatures around 850-950 °C/GPa from the Paleoarchean to Paleoproterozoic eras, then there is an increase in median dT/dP to 1010 °C/GPa during the Mesoproterozoic era. From there, a downward trend in median dT/dP can be observed, with values decreasing from 1010 °C/GPa to 300 °C/GPa during the Cenozoic era.

The upper whiskers demonstrate significant variation across the eras. Starting with 1725 °C/GPa in the Paleoarchean, then drops to 1333 °C/GPa in the Mesoarchean before increasing to 1926 °C/GPa in the Mesoproterozoic era. Subsequently, there is a decrease in the upper whisker to 774 °C/GPa during the Cenozoic era.

The lower whiskers of each era remain relatively stable throughout the examined periods. They show little variation from the Paleoarchean to the Cenozoic, ranging from 139 °C/GPa to 444 °C/GPa, with a median value of approximately 157.8 °C/GPa.

An observation regarding the scarcity of data for the Archean era is significant. As a result of this data imbalance, there are nearly as many outliers for the Cenozoic era as there are for the entire Paleoarchean era. This imbalance in data distribution between different geological eras can have implications and will be further discussed in 5.1 Temporal Data Imbalances.

Figure 4.13 plots the frequency of dT/dP calculations for each era. The Precambrian data displays a relatively even distribution across a range of values, with a central tendency around 700-900 °C/GPa, while the Phanerozoic data exhibits a more concentrated cluster around 300 °C/GPa, indicating a narrower range of temperature variations in response to pressure changes during this era. The distribution of Phanerozoic data rapidly thins out beyond this initial spike.

Figure 4.14 demonstrates a strong correlation between dT/dP and their associated uncertainties. The plot reveals that records with lower dT/dP values tend to have lower uncertainties, whereas records with higher dT/dP values exhibit greater uncertainties. This correlation is somewhat expected due to the nature of the dT/dP uncertainty equation (See 5.7 dT/dP Uncertainties and Pseudosection Modelling for a full discussion of that) in that the magnitude of dT/dP is a factor in determining dT/dP uncertainty.

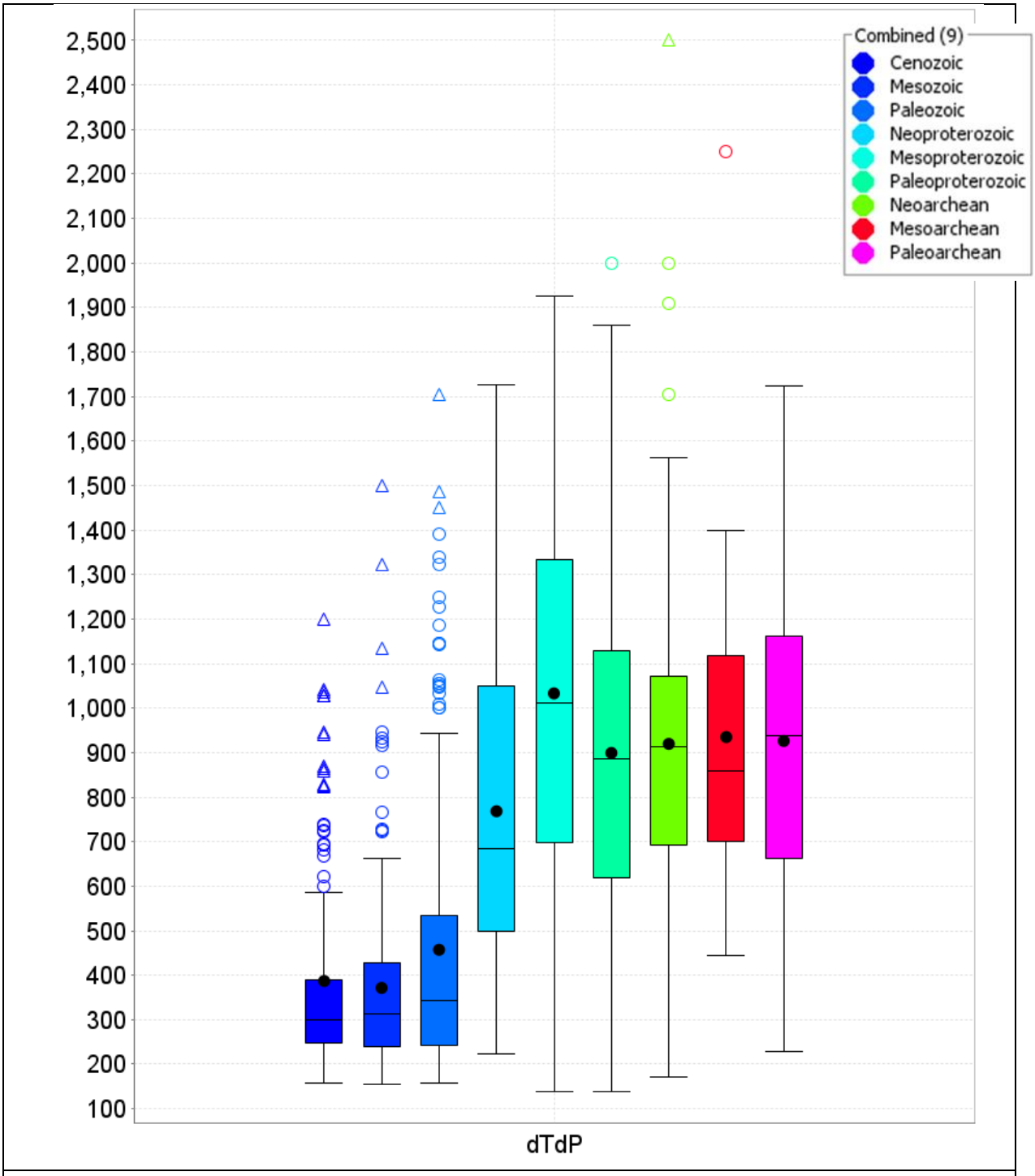

Figure 4.12 Box and whisker plot of dT/dP for all MetRec samples (eschewing one record at 3525 °C/GPa) divided by geological era. Black circle represents the mean. Black line represents the median. Central box is the middle 50% of data. Circles are data that is further than 1.5 times distance the from the box. Triangles is more than 3 times distance from the box. The Whiskers are the extreme values that are not outliers (i.e. outside the 50% box but less than 1.5 times distance from the box).

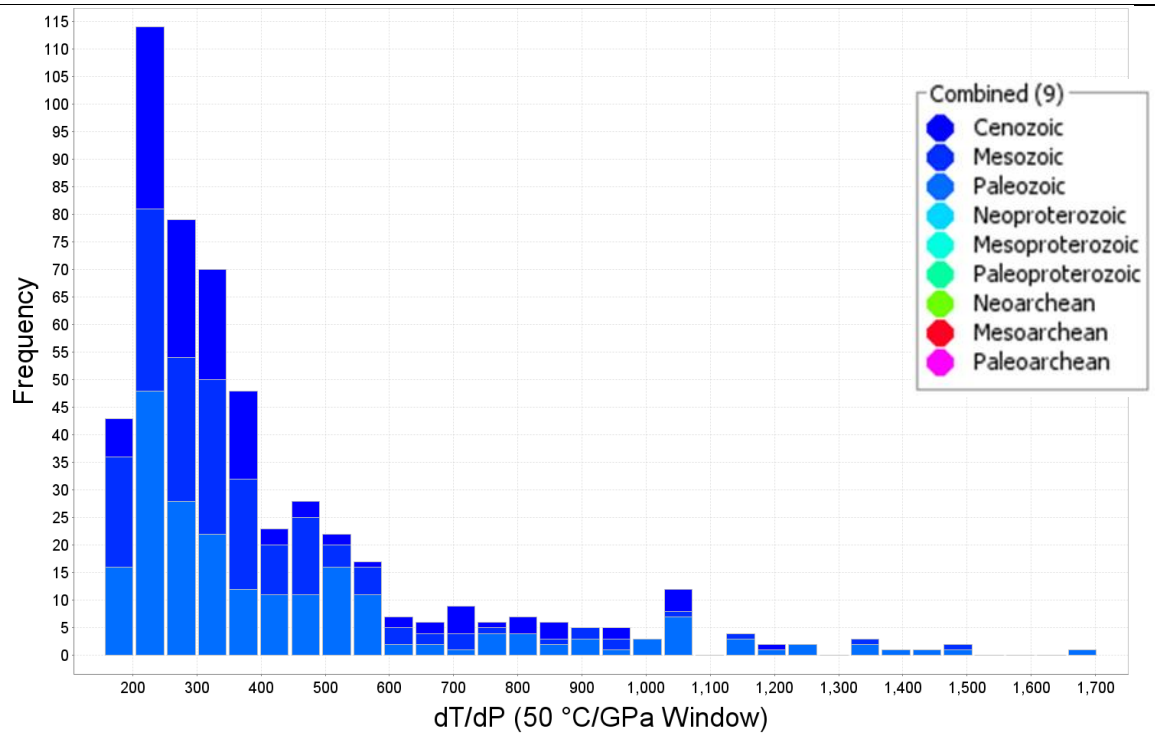

A)

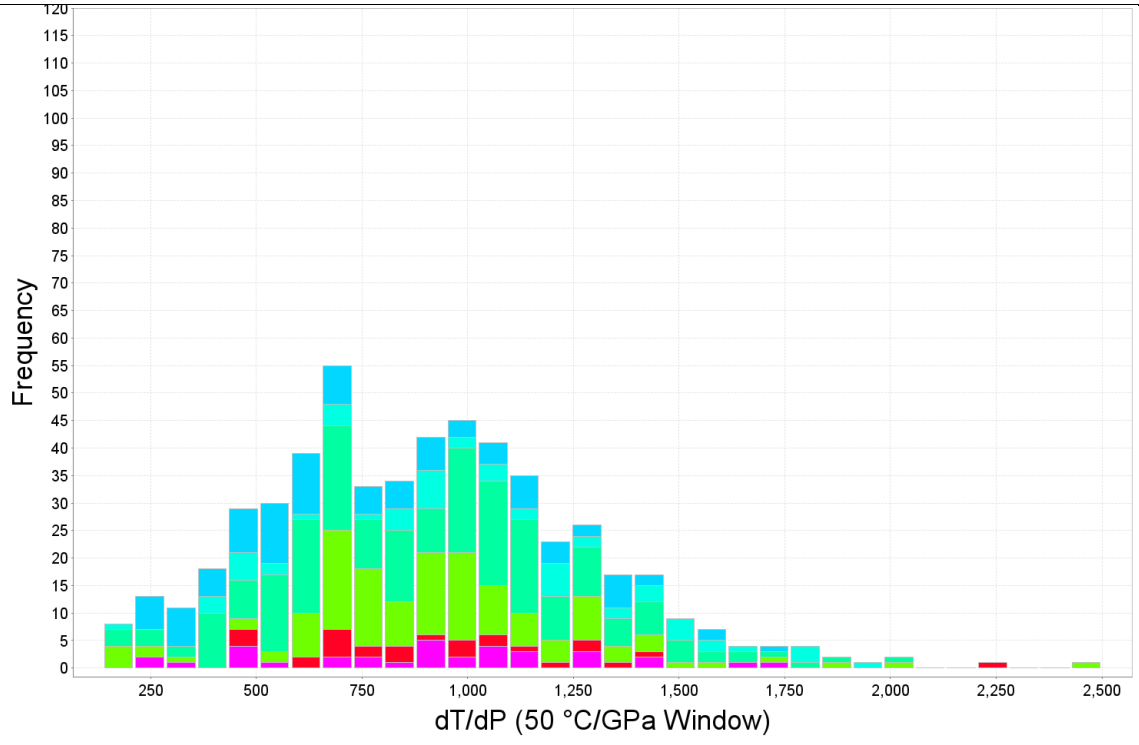

B)

Figure 4.13 Histogram of dT/dP (°C/GPa) distribution for all MetRec records. A) Phanerozoic and B) Precambrian.

The range of dT/dP uncertainties for records with quoted uncertainties is observed to be between 2.707 and 588 °C/GPa. Records with assumed uncertainties exhibit a wider range of uncertainties, spanning from 7.41 to 1361 °C/GPa.

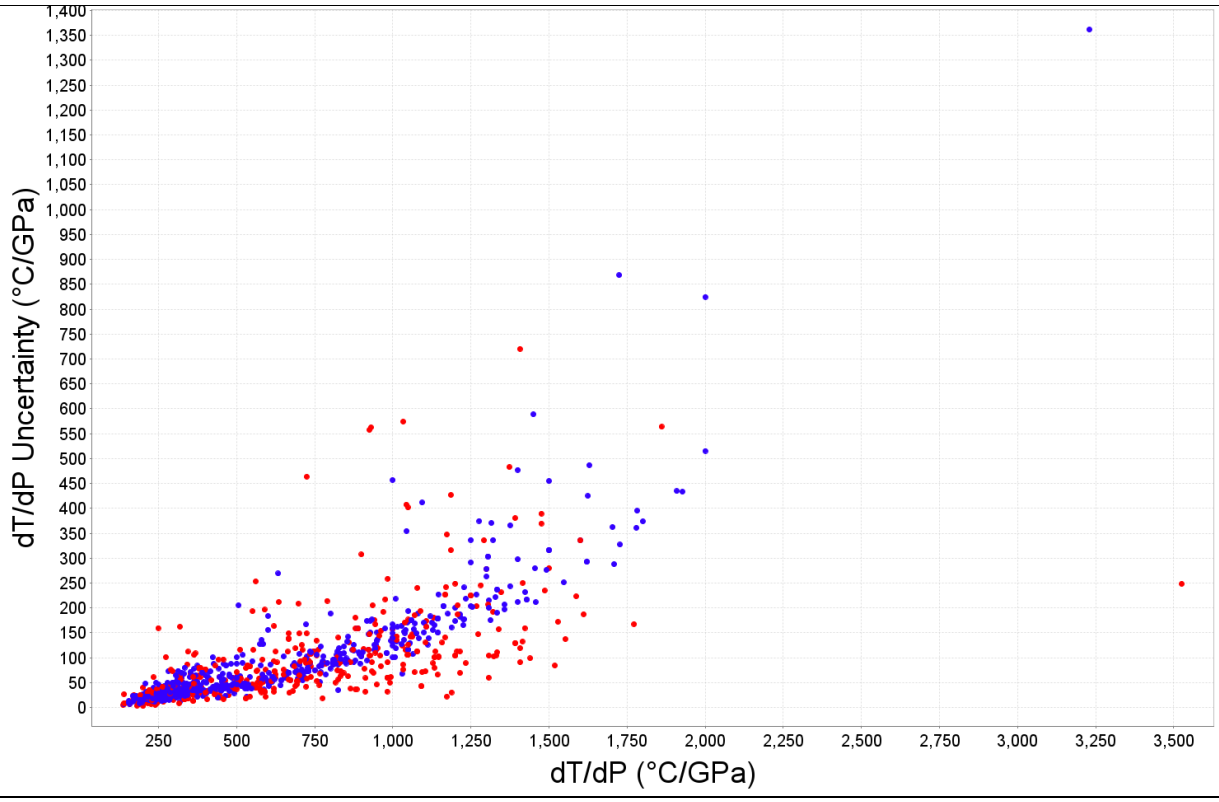

Figure 4.14 dT/dP Uncertainty (°C/GPa) against dT/dP (°C/GPa) for all MetRec samples. Samples are divided into two categories: red (method uncertainty) and blue (analytical uncertainty). See 3.1.2 Introducing New Fields for explanation of uncertainty types.

Figure 4.15 illustrates dT/dP through time using the updated polygonal classification scheme, showcasing the overlapping nature of records with different classifications in the dT/dP space. It is important to note that this overlap occurs because the polygonal classification considers pressure and temperature as independent parameters rather than a ratio between them. Consequently, certain sections, such as the high and contact groups, as well as the medium and low-grade groups, exhibit overlapping records. In this context, the figure highlights that some records initially classified as medium dT/dP may represent low-grade greenstone-associated rocks, which some authors might exclude from the medium dT/dP category. The updated

polygonal classification reveals a greater number of records falling into the low category as we go back in time.

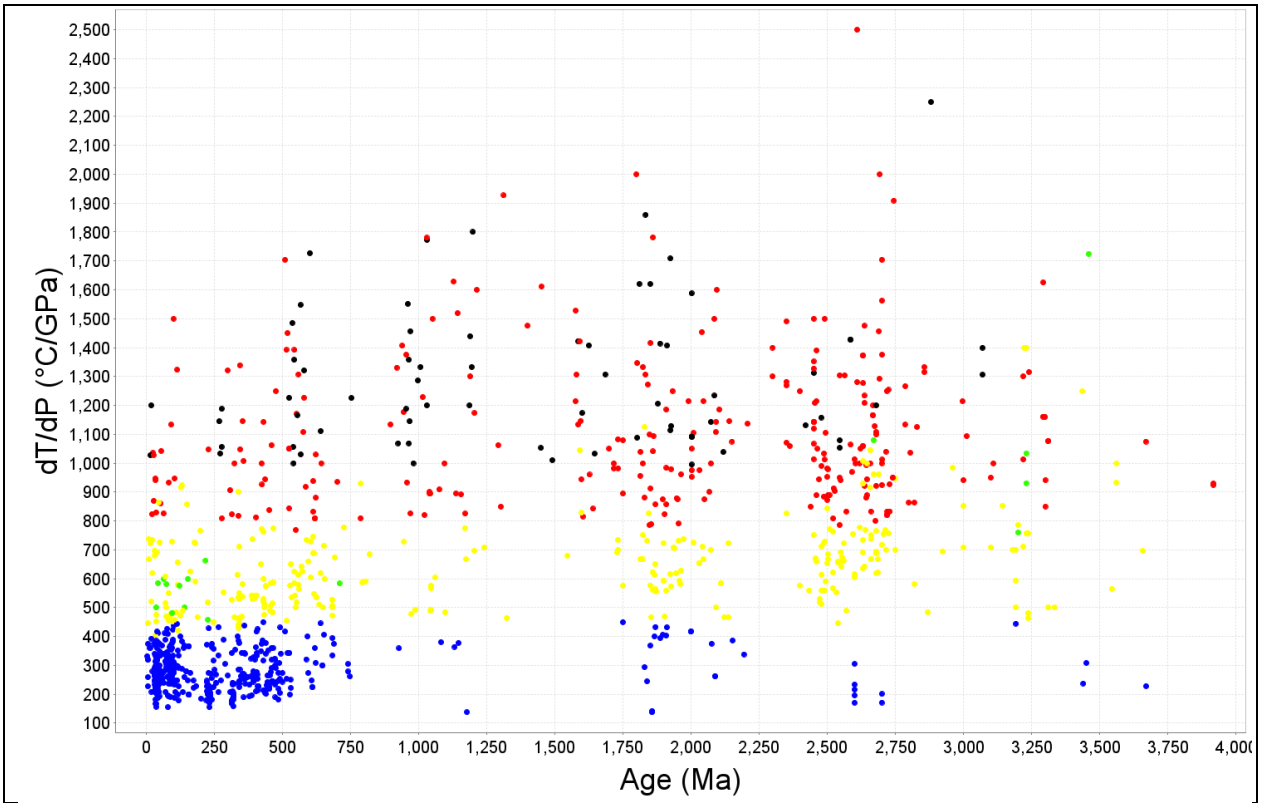

Figure 4.15 dT/dP (°C/GPa) through time for all MetRec records. Records are coloured according to the polygonal classification scheme discussed in 3.2.2 Nonlinear Categorization of dT/dP.

Figure 4.17 provides an overview of the distribution of records in PT-space by geological era. Despite the relatively small datasets available, the Neoarchean era exhibits a wide range of metamorphic facies, encompassing all major facies except for blueschist. The presence of greenschist, prehnite, and pumpellyite facies is not observed in the available records (which is expected, see 3.2.5 Eschewed Metamorphic Samples). Eclogites are intermittent in the record, appearing in alternate eras. Blueschist is observed from the Neoproterozoic era and continues until the present day.

A) Paleoarchean

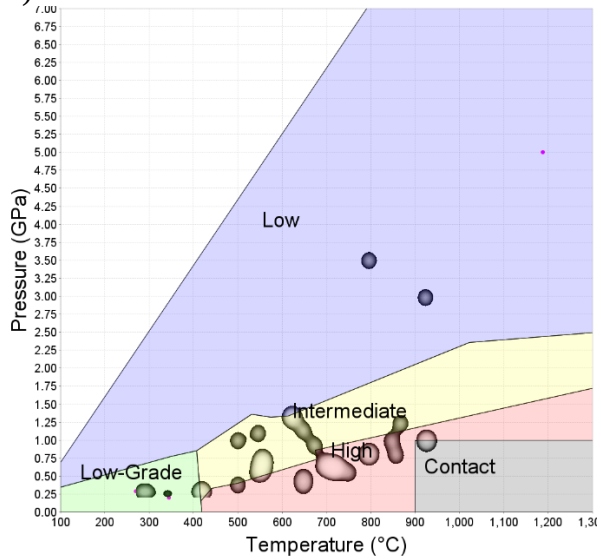

B) Mesoarchean

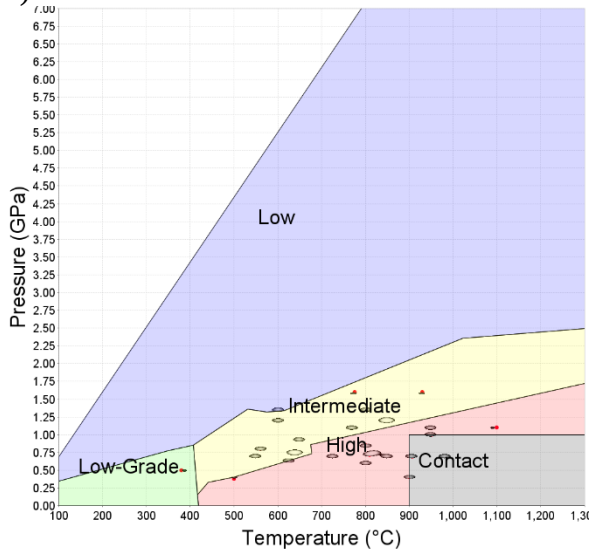

C) Neoarchean

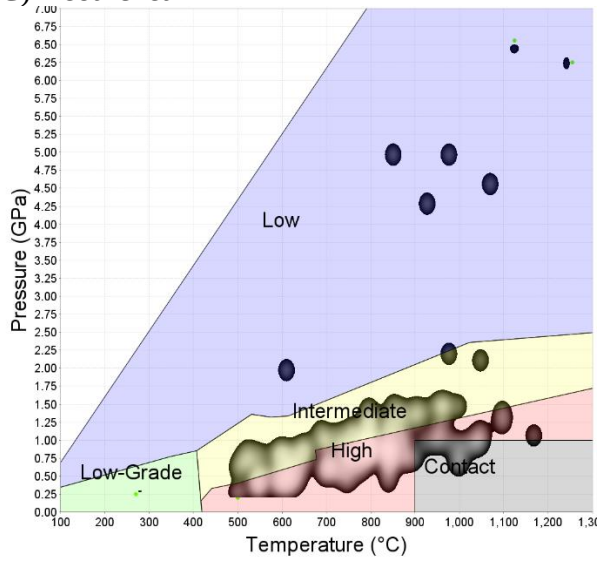

D) Paleoproterozoic

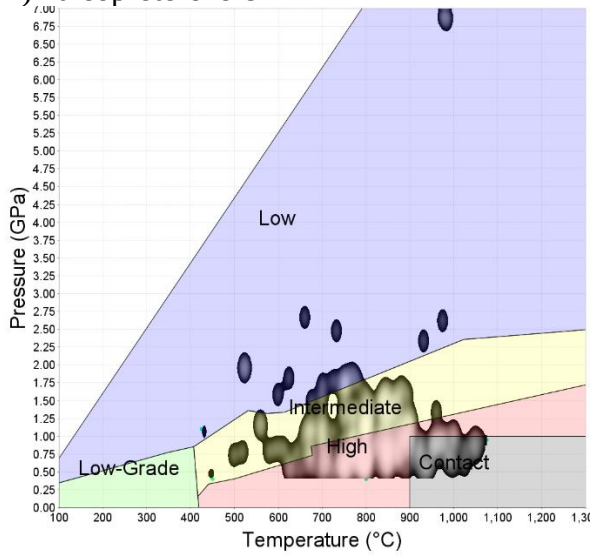

E) Mesoproterozoic

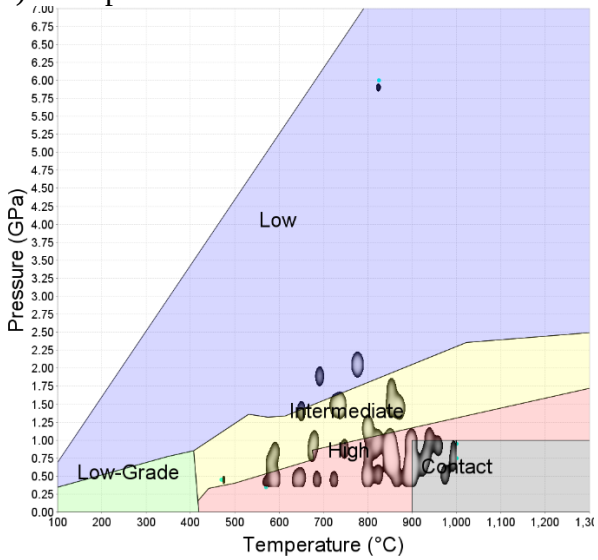

F) Neoproterozoic

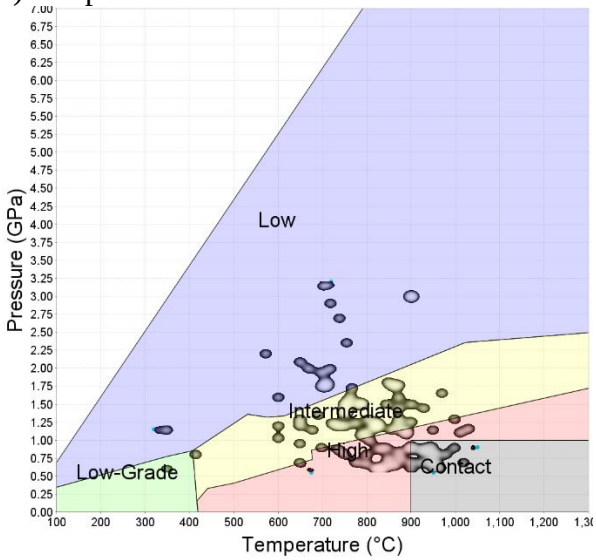

G) Paleozoic

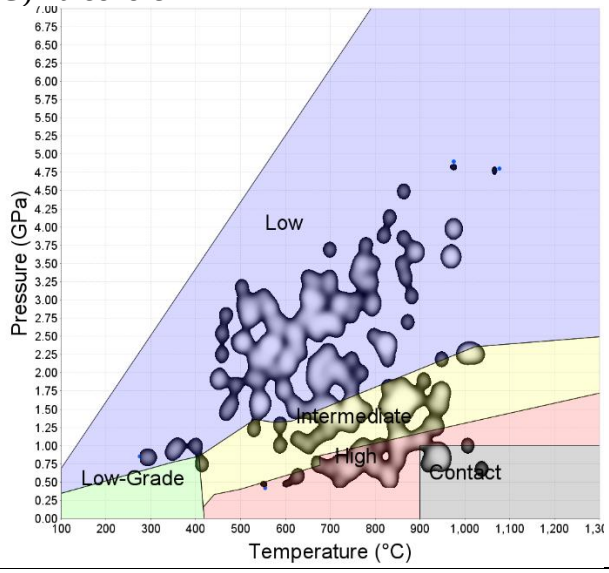

H) Mesozoic

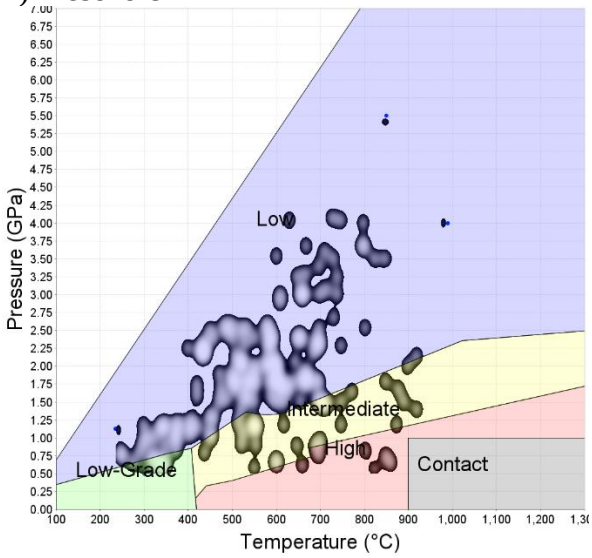

I) Cenozoic

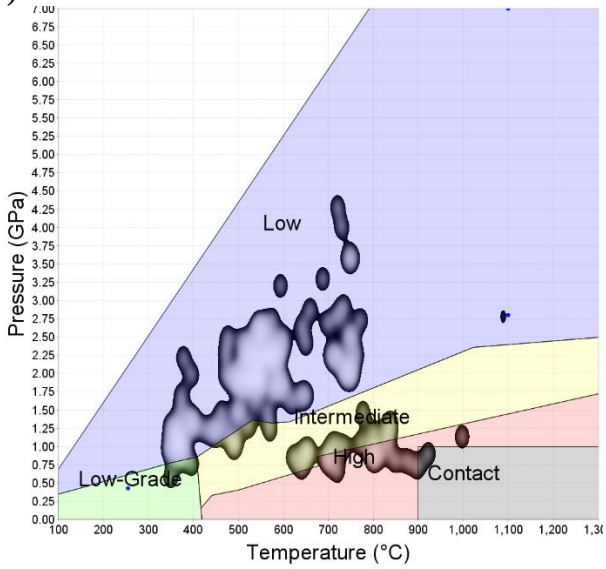

J) All Data

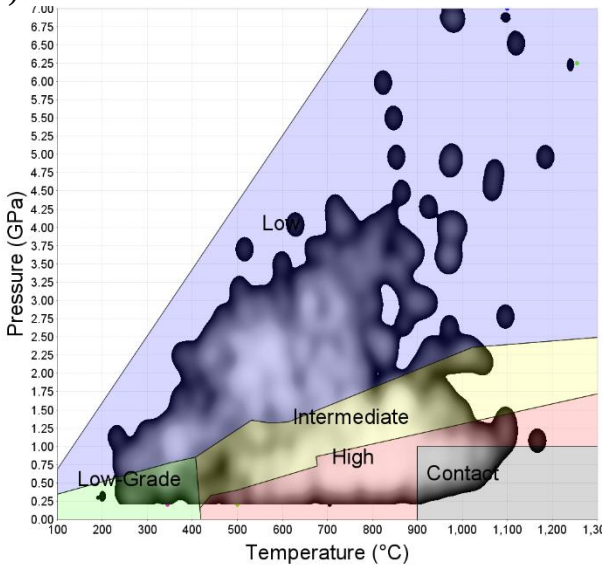

Figure 4.16 MetRec records plotted in PT space against polygonal classification scheme according to time slices. A) Paleoarchean and earlier, B) Mesoarchean, C) Neoarchean, D) Paleoproterozoic, E) Mesoproterozoic, F) Neoproterozoic, G) Paleozoic, H) Mesozoic, I) Cenozoic, and J) All Data. Grey heatmap acts as visual aid to represent the range of records found for each time. H) Overlaps all polygons.

A)_ Paleoarchean

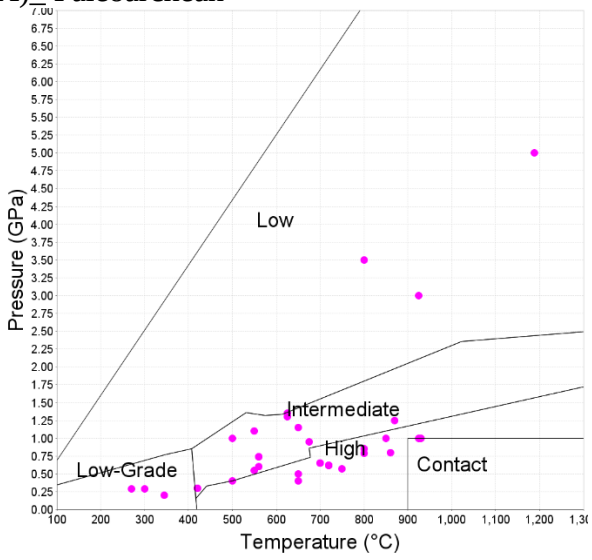

B) Mesoarchean

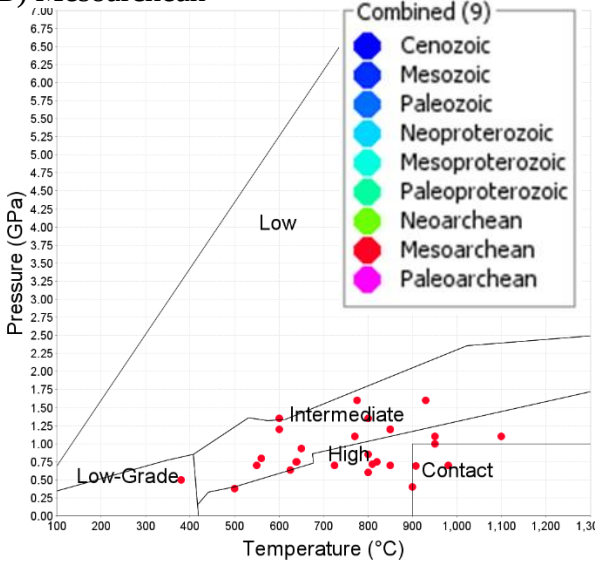

C) Neoarchean

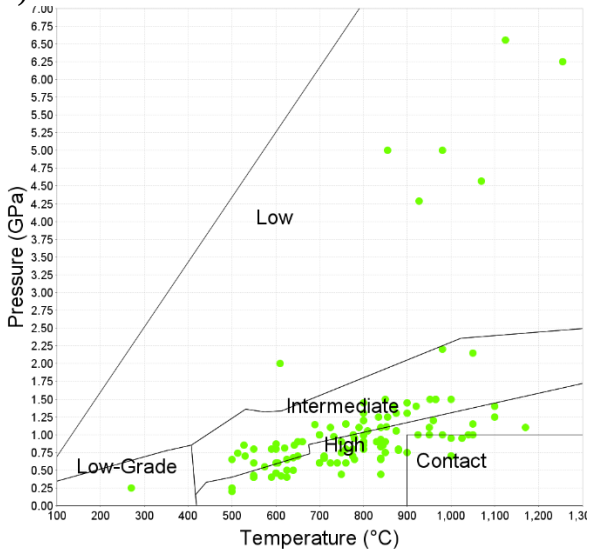

D) Paleoproterozoic

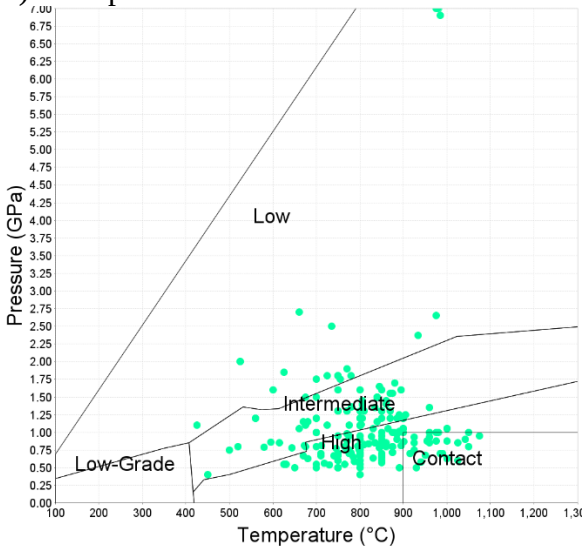

E) Mesoproterozoic

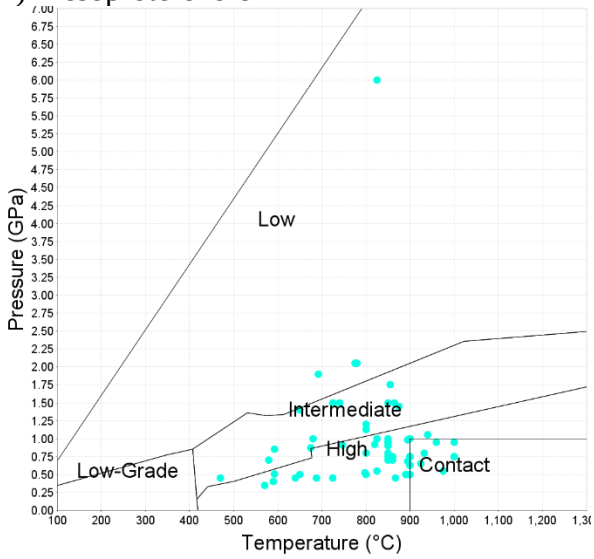

F) Neoproterozoic

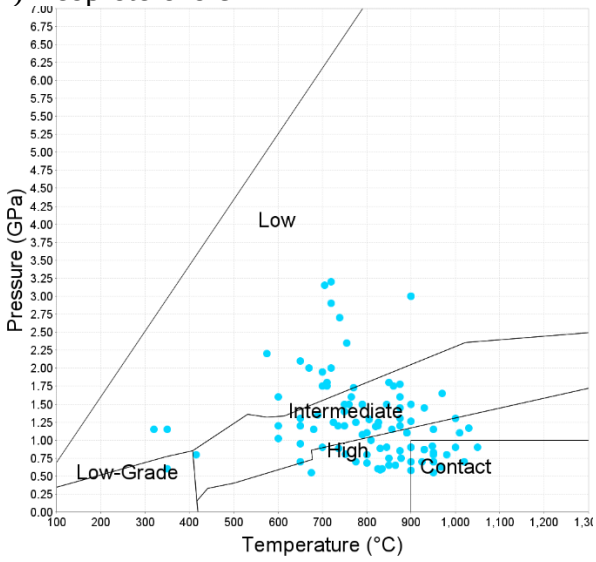

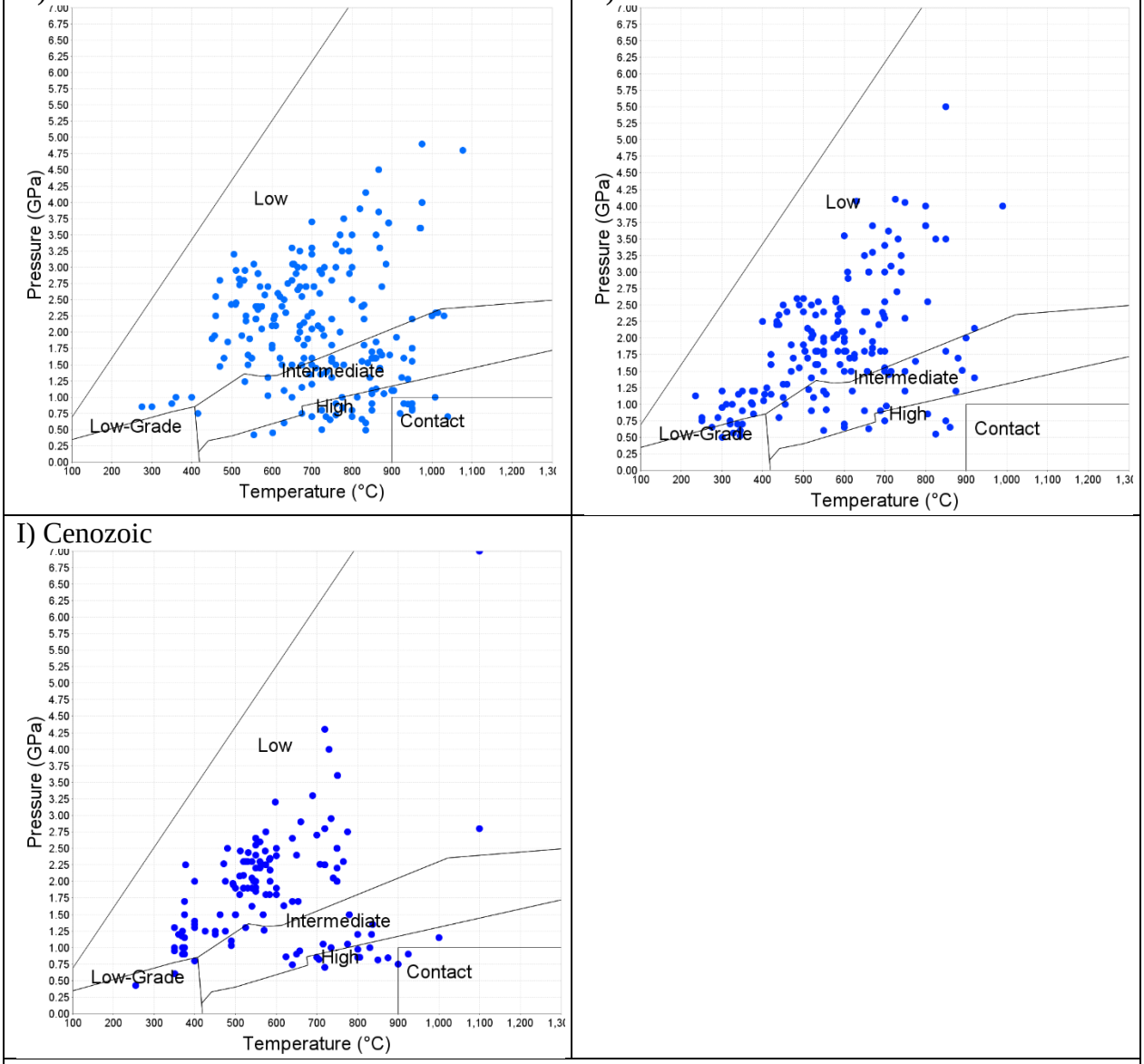

Figure 4.17 Pressure (GPa) against temperature (°C) against a metamorphic facies diagram (Zheng and Chen, 2017). The diagram is split into time slices from oldest to youngest: a) Paleoarchean, b) Mesoarchean, c) Neoarchean, d) Paleoproterozoic, e) Mesoproterozoic, f) Neoproterozoic, g) Paleozoic, h) Mesozoic, i) Cenozoic.

Figure 4.18, which focuses on the Phanerozoic era, a heatmap representation is used to identify the most common PT-space occupied by records, along with the associated metamorphic facies and polygonal classifications. The Phanerozoic era covers the entire range of known metamorphic facies.

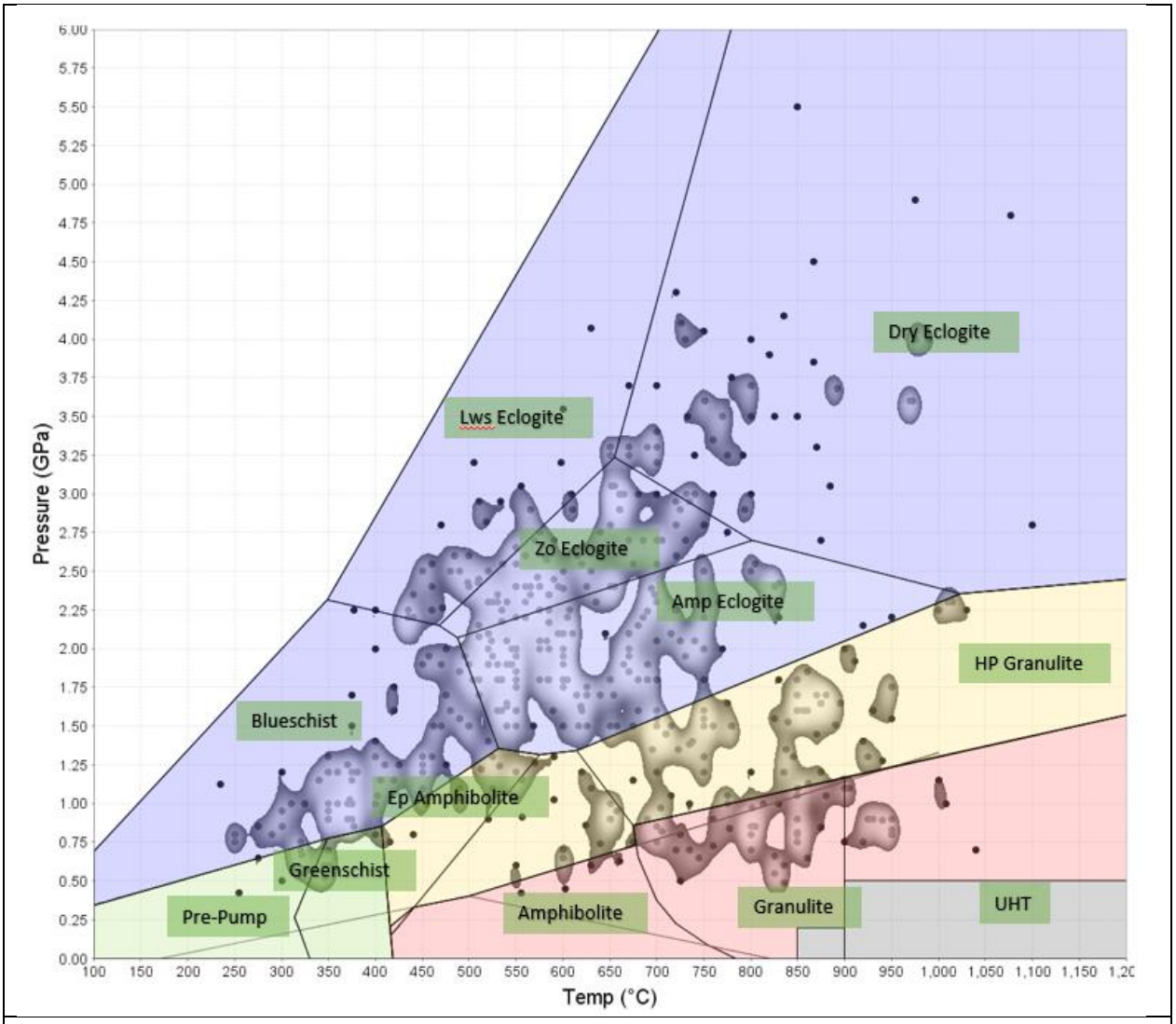

Figure 4.18 Heatmap for pressure (GPa) against temperature (°C) for Phanerozoic records in MetRec against metamorphic facies diagram (Zheng & Chen, 2017). Green labels represent metamorphic facies. Polygons are coloured according to polygonal dT/dP classification (See 3.2.2 Nonlinear Categorization of dT/dP). Blue = low, yellow = intermediate, red = high, green = low-grade, black = contact. Pre-Pump = Prehnite-pumpellyite facies, Amp = amphibolite, UHT = ultra-high temperature, Ep = epidote.

Figure 4.19 compares the Phanerozoic heatmap (as shown in the previous figure) with the range of Precambrian metamorphism. The Precambrian era, depicted in red, exhibits a higher density of records that cluster around the Amphibolite, Granulite, HP Granulite, and UHT facies. However, it is important to note that the Precambrian records cover all major facies, thanks in part to the occurrence of blueschist facies in the Neoproterozoic era.

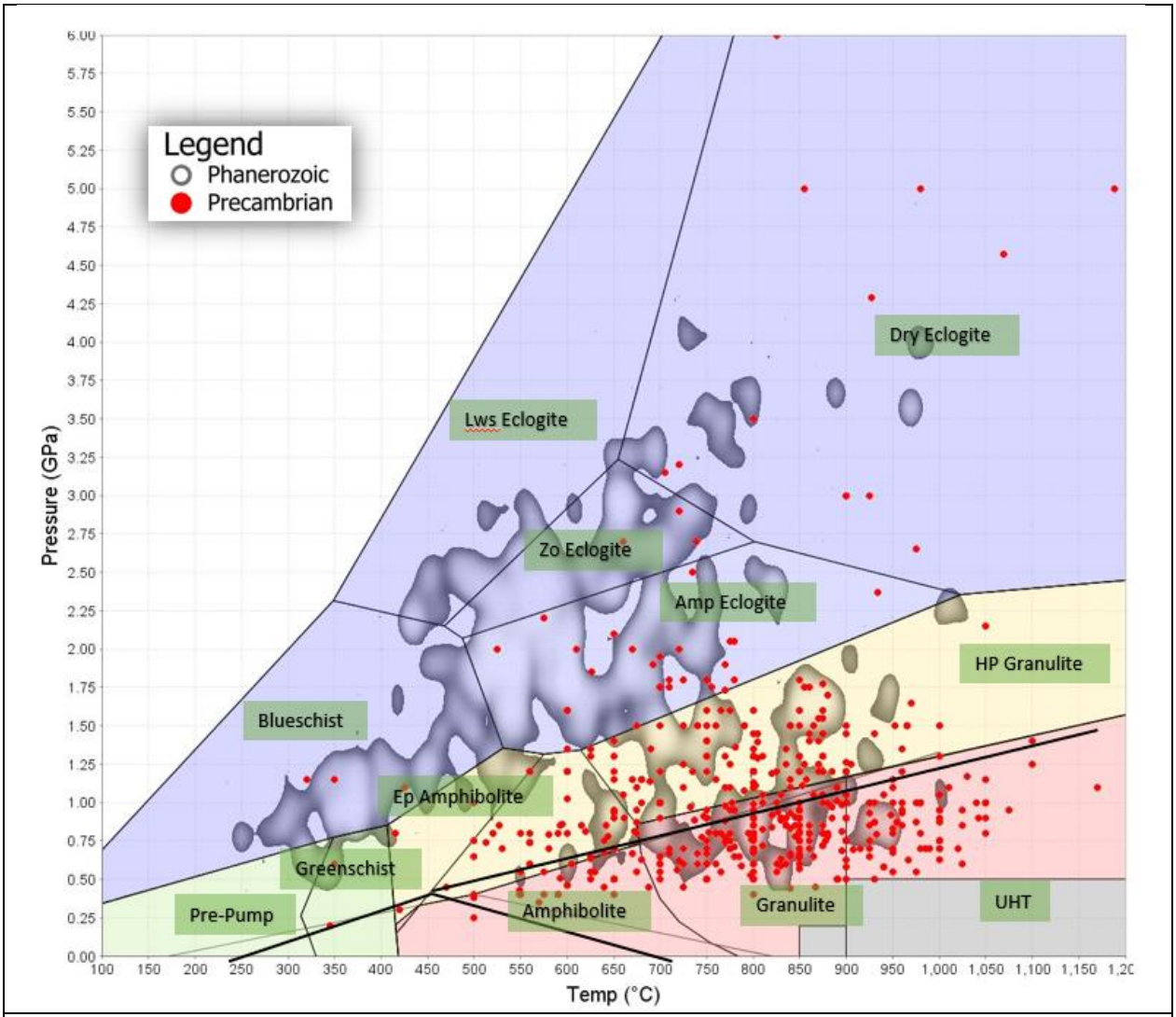

Figure 4.19 Pressure (GPa) against temperature (°C) diagram for Phanerozoic records against metamorphic facies diagram (Zheng & Chen, 2017). Comparison of heatmap of Phanerozoic records (black heatmap) against Precambrian samples (red). Green labels represent metamorphic facies. Polygons are coloured according to polygonal dT/dP classification (See 3.2.2 Nonlinear Categorization of dT/dP). Blue = low, yellow = intermediate, red = high, green = low-grade, black = contact.

Figure 4.20 presents a comparison between the quoted metamorphic facies classifications provided by publishing authors and the plotted facies of the PT grid. This figure highlights discrepancies between field-based classification of rocks and the facies classifications that can be derived from laboratory calculations. This comparison reveals instances where there may be inconsistencies or differences in the classification of metamorphic facies between the field observations and the calculated PT conditions. These discrepancies could arise due to various

factors, including the complexity and variability of metamorphic processes, the limitations of available data, or variations in interpretation and classification approaches by different authors.

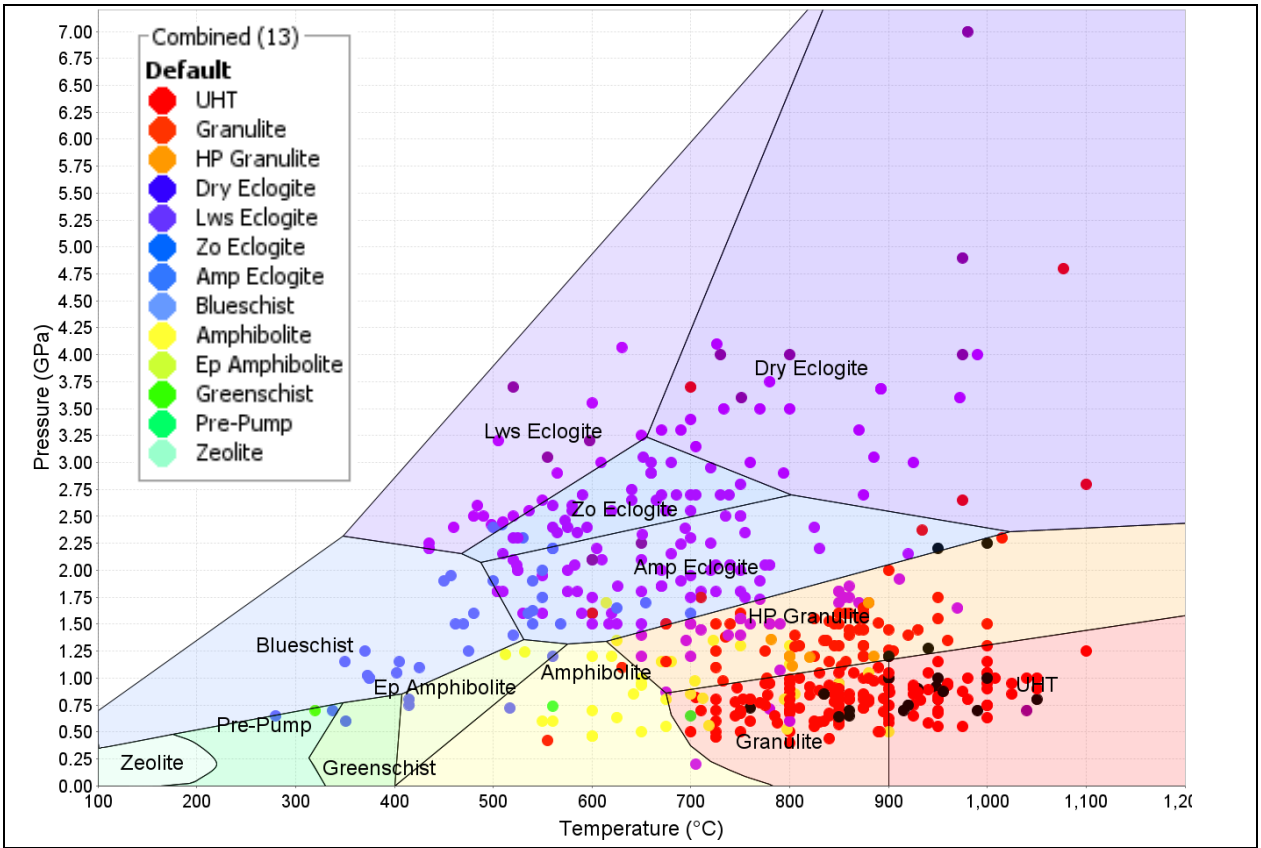

Figure 4.20 Pressure (GPa) against temperature (°C) for all MetRec records plotted against a metamorphic facies diagram (Zheng and Chen, 2017). Samples are coloured according to their quoted field-classification, that is the metamorphic facies assigned to the record by the authors of the original reference. This compares assumed field classifications against calculated metamorphic facies classifications.

4.5.1 **Metamorphic Samples against the Range of Modern Subduction Zones**

As discussed previously (see 2.1.9 The Range of Modern Subduction [Penniston-Dorland et al. (2015)), this paper quantified the PT-space in which subduction related rocks from the compilation of Penniston-Dorland et al. (2015). Figure 4.21 shows that range against sections in the low, intermediate, and high dT/dP categories. This challenges previous assumptions about the range of dT/dP values in subduction zones being relegated to the low dT/dP zone.

Figure 4.22 depicts the temporal distribution of samples that fall within this paper's range of subduction. These samples extend back to the Early Archean, suggesting that PT conditions conducive to subduction-related processes may have occurred throughout Earth's history. This figure also shows records which plot back to the Eoarchean and well above the 330-440 °C/GPa cut off of previous authors.

A) Penniston-Dorland Records

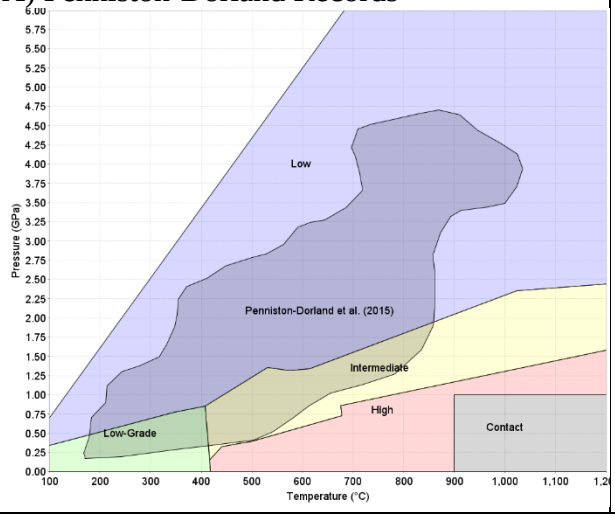

B) MetRec Records

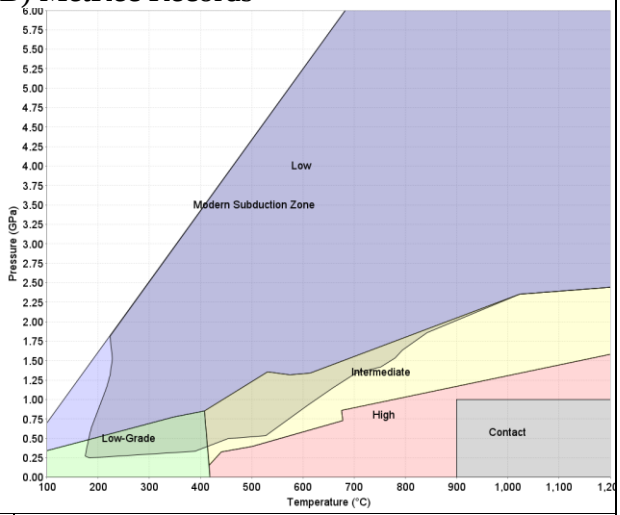

Figure 4.21 Polygonal classification diagram. A) Dark polygon represents the range of metamorphic samples found by Penniston-Dorland et al. (2015). B) Showing the location of additional samples from MetRec which would be considered subduction related.

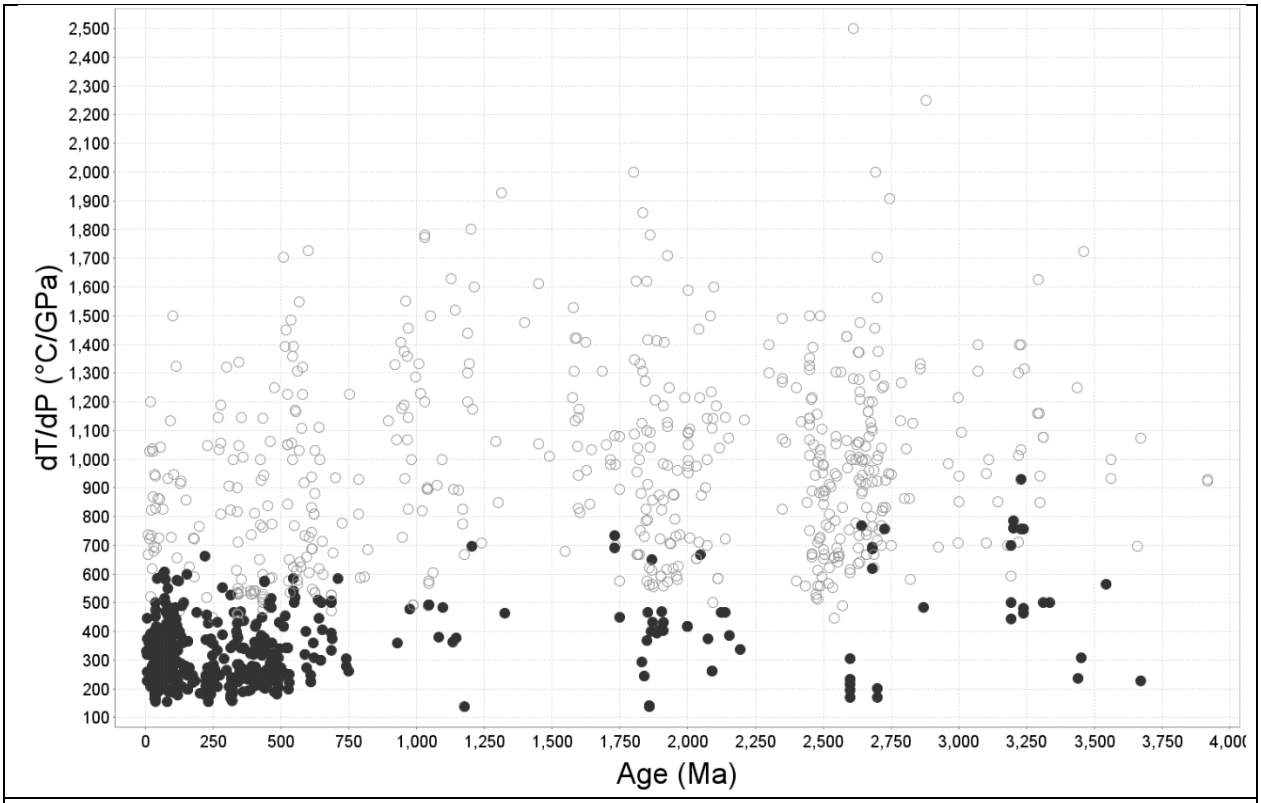

Figure 4.22 dT/dP (°C/GPa) against Age (Ma) for all samples. Black circles represent samples which plot inside the polygon from Figure 4.21b representing the range of modern subduction. Open grey cirlces plot outside of that polygon.

4.6 **Averaging Records**

This section provides the results of averaging oversampled areas as defined in 3.2.3 Averaging Oversampled Areas. This will provide a background for all records which had been sampled. This study created 14 ‘averaged’ records, which are records created from by averaging the age, temperature, and pressure estimates for records which are closely associated (See 3.2.3 Averaging Oversampled Areas for more information). This process created 4 records in China and 10 records in the Alps from 78 parent records. The results of this averaging are illustrated in Figure 4.23 which compares the dT/dP of the averaged samples against the parent samples which went into creating those.

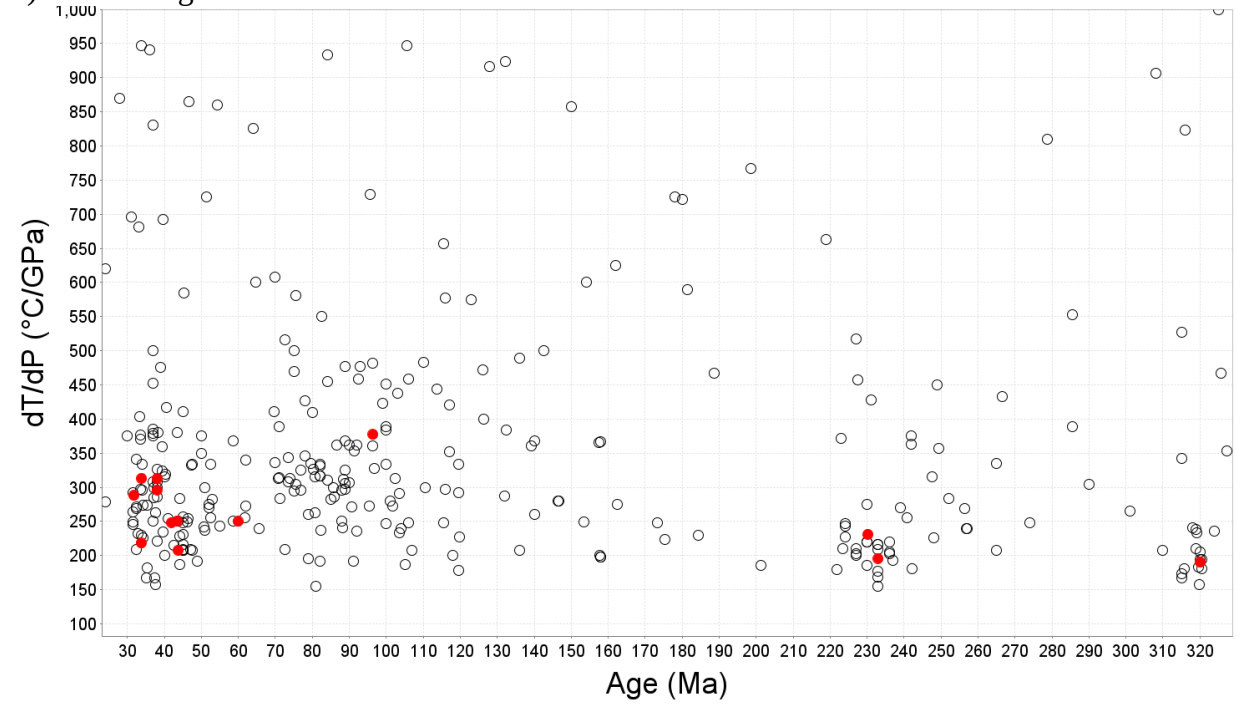

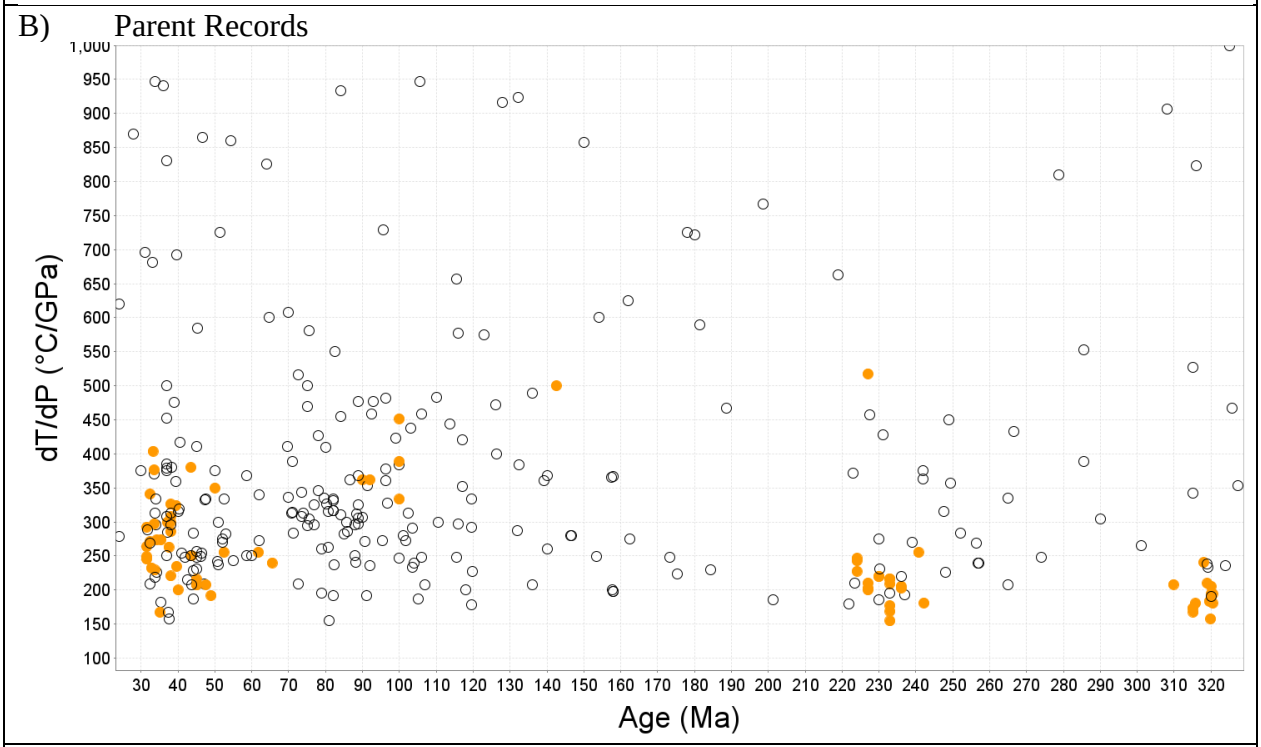

Figure 4.23 dT/dP (°C/GPa) against Age (Ma) for all MetRec records. A) Results of averaging records (closed red circles) and B) Parent records (closed orange circles).

4.7 Metamorphic Facies

Figure 4.24 presents a histogram of metamorphic facies based on plotted PT space. This shows blueschist records are scarce with 76 total records which begin to show in earnest after the 750 Ma mark. Eclogites are also rare and intermittent throughout the recorded timeline, with an increase in occurrence similar to blueschists from 750 Ma onwards. Amphibolites, although less common in the compilation, exhibit sporadic records with minor spikes at 2600 Ma and 100 Ma. High-pressure granulites display distinct spikes without intermediate records, occurring around 3200 Ma, 2600 Ma, 1900 Ma, and 1000 Ma. From 750 Ma onward, there is an increased occurrence of high-pressure granulites, with a decrease around 250 Ma. It's worth noting that the representation of greenschist/greenstone facies is limited in the database, and therefore, the records are not representative of the distribution of low-grade metamorphism through time. There may also be an underrepresentation of amphibolite grade metamorphism in the database.

Figure 4.27 shows the geographic distribution of blueschist records in the database (based on how records plot on the metamorphic facies diagram). There are sporadic blueschists across the globe, with almost all non-Alpine-Himalayan records being found on the end of continental blocks. The majority of records (51 out of 77 records) can be found in the Alpine-Himalayan series of orogens. The other records are found around the edges of modern plates.

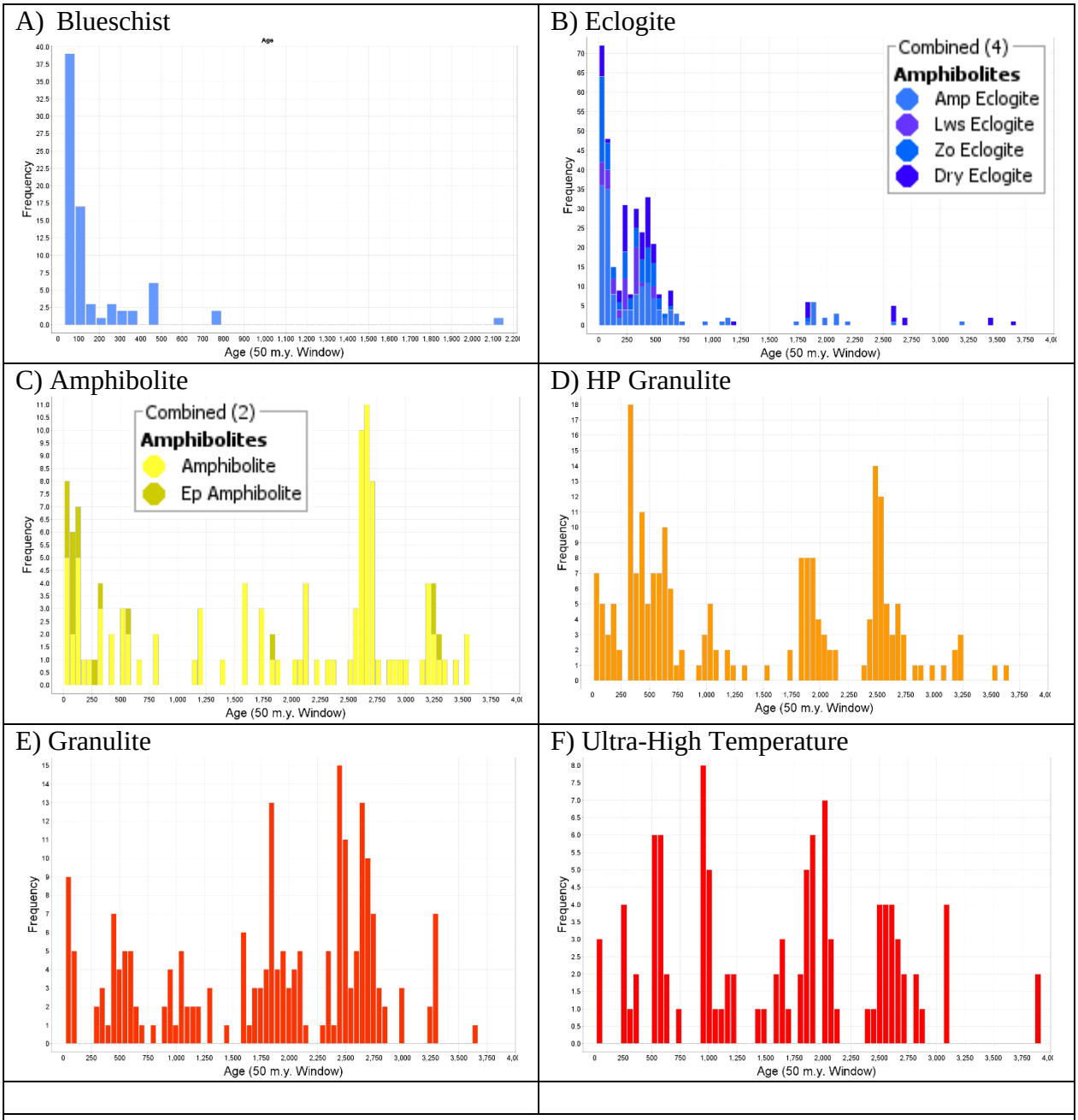

Figure 4.24 Histogram for samples by plotted metamorphic facies for all MetRec samples. A) Sub greenschist and greenschist, B) Blueschist and lawsonite eclogite, C) Eclogites, D) Amphibolites, E) High-pressure granulite, F) Granulite, and H) Ultra-high temperature.

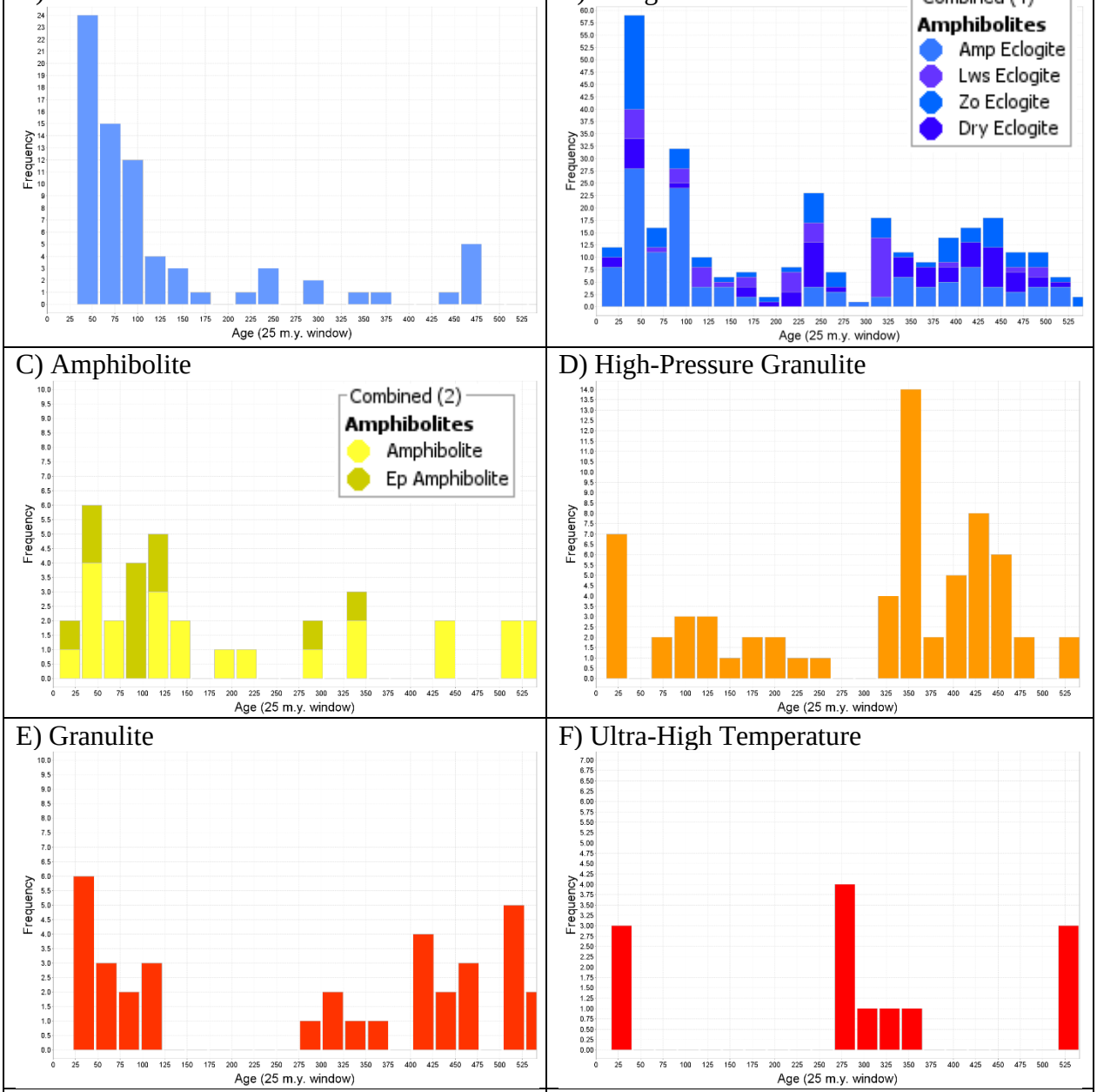

Figure 4.25 Histogram for Phanerozoic samples by plotted metamorphic facies for all MetRec samples. A) Sub greenschist and greenschist, B) Blueschist and lawsonite eclogite, C) Eclogites, D) Amphibolites, E) High-pressure granulite, F) Granulite, and H) Ultra-high temperature.

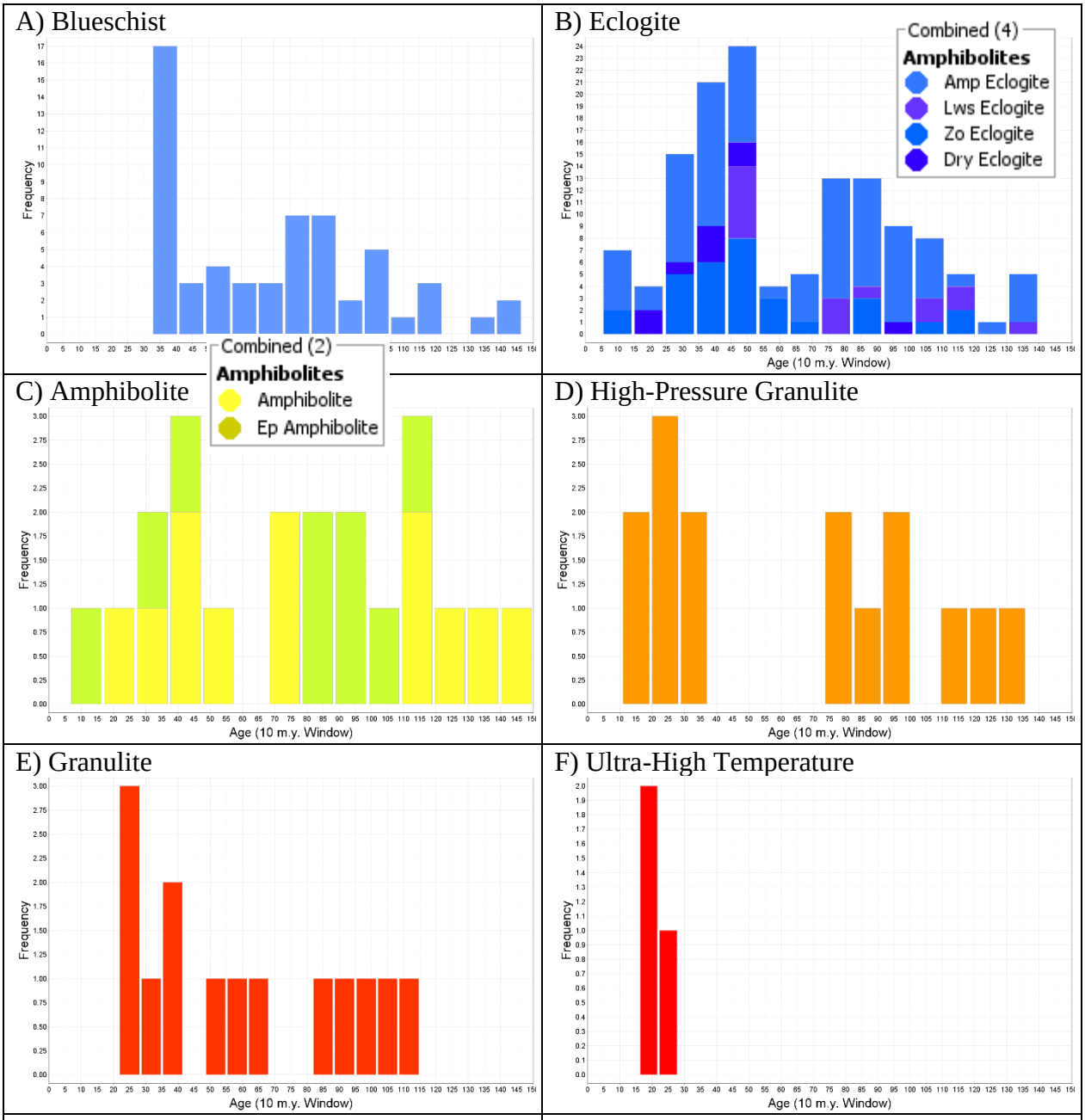

Figure 4.26 Histogram for samples younger than 150 Ma by plotted metamorphic facies for all MetRec samples. A) Sub greenschist and greenschist, B) Blueschist and lawsonite eclogite, C) Eclogites, D) Amphibolites, E) High-pressure granulite, F) Granulite, and H) Ultra-high temperature.

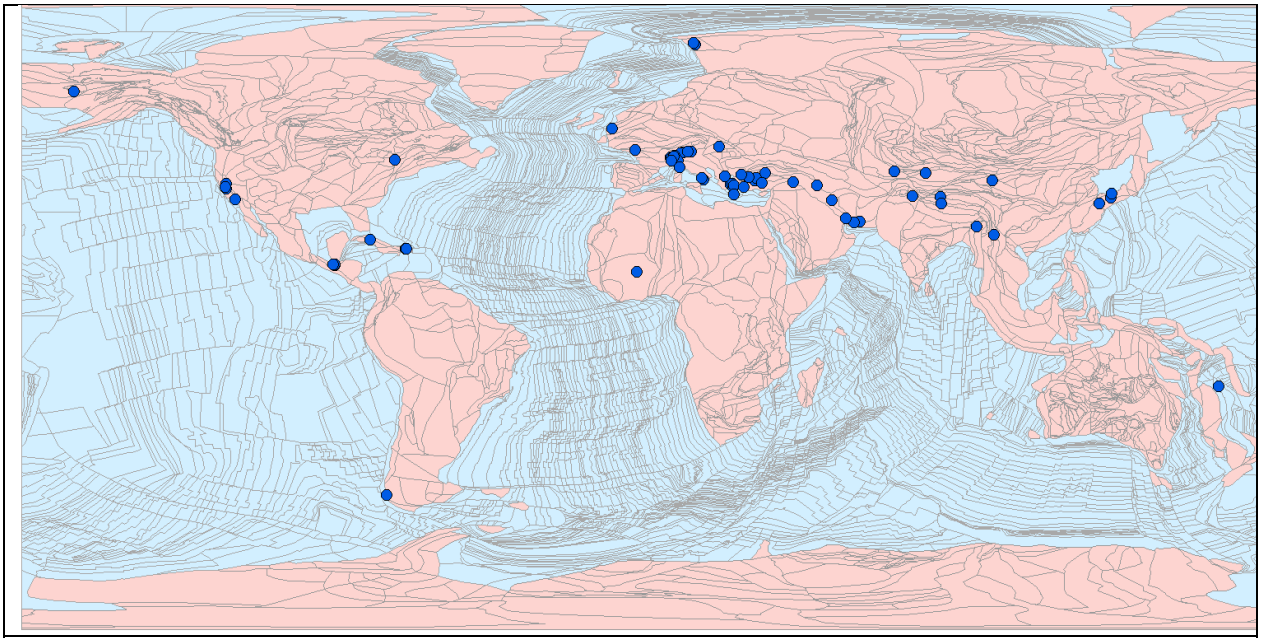

Figure 4.27 Modern day distribution of samples plotting in the blueschist range of the metamorphic facies diagram.

4.8 Upper/Lower Plate & Geodynamic Classifications

Figure 4.28 focuses on a subsample of Phanerozoic data and categorizes it into nine geodynamic settings based on a calculated geothermal gradient. The data is organized according to the estimated geotherm, allowing for a comparison between geodynamic settings and geothermal gradients. The geodynamic settings are arranged thus:

1. Continental Subduction
2. Lower Plate including blueschist
3. Retrograded Eclogite
4. Exhumed Lower Crust of Lower Plate
5. Upper Plate
6. Core Complex in Lower & Upper Plate, and Exhumed Lower Crust
7. Upper Plate Continental Arc
8. Upper Plate Arc or Magmatic Additions
9. Extension in Accretionary Complex

The results show that for the cool geotherm category (0-10 °C/km) only continental subduction and lower plate metamorphism (1 &2) show records. The moderate geotherm category (10 - 30 °C/km) contains records from all metamorphic categories (1-8) except extensions in accretionary complexes (9). The hot geotherm category shows records for upper plate (5), core complex (7), upper plate continental arc (7), upper plate arc (8), and extension (9). There is one sample of exhumed crust of the lower plate (4) that occurs at around 40 °C/km, which is an exception to the general trend observed in the other geodynamic settings.

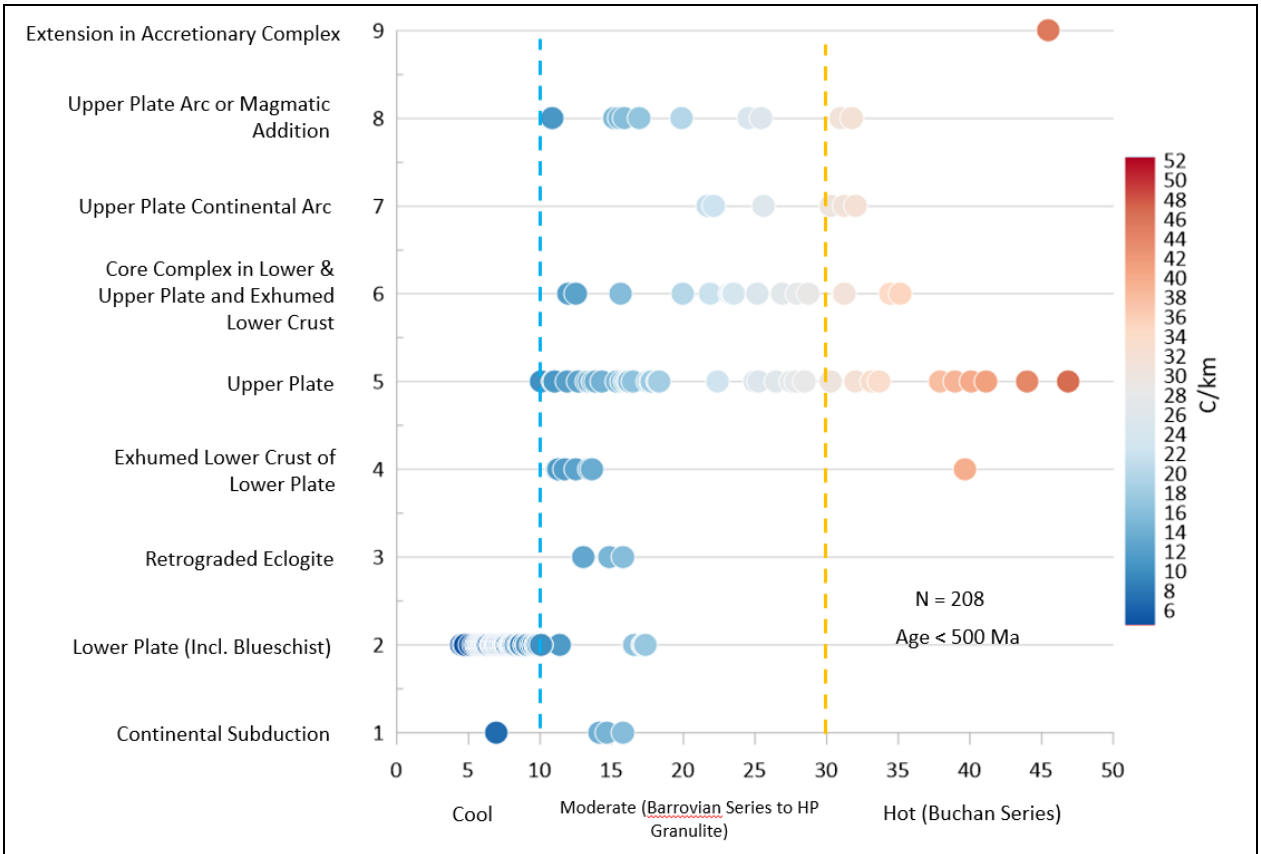

Figure 4.28 Geodynamic classification against calculated depth (°C/km). Dashed lines represent metamorphic classifications at 10 °C/km for Alpine-Barrovian series and 30 °C/km Barrovian-Buchan series. Colour of samples relate to °C/km as per legend on right. Depth estimated as 1 GPa = 33 km.

Figure 4.29 expands on Figure 4.28 by further organizing the geodynamic settings into upper and lower plate groups based on their respective geothermal gradients. These geodynamic settings were identified by inspection from primary literature. The lower plate groups exhibit a range of geothermal gradients from 5 °C/km to 18 °C/km, while the upper plate groups are

organized within the range of 10 °C/km to 50 °C/km. This division allows for a more detailed analysis and comparison of the geothermal gradients associated with different geodynamic settings. This division also illustrates the overlap between upper and lower plate geotherms which have not been previously acknowledged in previous literature.

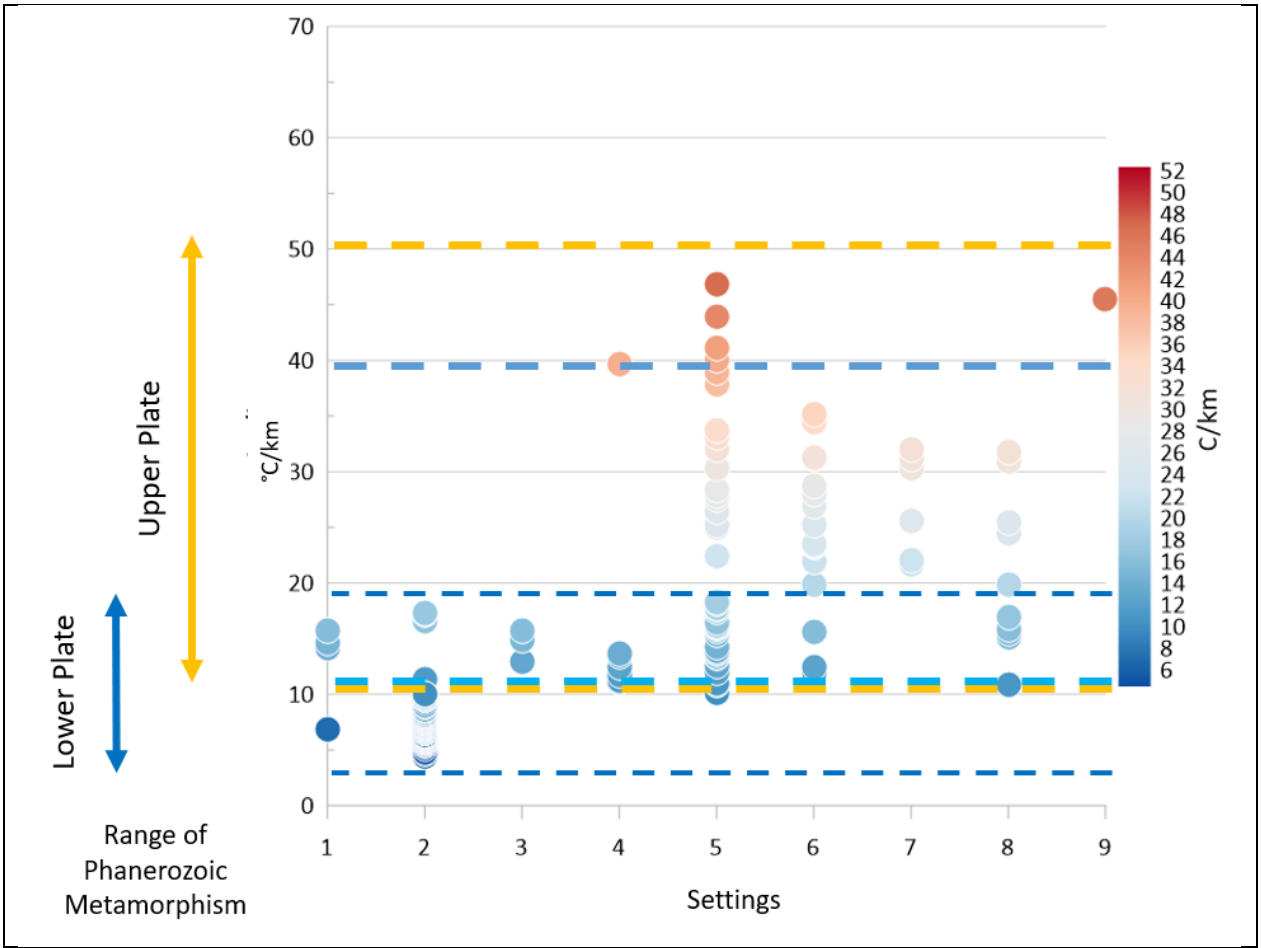

Figure 4.29 °C/km against geodynamic setting (see Figure 4.28 for more detail) for phanerozoic samples. Ranges for upper (gold) and lower plate (blue) on the left as well as dashed horizontal lines.

Figure 4.30 presents a comparison of the dT/dP values over time juxtaposed with the ranges of upper plate and lower plate geodynamic settings. The lower plate records, which encompass the Phanerozoic era, extend all the way back to the Paleoarchean. Additionally, there are records below the upper/lower plate overlap that date back to the Paleoproterozoic era.

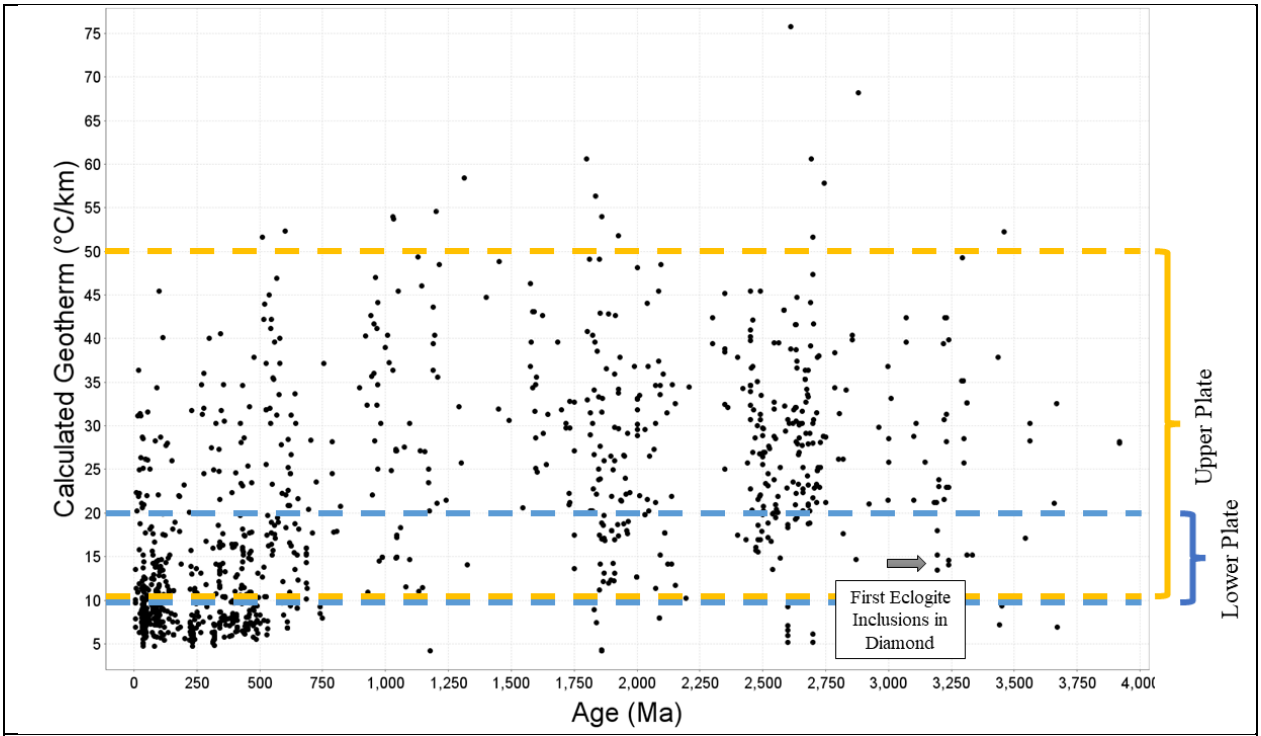

Figure 4.30 Calculated geotherm (°C/km) against age (Ma) for all Phanerozoic samples. Gold arrow marks the range for phanerozoic upper plate activity and blue marks the range for phanerozoic lower plate activity. Horizontal blue lines represent the boundary between Buchan series, Barrovian series, and Alpine series. Grey horizontal arrow at the bottom left shows the range of the Phanerozoic.

4.9 Supercontinent Cycles and Super GDU's

The main driver for non-contact metamorphism is the collision of tectonic plates as they travel horizontally across the globe. Using the work of Nguyen (2019), this study compared dT/dP classifications against the size of SuperGDU's and the number of SuperGDU's (Figure 4.31). The area of the largest SuperGDU (km^2) will grow during the accretion of supercontinents as the largest group of collided blocks begin to move together. The total number of independently moving SuperGDU's will increase during continental breakup as more blocks are moving separately.

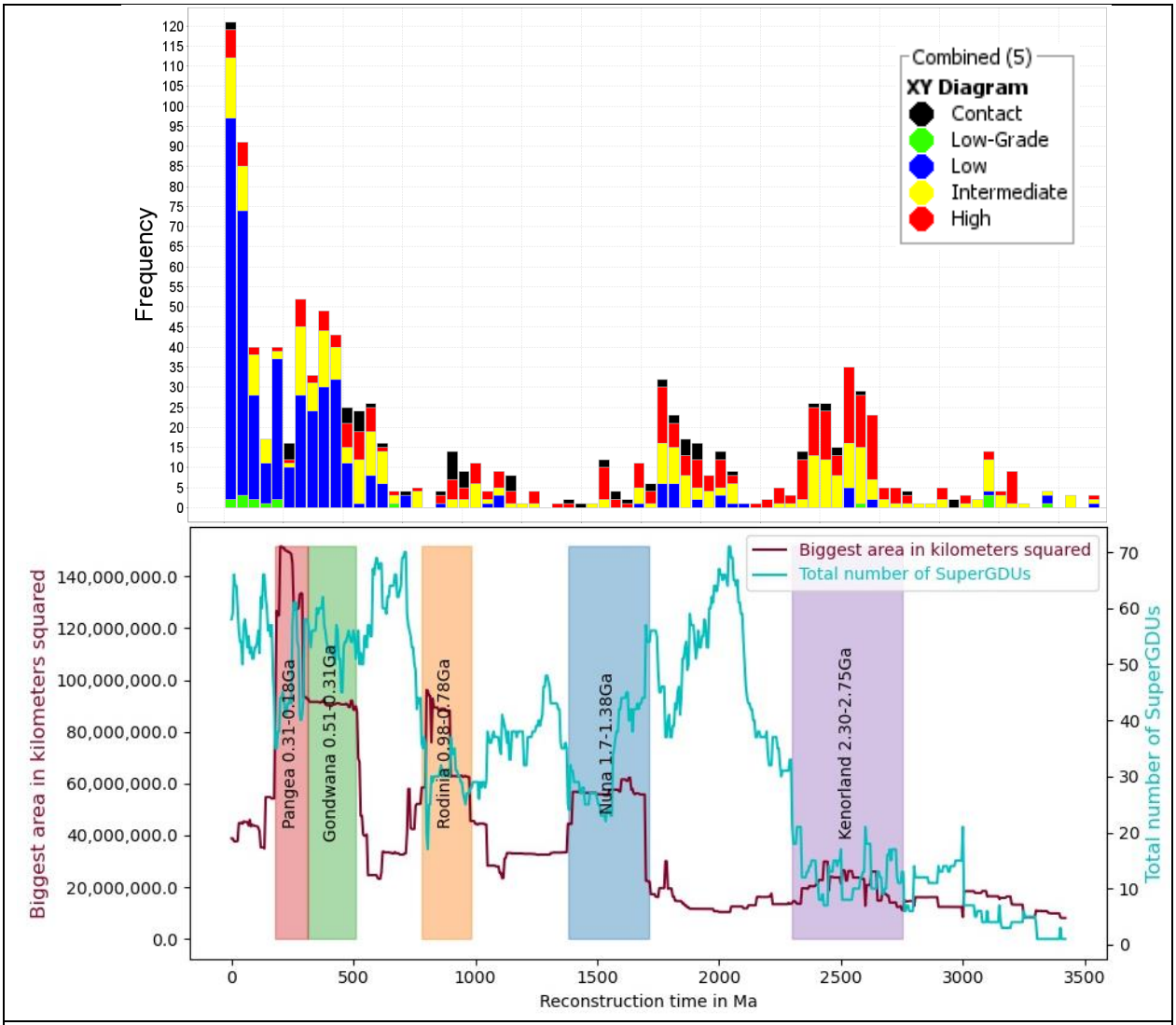

Figure 4.31 Comparison of largest SuperGDU size, total number of SuperGDU's, and frequency of dT/dP categories. Supercontinents and Kenorland are represented by columns in the background. Histogram columns are coloured according to the polygonal classification scheme discussed in 3.2.2 Nonlinear Categorization of dT/dP.

Pre-Kenorland, few samples exist. The majority of those which we have access to are medium category dT/dP, but high dT/dP and contact dT/dP categories are well-represented. Two samples of low category dT/dP appear however (these are from the Isua Greenstone Belt). SuperGDU size and number are low in this time period due to the low number of blocks from this period available for modelling. During Kenorland, the first spike of metamorphic records appears. This spike is composed of primarily medium/high category dT/dP samples, with a small number of contact dT/dP samples, and a few low category dT/dP samples. This spike is

contemporaneous with a spike in number of SuperGDU's. Records taper off into the ending of the Kenorland tenure and there's a gap until the accretion of Nuna.

A spike in records precedes the accretion of Nuna. These records trail slightly behind the largest spike in SuperGDU size but are not associated with a spike in SuperGDU size which comes later. This spike contains representatives from all categories. The Nuna-spike ends before the SuperGDU size spike begins. There are few records associated with Nuna's stable phase, those that exist are largely medium/high/contact dT/dP records.

The spike which precedes the stability phase of Rodinia follows the same pattern as the Nuna-spike: trails behind a SuperGDU number spike, contains all the four different dT/dP categories, and ends before the spike of SuperGDU size. It is much smaller than the Nuna-spike however.

Two spikes follow Rodinia: one associated with Gondwana begins following the rifting of Rodinia and drops with the finalization of Pangea; and a second spike appears since the breakup of Pangea, in the last 150 Ma. There is a large spike of low dT/dP. This final spike comes up into the present, inter-super continental time. The first spike around 250 Ma lasts 10 m.y. and overlaps with the estimated accretion and stabilization of Gondwana.

The number of SuperGDU's are generally highest during the inter-continental phases lowest during the supercontinent stability phases. The formation Gondwana is different from those previously seen as there is a noticeable drop going into the accretion of Gondwana, but it is less pronounced and sustained than either Nuna or Rodinia. The number of SuperGDU's for Gondwana/Pangea drops from a high around 70 to an average of ~60 – with dips into mid 40's. The lowest point for the period following Rodina is 30.

Kenorland shows spikes in number of independent blocks that are associated with metamorphic spikes but with so little data it is difficult to tell if these fit into an accretion-stability-breakup pattern. Two supercontinents (Nuna and Rodinia) show patterns which align with the accretion-stability-breakup pattern expected. Gondwana/Pangea follow the previous patterns but spikes grow throughout the formation of Gondwana. Lastly, a spike in independent blocks is associated with the inter-continental period we currently reside in. It would seem that

the pattern seen in Nuna and Rodinia appears twice, with it appearing in modified form in Kenorland and Pangea/Gondwana.

4.10 Spatial Associations

Spatial associations have been under-studied before now. Very little of the previous literature has explicitly taken spatial information into account. Looking at spatial associations gives the opportunity to understand how sampling biases are reflected in the dataset and to understand the relationship between supercontinent cycles and metamorphism as discussed previously.

Figure 4.32 shows the distribution of dT/dP categories across the modern globe. This map shows areas with large amounts of certain dT/dP categories in broad strokes. It can be seen that some orogens are well represented while other areas are not.

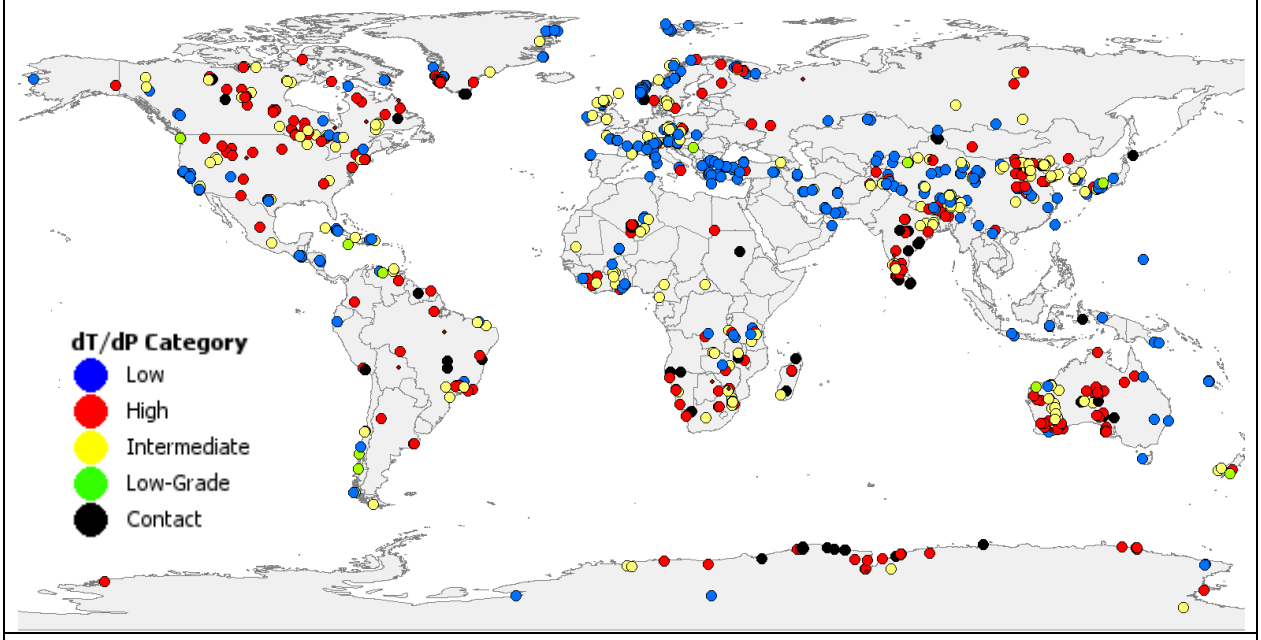

Figure 4.32 Global map of all MetRec records - with some averaged (refer to 3.2.3 Averaging Oversampled Areas).

Figure 4.34 and Figure 4.35 shows a plate reconstruction model at 60 Ma and 1048 Ma, respectively, with metamorphic records, igneous crystallization ages, and metamorphic ages.

These can be combined to get an interpretation of previous tectonic movements and metamorphic events. The plate reconstruction model is relative to mantle reference frame.

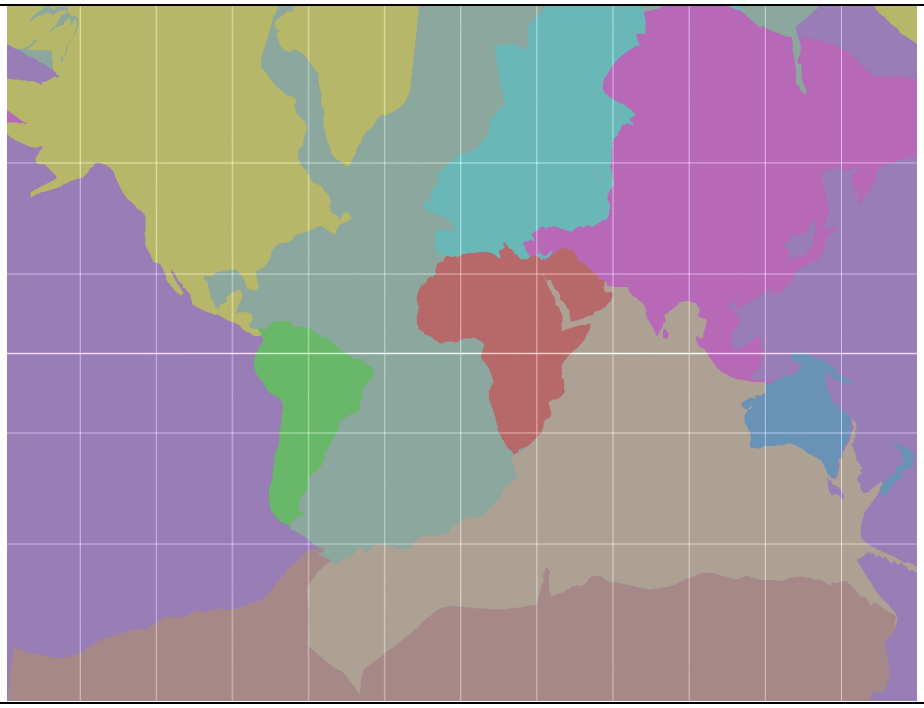

Figure 4.33 Colouration of the current SuperGDUs in the plate reconstruction model used in this study. Colouring: North America (yellow), South America (bright green), Europe (aquamarine), Africa (red), Asia (purple), Oceania (blue), Antarctica (brown). Oceans: Pacfic (dark purple), Arctic-Atlantic (dark green), Indian Ocean (tan). The distinctions are based on GDU's and there exists overllap between different oceans, namely that the Southern Ocean is not represented by its own colour. There is also some overlap between the northernmost Pacific and parts of the Arctic around Eastern Russia. Paleoplates model was used (Eglington et al., 2017; Evans and Eglington, 2022)

60 Ma Plate Reconstruction

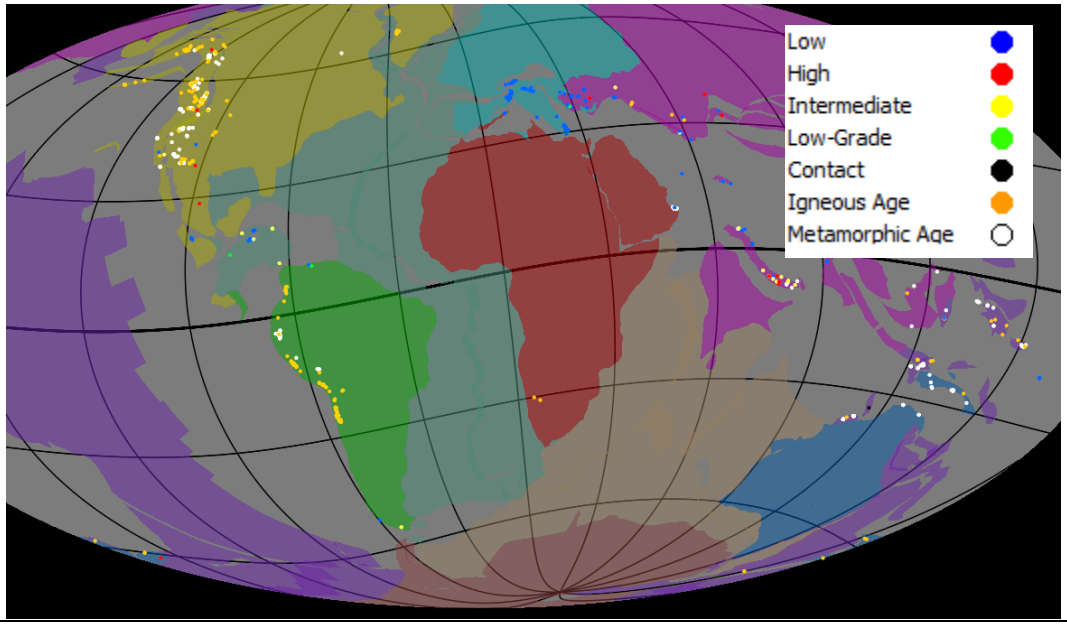

Figure 4.34 Snapshot of a plate reconstruction model (Paleoplates Model) in GPlates software, with data samples represented as dots coloured according to legend (Eglington et al., 2017; Evans and Eglington, 2022). This time slice is taken at 60 Ma in the Mollweide projection.

1048 Ma Plate Reconstruction

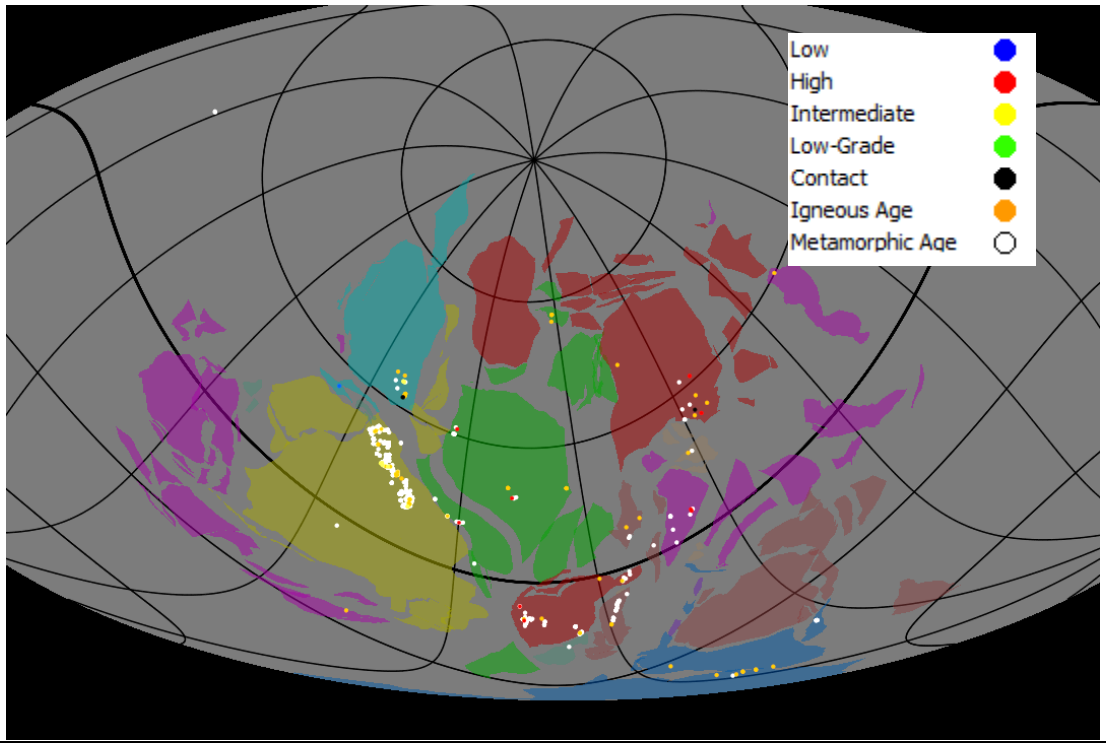

Figure 4.35 Snapshot of a plate reconstruction model (Paleoplates Model) in GPlates software, with data samples represented as dots coloured according to legend (Eglington et al., 2017; Evans and Eglington, 2022). This time slice is taken at 1048 Ma in the Mollweide projection.

5 Discussion

The MetRec database has established trends relating to the following: temporal data imbalances, spatial imbalances, questions of preservation, and trends in dT/dP through time.

5.1 Temporal Data Imbalances

There remains a significant data bias towards Phanerozoic records, despite a literature review which focused on pulling Precambrian data into the database. The incorporation of the remainder of the Penniston-Dorland (2015) compilation increases the number of records from younger than 750 Ma, but that does not account for all the bias still. It remains true that Phanerozoic samples are more readily accessed in the field than Archean samples.

It is evident that certain important and controversial areas of research have relatively fewer data points.

This observation serves as a reminder that the interpretation and analysis of the data should consider the limitations and biases introduced by the uneven distribution of records across geological eras, which something that has been missing from many statistical analyses. It emphasizes the need for caution when drawing conclusions or generalizing, particularly in areas where data are scarce or limited.

Figure 5.1 illustrates the amount of data in the Phanerozoic – there is as much data which can be considered outlier data to the box-and-whisker plot as there is for Paleoarchean and the Mesoarchean. There is also significant overlap between the two groups of data – if the low dT/dP category samples were not as well represented, the boxes for the Phanerozoic eras and the Archean eras would look very similar.

Table 5.1 provides a comparison of the number of records for each geological era against the number of records from the Phanerozoic. This table highlights that over 50% of the data in the

MetRec database is Phanerozoic. It is evident that certain important and controversial areas of research have relatively fewer data points.

This observation serves as a reminder that the interpretation and analysis of the data should consider the limitations and biases introduced by the uneven distribution of records across geological eras, which something that has been missing from many statistical analyses. It emphasizes the need for caution when drawing conclusions or generalizing, particularly in areas where data are scarce or limited.

Figure 5.1 illustrates the amount of data in the Phanerozoic – there is as much data which can be considered outlier data to the box-and-whisker plot as there is for Paleoarchean and the Mesoarchean. There is also significant overlap between the two groups of data – if the low dT/dP category samples were not as well represented, the boxes for the Phanerozoic eras and the Archean eras would look very similar.

Table 5.1 Comparison of the number of records for each geological era against the Phanerozoic. The table presents two perspectives: the expected number of records based on the density of Phanerozoic data and the number of samples required from each era to achieve a similar temporal density as the Phanerozoic.

Era	How many records in the Phanerozoic if it had the same density of sampling as the…		How many records in the … if it had the same density of sampling as the Phanerozoic	Current Records	% of Data
Phanerozoic				521	50.5
Neoproterozoic	112		442	99	9.6
Mesoproterozoic	53		288	61	5.9
Paleoproterozoic	109		866	190	18.4
Neoarchean	144		385	111	10.8
Mesoarchean	26		385	20	0.19
Neoarchean	31		385	24	0.23
Eoarchean	6		385	5	0.05

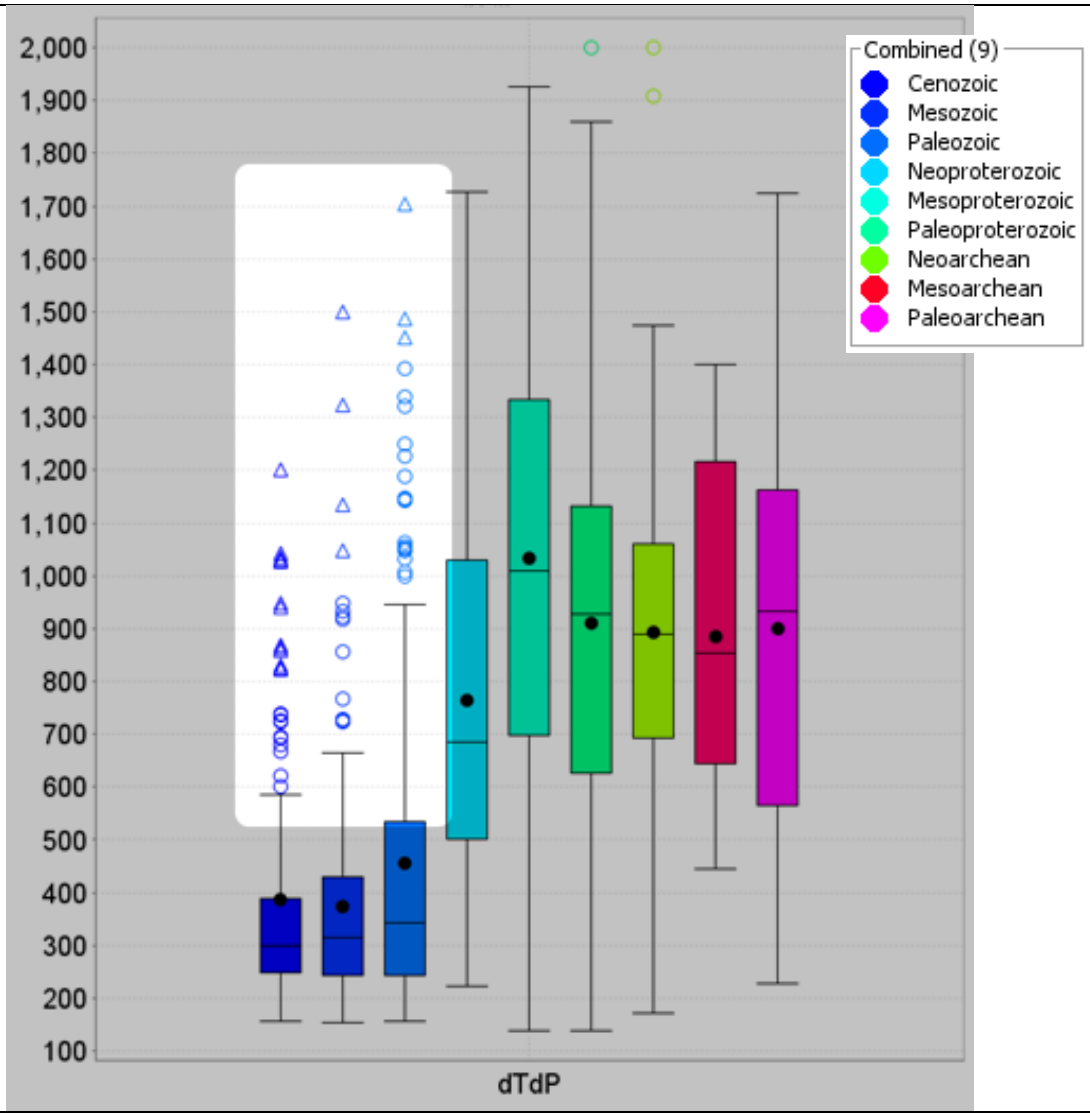

Figure 5.1 Highlighting the Phanerozoic outlier data (outside of the whiskers). It can be seen that while the majority of data in the Phanerozoic is below 550 °C there remain samples produced which overlap the same range as the Archean data.. Black circle represents the mean. Black line represents the median. Central box is the middle 50% of data. Circles are data that is further than 1.5 times distance the from the box. Triangles is more than 3 times distance from the box. The Whiskers are the extreme values that are not outliers (i.e. outside the 50% box but less than 1.5 times distance from the box). The triangles and circles emphasized by the red brackets represents a similar number of data points as for the entire Paleoarchean.

Figure 5.2 shows the frequency of dT/dP records for the Phanerozoic and establishes the predominance of low-dT/dP category records as classified by this study.

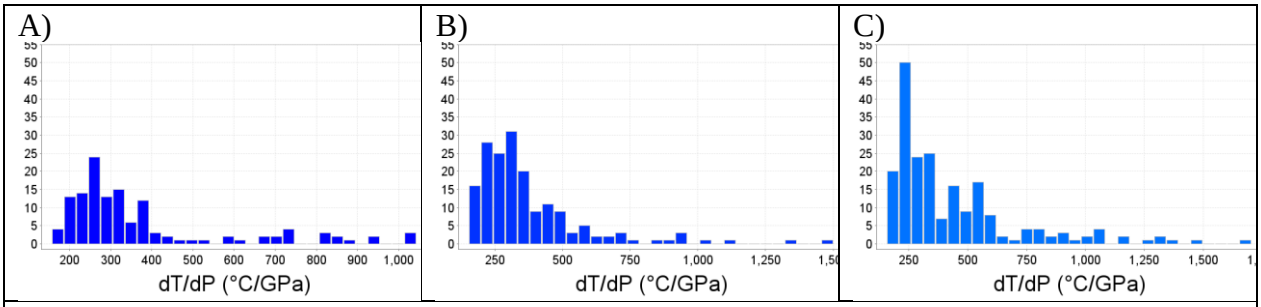

Figure 5.2 Comparison of the frequency of occurrences of different dT/dP records for the Phanerozoic. Figure is split into A) Cenozoic, B) Mesozoic, and C) Paleozoic.

5.1.1 **The Rarity of Blueschist Occurrences**

Despite the prevalence of low dT/dP category records in the Phanerozoic, there remain almost no blueschist samples. Despite records younger than 750 Ma making up 58% of the data, there are only 35 and 76 blueschist samples (field descriptions and plotted metamorphic facies respectively). Figure 5.3 shows the occurrences of blueschist samples through time. All but one blueschist record appear since the break up of Rodinia. Only two records exist from that far back and most records are since the break up of Pangea. Fifteen blueschist records survive from the tenure of Gondwana/Pangea and the rest have never experiences a supercontinent cycle.

This pattern is not seen with any of the eclogite varieties (Figure 5.4).

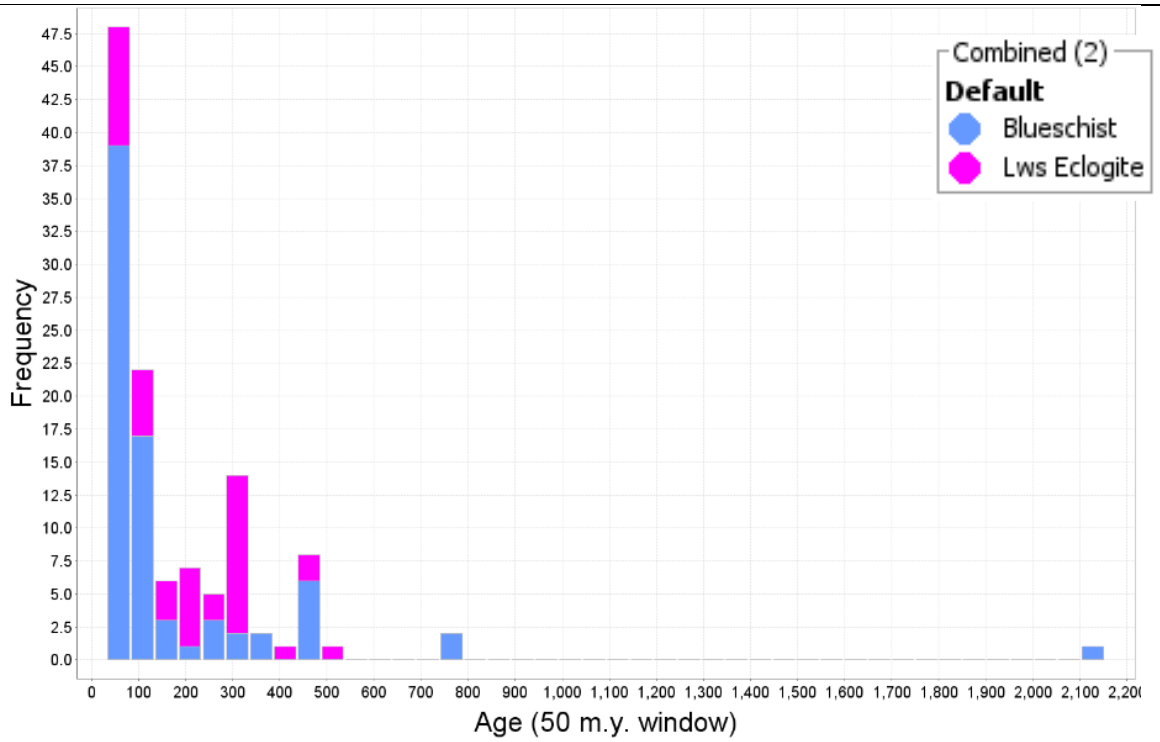

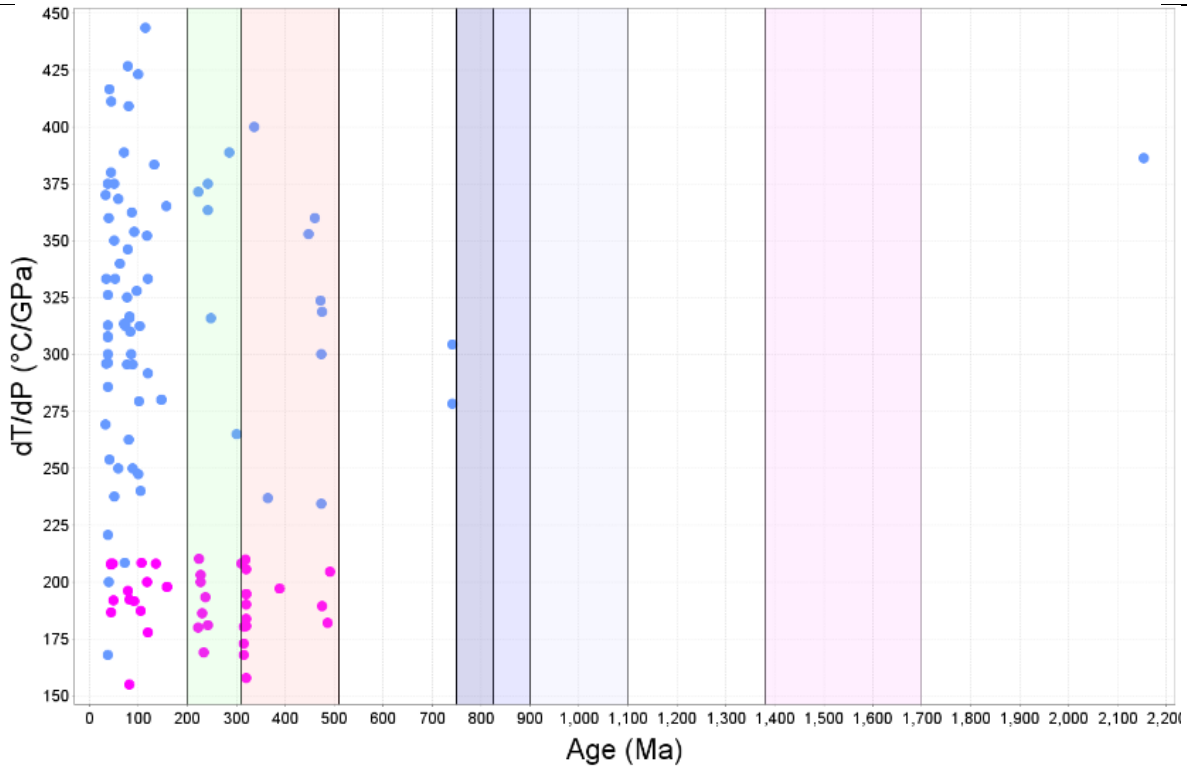

Figure 5.3 A) Histogram of subduction related samples through time. B) dT/dP (°C/GPa) for blueschist and lawsonite eclogite samples through time. Columns represent supercontinent, Nuna (pink), Rodinia (accretion, stability, and rifting in shades of purple), Gondwana (peach), Pangea (green).

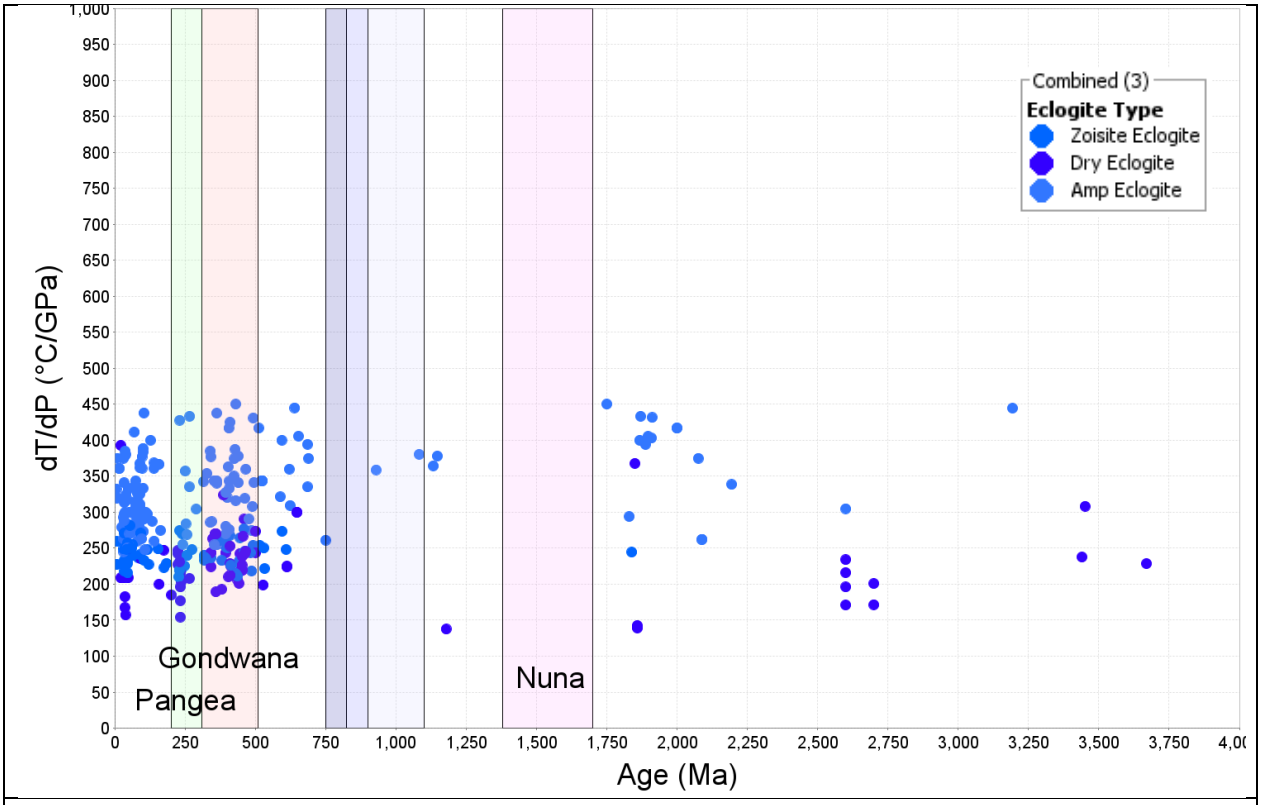

Figure 5.4 dT/dP (°C/GPa) for eclogite records through time. Columns represent supercontinent, Nuna (pink), Rodinia (accretion, stability, and rifting in shades of purple), Gondwana (peach), Pangea (green).

5.2 Spatial Biases

There has been much discussion around the differences between <750 Ma and >750 Ma rocks. Several theories have attempted to explain these differences as discussed previously (see 2 Literature Review & Previous Studies). The roles of spatial biases in datasets has not properly been addressed by previous authors. Here the distribution of records is discussed in terms of its impact on the results of the data.

As discussed previously (See 3.2.3 Averaging Oversampled Areas), there is a bias in the dataset towards samples from the Alpine-Himalayan orogens. When discussing the prevalence of low dT/dP category records and blueschist records since 750 Ma it is critical to mention the main orogens which are preserving blueschist records.

The distribution of blueschist occurrences is shown in Figure 5.5. The Alpine-Himalayan complex accounts for 51 of 77 blueschist samples (over 66%). The distribution of low dT/dP category samples is shown in Figure 5.6. There can be seen a distribution of records which clusters along the Alpine-Himalayan complex, which accounts for roughly half of all low-dT/dP category samples (235 of 424 records).

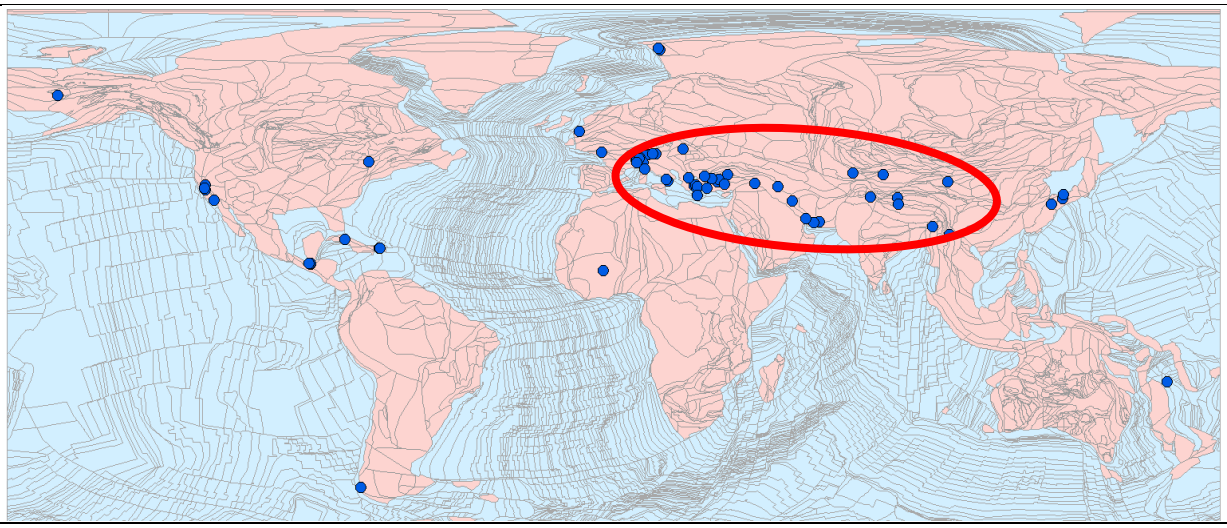

Figure 5.5 The distribution of blueschists against a modern geographical map. Blueschists are blue circles. Peach polygons are continental blocks and light blue polygons are oceanic blocks.

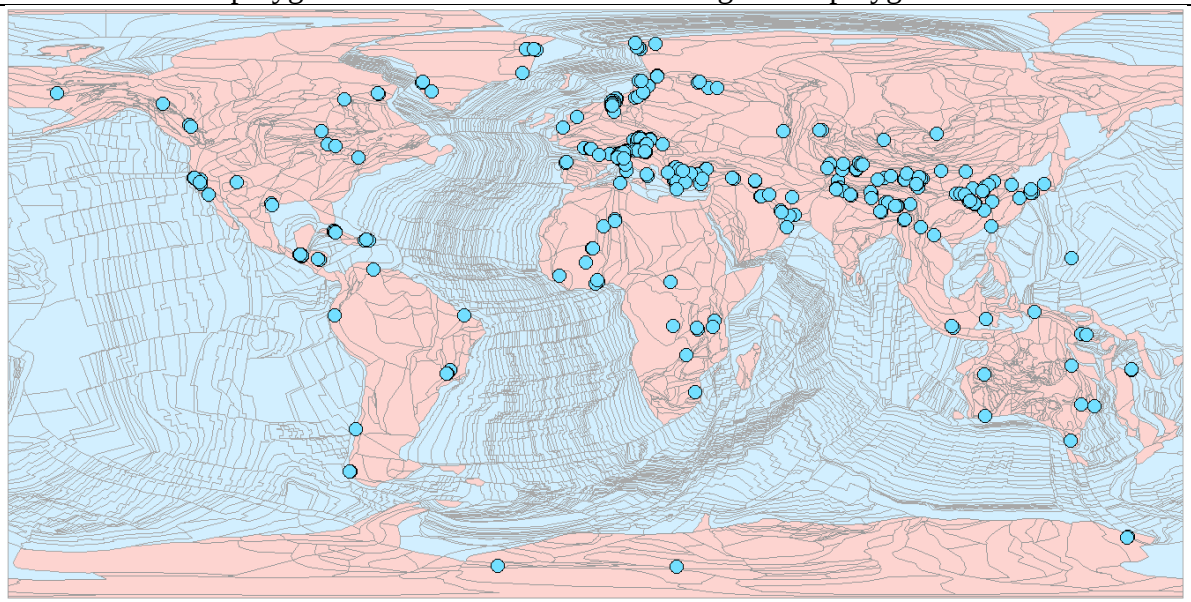

Figure 5.6 The distribution of low dT/dP records against a modern geographical map. Low-dT/dP category records are light-blue circles. Peach polygons are continental blocks and light blue polygons are oceanic blocks.

The Alpine-Himalayan complex is a critical source for both blueschist records and for low dT/dP category records. Removing these records would leave a global distribution of 26 blueschist records and 189 low dT/dP category records for the whole geologic time. This is summarized in Table 5.2 and in Figure 5.7.

Table 5.2 Comparison of records falling with the Alpine-Himalayan series of orogens and those falling outside of that complex.

Metamorphic Category	Distribution	
	Alpine-Himalayan	Global
Blueschist	51	26
Low	235	189
Low-Grade	7	11
Medium	107	173
High	22	231
Contact	1	67

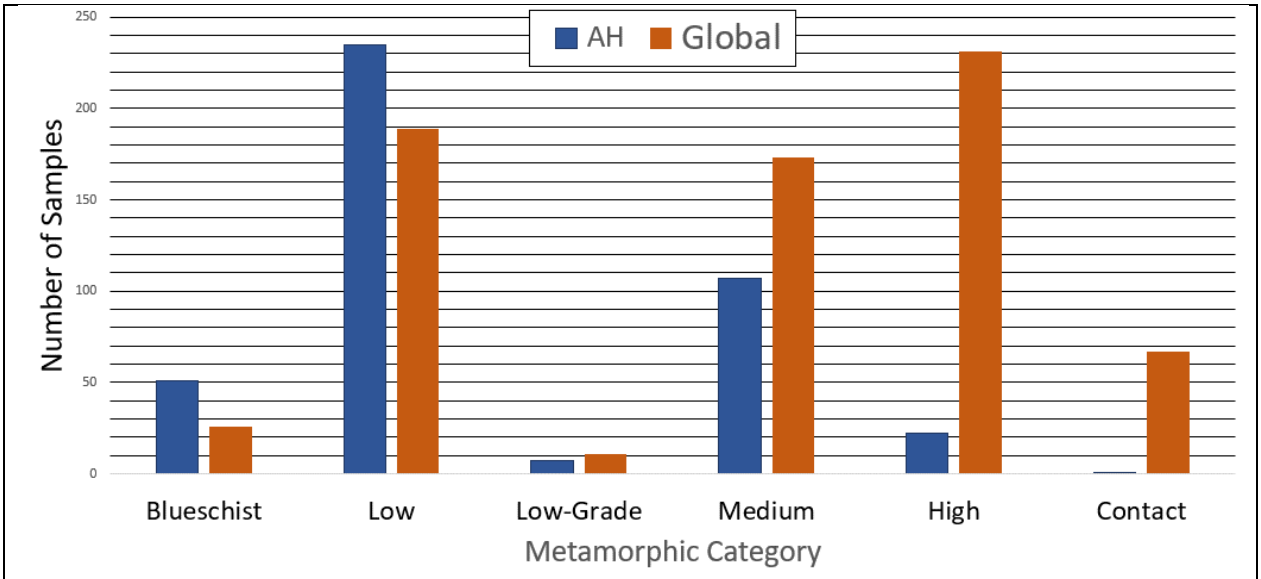

Figure 5.7 Comparison of records from the Alpine-Himalayan complex against records for the rest of the globe. Categories are broken into the polygonal classification set out by this study but also includes records plotting in the blueschist facies zone.

5.3 Matters of Preservation

When looking at the geographical distribution of blueschists, they can be divided into two categories: records which are found near the edge of continents and have thus far not been exposed to reworking during continental collision; and, the much larger group, of blueschists associated with the Alpine-Himalayan series of orogens which are massively over-represented in the literature and data compilations. One reason for this would be the population density along the these orogens. The Alps have a great amount of infrastructure which allows for studying the rocks with relative ease – compare this to South America with much less infrastructure and far greater difficulties in travel. The other reason would be that these orogens have sprung up because of tectonic movements and that many other areas will simply not produce such metamorphic samples because they have not been metamorphosed in the same way. Regardless, the overlap between mountains which are well travelled and an area which shows many instances of subduction has created a great number of low-dT/dP records.

Following the plate reconstruction modelling approach, there are many more GDU's for the time following Rodinia than for before it. This could reflect a preservation bias, in which the rocks following the breakup of Rodinia are better preserved and are more likely to be split into smaller parts because of the increase in information. Most theories addressing the sharp change to the appearance of blueschists and low dT/dP category records rely on a slow, long-term change which reaches a critical mass to start producing low-dT/dP metamorphism consistently. These theories do not account for matters or preservation or spatial biases.

5.4 Supercontinent Cyclicity

Analysis of the data from this study shows that previous trends are less chaotic than previously thought. It seems that filling the data set out smoothed out some of the trends we had seen previously. Trends such a strong bimodal distribution, a lack of low-dT/dP, sharp contacts of certain dT/dP categories at different times seem to be less pronounced than previously shown. Some trends, such as the association of samples becoming much more common during periods of continental accretion and super-continent cycles have stayed true and become more pronounced (Figure 5.8).

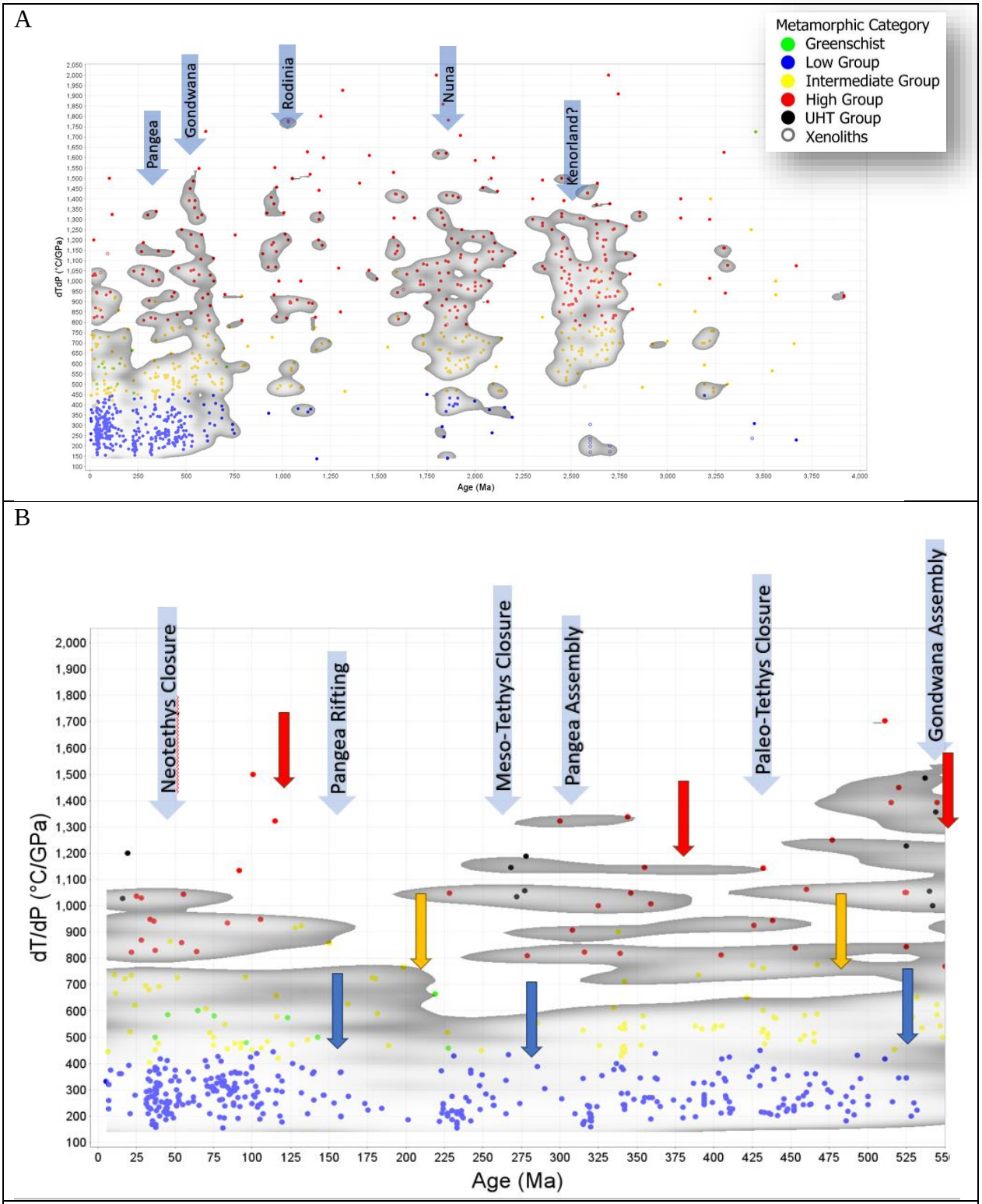

Figure 5.8 Heatmap for dT/dP (°C/GPa) against age (Ma). A) For all time periods and B) For the Phanerozoic. Blue labelled arrows mark generally understood timings for supercontinents amalgamation. Red, yellow, and blue arrows mark beginning periods of increased density of high, medium, and low dT/dP records respectively.

Figure 5.8 shows heatmaps for samples through time for the whole geologic timescale and again for the Phanerozoic. Times of increased density of records are highlighted with arrows and marks to show key geological and tectonic events which drive the production of metamorphic rocks are labelled. These tectonic events events are the real driver behind metamorphism and need to be kept in mind. Bringing in the geology to the data provides real insight into the numbers. We cannot just hope to get enough out of the PT estimates alone. Looking at things in a geologic and tectonic framework provides context for the data. One can see how and why certain samples appear or why they don't show up at certain times. This spatial context allows one to extrapolate for other areas.

In Figure 5.8 we can see association between sample density and large-scale supercontinent cycles. These associations also show large gaps between them, and this helps cement super continent cyclicity as one of the driving factors for metamorphism. One thing to keep in mind is the scale between the Phanerozoic data and the Precambrian data. There are as many Phanerozoic data as there are Precambrian data and as such it can be very difficult to see small variations in trends in the Precambrian data. Smaller events in the Phanerozoic may be represented by many samples but a Precambrian event of similar size could have one or no samples representing them.

One section which doesn't show an association between super continent formation and metamorphic samples is Rodinia. Rodinia is an outlier in this case. It is unclear currently if this is a matter of preservation and or a matter of sampling. What is clear is that filling in samples for Rodinia should be considered for future work.

Research in the field of secular trends in metamorphism is largely shaped by our ability to distill complex events into discrete variables for computing. The Earth's system is complex and intertwined, mixing, and evolving over billions of years. Examining these orogens with an eye to the system is the next step to understanding how the Earth has evolved. Factors such as super continent cyclicity, changes in mantle potential temperature, and orogens need to be considered together. Given the push towards large-scale, data driven endeavors, workers will need to keep the capturing and representation of these variables at the forefront of their research. Until the time comes when one can capture, represent, and work with every aspect of an orogen, there will always be the need to use proxies to help us grapple with these factors. Current research attempts

to maintain this honesty while pushing the boundaries of what has been done before. This will be the main challenge of this area of study. This report attempts to do that by adding new data to previous compilations, bringing updated and revised methods for capturing metamorphic data, and reworking analytical methods in meaningful and innovative ways. Even though metamorphic records vary in their proportions, all major metamorphic categories are present during each supercontinent. This leads to the conclusion that all major metamorphic categories are present back to the Archean.

Figure 5.9 shows a correlation between metamorphic samples and times of continental accretion. There are great lulls in the metamorphic conditions of rifting and break-up of continents, and we can see most of our samples overlap with times of accretion and continental collision. One notable exception is Rodinia, for which we have little and sparse data.

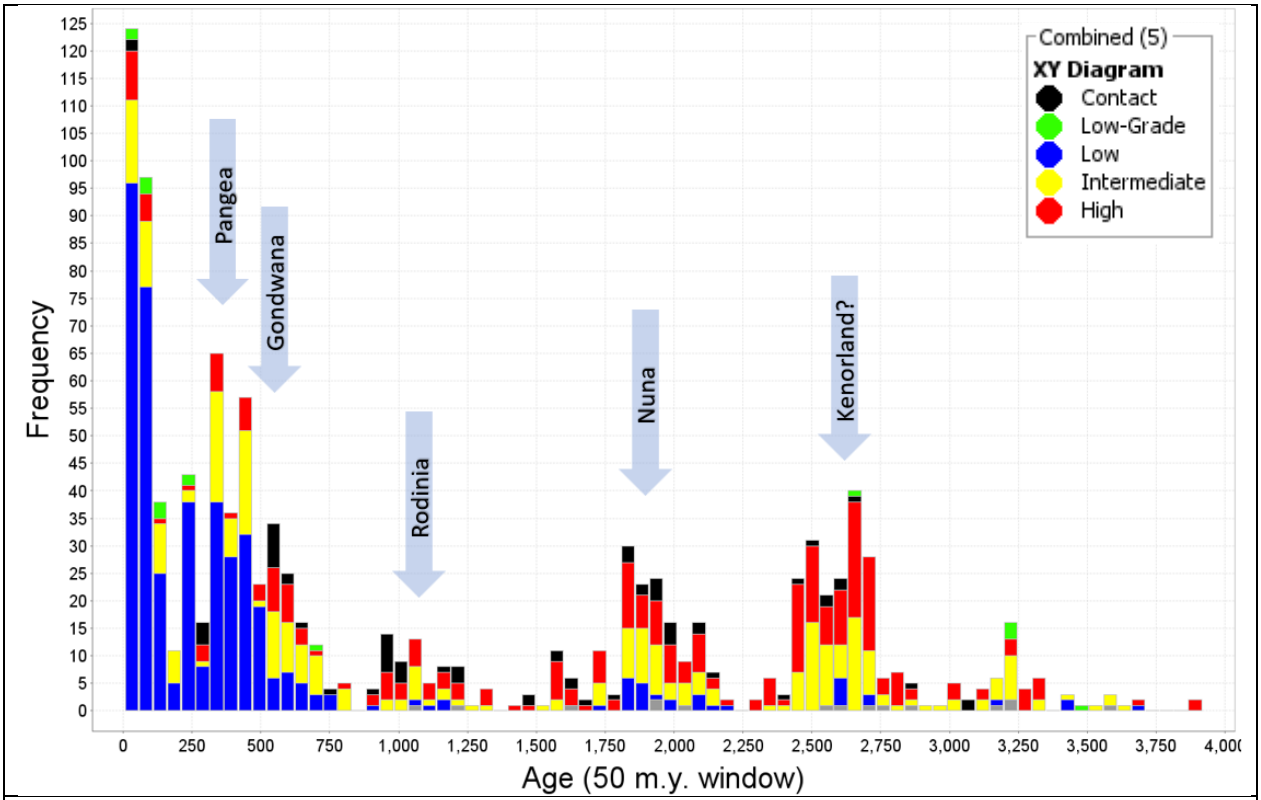

Figure 5.9 Histogram of all MetRec records by age with 50 m.y. windows.

Figure 5.10 summarizes the temporal associations between SuperGDU size, number of independent GDU's, and the frequency of dT/dP records in relation to supercontinent amalgamation.

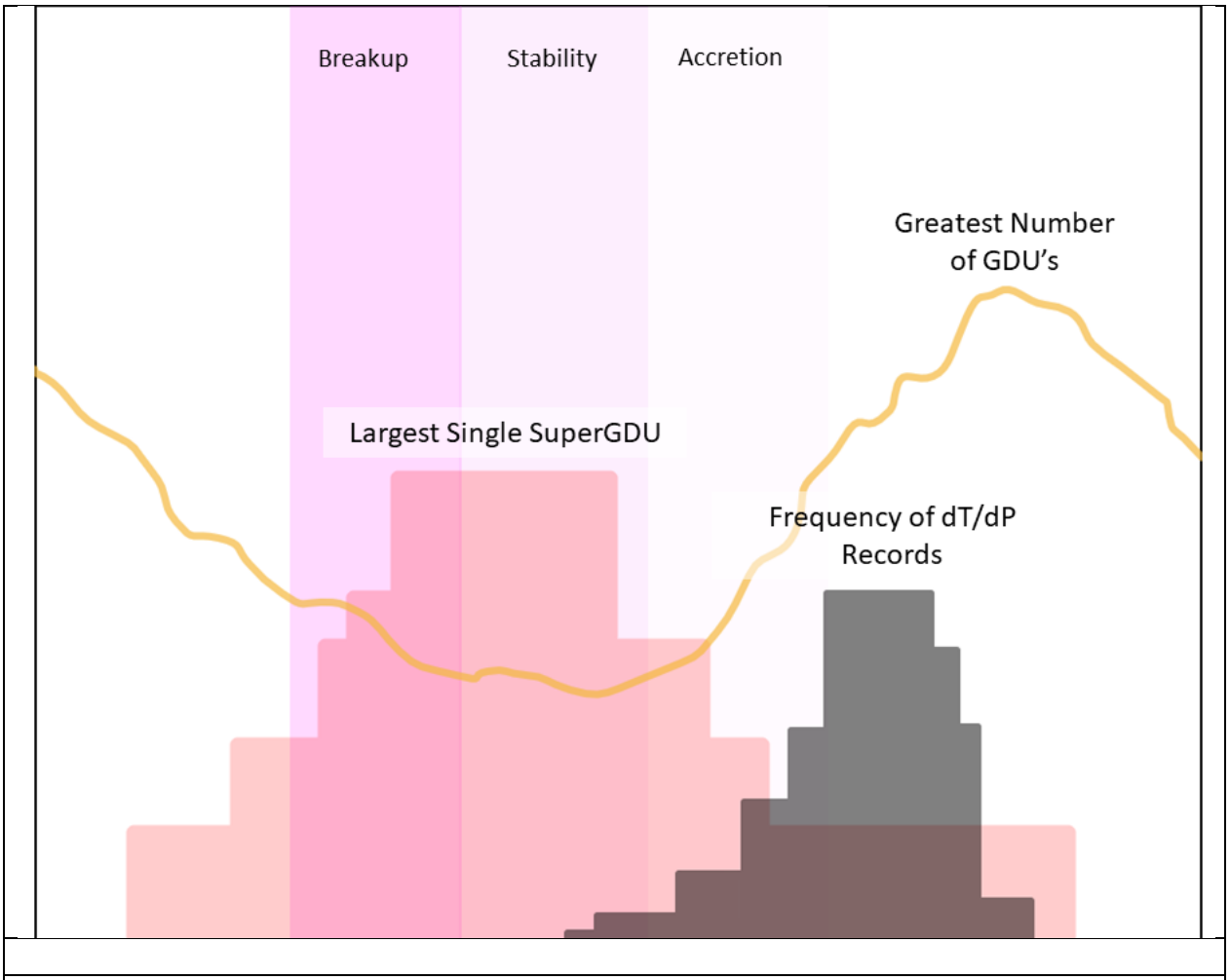

Figure 5.10 Cartoon representing the general trend between supercontinent phases of accretion-stability-breakup and the three factors introduced in Figure 4.31. Pink squares represent the size of the largest superGDU. The orange line represents the number of independent GDU's. The black squares represents the frequency of all metamophic records, not differentiated by dT/dP, in the databse. Purple columns show the tenure of supercontinents through amalgamation, stability and breakup.

5.5 Decreasing Mantle Potential Temperatures through Time and Their Affect on Metamorphic Temperatures

There has been much discussion surrounding the secular decrease in mantle potential temperature and its affect on metamorphic rocks. Previous compilations (Brown and Johnson, 2019; Brown et al., 2020a; Palin et al., 2020; Palin and Santosh, 2021b) have posited that a long-term decrease in mantle potential temperature would lead to the creation of low-temperature metamorphism. This postulating has been driven by the dearth of low-dT/dP (by previous compilation standards) beyond the Phanerozoic. Figure 5.11 is a series of box-and-whisker plots which show that temperatures have increased from the Paleoarchean through to the Phanerozoic where the median and lower range drop drastically. What is seen with this database, is the increase in the range of temperatures and median values from the Paleoarchean to Neoarchean, where they are relatively stable until the Phanerozoic. Moving into the Phanerozoic, upper range stays the same while the lower range and median drop. The change may seem drastic, but the lower range sits 100 °C below the Paleoarchean (234.5 °C vs 345.0 °C) and the median sits on par with the Paleoarchean (640 °C vs 675 °C). The trend is that average temperature value increase from Paleoarchean to Neoproterozoic before dropping back down – to Paleoarchean levels – in the Phanerozoic.

The evidence for a cooling mantle is clear and it is not the point of this study. What this study would support is that average metamorphic ranges are not tied to mantle potential temperature at all and are instead a product of changes in the tectonic regime. As continental crust develops and continents are developing from small things to super continents, we see an increase in median temperature (from Paleoarchean to Mesoarchean) – then a plateau as the continents stabilize into the normal tectonic regime we see today (from Mesoarchean to Neoproterozoic). The drop in temperature can be associated with better preservation of deep, high-pressure records.

It’s understandable that previous modelling conceived that a cooling mantle would engender the conditions for cold, modern subduction. The question yet remains of how much weight the Alpine-Himalayan data should have in these models. Proterozoic and Archean subduction zones hosted the conditions which overlap with some modern subduction zones. This

means that subduction zones like some modern ones could be taking place in a different form as far back as the Archean.

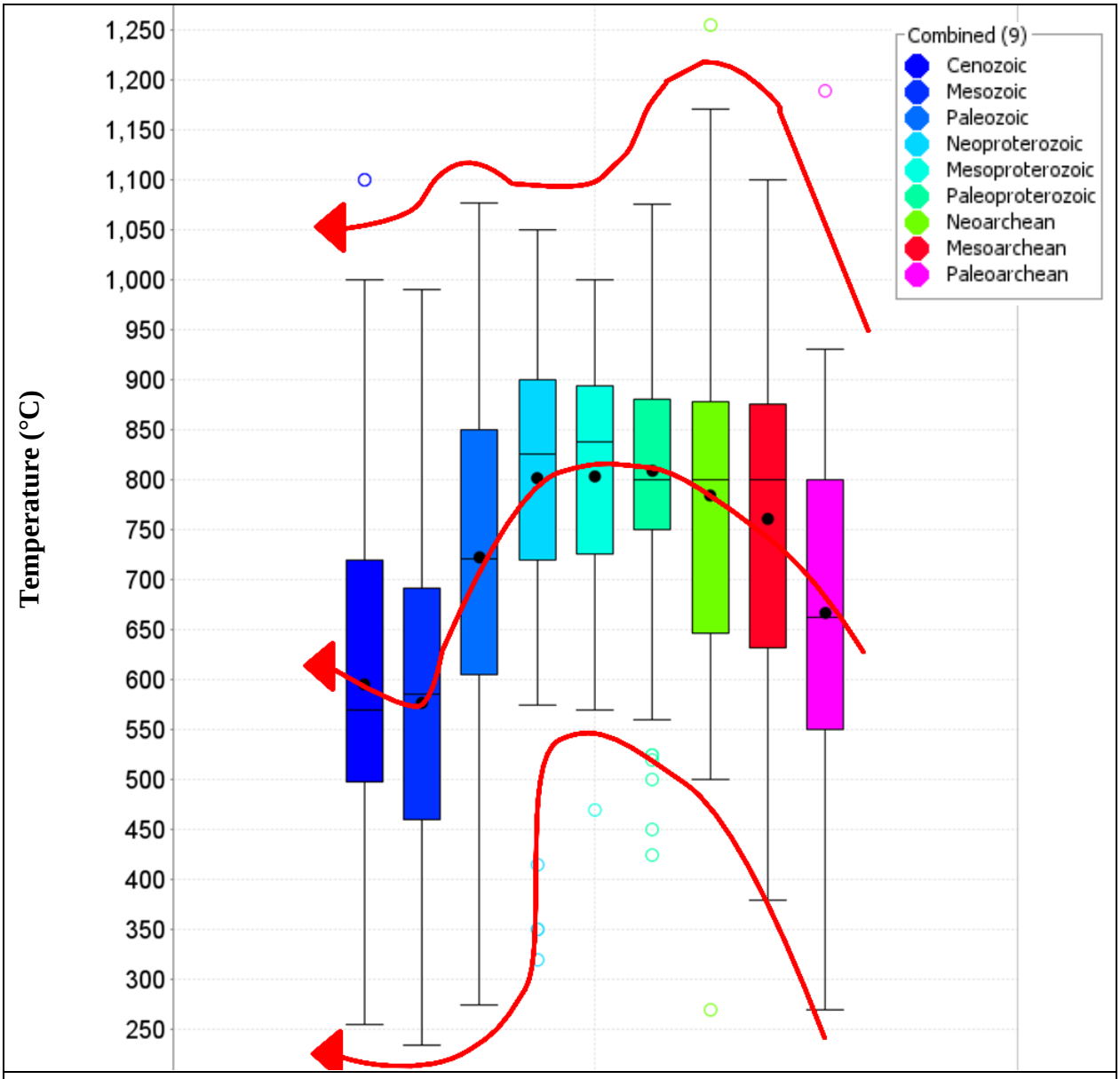

Figure 5.11 Box whisker plot for temperature estimates coloured by age according to legend. Black circle represents the mean. Black line represents the median. Central box is the middle 50% of data. Circles are data that is further than 1.5 times distance the from the box. Triangles is more than 3 times distance from the box. The Whiskers are the extreme values that are not outliers (i.e. outside the 50% box but less than 1.5 times distance from the box). Red arrows show the rough trends in upper range, median, and the lower range through time. Paleoarchean (n = 29), Mesoarchean (n = 20), Neoarchean (n = 111), Paleoproterozoic (n = 190), Mesoproterozoic (n = 61), Neoproterozoic (n = 99), Phanerozoic (n = 528).

5.6 Addressing the "Duality of Metamorphic Regimes"

From a statistical point of view, there is a difference in the nature of Phanerozoic metamorphism from that of Precambrian metamorphism. Previous compilations have shown stark contrast from the nature of records younger than 750 Ma and those which are older than that point. The cause of this change has been the focus of much discussion and debate. This study would posit that these changes are largely a matter of preservation and statistics.

Brown, Johnson, & Gardiner (2020a) argue that the onset of plate tectonics should be registered with the formation of Columbia as this marks the "onset of bimodal metamorphism." Holder et al. (2019) has shown that the previous datasets could show bimodal distribution through the use of Kernel Density Estimates (KDE). It has been increasingly common in recent literature to see the bimodal metamorphism as a sign of modern metamorphism. It is important to note that the use of bimodal metamorphism as an indicator for modern metamorphism stems from Holder et al. (2019).

It is the position of this paper that this bimodal distribution seen in the KDE of Holder et al. (2019) hold true for the dataset, but the reasons that it exists have not been examined. As discussed (5.2 Spatial Biases), there are many records in the Alps and Himalayas which are very low-dT/dP category and pull the Phanerozoic average down greatly. Disregarding these would allow the KDE to show less of an intense shift to a bimodal distribution. The use of these statistical methods is not suitable for such a small dataset.

5.7 dT/dP Uncertainties and Pseudosection Modelling

Uncertainty in dT/dP can be calculated using the following formula modified from Roddick (1987).

Equation 2 Calculated dT/dP uncertainty from Roddick (1987).

$$\frac{dT}{dP}Unc = \frac{dT}{dP} \times \sqrt{\left(\frac{UncP}{P}\right)^2 + \left(\frac{UncT}{T}\right)^2} \quad \text{.....(5.1)}$$

where $\frac{dT}{dP}Unc$ is the uncertainty in dT/dP, *UncP* is the uncertainty in pressure, and *UncT* is the uncertainty in temperature.

Calculated uncertainties for dT/dP are a product of the ratio of the value of temperature and pressure over the uncertainty for temperature and pressure respectively. This means that a high value with a small uncertainty will create a small dT/dP uncertainty (ex. 1000 °C ± 50 °C), but a low value with a relatively large uncertainty will create a large dT/dP uncertainty (ex. 100 °C ± 50 °C). This means that the assumption that pseudosection models have uncertainties of ±50 °C and ±0.1 GPa, for temperature and pressure respectively, will create large dT/dP uncertainties for low pressure records and small uncertainties for high pressure records as seen in Figure 5.12.

This comes about as the calculation is a result of the uncertainty in the temperature value over the uncertainty in the pressure value. When using the assumption of ±50 °C for temperature, one is almost always ensuring relatively flat uncertainty for temperature because the assumed temperature uncertainty is generally much lower than the value for temperature (see: 4.4.2 Temperature). The lowest temperature value for the MetRec dataset is 300°C, six times the value of the assumed pseudosection uncertainty. Contrast this with the range of pressures, where the lowest value is 0.2 GPa, only double the methodological uncertainty.

When the calculation proceeds for the uncertainty of dT/dP, it looks at the ratio of temperature uncertainty (generally low) over the pressure uncertainty (variable) and produces results that are striking. The range of dT/dP uncertainty (covered in section 4.5 dT/dP) varies from 2.7 °C/GPa to 868.3 °C/GPa. It is worth noting that the 2.7 °C/GPa record has a high pressure (4.15 GPa) and the 868.3 °C/GPa is a low pressure, low-grade prehnite-pumpellyite-greenschist (0.2 GPa).

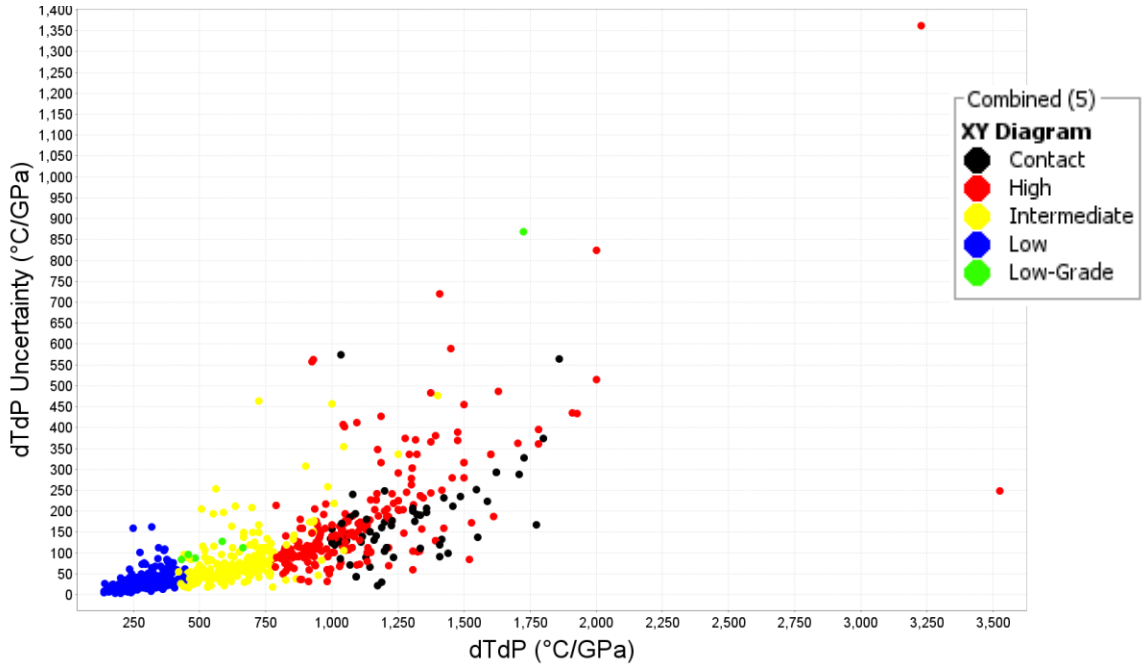

Figure 5.12 dT/dT Uncertainty (°C/GPa) against dT/dP (°C/GPa) for all MetRec samples. Samples are coloured according to the polygonal classification scheme discussed in 3.2.2 Nonlinear Categorization of dT/dP.

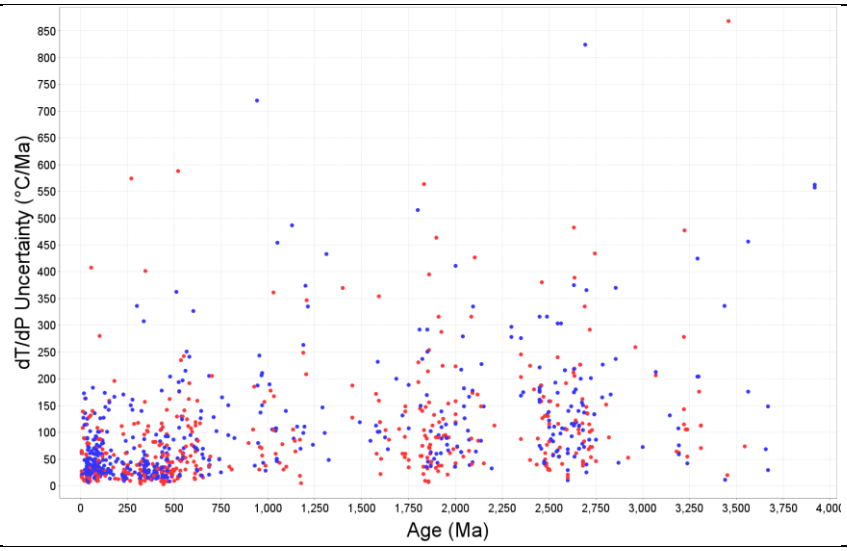

Figure 5.13 dT/dP Uncertainty (°C/GPa) against age (Ma) for all MetRec samples. Samples are divided into two categories: red (assumed method uncertainty) and blue (reported analytical uncertainty). The assumed method uncertainties indicate that the uncertainties for the PT estimates are assumed from the methods used for pressure and temperature. Reported analytical uncertainties are those uncertainties which have been calculated by the paper which originally published the PT estimate.

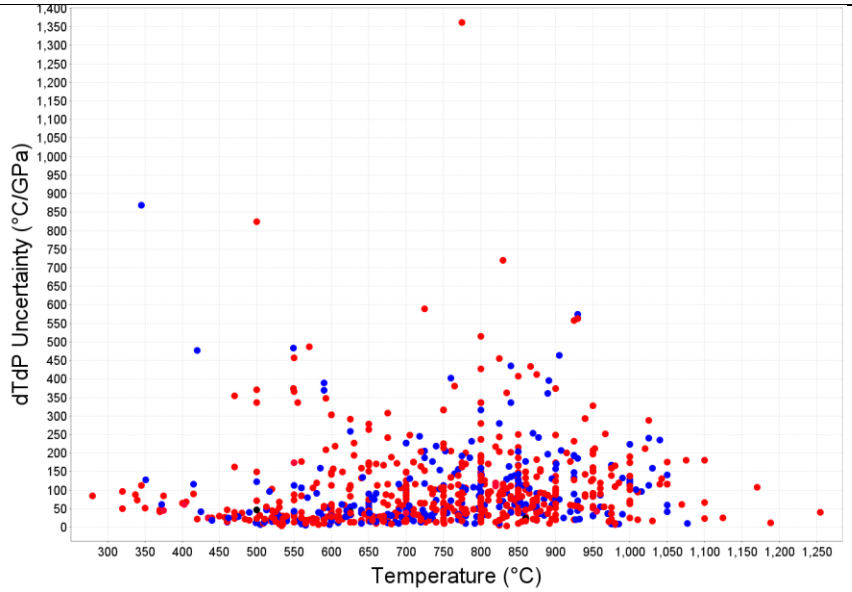

Figure 5.14 dT/dP Uncertainty (°C/GPa) against temperature (°C) for all MetRec samples. Samples are divided into two categories: red (method uncertainty) and blue (analytical uncertainty). The assumed method uncertainties indicate that the uncertainties for the PT estimates are assumed from the methods used for pressure and temperature. Reported analytical uncertainties are those uncertainties which have been calculated by the paper which originally published the PT estimate.

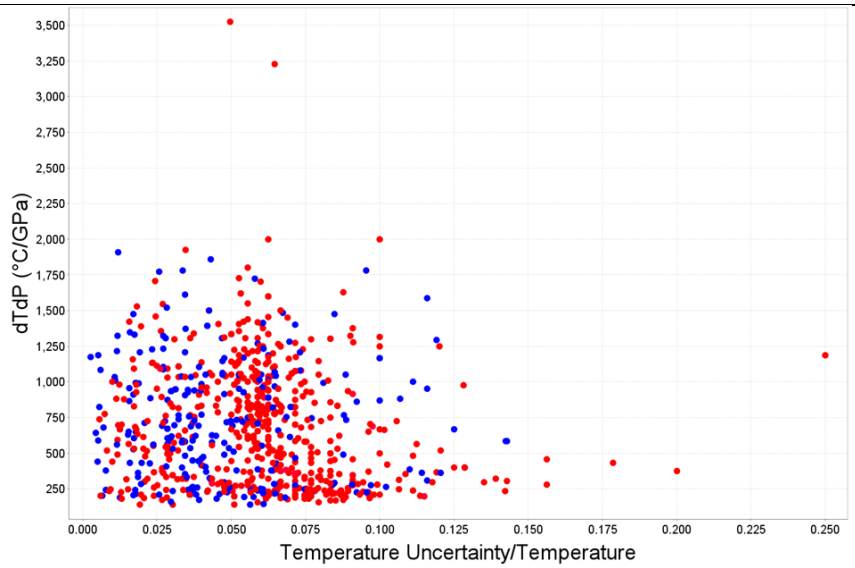

Figure 5.15 dT/dP Uncertainty (°C/GPa) against the ratio of temperature-to-temperature-uncertainty for all MetRec records. Samples are divided into two categories: red (method uncertainty) and blue (analytical uncertainty). The assumed method uncertainties indicate that the uncertainties for the PT estimates are assumed from the methods used for pressure and

temperature. Reported analytical uncertainties are those uncertainties which have been calculated by the paper which originally published the PT estimate.

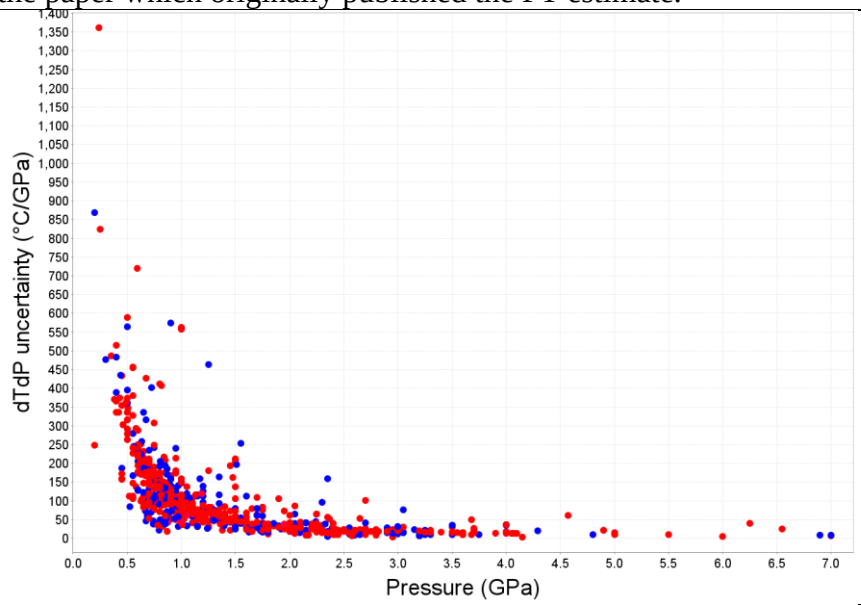

Figure 5.16 dT/dP Uncertainty (°C/GPa) against pressure (GPa) for all MetRec records. Samples are divided into two categories: red (method uncertainty) and blue (analytical uncertainty). The assumed method uncertainties indicate that the uncertainties for the PT estimates are assumed from the methods used for pressure and temperature. Reported analytical uncertainties are those uncertainties which have been calculated by the paper which originally published the PT estimate.

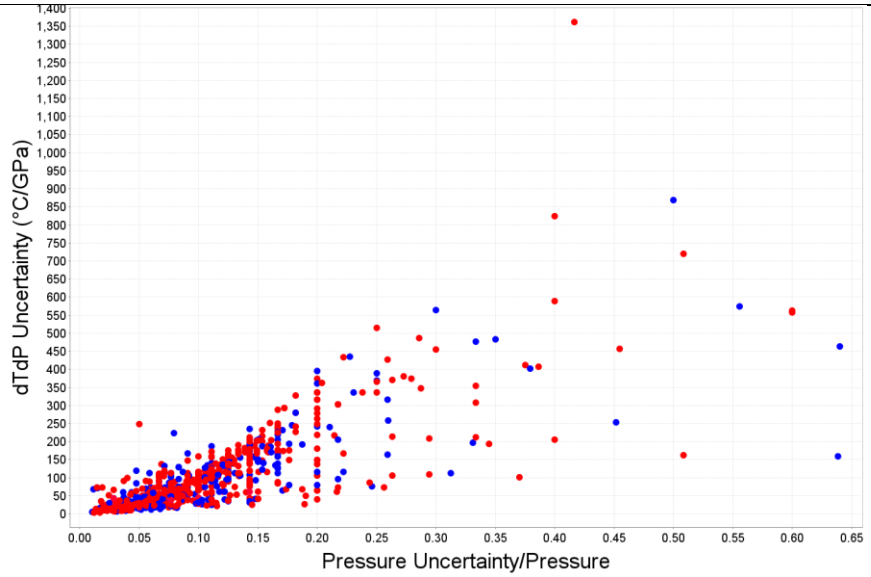

Figure 5.17 dT/dP Uncertainty (°C/GPa) against the ratio of pressure-to-pressure-uncertainty for all MetRec records. Samples are divided into two categories: red (method uncertainty) and blue (analytical uncertainty). The assumed method uncertainties indicate that the uncertainties for the PT estimates are assumed from the methods used for pressure and temperature. Reported analytical uncertainties are those uncertainties which have been calculated by the paper which originally published the PT estimate.

5.8 The effect of Contact-Category Metamorphism

As discussed in 2.2.4 Eschewed Metamorphic Samples, many previous compilations have chosen to not include contact metamorphic samples in their analyses because they do not represent changes in tectonic regime. Since this study has included all available data, it is important to discuss the impact of the contact-category samples which are included in MetRec. Table 5.3 summarizes the median values for temperature, pressure, and dT/dP and shows only marginal differences between these values whether contact-samples are included or not. The largest differences are 50 °C (Mesoproterozoic), 0.14 GPa (Mesoarchean), and 145 °C/GPa (Mesoarchean) for temperature, pressure, and dT/dP respectively. While this study agrees that the methodology to eschew known contact metamorphic samples from this study makes sense and should continue, it would posit that the inclusion of contact-category records is negligible to the outcomes of almost all current analyses.

Table 5.3 Summary of the affect of including contact-category metamorphic samples on the median values of temperature, pressure, and dT/dP at each geological era. The unchanged data is shown the on left and the contact-removed data is on the right for each category.

Geological Era	Temperature (°C)		Pressure (GPa)		dT/dP (°C/GPa)	
All Data	735	718	1.25	1.30	500	537
Cenozoic	570	568	1.90	1.90	300	300
Mesozoic	585	585	1.80	1.80	314	314
Paleozoic	723	715	2.00	2.05	343	340
Neoproterozoic	820	782	1.20	1.23	684	596
Mesoproterozoic	850	800	0.80	0.91	1010	895
Paleoproterozoic	800	800	0.90	0.97	928	857
Neoarchean	800	800	0.90	0.90	889	856
Mesoarchean	770	725	0.80	0.94	853	708
Paleoarchean	675	675	0.79	0.79	933	933

6 Conclusions & Recommendations

There is more work to be done when creating a database which fully describes the breadth and depth of metamorphic trends. This thesis is one step towards that and the addition of data to previous datasets, with emphasis on under-sampled areas and times, has shown that many previous conclusions are a product of limited datasets and sampling bias. These additions have filled in previously unknown areas and challenged assumptions. Some of these assumptions are around the availability of data (what time periods and areas can we get data from) and some around the interpretation of that data (what represents subduction? Where can we start to say we have real changes in the metamorphic record?). These challenges will surely be confronted again in the future.

The study of secular trends in metamorphism and the applications to the onset of plate tectonics will likely carry on for many years to come. Previous analysis of metamorphism has been varied and wide ranging but limited in terms of its data. Current research focuses on the thermobaric ratio but struggles with small datasets. Future analyses will certainly shed light on some of the areas in which we're currently struggling. Much of what has been studied so far has been focused on gathering data from easy and well populated areas. Areas such as the Alps, Himalayas, and some of the famous blueschist areas have carried much of the discussion while areas like South America have little in the way of data and thus do not contribute much despite having a varied geological history. Future work will need to consider these underrepresented areas. It has been common to assume that there is enough data, and that these smaller, more remote areas will change the interpretation little, but that remains to be seen. Future research and perhaps new technological advancements will continue to push datasets. This will allow one to perhaps start to use true statistical analyses with true statistical significance.

1. Subduction related rocks can be found well into the Archean. When these subduction zones were linked into a global framework is still under debate.

2. Using the findings of Penniston-Dorland et al. (2015), we have shown that there is the possibility that many events in the past could be the product of subduction.
3. Secular trends in metamorphism are tightly linked to supercontinent cycles: an abundance of data lining up with accretion and a dearth of data associated with breakup.
4. With the addition of new data which fills out old gaps, there is less bias in the record; trends seen in previous studies are not as relevant and should be reconsidered.

6.1 Recommendations for Future Work

6.1.1 Phanerozoic Data Bias

Increasing the amount of data is a clear objective for future work. The amount that the database can be increased however is limited by what papers are coming out and what has previously been studied. As such, the database will always be a reflection of what previous researchers have chosen to study.

The use of spatial associations, mapping and plate reconstruction software, will be key in understanding and interpreting the data which we do have access to. The bias, stemming from the intense density, of the Alpine-Himalayan complex is made clear when seen through mapping. Further associations will no doubt be made when used more often with plate reconstruction modelling.

6.1.2 Thermobaric Exaggeration (TBx)

As discussed in section 2.2.3 Thermobaric Exaggeration, there remains some exaggeration between the P-T-t path of a sample and the calculated dT/dP of that that sample. It would be the advice of this study that the relationships between TBx and other aspects of metamorphism (timing of metamorphic events, cooling rates, locality, proximity to edge of subduction zone or collision area) are studied in depth. To this end, this study recommends a literature review which would compile the data needed from P-T-t paths to be able to calculate TBx. Table 6.1 provides an example of the kind of comparisons which can be done using this sort of data. A dataset of this nature would also be able to provide a broad overview of the shape of most P-T-t paths in the literature, which would be a step towards utilizing P-T-t paths in a large-data capacity.

Table 6.1 Example orogens from which TBx can be calculated from a P-T-t path. Cooling rates taken from Chowdhury et al. (2021).

Name	dT/dP @Pmax	dT/dP @Tmax	TBx	dT/dP	Cooling Rate
Moine Thrust	545/0.85	590/0.66	0.71	694	>1000°C/m.y.
Southern Granulite Terrain	825/1.35	960/0.8	0.51	711	40°C/m.y.
Wyoming Province	775/0.66	790 / 0.59	0.89	1196	20-100°C/m.y.
Pikwitonei	930/0.86	980/0.84	0.93	1139	7°C/m.y.

7 References

Agard, P., Plunder, A., Angiboust, S., Bonnet, G., Ruh, J., 2018. The subduction plate interface: rock record and mechanical coupling (from long to short timescales). Lithos 320–321, 537–566. https://doi.org/10.1016/j.lithos.2018.09.029

Bhowmik, S.K., Chakraborty, S., 2017. Sequential kinetic modelling: A new tool decodes pulsed tectonic patterns in early hot orogens of Earth. Earth and Planetary Science Letters 460, 171–179. https://doi.org/10.1016/j.epsl.2016.12.018

Brown, Johnson, T., 2019. Time's arrow, time's cycle: Granulite metamorphism and geodynamics. Mineralogical Magazine 83, 323–338. https://doi.org/10.1180/mgm.2019.19

Brown, M., 2010. Paired metamorphic belts revisited. Gondwana Research, A Tribute to Miyashiro 18, 46–59. https://doi.org/10.1016/j.gr.2009.11.004

Brown, M., 2007. Metamorphic Conditions in Orogenic Belts: A Record of Secular Change. International Geology Review 49, 193–234. https://doi.org/10.2747/0020-6814.49.3.193

Brown, M., 2006. Duality of thermal regimes is the distinctive characteristic of plate tectonics since the Neoarchean. Geology 34, 961–964. https://doi.org/10.1130/G22853A.1

Brown, M., Johnson, T., 2018. Secular change in metamorphism and the onset of global plate tectonics. American Mineralogist 103, 181–196. https://doi.org/10.2138/am-2018-6166

Brown, M., Johnson, T., Gardiner, N.J., 2020a. Plate Tectonics and the Archean Earth. Annu. Rev. Earth Planet. Sci. 48, 291–320. https://doi.org/10.1146/annurev-earth-081619-052705

Brown, M., Johnson, T., Gardiner, N.J., 2020b. Plate Tectonics and the Archean Earth. Annu. Rev. Earth Planet. Sci. 48, 291–320. https://doi.org/10.1146/annurev-earth-081619-052705

Brown, M., Johnson, T., Spencer, C.J., 2022. Secular changes in metamorphism and metamorphic cooling rates track the evolving plate-tectonic regime on Earth. Journal of the Geological Society 179, jgs2022-050. https://doi.org/10.1144/jgs2022-050

Chowdhury, P., Chakraborty, S., Gerya, T.V., 2021. Time will tell: Secular change in metamorphic timescales and the tectonic implications. Gondwana Research 93, 291–310. https://doi.org/10.1016/j.gr.2021.02.003

Clarke, G.L., Powell, R., Fitzherbert, J.A., 2006. The lawsonite paradox: a comparison of field evidence and mineral equilibria modelling. Journal of Metamorphic Geology 24, 715–725. https://doi.org/10.1111/j.1525-1314.2006.00664.x

Collins, W., 2002. Nature of extensional orogens. Tectonics 21, 6–1. https://doi.org/10.1029/2000TC001272

Condie, K.C., Aster, R.C., van Hunen, J., 2016. A great thermal divergence in the mantle beginning 2.5 Ga: Geochemical constraints from greenstone basalts and komatiites. Geoscience Frontiers 7, 543–553. https://doi.org/10.1016/j.gsf.2016.01.006

Condie, K.C., Kroner, A., 2008. When did plate tectonics begin? Evidence from the geologic record.

Condie, K.C., Kröner, A., 2008. When did plate tectonics begin? Evidence from the geologic record, in: Special Paper 440: When Did Plate Tectonics Begin on Planet Earth? Geological Society of America, pp. 281–294. https://doi.org/10.1130/2008.2440(14)

Condie, K.C., Shearer, C.K., 2017. Tracking the evolution of mantle sources with incompatible element ratios in stagnant-lid and plate-tectonic planets. Geochimica et Cosmochimica Acta 213, 47–62. https://doi.org/10.1016/j.gca.2017.06.034

Currie, C.A., Hyndman, R.D., 2006. The thermal structure of subduction zone back arcs. Journal of Geophysical Research: Solid Earth 111. https://doi.org/10.1029/2005JB004024

Davies, G.F., 2009. Effect of plate bending on the Urey ratio and the thermal evolution of the mantle. Earth and Planetary Science Letters 287, 513–518. https://doi.org/10.1016/j.epsl.2009.08.038

Davies, G.F., 2006. Gravitational depletion of the early Earth's upper mantle and the viability of early plate tectonics. Earth and Planetary Science Letters 243, 376–382. https://doi.org/10.1016/j.epsl.2006.01.053

Davies, G.F., 1992. On the emergence of plate tectonics. GSA Today 20, 4. https://doi.org/10.1130/0091-7613(1992)020%3C0963:OTEOPT%3E2.3.CO;2

de Roever, W., 1956. Some differences between post-Paleozoic and older regional metamorphism. Geologie En Mijnbouw 18, 5.

Dhuime, B., Hawkesworth, C.J., Delavault, H., Cawood, P.A., 2018. Rates of generation and destruction of the continental crust: implications for continental growth. Philosophical Transactions of the Royal Society A: Mathematical, Physical and Engineering Sciences 376, 20170403. https://doi.org/10.1098/rsta.2017.0403

Dhuime, B., Wuestefeld, A., Hawkesworth, C.J., 2015. Emergence of modern continental crust about 3 billion years ago. Nature Geoscience 8, 552–555. https://doi.org/10.1038/ngeo2466

Eglington, B.M., Evans, D.A.D., Pehrsson, S.J., Huston, D.L., 2017. Reconstructing Phanerozoic and Proterozoic Earth Evolution: building on pre-existing efforts and data.

Eguchi, J., Seales, J., Dasgupta, R., 2020. Great Oxidation and Lomagundi events linked by deep cycling and enhanced degassing of carbon. Nat. Geosci. 13, 71–76. https://doi.org/10.1038/s41561-019-0492-6

Ernst, W.G., 1972. Occurrence and mineralogic evolution of blueschist belts with time. Am J Sci 272, 657–668. https://doi.org/10.2475/ajs.272.7.657

Evans, D.A.D., Eglington, B.M., 2022. Continuous Quantitative Model of Global Paleogeography Through 2.0 Billion Years.

Ganne, J., Feng, X., 2017. Primary magmas and mantle temperatures through time: A Not So Hot Mantle About 2.5 GYR Ago. Geochem. Geophys. Geosyst. 18, 872–888. https://doi.org/10.1002/2016GC006787

Gerya, T., Stöckhert, B., 2006. Two-dimensional numerical modeling of tectonic and metamorphic histories at active continental margins. Int J Earth Sci (Geol Rundsch) 95, 250–274. https://doi.org/10.1007/s00531-005-0035-9

Gerya, T.V., Stöckhert, B., Perchuk, A.L., 2002. Exhumation of high-pressure metamorphic rocks in a subduction channel: A numerical simulation. Tectonics 21, 6-1-6–19. https://doi.org/10.1029/2002TC001406

Grambling, J.A., 1981. Pressures and temperatures in Precambrian metamorphic rocks. Earth and Planetary Science Letters 53, 63–68. https://doi.org/10.1016/0012-821X(81)90026-1

Guotana, J.M., Morishita, T., Nishio, I., Tamura, A., Mizukami, T., Tani, K., Harigane, Y., Szilas, K., Pearson, D.G., 2022. Deserpentinization and high-pressure (eclogite-facies) metamorphic features in the Eoarchean ultramafic body from Isua, Greenland. Geoscience Frontiers 13, 101298. https://doi.org/10.1016/j.gsf.2021.101298

Hastie, A.R., Fitton, J.G., 2019. Eoarchaean tectonics: New constraints from high pressure-temperature experiments and mass balance modelling. Precambrian Research 325, 20–38. https://doi.org/10.1016/j.precamres.2019.02.006

Hawkesworth, C.J., Cawood, P.A., Kemp, T., Storey, C.D., Dhuime, B., 2009. A Matter of Preservation. Science 323.

Hawkesworth, C.J., Dhuime, B., Pietranik, A.B., Cawood, P.A., Kemp, A.I.S., Storey, C.D., 2010. The generation and evolution of the continental crust. Journal of the Geological Society 167, 229–248. https://doi.org/10.1144/0016-76492009-072

Herzberg, C., Condie, K., Korenaga, J., 2010. Thermal history of the Earth and its petrological expression. Earth and Planetary Science Letters 292, 79–88. https://doi.org/10.1016/j.epsl.2010.01.022

Holder, R.M., Viete, D.R., Brown, M., Johnson, T.E., 2019. Metamorphism and the evolution of plate tectonics. Nature 1–4. https://doi.org/10.1038/s41586-019-1462-2

Korenaga, J., 2021. Hadean geodynamics and the nature of early continental crust. Precambrian Research 359, 106178. https://doi.org/10.1016/j.precamres.2021.106178

Korenaga, J., 2018. Crustal evolution and mantle dynamics through Earth history. Philosophical Transactions of the Royal Society A: Mathematical, Physical and Engineering Sciences 376, 20170408. https://doi.org/10.1098/rsta.2017.0408

Korenaga, J., 2013. Initiation and Evolution of Plate Tectonics on Earth: Theories and Observations. Annu. Rev. Earth Planet. Sci. 41, 117–151. https://doi.org/10.1146/annurev-earth-050212-124208

Korenaga, J., 2008a. Urey ratio and the structure and evolution of Earth's mantle. Reviews of Geophysics 46. https://doi.org/10.1029/2007RG000241

Korenaga, J., 2008b. Urey ratio and the structure and evolution of Earth's mantle. Reviews of Geophysics 46. https://doi.org/10.1029/2007RG000241

Krebs, M., Maresch, W.V., Schertl, H.-P., Münker, C., Baumann, A., Draper, G., Idleman, B., Trapp, E., 2008. The dynamics of intra-oceanic subduction zones: A direct comparison between fossil petrological evidence (Rio San Juan Complex, Dominican Republic) and numerical simulation. Lithos, Rocks Generated under Extreme Pressure and Temperature Conditions: Mechanisms, Concepts, Models 103, 106–137. https://doi.org/10.1016/j.lithos.2007.09.003

McCoy-West, A.J., Chowdhury, P., Burton, K.W., Sossi, P., Nowell, G.M., Fitton, J.G., Kerr, A.C., Cawood, P.A., Williams, H.M., 2019. Extensive crustal extraction in Earth's early history inferred from molybdenum isotopes. Nat. Geosci. 12, 946–951. https://doi.org/10.1038/s41561-019-0451-2

Nguyen, H.A.T., 2019. Automatically Identifying and Examining Geodynamic Featurs in Plate Tectonic Models.

Nutman, A.P., 2022. Seeking Earth's oldest geological record: an unexpected discovery of well-preserved 3834 Ma metatonalite. Australian Journal of Earth Sciences 69, 188–199. https://doi.org/10.1080/08120099.2021.1980821

Nutman, A.P., Scicchitano, M.R., Friend, C.R.L., Bennett, V.C., Chivas, A.R., 2021. Isua (Greenland) ~3700 Ma meta-serpentinite olivine Mg# and δ18O signatures show connection between the early mantle and hydrosphere: Geodynamic implications. Precambrian Research 361, 106249. https://doi.org/10.1016/j.precamres.2021.106249

O'Neill, C., Turner, S., Rushmer, T., 2018. The inception of plate tectonics: a record of failure. Philos Trans A Math Phys Eng Sci 376, 20170414. https://doi.org/10.1098/rsta.2017.0414

Palin, R.M., Dyck, B., 2018. Metamorphic consequences of secular changes in oceanic crust composition and implications for uniformitarianism in the geological record. Geoscience Frontiers 9, 1009–1019. https://doi.org/10.1016/j.gsf.2018.04.004

Palin, R.M., Moore, J.D.P., Zhang, Z., Huang, G., Wade, J., Dyck, B., 2021. Mafic Archean continental crust prohibited exhumation of orogenic UHP eclogite. Geoscience Frontiers 101225. https://doi.org/10.1016/j.gsf.2021.101225

Palin, R.M., Santosh, M., 2021a. Plate tectonics: What, where, why, and when? Gondwana Research, SPECIAL ISSUE: GR-100 100, 3–24. https://doi.org/10.1016/j.gr.2020.11.001

Palin, R.M., Santosh, M., 2021b. Plate tectonics:What, where, why, and when? Gondwana Research.

Palin, R.M., Santosh, M., Cao, W., Li, S.-S., Hernández-Uribe, D., Parsons, A., 2020. Secular change and the onset of plate tectonics on Earth. Earth-Science Reviews 207, 103172. https://doi.org/10.1016/j.earscirev.2020.103172

Pattison, D.R.M., 1992. Stability of Andalusite and Sillimanite and the Al2SiO5 Triple Point: Constraints from the Ballachulish Aureole, Scotland. The Journal of Geology 100, 423–446. https://doi.org/10.1086/629596

Penniston-Dorland, S.C., Kohn, M.J., Manning, C.E., 2015. The global range of subduction zone thermal structures from exhumed blueschists and eclogites: Rocks are hotter than models. Earth and Planetary Science Letters 428, 243–254. https://doi.org/10.1016/j.epsl.2015.07.031

Profeta, L., Ducea, M.N., Chapman, J.B., Paterson, S.R., Gonzales, S.M.H., Kirsch, M., Petrescu, L., DeCelles, P.G., 2016. Quantifying crustal thickness over time in magmatic arcs. Sci Rep 5, 17786. https://doi.org/10.1038/srep17786

Roddick, J.C., 1987. Generalized numerical error analysis with applications to geochronology and thermodynamics. Geochimica et Cosmochimica Acta 51, 2129–2135. https://doi.org/10.1016/0016-7037(87)90261-4

Secular change in metamorphism tracks the emergence and evolution of plate... - Dr. Michael Brown, 2021. , Virtual Seminars in Precambrian Geology.

Shen, T., Hermann, J., Zhang, L., Lü, Z., Padrón-Navarta, J.A., Xia, B., Bader, T., 2015. UHP Metamorphism Documented in Ti-chondrodite- and Ti-clinohumite-bearing Serpentinized Ultramafic Rocks from Chinese Southwestern Tianshan. J. Petrology 56, 1425–1458. https://doi.org/10.1093/petrology/egv042

Shirey, S.B., Kamber, B.S., Whitehouse, M.J., Mueller, P.A., Basu, A.R., 2008a. A review of the isotopic and trace element evidence for mantle and crustal processes in the Hadean and Archean: Implications for the onset of plate tectonic subduction, in: Special Paper 440: When Did Plate Tectonics Begin on Planet Earth? Geological Society of America, pp. 1–29. https://doi.org/10.1130/2008.2440(01)

Shirey, S.B., Kamber, B.S., Whitehouse, M.J., Mueller, P.A., Basu, A.R., 2008b. A review of the isotopic and trace element evidence for mantle and crustal processes in the Hadean and Archean: Implications for the onset of plate tectonic subduction, in: Special Paper 440: When Did Plate Tectonics Begin on Planet Earth? Geological Society of America, pp. 1–29. https://doi.org/10.1130/2008.2440(01)

Sobolev, A.V., Asafov, E.V., Gurenko, A.A., Arndt, N.T., Batanova, V.G., Portnyagin, M.V., Garbe-Schönberg, D., Wilson, A.H., Byerly, G.R., 2019. Deep hydrous mantle reservoir provides evidence for crustal recycling before 3.3 billion years ago. Nature 571, 555–559. https://doi.org/10.1038/s41586-019-1399-5

Sobolev, S.V., Brown, M., 2019. Surface erosion events controlled the evolution of plate tectonics on Earth. Nature 570, 52–57. https://doi.org/10.1038/s41586-019-1258-4

Spencer, C.J., Mitchell, R.N., Brown, M., 2021. Enigmatic Mid-Proterozoic Orogens: Hot, Thin, and Low. Geophysical Research Letters 48, e2021GL093312. https://doi.org/10.1029/2021GL093312

Stern, R.J., 2005. Evidence from ophiolites, blueschists, and ultrahigh-pressure metamorphic terranes that the modern episode of subduction tectonics began in Neoproterozoic time. Geol 33, 557. https://doi.org/10.1130/G21365.1

Stern, R.J., Gerya, T., 2018. Subduction initiation in nature and models: A review. Tectonophysics, Understanding geological processes through modelling - A Memorial Volume honouring Evgenii Burov 746, 173–198. https://doi.org/10.1016/j.tecto.2017.10.014

Stern Robert J., 2018. The evolution of plate tectonics. Philosophical Transactions of the Royal Society A: Mathematical, Physical and Engineering Sciences 376, 20170406. https://doi.org/10.1098/rsta.2017.0406

Syracuse, E.M., van Keken, P.E., Abers, G.A., 2010. The global range of subduction zone thermal models. Physics of the Earth and Planetary Interiors 183, 73–90. https://doi.org/10.1016/j.pepi.2010.02.004

Tang, M., Chu, X., Hao, J., Shen, B., 2021. Orogenic quiescence in Earth's middle age. https://doi.org/10.1126/ science.abf1876

Tang, M., Ji, W.-Q., Chu, X., Wu, A., Chen, C., 2020. Reconstructing crustal thickness evolution from europium anomalies in detrital zircons. Geology 49, 76–80. https://doi.org/10.1130/G47745.1

Vernon, R.H., Clarke, G.L., 2008. Principles of metamorphic petrology, 3rd print. ed. Cambridge Univ. Press, Cambridge.

Wei, C.J., Clarke, G.L., 2011. Calculated phase equilibria for MORB compositions: a reappraisal of the metamorphic evolution of lawsonite eclogite. Journal of Metamorphic Geology 29, 939–952. https://doi.org/10.1111/j.1525-1314.2011.00948.x

Zheng, Y.-F., Chen, R.-X., 2017. Regional metamorphism at extreme conditions: Implications for orogeny at convergent plate margins. Journal of Asian Earth Sciences, The Structures and Processes of Subduction Zones 145, 46–73. https://doi.org/10.1016/j.jseaes.2017.03.009

Zheng, Y.-F., Zhao, G., 2020. Two styles of plate tectonics in Earth's history. Science Bulletin 65, 329–334. https://doi.org/10.1016/j.scib.2018.12.029